

The Application of Photomediated RAFT Polymerisation in 3D Printing

Author:

Zhang, Zhiheng

Publication Date:

2022

DOI:

<https://doi.org/10.26190/unsworks/24441>

License:

<https://creativecommons.org/licenses/by/4.0/>

Link to license to see what you are allowed to do with this resource.

Downloaded from <http://hdl.handle.net/1959.4/100734> in <https://unsworks.unsw.edu.au> on 2024-04-25



The Application of Photomediated RAFT Polymerisation in 3D Printing

Zhiheng Zhang

A thesis submitted in fulfilment of the requirements for the degree
of Doctor of Philosophy

School of Chemical Engineering

Faculty of Engineering

August 2022

Thesis Title and Abstract	Declarations	Inclusion of Publications Statement	Corrected Thesis and Responses
---------------------------	--------------	-------------------------------------	--------------------------------

ORIGINALITY STATEMENT

☒ I hereby declare that this submission is my own work and to the best of my knowledge it contains no materials previously published or written by another person, or substantial proportions of material which have been accepted for the award of any other degree or diploma at UNSW or any other educational institution, except where due acknowledgement is made in the thesis. Any contribution made to the research by others, with whom I have worked at UNSW or elsewhere, is explicitly acknowledged in the thesis. I also declare that the intellectual content of this thesis is the product of my own work, except to the extent that assistance from others in the project's design and conception or in style, presentation and linguistic expression is acknowledged.

COPYRIGHT STATEMENT

☒ I hereby grant the University of New South Wales or its agents a non-exclusive licence to archive and to make available (including to members of the public) my thesis or dissertation in whole or part in the University libraries in all forms of media, now or here after known. I acknowledge that I retain all intellectual property rights which subsist in my thesis or dissertation, such as copyright and patent rights, subject to applicable law. I also retain the right to use all or part of my thesis or dissertation in future works (such as articles or books).

For any substantial portions of copyright material used in this thesis, written permission for use has been obtained, or the copyright material is removed from the final public version of the thesis.

AUTHENTICITY STATEMENT

☒ I certify that the Library deposit digital copy is a direct equivalent of the final officially approved version of my thesis.

Thesis Title and Abstract	Declarations	Inclusion of Publications Statement	Corrected Thesis and Responses																
<p>UNSW is supportive of candidates publishing their research results during their candidature as detailed in the UNSW Thesis Examination Procedure.</p> <p>Publications can be used in the candidate's thesis in lieu of a Chapter provided:</p> <ul style="list-style-type: none">• The candidate contributed greater than 50% of the content in the publication and are the "primary author", i.e. they were responsible primarily for the planning, execution and preparation of the work for publication.• The candidate has obtained approval to include the publication in their thesis in lieu of a Chapter from their Supervisor and Postgraduate Coordinator.• The publication is not subject to any obligations or contractual agreements with a third party that would constrain its inclusion in the thesis.																			
<div><div><input checked="" type="checkbox"/> The candidate has declared that their thesis has publications - either published or submitted for publication - incorporated into it in lieu of a Chapter/s. Details of these publications are provided below..</div></div>																			
<div><div>Publication Details #1</div><table><tbody><tr><td>Full Title:</td><td>A Versatile 3D and 4D Printing System through Photocontrolled RAFT Polymerisation</td></tr><tr><td>Authors:</td><td>Zhang, Z.; Corrigan, N.; Bagheri, A.; Jin, J.; Boyer, C</td></tr><tr><td>Journal or Book Name:</td><td>Angewandte Chemie International Edition</td></tr><tr><td>Volume/Page Numbers:</td><td>58/17954-17963</td></tr><tr><td>Date Accepted/Published:</td><td>December 9, 2019</td></tr><tr><td>Status:</td><td>published</td></tr><tr><td>The Candidate's Contribution to the Work:</td><td>The candidate contributed greater than 50% to the work and is the primary author</td></tr><tr><td>Location of the work in the thesis and/or how the work is incorporated in the thesis:</td><td>This work is in lieu of Chapter 3 in the thesis</td></tr></tbody></table></div>				Full Title:	A Versatile 3D and 4D Printing System through Photocontrolled RAFT Polymerisation	Authors:	Zhang, Z.; Corrigan, N.; Bagheri, A.; Jin, J.; Boyer, C	Journal or Book Name:	Angewandte Chemie International Edition	Volume/Page Numbers:	58/17954-17963	Date Accepted/Published:	December 9, 2019	Status:	published	The Candidate's Contribution to the Work:	The candidate contributed greater than 50% to the work and is the primary author	Location of the work in the thesis and/or how the work is incorporated in the thesis:	This work is in lieu of Chapter 3 in the thesis
Full Title:	A Versatile 3D and 4D Printing System through Photocontrolled RAFT Polymerisation																		
Authors:	Zhang, Z.; Corrigan, N.; Bagheri, A.; Jin, J.; Boyer, C																		
Journal or Book Name:	Angewandte Chemie International Edition																		
Volume/Page Numbers:	58/17954-17963																		
Date Accepted/Published:	December 9, 2019																		
Status:	published																		
The Candidate's Contribution to the Work:	The candidate contributed greater than 50% to the work and is the primary author																		
Location of the work in the thesis and/or how the work is incorporated in the thesis:	This work is in lieu of Chapter 3 in the thesis																		

Publication Details #2

Full Title:	Effect of Thiocarbonylthio Compounds on Visible-Light-Mediated 3D Printing
Authors:	Zhang, Z.; Corrigan, N.; Boyer, C
Journal or Book Name:	Macromolecules
Volume/Page Numbers:	54/1170-1182
Date Accepted/Published:	January 29, 2021
Status:	published
The Candidate's Contribution to the Work:	The candidate contributed greater than 50% to the work and is the primary author
Location of the work in the thesis and/or how the work is incorporated in the thesis:	This work is in lieu of Chapter 4 in the thesis

Publication Details #3

Full Title:	A Photoinduced Dual-Wavelength Approach for 3D Printing and Self-Healing of Thermosetting Materials
Authors:	Zhang, Z.; Corrigan, N.; Boyer, C
Journal or Book Name:	Angewandte Chemie International Edition
Volume/Page Numbers:	61/e202114111
Date Accepted/Published:	March 7, 2022
Status:	published
The Candidate's Contribution to the Work:	The candidate contributed greater than 50% to the work and is the primary author
Location of the work in the thesis and/or how the work is incorporated in the thesis:	This work is in lieu of Chapter 5 in the thesis

Candidate's Declaration



I confirm that where I have used a publication in lieu of a chapter, the listed publication(s) above meet(s) the requirements to be included in the thesis. I also declare that I have complied with the Thesis Examination Procedure.

Acknowledgements

First and foremost, I would like to express my greatest gratitude to my supervisor, Prof. Cyrille Boyer for the invaluable mentorship and support throughout my PhD. Your guidance has been paramount in my academic development and has always encouraged me to be adventurous. Your tremendous dedication towards research and your enthusiasm in work will always motivate me for my future career development. My sincerest appreciation to my joint supervisor Dr. Nathaniel Corrigan for your kindness in sharing all your knowledge and experience to assist me patiently and earnestly in any way you could. Without your help, my research career would not have been possible.

I would also like to thank our very supportive lab manager, Mr. Eh Hau Pan for your excellent work in lab management and maintenance, keeping everything running smoothly. Also, thanks to Dr. Karen Privat from Electron Microscope Unit for your technical support and professional suggestion in my research projects.

Thanks also to all my group members and PhD friends: Ke Liu, Liwen Zhang, Chenyu Wu, Huijie Zhu, Xiaoyu Cong, Zi Wang, Xiaobing Shi, Gervase Ng, Sihao Xu, Valentin Bobrin, Kenny Lee, Erna Wulandari, Peter Judzewitsch, Tony Zhang, Zilong Wu, Ruizhe Liu, Dewen Zhou, Nicole, Fumi Ishizuka, Hyun Jin Kim, Zhiwei Li, Kenward Jung. Thank you for sharing your knowledge and providing me with sincere help for my research progress and thanks for making the office and the lab an enjoyable place.

Special thanks to my best friends outside of research, Shawn, Ashley, Ben, Caroline, Modi, Yangyang, Mark and Nick, thanks for being there to support me all the time.

Finally, I would like to show my deepest appreciation to my family members, my grandparents, my parents, my parents-in-law, my wife Cassie and my daughter Alina, my elder brother Tao and sister Hong. Thank you for your unconditional love and support throughout my journey.

Abstract

Vat photopolymerisation (VP) is a promising additive manufacturing technology which enables the construction of complex 3D objects via versatile photochemistries. VP techniques have demonstrated superior advantages in imparting spatiotemporal control and providing high build rates and high printing resolution. However, current photocuring methods are based on non-living free radical or cationic polymerisation which offer limited control over chain growth, network formation and thus the final properties of 3D printed materials. Moreover, inert polymer chains produced during the polymerisation are incapable of being reactivated for post-functionalisation of pre-formed polymers. To fabricate materials with controlled properties and post-modifiable networks, photomediated reversible addition-fragmentation chain transfer (RAFT) polymerisation techniques were employed in VP. The addition of RAFT agents in photoresins provided control over polymer chain growth and network formation. Also, the retention of thiocarbonylthio polymer chain-ends in the network imparted living characteristics to 3D printed materials, which were easily post-modified with diverse functions and properties.

This work firstly explored photoinduced electron/energy transfer-reversible addition-fragmentation chain transfer (PET-RAFT) polymerisation in 3D printing under visible light irradiation in the open air. The use of an organic dye in conjunction with a tertiary amine as co-catalyst allowed fast printing speeds. The inclusion of RAFT agents in photoresins provided control over the mechanical properties of 3D printed materials. The presence of latent RAFT agents in the resin allowed post-functionalisation of these materials. Based on this study, photoresins containing RAFT agents with different activating Z groups and leaving R groups were investigated for their application in 3D printing. Also, the impact of the concentration of trithiocarbonates on mechanical properties of 3D printed materials was demonstrated. In addition, the 3D printed materials containing RAFT agents were easily post-modified via one-pot *in situ* aminolysis and thiol-Michael additions. Finally, the inclusion of RAFT agents in 3D printed thermosets materials conferred self-healing functionality. Materials containing trithiocarbonate units that were 3D printed under visible light can perform rapid self-repair via a secondary polymerisation mechanism under UV light irradiation under open-air conditions and at room temperature. This study promisingly paves the way for the fabrication of novel 3D printed thermosets with self-healing properties.

List of Publications

Publications directly contributing to this thesis

Zhang, Z.; Corrigan, N.; Bagheri, A.; Jin, J.; Boyer, C. A Versatile 3D and 4D Printing System through Photocontrolled RAFT Polymerisation. *Angewandte Chemie International Edition* **2019**, 58(50), 17954-17963.

Zhang, Z.; Corrigan, N.; Boyer, C. Effect of Thiocarbonylthio Compounds on Visible-Light-Mediated 3D Printing. *Macromolecules* **2021**, 54(3), 1170-1182.

Zhang, Z.; Corrigan, N.; Boyer, C. A Photoinduced Dual-Wavelength Approach for 3D Printing and Self-Healing of Thermosetting Materials. *Angewandte Chemie International Edition* **2022**, 61(11), e202114111.

Other publications

Zhang, L.; Shi, X.; **Zhang, Z.**; Kuchel, R. P.; Namivandi-Zangeneh, R.; Corrigan, N.; Jung, K.; Liang, K.; Boyer, C., Porphyrinic Zirconium Metal–Organic Frameworks (MOFs) as Heterogeneous Photocatalysts for PET-RAFT Polymerization and Stereolithography. *Angewandte Chemie International Edition* **2021**, 60(10), 5489-5496.

Conference presentations

Z. Zhang. A Versatile 3D and 4D Printing System through Photocontrolled RAFT Polymerisation. *37th Australasian Polymer Symposium*, 2019. Twin Waters, QLD, Australia

Z. Zhang. Effect of Thiocarbonylthio Compounds on Visible-Light-Mediated 3D Printing. *RACI NSW Polymer Group 2-Day symposium (via Zoom)*, 2021. The University of Sydney, NSW, Australia

Table of Contents

Acknowledgements.....	i
Abstract.....	ii
List of Publications.....	iii
Table of Contents	iv
List of Figures	vii
List of Tables	xvii
List of Abbreviations and Symbols.....	xix
Chapter 1. Introduction.....	1
1.1 Thesis Motivation	2
1.2 Thesis Outline	5
1.3 References	8
Chapter 2. Literature Review	12
2.1 Reversible Deactivation Radical Polymerisation (RDRP).....	14
2.1.1 Benefits of RDRP	16
2.1.2 Reversible addition-fragmentation chain transfer polymerisation (RAFT)	19
2.2 Photomediated RAFT Polymerisation	31
2.2.1 Benefits of light verses heat	31
2.2.2 RAFT polymerisation initiated by conventional photoinitiators	39
2.2.3 RAFT polymerisation via iniferter polymerisation mechanism.....	42
2.2.4 Photoinduced electron/energy transfer (PET)-RAFT polymerisation	47
2.3 Vat Photopolymerisation 3D printing	54
2.3.1 Laser scanning stereolithography (SLA)	55
2.3.2 Mask projection stereolithography (MPSL)	59
2.3.3 Volumetric stereolithography	63
2.4 Summary	66
2.5 Reference.....	68
Chapter 3. A Versatile 3D and 4D Printing System through Photocontrolled RAFT Polymerisation	88

3.1	Introduction.....	89
3.2	Experimental Section.....	92
3.2.1	Materials.....	92
3.2.2	Instrumentation	92
3.2.3	Experimental procedure	93
3.3	Results and Discussion.....	97
3.3.1	Optimisation of resin formulations	97
3.3.2	Controlling mechanical properties of RAFT containing 3D printed materials	107
3.3.3	4D printed materials through spatially controlled aqueous photopolymerisation.....	111
3.3.4	Reactivation of trithiocarbonate groups for post-modification of 3D printed materials	113
3.4	Conclusion.....	116
3.5	Reference.....	117

Chapter 4. Effect of Thiocarbonylthio Compounds on Visible Light Mediated 3D

Printing	124
4.1 Introduction.....	125
4.2 Experimental Section	128
4.2.1 Materials.....	128
4.2.2 Instrumentation	128
4.2.3 Experimental procedure	129
4.3 Results and Discussion.....	133
4.3.1 Optimisation of resin formulations	133
4.3.2 Kinetics comparison between different RAFT agents	135
4.3.3 3D printing and mechanical properties comparison with various RAFT agents	141
4.3.4 Post-modification of 3D printed objects	149
4.4 Conclusion.....	154
4.5 Reference.....	155

Chapter 5. Effect of Thiocarbonylthio Compounds on Visible Light Mediated 3D

Printing	161
-----------------------	------------

5.1	Introduction.....	162
5.2	Experimental Section.....	165
5.2.1	Materials.....	165
5.2.2	Instrumentation	165
5.2.3	Experimental procedure	166
5.3	Results and Discussion.....	171
5.3.1	Optimisation of resin formulations	171
5.3.2	Self-healing of 3D printed materials	173
5.4	Conclusion.....	188
5.5	Reference.....	189
 Chapter 6. Concluding Remarks and Outlook.....		195
6.1	Conclusion.....	196
6.2	Future Perspectives	199

List of Figures

Figure 2.1 General mechanisms of reversible deactivation radical polymerisation.	15
Figure 2.2 Typical behaviour in RDRP systems. (A) a linear relationship between monomer conversion and number average molecular weight; (B) chain length distribution approaching a Poisson distribution and the complete shift in molecular weight upon chain extensions. Figure adapted from Ref. [12].	16
Figure 2.3 General chemical structures of four main classes of RAFT agents.	19
Figure 2.4 Mechanism of RAFT polymerisation showing the steps of initiation, reversible chain transfer/propagation (also known as pre-equilibrium), reinitiation, chain equilibration/propagation (also known as main equilibrium) and termination.	21
Figure 2.5 Zwitterionic canonical forms of xanthates and dithiocarbamates.	23
Figure 2.6 Schematic presentations of the polymer network synthesis process for conventional (top) and RAFT (bottom) polymerisations.	26
Figure 2.7 Demonstration of the modification of parent gels with the TTC units in the network in the presence of a photocatalyst (10-phenylphenothiazine, PTH) and monomers (<i>N</i> -isopropylacrylamide, NIPAAM) under blue light irradiation.	28
Figure 2.8 Proposed mechanism of self-healing process via reshuffling reaction of TTC units between network strands under UV light irradiation.	29
Figure 2.9 Processes of RAFT end-group transformation via ω -end modification approaches (R^{\bullet} = radical; [H] = hydrogen donor; M = monomer).	30
Figure 2.10 RAFT polymerisation of MA using chlorophyll a as photocatalyst in the presence (“ON”) or in the absence (“OFF”) of light.	32
Figure 2.11 Demonstration of the formation of patterned polymer brushes via SI-PET-RAFT process. (a) Schematic of spatial control via SI-PET-RAFT in the polymerisation of DMAm on a DDMAT-functionalised substrate; (b) Optical micrograph of DMAm polymer brush (light) reproduction of an original photomask (inset) on silica (dark).	33

Figure 2.12 The effect of UV light intensity on polymerisation rates.	34
Figure 2.13 Examples of chromophores used in photopolymerisation. PTH: 10-phenylpheothiazine, Ir(ppy) ₃ : tris[2-phenylpyridinato-C2,N]iridium(III), MPP: 2,4,6-tris(<i>p</i> -methoxyphenyl)pyrylium tetrafluoroborate, Pent: 6,13-bis(triisopropylsilylethynyl)pentacene, ZnTPP: 5,10,15,20-tetraphenyl-21H,23H-porphine zinc, BChl <i>a</i> : bacteriochlorophyll <i>a</i> , TPO: (2,4,6-trimethylbenzoyl)diphenylphosphine oxide, EY: eosin Y, DTC: methyl 2-((9H-carbazole-9-carbonothioyl)thio)-2-methylpropanoate, CDTA: 4-cyano-4-[(dodecylsulfanylthiocarbonyl)sulfanyl]pentanoic acid, OBN: oil blue N, AlPc: aluminium phthalocyanine.	36
Figure 2.14 Reaction route for the synthesis of graft copolymers via the selective photoactivation of two PCs, PheoA and ZnTPP, in a one-pot, two-step process.	37
Figure 2.15 Synthesis of three types of STEM-0 networks (A–C, Step 1) under green light irradiation followed by post-modification in the presence of new monomers under blue light to generate STEM-1 gels (A–C, Step 2).	38
Figure 2.16 Schematic process of RAFT photoiniferter polymerisation.	42
Figure 2.17 Temporal control over the polymerisation of NIPAAm in the presence of bis-norbornene trithiocarbonate under UV light irradiation.	44
Figure 2.18 Demonstration of the expandable network via RAFT photo-iniferter polymerisation under sunlight exposure.	46
Figure 2.19 Proposed mechanism of PET-RAFT polymerisation in the presence of photocatalyst: (A) electron transfer and (B) energy transfer mechanism. PC: photocatalyst.	47
Figure 2.20 Proposed mechanism for PET-RAFT polymerisation mediated by ZnTPP in DMSO in the presence of oxygen. ³ Σ = ground state oxygen, ¹ Δ = singlet oxygen, TTA = triplet-triplet annihilation, DMSO ₂ = dimethyl sulfone.	50

Figure 2.21 Proposed mechanisms for PET-RAFT polymerisation mediated by eosin Y in the absence (A) and presence (B) of triethylamine (TEA) and their oxygen tolerance.	51
Figure 2.22 The concept of stereolithography.	55
Figure 2.23 Different orientations of samples printed on platform (CAD representation).	56
Figure 2.24 Dentures 3D printed via SLA process in three different directions (0°, 45°, and 90°).	57
Figure 2.25 Comparison between the working principle of (a) SLA and (b) DLP 3D printers.	59
Figure 2.26 Optical images of 3D printed longhorns with corresponding resins indicated with the optimised resin composition and a slicing thickness of 100 µm.....	60
Figure 2.27 Demonstration of the working principle of CLIP 3D printer.	61
Figure 2.28 The slope feature of the open book fabricated with the same build speed of 40 mm/h but with different slicing thicknesses (100, 20 and 0.4 µm).....	62
Figure 2.29 Demonstration of CAL volumetric fabrication. (A) the concept of CAL volumetric fabrication; (B) the components of CAL system; (C) time-sequenced views of the object during a CAL print; (D) the printed object after washing away uncured resin; (E) the object from (D) painted for clarity; (F) the same geometry of (D) in larger size; (G) opaque version of the geometry in (F) by using crystal violet dye in the resin. Scale bars: 10 mm.	64
Figure 2.30 Demonstration of the volumetric bioprinting process. (A) the cell-laden gel resin container connected to a rotating platform; (B) the schematic of volumetric fabrication; (C) the final printed hydrogel-based human auricle model. Printing time = 22.7 s; scale bar = 2 mm.	65
Figure 3.1 Thiocarbonylthio containing photopolymerisation resins. (A) reaction components; (B) proposed PET-RAFT mechanism. PC: photocatalyst; NR ₃ : tertiary amine; PET: photoinduced electron transfer.	98

Figure 3.2 Kinetics of polymerisation for DMAm / PEGDA mixtures in the presence of EY or EB as PC, with varied molar ratios of BTPA as RAFT agent at a molar concentration of [DMAm] : [PEGDA] : [TEtOHA] : [PC] : [BTPA] = 1000 : 50 : 20 : 0.1 : variable. Note: All reactions were performed using a solids content of 50 wt% under green light ($\lambda_{\max} = 525$ nm and $I_0 = 4.3$ mW/cm²). 100

Figure 3.3 Kinetics of polymerisation for DMAm / PEGDA mixtures using EB or EY as catalyst and varied concentrations of BTPA and TEtOHA. (A) [EB] : [DMAm] : [PEGDA] : [BTPA] : [TEtOHA] = 0.1 : 1000 : 50 : 1 : variable; (B) [EB] : [DMAm] : [PEGDA] : [BTPA] : [TEtOHA] = 0.1 : 1000 : 50 : 0 : variable. (C) [EY] : [DMAm] : [PEGDA] : [BTPA] : [TEtOHA] = 0.1 : 1000 : 50 : 1 : variable; (D) [EY] : [DMAm] : [PEGDA] : [BTPA] : [TEtOHA] = 0.1 : 1000 : 50 : 0 : variable. Note: All reactions were performed using a solids content of 50 wt% under green light ($\lambda_{\max} = 525$ nm and $I_0 = 4.3$ mW/cm²). 101

Figure 3.4 Kinetics of polymerisation for DMAm / PEGDA mixtures with varied molar ratio of EB as PC at a fixed molar concentration of [DMAm] : [PEGDA] : [TEtOHA] : [BTPA] = 1000 : 50 : 20 : 1. Note: All reactions were performed using a solids content of 50 wt% under green light ($\lambda_{\max} = 525$ nm and $I_0 = 4.3$ mW/cm²). 103

Figure 3.5 Kinetics of polymerisation for DMAm / PEGDA mixtures using BTPA as RAFT agent at different concentrations of EB and TEtOHA and different total solids content. (A) solid content = 25%; (B) solid content = 50%; (C) solid content = 75%. Conditions: [EB] : [DMAm] : [PEGDA] : [BTPA] : [TEtOHA] = 0.01/0.025 : 1000 : 50 : 1 : 10/20. Polymerisation was performed under 4.3 mW/cm² green light ($\lambda_{\max} = 525$ nm), using a droplet (20 μ L) of reaction mixture. Vinyl bond conversion over time was quantified by ATR-FTIR spectroscopy..... 104

Figure 3.6 Kinetics of polymerisation for DMAm / PEGDA mixtures using BTPA as RAFT agent at different total solids content of DMAm and PEGDA and varied DMAm / PEGDA ratios. (A) bulk (solvent free) reaction using a ratio of [EB] : [BTPA] : [TEtOHA] = 0.01 : 1 : 20 and a constant BTPA molality of 8.96 mmol/kg; (B) solids content 50 wt% monomer and crosslinker using a ratio of [EB] : [BTPA] : [TETOHA] = 0.01 : 1 : 20 and a constant BTPA molality of 8.96 mmol/kg. *N.B.* DMAm : PEGDA ratio of 95 : 5 actually performed using a ratio of 1000 : 50 (approximately 95 :5). Conditions: Polymerisation

was performed under 4.3 mW/cm² green light ($\lambda_{\text{max}} = 525$ nm), using a droplet (20 μL) of reaction mixture. Vinyl bond conversion over time was quantified by ATR-FTIR spectroscopy..... 106

Figure 3.7 Samples 3D printed with photocontrolled RAFT polymerisation. (A) effect of changing the DMAM : PEGDA ratio on the storage modulus (E') and glass transition temperature (T_g), while holding the EB, BTPA, and TEtOHA concentrations constant; (B) effect of changing RAFT concentrations using a ratio [EB] : [DMAM] : [PEGDA] : [BTPA] : [TEtOHA] = 0.01 : 164 : 382: variable : 20 in bulk; (C) sample printed with a layer thickness of 20 μm and cure time per layer of 13 s using a recipe of [EB] : [DMAM] : [PEGDA] : [BTPA] : [TEtOHA] = 0.01 : 164 : 382 : 1 : 20; (D) Storage modulus (E') and Tan δ for sample shown in **Figure 3.7C** at a frequency of 1 Hz determined by DMA. Error bars were calculated using duplicate samples. 109

Figure 3.8 3D printed object definition using a 100 μm layer slicing thickness and various layer cure times with the resin formulation of [EB] : [DMAM] : [PEGDA] : [BTPA] : [TEtOHA] = 0.01 : 164 : 382 : 1 : 20 in bulk. (A) 13 s exposure time per layer; (B) 20 s exposure time per layer; (C) 25 s exposure time per layer; (D) 30 s exposure time per layer..... 110

Figure 3.9 Mechanical properties of 3D printed materials by using the resin formulation of [EB] : [DMAM] : [PEGDA] : [BTPA] : [TEtOHA] = 0.01 : 164 : 382 : 1 : 20 in bulk. (A) effect of layer slicing thickness and irradiation time per layer on resulting storage modulus (E') and glass transition temperature (T_g). First number on x-axis label indicates layer thickness in μm and second number indicated exposure time per layer in seconds; (B) effect of post-curing times under 4.3 mW/cm² green light ($\lambda_{\text{max}} = 525$ nm) irradiation on resulting storage modulus (E') and glass transition temperature (T_g)..... 111

Figure 3.10 Swelling and desolvation induced actuation of a material 3D printed with spatially resolved light doses. (A) designed geometrical properties of cross; (B) top view of swollen cross geometry (layer exposed to higher light dose on bottom of object); (C) cross with layer exposed to higher light dose on the bottom, after 5 mins in water; (D) flipped swollen cross before dehydration (layer exposed to higher light dose on top); (E) cross after 80 seconds of dehydration; (F) cross after 7 mins of dehydration. 113

Figure 3.11 Secondary polymerisation from 3D printed materials to change the surface properties. (A) colour change in 3D printed films via post-curing under green light irradiation. From top: 3D printed film before post-curing, after post-curing for BTPA containing resins, and after post-curing for RAFT agent-free resins; (B) absorbance spectra before and after post-curing for films 3D printed in the presence and absence of RAFT agents; (C) high surface wettability of 3D printed DMAM/PEDGA networks; (D) decreased surface wettability for BA functionalised material; (E) spatially resolved fluorescence of 3D printed materials containing RAFT agent through photoinduced surface-functionalisation in the presence of pyrene-MMA. 114

Figure 4.1 Kinetics of polymerisation for PEGA / PEGDA mixtures using BTPA as RAFT agent. (A) vinyl bond conversions *vs* time for varied molar ratios of BTPA as RAFT agent at molar concentrations of [PEGA] : [PEGDA] : [BTPA] : [EB] : [TEtOHA] = 1000 : 500 : [variable] : 0.025 : 20; (B) vinyl bond conversion *vs* time for varied TEtOHA molar ratios at molar concentrations of [PEGA] : [PEGDA] : [BTPA] : [EB] : [TEtOHA] = 1000 : 500 : 50 : 0.025 : [variable]; (C) vinyl bond conversion *vs* time for varied EB molar ratios at molar concentrations of [PEGA] : [PEGDA] : [BTPA] : [EB] : [TEtOHA] = 1000 : 500 : 50 : [variable] : 40. Note: All reactions were performed in bulk under green light ($\lambda_{\text{max}} = 525 \text{ nm}$ and $I_0 = 4.3 \text{ mW/cm}^2$). 134

Figure 4.2 Various RAFT agents used in this work composed of thiocarbonylthio group (orange), activating Z group (red) and leaving R group (blue), 2-(butylthiocarbonothioylthio) propanoic acid (**BTPA**), 4-cyano-4-[(dodecylsulfanylthiocarbonyl)sulfanyl]pentanoic acid (**CDTPA**), dibenzyl trithiocarbonate (**DBTTC**), 4-cyano-4-(phenylcarbonothioylthio) pentanoic acid (**CPADB**), methyl 2-((ethoxycarbonothioyl)thio) propanoate (**Xanthate**), cyanomethyl (3,5-dimethyl-1H-pyrazole)-carbodithioate (**DTC1**) and 2-cyanobutan-2-yl 4-chloro-3,5-dimethyl-1H-pyrazole-1-carbodithioate (**DTC2**)..... 136

Figure 4.3 Kinetics of polymerisation for PEGA / PEGDA mixtures using various RAFT agents. (A) vinyl bond conversions *vs* time for varied RAFT agents at a fixed molar concentration of [PEGA] : [PEGDA] : [RAFT] : [EB] : [TEtOHA] = 571 : 1333 : 5 : 0.2 : 40; (B) vinyl bond conversions *vs* time for varied RAFT agents at a fixed molar concentration of [PEGA] : [PEGDA] : [RAFT] : [EB] : [TEtOHA] = 571 : 1333 : 50 :

0.2 : 40. Note: All reactions were performed in bulk under green light ($\lambda_{\text{max}} = 525 \text{ nm}$ and intensity = 4.3 mW/cm^2). 138

Figure 4.4 Values of ΔH_{stab} , ΔH_{frag} and RSE of R^\bullet (kJ/mol) for RAFT agents in the present work.⁶³⁻⁶⁴ The values of ΔH_{stab} and ΔH_{frag} are associated with the effect of Z group, while the value of RSE of R^\bullet is associated with the effect of R group. The value of RSE of R^\bullet of acrylate (assumed to have the structure $\text{CH}(\text{CH}_3)(\text{CO})\text{OCH}_3$) was used as a reference for the secondary acrylic propagating radical species in the system. 139

Figure 4.5 Rectangular sample 3D printed via PET-RAFT polymerisation. (A) sample 3D printed with a layer thickness of $20 \mu\text{m}$ and cure time per layer of 20 s using a recipe of $[\text{BTPA}] : [\text{PEGA}] : [\text{PEGDA}] : [\text{EB}] : [\text{TEtOHA}] = 5 : 571 : 1333 : 0.2 : 40$; (B) storage modulus (E') and $\tan \delta$ for the sample at a frequency of 1Hz determined by DMA... 142

Figure 4.6 Schematic presentations of polymer network synthesis process: (A) highly crosslinked nanogels formation via free radical polymerisation (FRP) and the resulting heterogenous network structures; (B) RAFT polymerisation process leading to more homogeneous network structure via the formation of more highly branched polymers in the earlier stages of the polymerisation..... 145

Figure 4.7 Kinetics of polymerisation for PEGA / PEGDA mixtures using varied molar ratios of BTPA as RAFT agent at a fixed molar concentration of $[\text{PEGA}] : [\text{PEGDA}] : [\text{EB}] : [\text{TEtOHA}] = 571 : 1333 : 0.2 : 40$, performed in bulk. Note: All reactions were performed under green light ($\lambda_{\text{max}} = 525 \text{ nm}$ and intensity = 4.3 mW/cm^2). 147

Figure 4.8 3D printed theatre complex. (A) original .stl file image; (B) the theatre complex printed using the resin formulation of $[\text{PEGA}] : [\text{PEGDA}] : [\text{RAFT}] : [\text{EB}] : [\text{TEtOHA}] = 571 : 1333 : 5 : 0.2 : 40$; (C) side view of the theatre complex. 149

Figure 4.9 Aminolysis of 3D printed materials to change 3D printed material properties. (A) sample printed with a layer thickness of $20 \mu\text{m}$ and cure time per layer of 40 s using a recipe of $[\text{PEGA}] : [\text{PEGDA}] : [\text{BTPA}] : [\text{EB}] : [\text{TEtOHA}] = 571 : 1333 : 25 : 0.2 : 40$; (B) sample post-cured for 10 min under green light ($\lambda_{\text{max}} = 525 \text{ nm}$, 7.1 mW/cm^2); (C) absorbance spectra of the sample 3D printed in the presence of BTPA before and after post-curing for 10 min under green light ($\lambda_{\text{max}} = 525 \text{ nm}$, 7.1 mW/cm^2); (D) sample aminolysed for 120 min with a molar ratio of $[\text{hexylamine}] : [\text{BTPA}] = 100 : 1$ in 10 ml

DMF solution at room temperature; (E) absorbance spectra before and after aminolysis for samples 3D printed in the presence of BTPA; (F) absorbance spectra before and after aminolysis of a mixture with a molar ratio of [BTPA] : [hexylamine] = 1 : 100 in a total volume of 4 ml DMF solution at room temperature. 151

Figure 4.10 Post-modification of 3D printed objects. (A) schematic showing process of one-pot transformation of RAFT agent end groups via performing aminolysis of thiocarbonylthio groups and thiol-Michael addition to introducing fluorescent PyMMA group; (B) fluorescence images of 3D printed samples. From top to bottom: original 3D printed sample before post-curing, post-cured 3D printed sample exposed to a solution of PyMMA in DMF for 1 h, post-cured 3D printed sample exposed to a solution of PyMMA and hexylamine in DMF for 1 h; (C) fluorescence image of the post-modified 3D printed theatre complex. The object was printed using the resin formulation of [PEGA] : [PEGDA] : [BTPA] : [EB] : [TEtOHA] = 571 : 1333 : 5 : 0.2 : 40 with a layer thickness of 20 μm and cure time per layer of 40 s. 152

Figure 5.1 Kinetics of polymerisation for HEA/EGDMA mixtures using DBTTC as RAFT agent. (A) vinyl bond conversions vs time for varied [DBTTC] : [HEA] molar ratios with constant TPO molar ratio [DBTTC] : [TPO] = 1 : 0.5 and fixed molar ratio of [HEA] : [EGDMA] = 10 : 1; (B) vinyl bond conversion vs time for varied TPO molar ratios at molar concentration of [DBTTC] : [HEA] : [EGDMA] : [TPO] = 1 : 60 : 6 : [variable]; (C) vinyl bond conversion vs time for varied [HEA] : [EGDMA] molar ratios at a ratio of [DBTTC] : [TPO] = 1 : 0.5, the recipes were design to maintain fixed molar concentrations of DBTTC and TPO. As such, the molar ratios used in these experiments were [DBTTC] : [HEA] : [EGDMA] : [TPO] = 1 : 60 : 6 : 0.5 ([HEA] : [EGDMA] = 60 : 6), [DBTTC] : [HEA] : [EGDMA] : [TPO] = 1 : 63.2 : 4.2 : 0.5 (approximately [HEA] : [EGDMA] = 60 : 4), and [DBTTC] : [HEA] : [EGDMA] : [TPO] = 1 : 64.9 : 3.2 : 0.5 (approximately [HEA] : [EGDMA] = 60 : 3). Note: All reactions were performed under violet light ($\lambda_{\text{max}} = 405 \text{ nm}$ and $I_0 = 3.6 \text{ mW/cm}$). 173

Figure 5.2 Dumbbell-shaped samples 3D printed using a resin formulation of [DBTTC] : [HEA] : [EGDMA] : [TPO] = 1 : 60 : 4 : 0.5 at a layer slicing thickness of 50 μm . (A) Dumbbell-shaped samples printed using a single layer cure time of 80 s/layer and (B) a single layer cure time of 60 s/layer. 174

Figure 5.3 Self-healing process of 3D printed samples. (A) demonstration of the self-healing process on a dumbbell shaped object 3D printed using a resin formulation of [DBTTC] : [HEA] : [EGDMA] : [TPO] = 1 : 60 : 4 : 0.5; SEM images of (B) the top surface of the healed sample, (C) cross-sectional view of the healed sample, and (D) the magnified cross-sectional view of the healed sample showing disappearance of interfacial region after healing process.	176
Figure 5.4 Storage modulus (E') and Tan δ for samples 3D printed with different resin formulations at a frequency of 1 Hz measured by DMA. (A) sample printed with the resin containing [DBTTC] : [HEA] : [EGDMA] : [TPO] = 1 : 60 : 4 : 0.5 at a cure time per layer of 80 s; (B) sample printed with the resin containing [DBTTC] : [HEA] : [EGDMA] : [TPO] = 0 : 60 : 4 : 0.5 at a cure time per layer of 20 s.	176
Figure 5.5 Stress-strain curves of the original sample and healed samples at various healing time. The dumbbell-shaped sample 3D printed by using the resin formulation of [DBTTC] : [HEA] : [EGDMA] : [TPO] = 1 : 60 : 4 : 0.5 at a layer slicing thickness of 50 μ m and a single layer cure time of 80 s/layer.	179
Figure 5.6 Healing efficiency of samples 3D printed with the resin of [DBTTC] : [HEA] : [EGDMA] : [TPO] = 1 : 60 : 4 : 0.5 at various healing time. (A) tensile strength recovery, and (B) elongation at break recovery of samples after irradiation under UV light at room temperature over time.	179
Figure 5.7 Storage modulus (E') and Tan δ for sample 3D printed with the resin containing [DBTTC] : [AA] : [HEA] : [EGDMA] : [TPO] = 1 : 6 : 54 : 4 : 0.5 at a cure time per layer of 100 s at a frequency of 1 Hz measured by DMA.	180
Figure 5.8 Kinetics of polymerisation with varied DBTTC concentration at fixed molar concentration of [HEA] : [EGDMA] : [TPO] = 60 : 4 : 0.5.	182
Figure 5.9 Mechanical property recovery vs time for 3D printed samples. (A) tensile strength recovery, and (B) elongation at break recovery for samples 3D printed using varied concentrations of DBTTC in the resin at a fixed molar ratio of [HEA] : [EGDMA] : [TPO] = 60 : 4 : 0.5. Self-healing was performed under UV light irradiation at room temperature with PEGDA at the material interface.	183

Figure 5.10 Kinetics of polymerization with different RAFT agents at fixed molar ratio of [RAFT] : [HEA] : [EGDMA] : [TPO] = 1 : 60 : 4 : 0.5.	184
Figure 5.11 Mechanical property recovery vs time for 3D printed samples. (A) tensile strength recovery, and (B) elongation at break recovery for samples 3D printed with varied RAFT agents in the resin at a fixed molar ratio of [RAFT] : [HEA] : [EGDMA] : [TPO] = 1 : 60 : 4 : 0.5. Self-healing was performed under UV light irradiation at room temperature with PEGDA at the material interface.	186
Figure 5.12 Photoinduced self-healing of geometrically complex objects 3D printed via photo-RDRP. Top: 200 g weightlifting test on a hook before and after self-healing. Hook was 3D printed using the resin formulation [DBTTC] : [HEA] : [EGDMA] : [TPO] = 1 : 60 : 4 : 0.5 and was self-healed under 365 nm irradiation for 60 min in air at room temperature. Bottom: model violin 3D printed using the resin formulation [DBTTC] : [HEA] : [EGDMA] : [TPO] = 0.25 : 60 : 4 : 0.5 self-healed under 365 nm irradiation for 60 min in air at room temperature.	187

List of Tables

Table 2.1 Guidelines for selection of the Z group and R group of RAFT agents for polymerisation of different monomers.....	24
Table 2.2 Examples of photocatalysts used in PET-RAFT polymerisations.	52
Table 3.1 Effect of changing catalyst and concentrations of TEtOHA and BTPA on the polymerisation kinetics of DMAM / PEGDA mixtures performed in 50 wt% solutions of water.....	102
Table 3.2 Effect of changing catalyst and TEtOHA molar ratios, and the solids content of monomer and crosslinker on the polymerization kinetics of DMAM / PEGDA mixtures.	105
Table 3.3 Effect of changing monomer and crosslinker molar ratios in an aqueous system (50 wt%) and in the absence of solvent (bulk) on the polymerisation kinetics of DMAM / PEGDA mixtures.	107
Table 4.1 Kinetics of polymerisation for PEGA / PEGDA mixtures using various RAFT agents.	137
Table 4.2 The mechanical properties of samples 3D printed with various RAFT agents.	143
Table 4.3 Mechanical properties of 3D printed samples containing BTPA and Xanthate.	144
Table 4.4 The mechanical properties of samples 3D printed with varied concentrations of BTPA.	148
Table 5.1 Mechanical properties of samples 3D printed with the resin of [DBTTC] : [HEA] : [EGDMA] : [TPO] = 1 : 60 : 4 : 0.5 self-healing at various healing time.	178
Table 5.2 Mechanical properties of samples 3D printed with the resin containing varied molar ratio of [AA] : [HEA] at a fixed molar ratio of [DBTTC] : [EGDMA] : [AA+HEA] : [TPO] = 1 : 4 : 60 : 0.5 self-healing under 365 nm irradiation for 60 min.	181

Table 5.3 Mechanical properties of original samples 3D printed with various concentrations of DBTTC in the resin at a fixed molar ratio of [HEA] : [EGDMA] : [TPO] = 60 : 4 : 0.5.	182
Table 5.4 Mechanical properties of samples 3D printed with the resin of [DBTTC] : [HEA] : [EGDMA] : [TPO] = 0.5 : 60 : 4 : 0.5 self-healing at various healing time. ..	183
Table 5.5 Mechanical properties of samples 3D printed with the resin of [DBTTC] : [HEA] : [EGDMA] : [TPO] = 0.25 : 60 : 4 : 0.5 self-healing at various healing time.	184
Table 5.6 Mechanical properties of samples 3D printed with the resin of [BSTP] : [HEA] : [EGDMA] : [TPO] = 1 : 60 : 4 : 0.5 self-healing at various healing time	185

List of Abbreviations and Symbols

Abbreviations

AA	acrylic acid
AlPc	aluminium phthalocyanine
AM	acrylamide
AN	acrylonitrile
ASTM	American Society for Testing and Materials
ATR-FTIR	Attenuated total reflectance-fourier-transform infrared
ATRP	Atom transfer radical polymerisation
BA	butyl acrylate
BChl <i>a</i>	bacteriochlorophyll <i>a</i>
bisPEMAT	bis[(2-propionate)ethyl methacrylate] trithiocarbonate
BSTP	3-(((benzylthio)carbonothioylthio)propionic acid
BTPA	2-(butylthiocarbonothioylthio) propanoic acid
BTPEMA	(2-(2-(n-butyltrithiocarbonate)-propionate)ethyl methacrylate
BzMIm	benzyl maleimide
CAD	Computer-assisted designs
CAL	Computed axial lithography
CDB	cumyl dithiobenzoate
CDTPA	4-cyano-4-[(dodecylsulfanylthiocarbonyl)sulfanyl]pentanoic acid
CLIP	continuous liquid interface production
CPADB	4-cyano-4-(phenylcarbonothioylthio) pentanoic acid
CPD	2-cyanopropan-2-yl benzodithioate
CPFDB	2-cyanoprop-2-yl(4-fluoro)dithiobenzoate
DAAm	diacetone acrylamide
DBTTC	dibenzyl trithiocarbonate
DDMAT	<i>S</i> -1-dodecyl- <i>S</i> '-(α,α' -dimethyl- α'' -acetic acid) trithiocarbonate
DLP	Digital light processing
DMA	Dynamic mechanical analysis
DMAm	<i>N,N</i> -dimethylacrylamide
DMF	dimethylformamide
DMSO	dimethyl sulfoxide
DMSO ₂	dimethyl sulfone
DP	degree of polymerisation
DTC	methyl 2-((9H-carbazole-9-carbonothioylthio)-2-methylpropanoate
DTC1	cyanomethyl (3,5-dimethyl-1H-pyrazole)-carbodithioate

DTC2	2-cyanobutan-2-yl 4-chloro-3,5-dimethyl-1H-pyrazole-1-carbodithioate
DTPA	2-((dodecylthio)carbonylthio)thio)propanoic acid
DTRP	Degenerative transfer radical polymerisation
EB	erythrosin B
EGDMA	ethylene glycol dimethacrylate
equiv.	equivalent
EY	eosin Y
FRP	Free radical polymerisation
FTNIR	Fourier Transform Near-Infrared
g-C ₃ N ₄	graphitic carbon nitride
GMA	glycidyl methacrylate
HEA	2-hydroxyethyl acrylate
Ir(ppy) ₃	tris[2-phenylpyridinato-C2,N]iridium(III)
LAMs	Less activated monomers
LCD	Liquid crystal display
LED	Light emitting diode
MA	methyl acrylate
MADIX	Macromolecular design via the interchange of xanthates
MAM	methacrylamide
MAMs	More activated monomers
MMA	methyl methacrylate
MPP	2,4,6-tris(p-methoxyphenyl)pyrylium tetrafluoroborate
MPSL	Mask projection stereolithography
NIPAAM	<i>N</i> -isopropylacrylamide
NIR	Near-infrared
NMP	Nitroxide-mediated polymerisation
NMR	Nuclear magnetic resonance
NVP	<i>N</i> -vinylpyrrolidone
OBN	oil blue N
P	poly (prefix)
PB	phloxine B
PC	photoredox catalyst
PEGA	poly(ethylene glycol) methyl ether acrylate
PEGDA	poly(ethylene glycol) diacrylate
Pent	6,13-bis(triisopropylsilylethynyl)pentacene
PET-RAFT	Photoinduced electron/energy transfer -reversible addition-fragmentation chain transfer polymerisation
PheoA	pheophorbide <i>a</i>
PISA	Visible light initiated polymerisation-induced self-assembly
PTH	10-phenylphenothiazine
Pyrene-MMA	1-pyrenemethyl methacrylate
RAFT	Reversible addition fragmentation chain transfer polymerisation

RB	rose bengal
RDRP	Reversible-deactivation radical polymerisation
$\text{Ru}(\text{bpy})_3\text{Cl}_2$	tris(bipyridine) ruthenium(II) chloride
SEM	Scanning electron microscopy
SI-PET-RAFT	Surface-initiated (SI) PET-RAFT
SLA	Stereolithography
SPTP	sodium phenyl-2,4,6-trimethylbenzoylphosphinate
SRMP	Stable radical-mediated polymerisation
St	styrene
STEM	Structurally tailored and engineered macromolecular
STL	Standard tessellation language
TEA	triethylamine
TEtOHA	triethanolamine
TPO	(2,4,6-trimethylbenzoyl)diphenylphosphine oxide
TTA	Triplet-triplet annihilation
TTC	trithiocarbonate
UHMW	Ultrahigh molecular weight
UV	Ultraviolet
UV-Vis	Ultraviolet-visible
VAc	vinyl acetate
VP	Vat photopolymerisation
Xanthate	methyl 2-((ethoxycarbonothioyl)thio) propanoate
ZnTPP	5,10,15,20-tetraphenyl-21H,23H-porphine zinc
3D	Three dimensional

Symbols

X	dormant group
P_x^\bullet	propagating radical
R^\bullet	carbon-centered radical
A^{m}	transition metal complex
C_{tr}	RAFT equilibrium transfer coefficient
$C_{\text{-tr}}$	RAFT equilibrium transfer coefficient
k_{tr}	RAFT equilibrium rate constant
$k_{\text{-tr}}$	RAFT equilibrium rate constant
k_{b}	RAFT equilibrium rate constant
$k_{\text{-b}}$	RAFT equilibrium rate constant
k_{add}	RAFT equilibrium rate constant
$k_{\text{-add}}$	RAFT equilibrium rate constant
ϕ	RAFT equilibrium partition coefficient

k_p	propagation rate constant
M	monomer
$[H]$	hydrogen donor
λ_{\max}	wavelength of maximum absorbance
λ	wavelength
M_n	number average molecular weight
\bar{D}	dispersity
T_g	glass transition temperature
E'	storage modulus
$^{\circ}C$	degree Celsius
$^{\circ}$	degree
Hz	hertz
MPa	megapascal
KPa	kilopascal
l	length
w	width
t	thickness
mW	milliwatt
$^3\Sigma$	triplet (ground state) oxygen
$^1\Delta$	singlet oxygen
I_0	Intensity
Φ	quantum yield
wt%	weight ratio
vol%	volume ratio
J	Joule
*	electronically excited state
α	vinyl bond conversion
ΔH_{stab}	RAFT agent stability
ΔH_{frag}	RAFT agent fragmentation efficiency
RSE	radical stabilisation energies
Tan δ	damping coefficient

Chapter 1. Introduction

1.1 Thesis Motivation

Polymers are an important class of engineering materials that have been mass produced since their discovery over a century ago, from low cost commodity polymers (such as, polyethylene, polypropylene, polystyrene, or polyvinyl chloride) to high cost engineered polymers (such as, polycarbonate, polyimide, nylon 6 or polyetheretherketone).¹⁻² The exceedingly diverse physical and chemical properties of these polymers allows their application in packaging, clothing, building construction, aircraft and automotive industry, and many others.³ Despite these polymeric materials being mature, driven by the high demand for products with improved quality and performance and advanced functionalities, the evolution of synthetic methods in polymer chemistry is of critical significance.

Recently, reversible-deactivation radical polymerisation (RDRP) techniques, such as nitroxide-mediated polymerisation (NMP),⁴⁻⁵ atom transfer radical polymerisation (ATRP),⁶⁻⁷ reversible addition fragmentation chain transfer polymerisation (RAFT),⁸⁻¹² have drawn large attention, mainly attributed to the ability to provide good control over macromolecular syntheses. Unlike free radical polymerisation which invariably leads to broad polymer chain length distributions and dead polymer chains, RDRP significantly suppresses termination of growing polymer chains by establishing a dormant-active equilibrium; the rapid reversible activation and deactivation dynamic equilibrium allows all active polymer chains to grow simultaneously and imparts living characteristics to the polymerisation.¹³⁻¹⁵ As a result, polymers with tailored molecular weight distributions and well-defined structures can be produced, obtaining superior physical and chemical properties ready for future applications.

Among various RDRP techniques, RAFT polymerisation is extensively employed due to its remarkable advantages in polymer syntheses.¹⁶⁻²⁰ First, a wide selection of RAFT agents with different leaving R groups and activating Z groups dramatically improve the effectiveness of RAFT polymerisation toward a broad scope of monomers, including the “more activated” monomers (MAMs) (such as methyl acrylate (MA) or acrylamide (AM)) and the “less activated” monomers (LAMs) (such as vinyl acetate (VAc) or *N*-vinylpyrrolidone (NVP)).^{9, 21-22} Moreover, RAFT polymerisation can proceed in a variety of reaction media and exhibits a high tolerance to a broad range of reaction temperatures

and high reaction pressures.^{11, 23-29} More importantly, RAFT crosslinking polymerisation provides great benefits in preparing homogeneous networks and the retention of the dormant thiocarbonylthio polymer chain-ends throughout the RAFT polymerisation can be reactivated to enable post-functionalisation of the pre-formed polymers with diverse properties and functionalities under external stimuli.³⁰⁻³⁴ These attributes significantly increase the versatility and applicability of RAFT polymerisation in many applications, such as drug delivery, electronics, or biosensors.³⁵⁻³⁹

With the increasing demand for a cost-effective and environmentally friendly manufacture of polymer materials, the techniques of using light as the energy source to mediate RAFT polymerisation has emerged as a powerful tool.⁴⁰⁻⁴² To compare with thermally induced RAFT polymerisation, light mediated processes can proceed at ambient temperature and have more advantages in providing spatiotemporal control.⁴³⁻⁴⁶ Further, polymerisation rates can be simply and instantaneously controlled via the change of light intensity or wavelength.⁴⁷⁻⁴⁸ More significantly, various oxygen tolerant strategies enable photomediated RAFT polymerisation to be conducted in the open air, which significantly simplifies reaction procedures by eliminating deoxygenation process.⁴⁹⁻⁵² In spite of these benefits, the application of photomediated RAFT polymerisation techniques is still underexplored.

Concurrently with the advancement of RDRP, 3D printing technology has developed rapidly in the past few decades, causing immeasurable influence on materials science. In comparison with traditional manufacturing which requires complicated processing procedures, such as forging or machining, 3D printing adopts a layer-by-layer model generation principle, allowing faster fabrication of customised materials with complex geometries and functions tailored for various applications.⁵³⁻⁵⁴ Among the most common 3D printing technologies, such as directed energy deposition, binder jetting or material extrusion, vat photopolymerisation (VP) has garnered great attention in polymer science due to the application of versatile photochemistry which enables the production of materials with diverse physical and chemical properties via photoinduced polymerisation.⁵⁵⁻⁵⁶ Furthermore, VP techniques, such as stereolithography (SLA), digital light processing (DLP) or volumetric stereolithography, are superior in providing fast printing speed and high printing resolution.⁵⁷⁻⁶¹ The photoresins used in VP typically consist of multifunctional (meth)acrylate- or epoxide-based monomers and oligomers and

photoinitiating species; under light irradiation at a specific area, the liquid photoresin can be converted into solid materials within seconds.^{56, 62}

However, current photopolymerisation based 3D printing techniques remain a great challenge in fabricating materials with the ability to be transformed or reprocessed after printing, such as stimuli-responsiveness or self-healing. This is mainly because these techniques currently adopt conventional photocuring mechanism which is primarily reliant on non-living free radical or cationic polymerisation, offering limited control over chain growth and producing irreversible crosslinked networks incapable of reactivation for further chain extension.⁶³⁻⁶⁴ Such photocuring method critically prevents post-functionalisation of 3D printed materials, and finally leads to the generation of a vast majority of undegradable or unrecyclable wastes.

In this regard, the application of photomediated RAFT polymerisation in VP is promising for several reasons. First of all, RAFT polymerisation controls polymer chain growth and network formation, thus allowing the tuning of final properties of crosslinked polymers. Moreover, the dormant thiocarbonylthio species in the network can be repeatedly activated by external stimuli to post-modify the pre-formed networks. More importantly, the high oxygen tolerance and multiple photoinitiating system choices makes photomediated RAFT polymerisation more practical and robust in 3D printing environment. Therefore, this thesis aims to apply photomediated RAFT polymerisation techniques in VP to impart living characteristics to 3D printing and fabricate novel and functional materials.

1.2 Thesis Outline

As outlined above, photomediated RAFT polymerisation has been extensively employed in many applications but underexplored in 3D printing; VP techniques have developed rapidly but fabricate materials incapable of post-functionalisation. As such, it is expected that the application of photomediated RAFT polymerisation in VP will facilitate the fabrication of 3D printed materials with controlled properties and impart living characteristics to these materials.

Therefore, **Chapter 2** starts with the introduction of RDRP and its advantages in polymeric materials syntheses, followed by a comprehensive review of RAFT polymerisation mechanisms with RAFT crosslinking polymerisation and RAFT end-group functionalisation highlighted. The majority of **Chapter 2** is focused on the review of photomediated RAFT polymerisation, including the illustration of the benefits of using light to initiate RAFT polymerisation and three different photomediated RAFT polymerisation mechanisms, RAFT polymerisation initiated by conventional photoinitiators, RAFT polymerisation via iniferter polymerisation and photoinduced electron/energy transfer (PET)-RAFT polymerisation. Finally, some major VP 3D printing techniques, including laser scanning stereolithography, mask projection stereolithography and volumetric stereolithography, and their applications, are reviewed.

In **Chapter 3**, a rapid visible light mediated PET-RAFT polymerisation process was applied to a 3D printing system. The photoresins contained a metal-free dye (erythrosin B) in conjunction with a tertiary amine co-catalyst and a trithiocarbonate RAFT agent to afford polymerisation without prior deoxygenation. The reaction components are non-toxic, metal free and environmentally friendly (water based photoresin), which tailors these systems toward the fabrication of biomaterials. Following optimisation of the resin formulation by varying the ratio of photocatalyst and tertiary amine, a variety of 3D printing conditions were investigated to prepare functional materials using green light. Furthermore, the mechanical properties of these 3D printed materials were tested under different conditions. Interestingly, the concentration of trithiocarbonate impacts the mechanical properties and the performance of these materials. Remarkably, the use of a photoinduced polymerisation process provided facile spatial control over the network structure by varying the light dose to each layer of the 3D printed material; using this

strategy, a 4D printing process was demonstrated via 3D printing and subsequent swelling and dehydration induced actuation. Furthermore, the trithiocarbonate species incorporated in the polymer networks were able to be reactivated after the initial 3D printing process, which enabled post-functionalisation of the printed materials via secondary photopolymerisation processes. This RAFT-mediated 3D and 4D printing process should provide access to a range of new functional and stimuli-responsive materials. This chapter is based on the published work: Zhang et.al., A Versatile 3D and 4D Printing System through Photocontrolled RAFT Polymerisation. *Angewandte Chemie International Edition* **2019**, 58, 17954-17963.

In the previous chapter, visible light-induced PET-RAFT polymerisation by using trithiocarbonate as RAFT agent was successfully applied in 3D printing. However, there is a lack of understanding of the impacts of RAFT agents with different structures on 3D printing process. Therefore, in **Chapter 4**, RAFT agents with different activating Z groups and leaving R groups were incorporated in resin formulations and applied to open-air 3D printing systems under green light irradiation. The Z and R groups of RAFT agents influenced the polymerisation kinetics and 3D printing process (cure time) and affected the mechanical properties of 3D printed materials. The impacts of the concentration of trithiocarbonate on mechanical properties were also investigated. The 3D printed materials containing RAFT agents were easily post-modified after printing via one-pot *in situ* aminolysis and thiol-Michael additions. The RAFT mediated photoinduced polymerisation appears a promising method for producing novel and functional materials. This chapter is based on the published work: Zhang et.al., Effect of Thiocarbonylthio Compounds on Visible-Light-Mediated 3D Printing. *Macromolecules* **2021**, 54, 1170-1182.

VP-based 3D printing techniques have been widely used to produce high-resolution 3D thermosetting materials. However, the lack of repairability of these thermosets leads to the production of waste. Consideration of the incorporation of RAFT agents in the network can be reactivated to enable a secondary polymerisation process, in **Chapter 5**, RAFT agents were added to resin formulations to allow visible light mediated 3D printing of materials with self-healing capabilities. The self-healing process was based on the reactivation of RAFT agent embedded in the thermosets under UV light, which enabled reformation of the polymeric network. The self-healing process can be performed at room

temperature without prior deoxygenation. The impact of the type and concentration of RAFT agents in the polymer network on the healing efficiency was explored. Resins containing RAFT agents enable 3D printing of thermosets with self-healing properties, broadening the scope of future applications for polymeric thermosets in various fields. This chapter is based on the published work: Zhang et.al., A Photoinduced Dual-Wavelength Approach for 3D Printing and Self-Healing of Thermosetting Materials. *Angewandte Chemie International Edition* **2022**, 61, e202114111.

Finally, **Chapter 6** briefly summarises the main outcomes of this thesis and outlines some future perspectives for photomediated RAFT polymerisation in VP.

1.3 References

1. Feldman, D., Polymer History. *Designed Monomers and Polymers* **2008**, *11*(1), 1-15.
2. Cheremisinoff, P., *Handbook of engineering polymeric materials*. CRC Press: 1997.
3. Brazel, C. S.; Rosen, S. L., *Fundamental principles of polymeric materials*. John Wiley & Sons: 2012.
4. Hawker, C. J.; Bosman, A. W.; Harth, E., New polymer synthesis by nitroxide mediated living radical polymerizations. *Chemical Reviews* **2001**, *101*(12), 3661-88.
5. Moad, G.; Rizzardo, E., Chapter 1 The History of Nitroxide-mediated Polymerization. In *Nitroxide Mediated Polymerization: From Fundamentals to Applications in Materials Science*, The Royal Society of Chemistry: 2016; pp 1-44.
6. Matyjaszewski, K., Atom Transfer Radical Polymerization (ATRP): Current Status and Future Perspectives. *Macromolecules* **2012**, *45*(10), 4015-4039.
7. Matyjaszewski, K.; Tsarevsky, N. V., Macromolecular Engineering by Atom Transfer Radical Polymerization. *Journal of the American Chemical Society* **2014**, *136*(18), 6513-6533.
8. Hill, M. R.; Carmean, R. N.; Sumerlin, B. S., Expanding the scope of RAFT polymerization: recent advances and new horizons. *Macromolecules* **2015**, *48*(16), 5459-5469.
9. Moad, G.; Rizzardo, E.; Thang, S. H., Living Radical Polymerization by the RAFT Process – A Third Update. *Australian journal of chemistry* **2012**, *65*(8), 985-1076.
10. Perrier, S.; Takolpuckdee, P., Macromolecular design via reversible addition–fragmentation chain transfer (RAFT)/xanthates (MADIX) polymerization. *Journal of Polymer Science Part A: Polymer Chemistry* **2005**, *43*(22), 5347-5393.
11. Moad, G.; Rizzardo, E.; Thang, S. H., Radical addition–fragmentation chemistry in polymer synthesis. *Polymer* **2008**, *49*(5), 1079-1131.
12. Rizzardo, E.; Chiefari, J.; Mayadunne, R. T. A.; Moad, G.; Thang, S. H., Synthesis of Defined Polymers by Reversible Addition—Fragmentation Chain Transfer: The RAFT Process. In *Controlled/Living Radical Polymerization*, American Chemical Society: 2000; pp 278-296.
13. Braunecker, W. A.; Matyjaszewski, K., Controlled/living radical polymerization: Features, developments, and perspectives. *Progress in Polymer Science* **2007**, *32*(1), 93-146.
14. Shipp, D. A., Reversible-Deactivation Radical Polymerizations. *Polymer Reviews* **2011**, *51*(2), 99-103.
15. Matyjaszewski, K.; Müller, A. H. E., *Controlled and Living Polymerizations: From Mechanisms to Applications*. John Wiley & Sons: 2009.
16. Moad, G.; Rizzardo, E.; Thang, S. H., Living Radical Polymerization by the RAFT Process. *Australian journal of chemistry* **2005**, *58*(6), 379-410.
17. Moad, G.; Rizzardo, E.; Thang, S. H., Living Radical Polymerization by the RAFT Process A First Update. *Australian journal of chemistry* **2006**, *59*(10), 669-692.
18. Moad, G.; Rizzardo, E.; Thang, S. H., Living Radical Polymerization by the RAFT Process A Second Update. *Australian journal of chemistry* **2009**, *62*(11), 1402-1472.
19. Moad, G.; Rizzardo, E.; Thang, S. H., Toward Living Radical Polymerization. *Accounts of Chemical Research* **2008**, *41*(9), 1133-1142.
20. Rizzardo, E.; Chen, M.; Chong, B.; Moad, G.; Skidmore, M.; Thang, S. H., RAFT Polymerization: Adding to the Picture. *Macromolecular Symposia* **2007**, *248*(1), 104-116.

21. Keddie, D. J.; Moad, G.; Rizzardo, E.; Thang, S. H., RAFT Agent Design and Synthesis. *Macromolecules* **2012**, *45*(13), 5321-5342.
22. Barner-Kowollik, C., *Handbook of RAFT polymerization*. John Wiley & Sons: 2008.
23. Arita, T.; Buback, M.; Janssen, O.; Vana, P., RAFT-Polymerization of Styrene up to High Pressure: Rate Enhancement and Improved Control. *Macromolecular Rapid Communications* **2004**, *25*(15), 1376-1381.
24. Rzaev, J.; Penelle, J., HP-RAFT: A Free-Radical Polymerization Technique for Obtaining Living Polymers of Ultrahigh Molecular Weights. *Angewandte Chemie International Edition* **2004**, *43*(13), 1691-1694.
25. Monteiro, M. J.; Bussels, R.; Beuermann, S.; Buback, M., High Pressure 'Living' Free-Radical Polymerization of Styrene in the Presence of RAFT. *Australian journal of chemistry* **2002**, *55*(7), 433-437.
26. Arita, T.; Buback, M.; Vana, P., Cumyl Dithiobenzoate Mediated RAFT Polymerization of Styrene at High Temperatures. *Macromolecules* **2005**, *38*(19), 7935-7943.
27. Xu, J.; He, J.; Fan, D.; Tang, W.; Yang, Y., Thermal Decomposition of Dithioesters and Its Effect on RAFT Polymerization. *Macromolecules* **2006**, *39*(11), 3753-3759.
28. Martin, L.; Gody, G.; Perrier, S., Preparation of complex multiblock copolymers via aqueous RAFT polymerization at room temperature. *Polymer Chemistry* **2015**, *6*(27), 4875-4886.
29. Chiefari, J.; Chong, Y.; Ercole, F.; Krstina, J.; Jeffery, J.; Le, T. P.; Mayadunne, R. T.; Meijs, G. F.; Moad, C. L.; Moad, G., Living free-radical polymerization by reversible addition-fragmentation chain transfer: the RAFT process. *Macromolecules* **1998**, *31*(16), 5559-5562.
30. Yu, Q.; Zhu, Y.; Ding, Y.; Zhu, S., Reaction behavior and network development in RAFT radical polymerization of dimethacrylates. *Macromolecular Chemistry and Physics* **2008**, *209*(5), 551-556.
31. Roy, S. G.; Haldar, U.; De, P., Remarkable swelling capability of amino acid based cross-linked polymer networks in organic and aqueous medium. *ACS Applied Materials & Interfaces* **2014**, *6*(6), 4233-4241.
32. Chen, M.; Gu, Y.; Singh, A.; Zhong, M.; Jordan, A. M.; Biswas, S.; Korley, L. T.; Balazs, A. C.; Johnson, J. A., Living Additive Manufacturing: Transformation of Parent Gels into Diversely Functionalized Daughter Gels Made Possible by Visible Light Photoredox Catalysis. *ACS Central Science* **2017**, *3*(2), 124-134.
33. Shanmugam, S.; Cuthbert, J.; Flum, J.; Fantin, M.; Boyer, C.; Kowalewski, T.; Matyjaszewski, K., Transformation of gels via catalyst-free selective RAFT photoactivation. *Polymer Chemistry* **2019**, *10*(19), 2477-2483.
34. Amamoto, Y.; Kamada, J.; Otsuka, H.; Takahara, A.; Matyjaszewski, K., Repeatable photoinduced self-healing of covalently cross-linked polymers through reshuffling of trithiocarbonate units. *Angewandte Chemie International Edition* **2011**, *50*(7), 1660-1663.
35. Moad, G.; Chen, M.; Häussler, M.; Postma, A.; Rizzardo, E.; Thang, S. H., Functional polymers for optoelectronic applications by RAFT polymerization. *Polymer Chemistry* **2011**, *2*(3), 492-519.
36. Williams, P. E.; Moughton, A. O.; Patterson, J. P.; Khodabakhsh, S.; O'Reilly, R. K., Exploring RAFT polymerization for the synthesis of bipolar diblock copolymers and their supramolecular self-assembly. *Polymer Chemistry* **2011**, *2*(3), 720-729.

37. Boyer, C.; Bulmus, V.; Davis, T. P.; Ladmiral, V.; Liu, J.; Perrier, S., Bioapplications of RAFT Polymerization. *Chemical Reviews* **2009**, *109*(11), 5402-5436.
38. Smith, D.; Holley, A. C.; McCormick, C. L., RAFT-synthesized copolymers and conjugates designed for therapeutic delivery of siRNA. *Polymer Chemistry* **2011**, *2*(7), 1428-1441.
39. Moad, G.; Rizzardo, E.; Thang, S. H., RAFT Polymerization and Some of its Applications. *Chemistry – An Asian Journal* **2013**, *8*(8), 1634-1644.
40. Li, S.; Han, G.; Zhang, W., Photoregulated reversible addition–fragmentation chain transfer (RAFT) polymerization. *Polymer Chemistry* **2020**, *11*(11), 1830-1844.
41. Chen, M.; Zhong, M.; Johnson, J. A., Light-Controlled Radical Polymerization: Mechanisms, Methods, and Applications. *Chemical Reviews* **2016**, *116*(17), 10167-10211.
42. Dadashi-Silab, S.; Doran, S.; Yagci, Y., Photoinduced Electron Transfer Reactions for Macromolecular Syntheses. *Chemical Reviews* **2016**, *116*(17), 10212-75.
43. Shanmugam, S.; Xu, J.; Boyer, C., Utilizing the electron transfer mechanism of chlorophyll a under light for controlled radical polymerization. *Chemical Science* **2015**, *6*(2), 1341-1349.
44. Li, M.; Fromel, M.; Ranaweera, D.; Rocha, S.; Boyer, C.; Pester, C. W., SI-PET-RAFT: Surface-Initiated Photoinduced Electron Transfer-Reversible Addition–Fragmentation Chain Transfer Polymerization. *ACS Macro Letters* **2019**, *8*(4), 374-380.
45. Xu, J.; Shanmugam, S.; Fu, C.; Aguey-Zinsou, K. F.; Boyer, C., Selective Photoactivation: From a Single Unit Monomer Insertion Reaction to Controlled Polymer Architectures. *Journal of the American Chemical Society* **2016**, *138*(9), 3094-106.
46. Zhang, L.; Wu, C.; Jung, K.; Ng, Y. H.; Boyer, C., An Oxygen Paradox: Catalytic Use of Oxygen in Radical Photopolymerization. *Angewandte Chemie International Edition* **2019**, *58*(47), 16811-16814.
47. Wang, H.; Li, Q.; Dai, J.; Du, F.; Zheng, H.; Bai, R., Real-Time and in Situ Investigation of “Living”/Controlled Photopolymerization in the Presence of a Trithiocarbonate. *Macromolecules* **2013**, *46*(7), 2576-2582.
48. Shanmugam, S.; Xu, J.; Boyer, C., Exploiting Metalloporphyrins for Selective Living Radical Polymerization Tunable over Visible Wavelengths. *Journal of the American Chemical Society* **2015**, *137*(28), 9174-9185.
49. Xu, J.; Jung, K.; Atme, A.; Shanmugam, S.; Boyer, C., A robust and versatile photoinduced living polymerization of conjugated and unconjugated monomers and its oxygen tolerance. *Journal of the American Chemical Society* **2014**, *136*(14), 5508-5519.
50. Corrigan, N.; Rosli, D.; Jones, J. W. J.; Xu, J.; Boyer, C., Oxygen Tolerance in Living Radical Polymerization: Investigation of Mechanism and Implementation in Continuous Flow Polymerization. *Macromolecules* **2016**, *49*(18), 6779-6789.
51. Xu, J.; Shanmugam, S.; Duong, H. T.; Boyer, C., Organo-photocatalysts for photoinduced electron transfer-reversible addition–fragmentation chain transfer (PET-RAFT) polymerization. *Polymer Chemistry* **2015**, *6*(31), 5615-5624.
52. Fu, Q.; Xie, K.; McKenzie, T. G.; Qiao, G. G., Trithiocarbonates as intrinsic photoredox catalysts and RAFT agents for oxygen tolerant controlled radical polymerization. *Polymer Chemistry* **2017**, *8*(9), 1519-1526.
53. Ligon, S. C.; Liska, R.; Stampfl, J.; Gurr, M.; Mulhaupt, R., Polymers for 3D Printing and Customized Additive Manufacturing. *Chemical Reviews* **2017**, *117*(15), 10212-10290.
54. Wendel, B.; Rietzel, D.; Kühnlein, F.; Feulner, R.; Hülde, G.; Schmachtenberg, E., Additive Processing of Polymers. *Macromolecular Materials and Engineering* **2008**, *293*(10), 799-809.

55. Zhang, J.; Xiao, P., 3D printing of photopolymers. *Polymer Chemistry* **2018**, 9(13), 1530-1540.
56. Layani, M.; Wang, X.; Magdassi, S., Novel Materials for 3D Printing by Photopolymerization. *Advanced Materials* **2018**, 30(41), 1706344.
57. Hull, C. W. Apparatus for production of three-dimensional objects by stereolithography. U.S. Patent 4575330, 1986.
58. Steyrer, B.; Neubauer, P.; Liska, R.; Stampfl, J., Visible Light Photoinitiator for 3D-Printing of Tough Methacrylate Resins. *Materials* **2017**, 10(12), 1445.
59. Ahn, D.; Stevens, L. M.; Zhou, K.; Page, Z. A., Rapid High-Resolution Visible Light 3D Printing. *ACS Central Science* **2020**, 6(9), 1555-1563.
60. Tumbleston, J. R.; Shirvanyants, D.; Ermoshkin, N.; Januszewicz, R.; Johnson, A. R.; Kelly, D.; Chen, K.; Pinschmidt, R.; Rolland, J. P.; Ermoshkin, A.; Samulski, E. T.; DeSimone, J. M., Additive manufacturing. Continuous liquid interface production of 3D objects. *Science* **2015**, 347(6228), 1349-1352.
61. Kelly Brett, E.; Bhattacharya, I.; Heidari, H.; Shusteff, M.; Spadaccini Christopher, M.; Taylor Hayden, K., Volumetric additive manufacturing via tomographic reconstruction. *Science* **2019**, 363(6431), 1075-1079.
62. Pagac, M.; Hajnys, J.; Ma, Q.-P.; Jancar, L.; Jansa, J.; Stefek, P.; Mesicek, J., A Review of Vat Photopolymerization Technology: Materials, Applications, Challenges, and Future Trends of 3D Printing. *Polymers* **2021**, 13(4), 598.
63. Bagheri, A.; Fellows, C. M.; Boyer, C., Reversible Deactivation Radical Polymerization: From Polymer Network Synthesis to 3D Printing. *Advanced Science* **2021**, 8(5), 2003701.
64. Bagheri, A.; Jin, J., Photopolymerization in 3D Printing. *ACS Applied Polymer Materials* **2019**, 1(4), 593-611.

Chapter 2. Literature Review

Polymeric materials are nowadays an integral part of numerous commercial products and a commodity in our daily life. To meet the high demand for materials with various properties, such as biocompatibility, self-reparability and recyclability, advances in polymer chemistry are crucial. Conventional chain growth polymerisations, particularly free radical polymerisation allows access to a broad scope of materials but lacks the ability to finely control the polymerisation to make tailored macromolecules. The irreversible chain transfer and termination reactions present in conventional free radical polymerisation invariably leads to broad chain length distributions and dead polymer chains. Therefore, polymerisation techniques which enable a high degree of control and decrease the occurrence of unavoidable termination events are of great need.

Szwarc firstly applied the living concept in polymer science in 1956.¹ Living polymers were successfully produced via an anionic polymerisation which was initiated by the green complex naphthalene anion, sodium cation in tetrahydrofuran in the absence of air. As the ions formed during the reaction were well dissolved in tetrahydrofuran, the electron transfer from a carbanionic end of a growing polymer to the sodium cation became energetically unprofitable, in turn impeding the occurrence of termination. As a result, the polymerisation proceeded and stopped until the monomer supply was exhausted. It was also claimed polymerisation can be terminated in the presence of oxygen or water. Based on this finding, block copolymers were produced with the addition of a second monomer to the living polymers formed from the first monomer. This work laid great foundation to the synthesis of polymers with engineered and accurately designed macromolecular structures, compositions, and topologies. However, to compare with radical polymerisation, the stringent reaction conditions, such as the avoidance of oxygen and water, and the lower compatibility with vinylic monomers limit the applications of anionic polymerisation. Therefore, imparting living characteristics to radical polymerisation would be useful.

2.1 Reversible Deactivation Radical Polymerisation (RDRP)

One of the first examples of “living” radical polymerisation was demonstrated by Otsu and co-workers, who firstly introduced the initiator-transfer agent-terminator (iniferter) concept in the polymerisation of methyl methacrylate (MMA) or styrene (St) in 1982.² In their work, a tetraethylthiuram disulfide iniferter was initially activated by heat to prepare PMMA and PSt in the absence of light. As the dialkyl dithiocarbamate group can be cleaved into radicals under irradiation, the pre-formed polymers were subsequently reactivated by UV light in the presence of additional monomers, eventually generating block copolymers. Although the dispersity was high, it impressively revealed the living character of dormant polymer chains via a radical polymerisation process.

Motivated by the versatility and compatibility of radical polymerisation, including the high tolerance to a wide variety of functional and non-functional monomers and mild reaction conditions, enormous work has been done to develop effective living radical polymerisation strategies.³⁻⁹ These strategies were developed based on three different polymerisation mechanisms: stable radical-mediated polymerisation (SRMP), atom transfer radical polymerisation (ATRP), and degenerative transfer radical polymerisation (DTRP).¹⁰⁻¹⁴

In SRMP, chemical species undergo unimolecular bond cleavage to generate a propagating radical and a dormant group X as shown in **Figure 2.1**. One example of SRMP is nitroxide-mediated polymerisation (NMP), where X is a nitroxide. NMP proceeds under a reversible deactivation mechanism between the stable nitroxide radical (X) and the propagating carbon-centered radical (P_n^\bullet) to form a dormant alkoxyamine species ($P_n\text{-X}$). Under high temperature, the thermally unstable dormant species can undergo homolytic cleavage of the alkoxyamine C-ON bond to regenerate the nitroxide radical (X) and the propagating radical (P_n^\bullet), in turn establishing an activation-deactivation equilibrium.

As for ATRP, a transition metal complex (activator, A^m), can abstract a halogen atom X from a halide initiator (R-X), to generate an oxidised halogenated metal complex (deactivator, $A^{m+1}X$) and an organic carbon-centered radical R^\bullet . The R^\bullet can subsequently undergo radical addition to vinyl bonds to start propagation. In a well-controlled ATRP,

very few polymer chains undergo termination reactions. Instead, the propagating radical P_n^\bullet can be rapidly trapped by the deactivator ($A^{m+1}X$) to form a halide-capped dormant chain (P_n-X), accompanied by the reformation of the activator (A^m). (**Figure 2.1**). One example of ATRP is to use copper(I) complex as the activator and bromides as the halide species to form propagating radicals and copper(II) complex as the deactivator.

DTRP employs a chain transfer agent and involves reversible transfer of propagating radicals between dormant species (**Figure 2.1**). With the addition of a propagating radical (P_n^\bullet) to a chain transfer agent, an intermediate radical is formed, followed by fragmentation to provide a new propagating radical and a dormant polymeric compound (P_n-X). The propagating radical can then reinitiate unreacted monomers to form new propagating species (P_m^\bullet). Rapid equilibrium can be subsequently established between the propagating radicals (P_n^\bullet and P_m^\bullet) and the dormant species (P_m-X or P_n-X) to allow an equal probability for all chains to grow. One example of DTRP is to employ thiocarbonylthio compounds as chain transfer agents, which is commonly known as reversible addition fragmentation chain transfer polymerisation, RAFT.

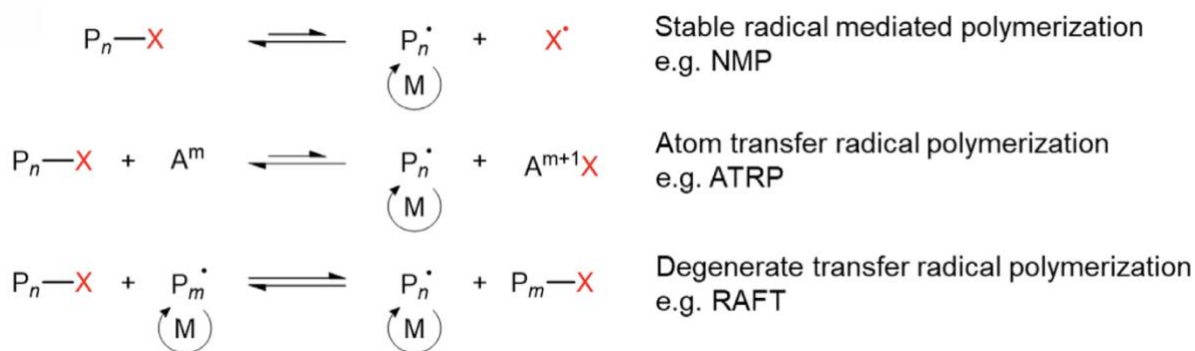


Figure 2.1 General mechanisms of reversible deactivation radical polymerisation.¹²

As these polymerisation methods were named in many different ways (e.g., living or controlled/living radical polymerisations), the IUPAC recommended the use of the term reversible-deactivation radical polymerisation (RDRP) in 2010.¹⁵ With the improvements and evolution of various RDRP techniques, a wide range of polymeric materials have been generated for the applications in drug delivery, therapeutics, nanoparticles, sensors, adhesives, coatings, and others.¹⁶⁻¹⁸

2.1.1 Benefits of RDRP

So far, there have been many effective RDRP techniques, with NMP, ATRP and RAFT polymerisation being the most widely used. Although these techniques differ in reaction mechanisms and employ distinct control agents, they all undergo a dormant-active equilibrium process that allows all active polymer chains to grow simultaneously. The rapid reversible activation and deactivation dynamic equilibrium established with the aid of the control agent can significantly reduce the fraction of terminated chains, in turn imparting living characteristics into the polymerisation.

One of the main benefits of RDRP techniques is that molecular weights of linear polymers can be accurately controlled by adjusting the relative concentrations of control agent and monomer in the system. Increasing the initial concentration of control agent relative to the initial concentration of monomer can result in the production of polymers with lower molecular weights. For an effective RDRP process, the rates of initialization and the dormant-active equilibrium are rapid with respect to propagation.¹⁹ Therefore, all polymer chains can grow evenly at the same rate. As such, the molecular weight of each polymer chain will become comparable during the polymerisation, increasing linearly with monomer conversions (**Figure 2.2A**).¹² Finally, the chain length distribution will approach a Poisson distribution, obtaining polymers with low dispersity (**Figure 2.2B**). The linear relationship between polymer molecular weight and monomer conversion in RDRP provides an efficient way to achieve polymeric materials with predictable molecular weights.

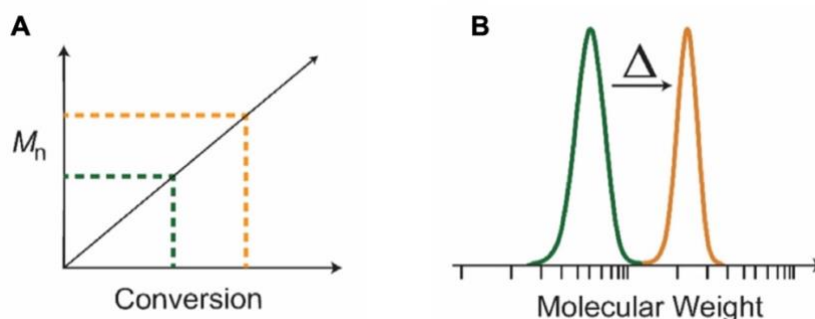


Figure 2.2 Typical behaviour in RDRP systems. (A) a linear relationship between monomer conversion and number average molecular weight; (B) chain length distribution approaching a Poisson distribution and the complete shift in molecular weight upon chain extensions. Figure adapted from Ref. [12].

Regardless of different mechanisms of varied RDRP techniques, the retention of the chain-end functionality of the control agent throughout the polymerisation allows dormant polymer chains to be reactivated, enabling repeated chain extension in the presence of additional monomers. As such, polymeric materials with well-defined macromolecular topology, including block and graft copolymers, stars, branched and brush polymers, can be readily synthesised.²⁰⁻³¹ Further, with the addition of multivinyl monomers in the reaction mixture, topologically diverse crosslinked polymers can be formed via RDRP. To compare with uncontrolled polymerisation techniques, RDRP is advantageous in preparing homogeneous polymer networks. This is mainly because the high initiation to propagation rates of RDRP allows all chains to be initiated at the early stage of the polymerisation. Subsequently, the dormant-active equilibrium leaves sufficient time for chains to diffuse and relax, leading to the consumption of all the monomers or crosslinkers in the system. This facilitates the formation of more uniform branched copolymers and finally a more homogeneous network.³²⁻³³

RDRP also exhibits a broad tolerance to various reaction conditions. Unlike ionic polymerisation which must be conducted in the absence of water, RDRP process can proceed in the presence of many different solvents, such as organic or protic solvents,^{7, 34-35} ionic liquids,³⁶⁻³⁸ supercritical carbon dioxide,³⁹ and others, including water.¹² Moreover, although radicals generated in RDRP are sensitive to oxygen, various oxygen tolerant strategies have been explored to enable the polymerisation to proceed in the open air.⁴⁰ Further, as early RDRP systems were mainly reliant on heat to activate the polymerisation, their applications were limited in the fields sensitive to temperature, such as bioapplications. In this regard, a variety of RDRP systems using different stimulus to induce reactions have been excitingly explored, including photomediated RDRP,⁴¹⁻⁴² electrochemical RDRP,⁴³⁻⁴⁴ mechano-initiated RDRP,⁴⁵⁻⁴⁶ and enzyme-initiated RDRP.⁴⁷⁻

48

In addition, RDRP possesses high compatibility with a broad scope of monomers, including (meth)acrylates, (meth)acrylamide, St, acrylonitrile (AN), vinyl acetate (VAc), *N*-vinylpyrrolidone (NVP), acrylic acid (AA) and many others.^{23, 49-57} These monomers can also contain various functional groups, such as carboxylic acids, hydroxyls, esters, dialkylamino groups, and many others, which remain intact throughout the polymerisation and can be potentially post-modified to enhance polymer functionality.

Due to the abovementioned advantages, RDRP has become the most versatile and robust radical polymerisation approach. Among various RDRP techniques, RAFT polymerisation exhibits a higher tolerance to a wider range of monomers and reaction conditions. For instance, the “less activated” monomers (LAMs), such as VAc or NVP, are challenging to be polymerised by using other RDRP techniques, but can be polymerised via RAFT with a good molecular weight control and low dispersities.^{49, 55, 58-60} Moreover, with the assistance of various oxygen tolerant strategies, RAFT polymerisation can be performed in the air, which significantly simplifies experiment setup and reaction procedures.^{40, 61} In addition, the fast initiation rate of RAFT polymerisation is critically important for the whole research work of the thesis. Upon all these advantages, the following sections will therefore elaborate more on RAFT polymerisation. More research work on other RDRP techniques can be found in more comprehensive review papers.^{12, 49-50, 62-69}

2.1.2 Reversible addition-fragmentation chain transfer polymerisation (RAFT)

Reversible addition-fragmentation chain transfer (RAFT) polymerisation is one of the most effective and versatile RDRP techniques. RAFT relies on a degenerative chain transfer process to control the exchange between the active and dormant species during polymerisation. The early reports of applying addition-fragmentation chain transfer techniques to control molecular weight can trace back to the 1980s.^{2, 70-73} However, imparting living character to the radical polymerisation via reversible addition-fragmentation chain transfer method appeared in 1995.⁷⁴⁻⁷⁶ Building upon the work in 1998, a group of researchers from Commonwealth Scientific and Industrial Research Organization (CSIRO) Australia utilised thiocarbonylthio compounds (RSC(Z)=S) as the chain transfer agents and designated the process RAFT polymerization.⁷ The design and synthesis of thiocarbonylthio species (RAFT agents) with diverse structures significantly improved the effectiveness of RAFT polymerisation toward various monomer systems. So far, a wide range of RAFT agents have been developed (**Figure 2.3**), including the four main classes of dithioesters ($\text{Z} = \text{alkyl or aryl}$),⁷⁷ trithiocarbonates ($\text{Z} = \text{SR}'$),²² dithiocarbamates ($\text{Z} = \text{NR}'\text{R}''$)⁷⁸⁻⁸¹ and xanthates ($\text{Z} = \text{OR}'$).⁸²⁻⁸³ The polymerization process employing xanthates as the chain transfer agent was termed macromolecular design via the interchange of xanthates (MADIX).⁸³ The RAFT and MADIX processes are actually identical in mechanisms, but only differ by the structure of the thiocarbonylthio compounds.^{51, 84}

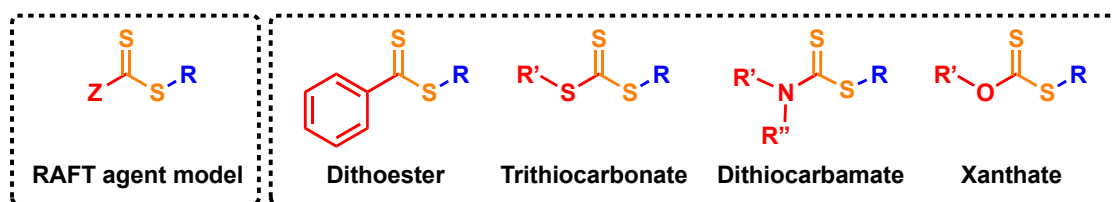


Figure 2.3 General chemical structures of four main classes of RAFT agents.

Apart from being able to confer living characteristics to the polymerisation, another benefit of the RAFT process is that it can proceed in various reaction media, including bulk,⁷ organic or protic solvents,^{7, 34-35} emulsion and mini-emulsion,⁸⁵⁻⁸⁷ Lewis acid⁸⁸⁻⁹⁰ and some unconventional solvents such as ionic liquids.³⁶⁻³⁷ Further, RAFT polymerisation demonstrates a high tolerance to the majority of monomers,^{23, 51-57} a broad range of reaction temperatures (typically from ambient to 180 °C) and high reaction

pressures (up to 5 kbar).^{54, 91-96} These attributes increase the versatility and applicability of RAFT polymerisation. It is reported that RAFT polymerisation has been successfully applied in the fields of bioapplications, electronic polymers, stimuli-responsive polymers and industrial polymeric materials.^{18, 97-99} More information regarding to the applications of RAFT polymerisation can be found in other reviews.^{12, 17, 100-101} The following sections will focus on the mechanism of RAFT polymerisation, how to make the right selection of the RAFT agents and RAFT crosslinking polymerisation.

2.1.2.1 Mechanism of RAFT polymerisation

The mechanism of RAFT polymerisation is shown in **Figure 2.4**. In general, RAFT polymerisation comprises initiation, pre-equilibrium, re-initiation, main equilibrium and termination.^{51, 102-103} In the initiation process, initiators are used to generate free radicals which are capable of initiating polymerisation to form propagating radicals (P_n^\bullet). Subsequently, the propagating radical (P_n^\bullet) can add to the thiocarbonylthio compound ($RSC(Z)=S$, **(1)**) to form an intermediate radical species **(2)**. Followed by the fragmentation of the radical intermediate **(2)**, a polymeric thiocarbonylthio compound ($P_nS(Z)C=S$, **(3)**) and a RAFT agent derived radical (R^\bullet) are generated. The radical (R^\bullet) re-initiates unreacted monomers and continues propagation to form new polymeric propagating species (P_m^\bullet). Afterwards, the main equilibrium is rapidly established between the propagating radicals (P_n^\bullet and P_m^\bullet) and the dormant thiocarbonylthio compounds **(3)** by way of the intermediate **(4)**, providing an equal probability for all chains to grow. As such, polymers with low dispersity can be obtained via RAFT process. When the polymerisation is complete, most of chains possess the thiocarbonylthio end-group and remain dormant. However, biomolecular termination of free polymeric radicals leads to dead polymer.

propagating radicals P_n^\bullet and P_m^\bullet , which provides the same rate constants k_{add} , $k_{-\beta}$ and a partition coefficient ϕ of 0.5.

$$k_{\text{tr}} = k_{\text{add}}\phi = k_{\text{add}} \frac{k_{\beta}}{k_{-\text{add}} + k_{\beta}} \quad \text{Eq. 1}$$

$$k_{-\text{tr}} = k_{-\beta}(1 - \phi) = k_{-\beta} \frac{k_{-\text{add}}}{k_{-\text{add}} + k_{\beta}} \quad \text{Eq. 2}$$

$$\phi = \frac{k_{\beta}}{k_{-\text{add}} + k_{\beta}} \quad \text{Eq. 3}$$

2.1.2.2 Choice of RAFT agents

So far, a wide range of RAFT agents ($\text{RSC}(\text{Z})=\text{S}$) have been reported. The effectiveness of these RAFT agents in the polymerisation of different monomers is strongly determined by the properties of the leaving R groups and the activating Z groups.

The Z group plays a vital role in affecting the rate of addition of propagating radicals to the $\text{C}=\text{S}$ double bond of a thiocarbonyl group.^{51, 84, 104} The rate is higher when Z is aryl, alkyl (dithioesters), or SR' (trithiocarbonates), but lower when Z is OR' (xanthates) or $\text{NR}'\text{R}''$ (dithiocarbamates). The low activity of xanthates and dithiocarbamates derivatives can be attributed to the zwitterionic canonical forms shown in **Figure 2.5**. The interaction between the oxygen or nitrogen lone pairs and the $\text{C}=\text{S}$ double bond reduces the double bond character, in turn impeding the free radical addition.^{78, 104} The activity can be enhanced when the lone pair on the oxygen or nitrogen atom is conjugated to a π -system or interacts with an electron-withdrawing group on the Z substituents.^{78-79, 105-106} In addition, the Z group determines the stability of the intermediate RAFT radicals formed during the pre-equilibrium or the main equilibrium. If the intermediate radical is significantly stabilised, for instance by a phenyl Z group, the rate of fragmentation may become very slow. As a result, the polymerisation can be inhibited or retarded. Many previous reports have revealed the occurrence of retardation when the RAFT agent is dithioester with a Z of aryl group. This is more apparent when a higher concentration of RAFT agents is employed.¹⁰⁷⁻¹¹⁰

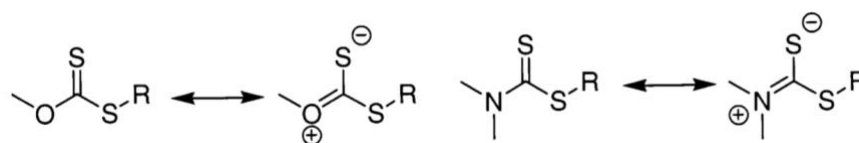
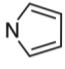
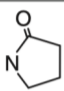
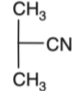
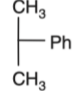
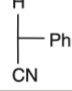
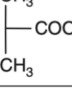
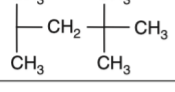
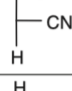
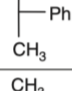
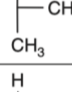
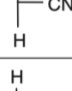
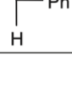


Figure 2.5 Zwitterionic canonical forms of xanthates and dithiocarbamates.¹⁰⁴

Radically polymerisable monomers can be broadly classified into two categories, known as the “more activated” monomers (MAMs) and the “less activated” monomers (LAMs). MAMs have C=C double bonds conjugated with an aromatic ring (e.g., St and vinylpyridine), a carbonyl group (e.g., MMA, methyl acrylate (MA), methacrylamide (MAM), acrylamide (AM)) or a nitrile (e.g., AN). LAMs have C=C double bonds adjacent to a saturated carbon (e.g., diallyldimethylammonium chloride), on oxygen or nitrogen lone pair (e.g., VAc) or NVP) or the heteroatom of a heteroaromatic ring (e.g., *N*-vinylcarbazole).^{51, 84} MAMs and LAMs have different activities, with the former being less reactive in radical addition but the latter highly reactive. As a result, to provide good control, the selection of the RAFT agent with a suitable Z group to mediate the polymerisation of a specific monomer is of great significance.

A general guideline of Z selection is shown in **Table 2.1**.⁵¹ More active RAFT agents, such as dithioesters (Z = alkyl or aryl) or trithiocarbonates (Z = SR'), are more suitable for controlling polymerisation of MAMs, while less active RAFT agents, such as dithiocarbamates (Z = NR'R'') and xanthates (Z = OR') are ineffective with MAMs.^{57, 79, 104, 111} This is mainly because MAM propagating radicals are less reactive and will not add effectively to less active RAFT agents (e.g. dithiocarbamate or xanthate). As a result, a more active RAFT agent is required for effective radical addition, in turn performing good control over polymerisation. On the contrary, less active RAFT agents provide good control over the polymerisation of LAMs, while more active RAFT agents may inhibit or retard polymerisation of LAMs.^{57, 79, 104, 111} It is reported that the intermediate radical formed by the addition of a less activated monomer is more stable and not in favour of fragmentation.^{57, 112} As such, a Z group which can destabilise the intermediate radical is essential to promote fragmentation. The less active RAFT agents such as dithiocarbamates (Z = NR'R'') and xanthates (Z = OR') have the Z group containing nitrogen or oxygen. The lone pairs of the heteroatoms can effectively induct toward the intermediate radical to destabilise it and facilitate fragmentation process.^{57, 112}

Table 2.1 Guidelines for selection of the Z group and R group of RAFT agents for polymerisation of different monomers.^{51a}

Class	Aryl dithioester	Trithiocarbonate	Alkyl or aralkyl dithioester	Aromatic dithiocarbamate	Lactam dithiocarbamate	O-aryl xanthate	O-alkyl xanthate	N-alkyl-N-aryl dithiocarbamate	N,N-dialkyl dithiocarbamate
R \ Z	Ph	SCH ₃	CH ₃			OPh	OCH ₃	NPh(CH ₃)	N(CH ₃) ₂
	MMA St MA VAc	MMA St MA VAc	MMA St MA VAc	MMA St MA VAc	MMA St MA VAc	MMA St MA VAc	MMA St MA VAc	MMA St MA VAc	MMA St MA VAc
	MMA St MA VAc	MMA St MA VAc	MMA St MA VAc	MMA St MA VAc	MMA St MA VAc	MMA St MA VAc	MMA St MA VAc	MMA St MA VAc	MMA St MA VAc
	MMA St MA VAc	MMA St MA VAc	MMA St MA VAc	MMA St MA VAc	MMA St MA VAc	MMA St MA VAc	MMA St MA VAc	MMA St MA VAc	MMA St MA VAc
	MMA St MA VAc	MMA St MA VAc	MMA St MA VAc	MMA St MA VAc	MMA St MA VAc	MMA St MA VAc	MMA St MA VAc	MMA St MA VAc	MMA St MA VAc
	MMA St MA VAc	MMA St MA VAc	MMA St MA VAc	MMA St MA VAc	MMA St MA VAc	MMA St MA VAc	MMA St MA VAc	MMA St MA VAc	MMA St MA VAc
	MMA St MA VAc	MMA St MA VAc	MMA St MA VAc	MMA St MA VAc	MMA St MA VAc	MMA St MA VAc	MMA St MA VAc	MMA St MA VAc	MMA St MA VAc
	MMA St MA VAc	MMA St MA VAc	MMA St MA VAc	MMA St MA VAc	MMA St MA VAc	MMA St MA VAc	MMA St MA VAc	MMA St MA VAc	MMA St MA VAc
	MMA St MA VAc	MMA St MA VAc	MMA St MA VAc	MMA St MA VAc	MMA St MA VAc	MMA St MA VAc	MMA St MA VAc	MMA St MA VAc	MMA St MA VAc
	MMA St MA VAc	MMA St MA VAc	MMA St MA VAc	MMA St MA VAc	MMA St MA VAc	MMA St MA VAc	MMA St MA VAc	MMA St MA VAc	MMA St MA VAc
	MMA St MA VAc	MMA St MA VAc	MMA St MA VAc	MMA St MA VAc	MMA St MA VAc	MMA St MA VAc	MMA St MA VAc	MMA St MA VAc	MMA St MA VAc
CH ₃	MMA St MA VAc	MMA St MA VAc	MMA St MA VAc	MMA St MA VAc	MMA St MA VAc	MMA St MA VAc	MMA St MA VAc	MMA St MA VAc	MMA St MA VAc

^aBold blue = controls well; regular black = controls, but not so well; bold grey = does not control.

The R group is of great importance in the pre-equilibrium of the polymerisation. It should be a better leaving group with respect to the propagating radical to force the equilibrium

to move toward product side, fragmenting rapidly to generate radical R^\bullet .^{51, 84} Also, the radical R^\bullet must efficiently reinitiate monomers to avoid retardation.¹¹³ A general guideline of R selection is shown in **Table 2.1**.⁵¹

The stability of radical R^\bullet plays a role in determining the fragmentation rate. Increased radical stability makes R group a better leaving group; however, if the radical R^\bullet is too stabilised, the reinitiation rate constant k_i becomes lower than the propagation rate constant k_p . As a result, it cannot effectively add to a monomer and reinitiate polymerisation.^{84, 97, 113} Steric effect is another important factor in determining the leaving ability of radical R^\bullet . For example, in the polymerisation of MMA, iso-octyl dithiobenzoate ($R = -C(CH_3)_2CH_2(CH_3)_3$) demonstrated a higher transfer coefficients than *tert*-butyl dithiobenzoate ($R = C(CH_3)_3$) and benzyl dithiobenzoate ($R = -CH_2Ph$).¹¹³ The bulky structure of the R group of iso-octyl dithiobenzoate enhanced the leaving ability. However, the steric bulk may also incur steric hindrance, which may affect the R group reinitiating capability. Introducing electron withdrawing groups on the R group can increase the electrophilicity of the leaving radical, in turn enhancing its affinity for electron rich C=C double bonds to reinitiate monomer, despite the steric bulk.^{97, 113} Moreover, this polar effect can also increase fragmentation rates of the R group.

2.1.2.3 RAFT crosslinking polymerisation

Free radical polymerisation (FRP) of vinyl monomers and divinyl crosslinkers has been largely employed for the synthesis of highly crosslinked networks and gels. The network structures of these polymeric materials are critically important to the performance in various fields, such as dental materials, coatings, drug delivery, artificial organs and microelectronic devices.¹¹⁴⁻¹¹⁶ However, FRP process usually leads to the formation of a heterogeneous network which seriously impacts the mechanical properties of the final products.¹¹⁷⁻¹¹⁹ In FRP, the low rate of initiation compared to propagation leads to a very low concentration of polymer chains at the early stage of the polymerisation. As a result, intermolecular crosslinking reaction is limited. Instead, pendent vinyl bonds are rapidly consumed by propagating radicals via intramolecular cyclization reactions, generating densely crosslinked domains (nanogels).^{117, 120-123} These nanogels are loosely connected toward the later stages of the reaction to form networks with highly variable crosslink densities.

In contrast to FRP, RAFT crosslinking polymerisation provides great benefits in preparing homogeneous networks. In a RAFT system, all primary chains can be initiated at the very beginning of polymerisation. Due to rapid exchange reaction between propagating radicals and dormant chains, chain growth is frequently interrupted. As a result, all chains grow in a reduced rate, which leaves sufficient time for chain relaxation and diffusion, in turn promoting intermolecular crosslinking and reduce intramolecular cyclisation. This process significantly minimises nanogels formation and gives rise to more homogeneous networks.¹²⁴⁻¹²⁸ **Figure 2.6** compares the gelation process by free radical polymerisation vs RAFT polymerisation.¹²⁶

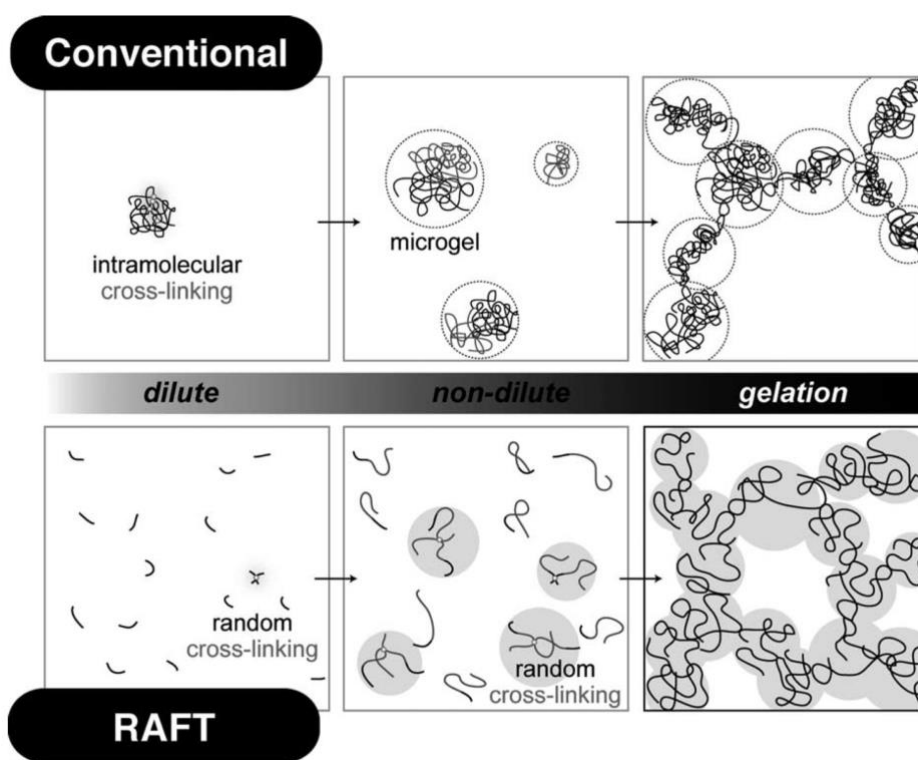


Figure 2.6 Schematic presentations of the polymer network synthesis process for conventional (top) and RAFT (bottom) polymerisations.¹²⁶

Several studies have been attempted to fabricate polymeric materials with a network of enhanced homogeneity via RAFT crosslinking polymerisation. For instance, Zhu and co-workers investigated the homogeneity of networks formed via FRP and RAFT polymerisation of oligo(ethylene glycol) dimethacrylates.¹²⁵ The dynamic mechanical analysis (DMA) results showed that the breadths of glass transition regions of the two networks were distinct. The network formed via RAFT polymerisation exhibited a narrower $\tan \delta$ peak than that of the counterpart formed via FRP, indicating a more

homogeneous network of the former. The heterogeneous distribution of highly crosslinked nanogels formed in FRP network led to a wide distribution of relaxation times and then a wide glass transition region. In another research, De and co-workers synthesised crosslinked polymer gels in the presence of a trithiocarbonate RAFT agent in organic and aqueous solvents.¹²⁴ They found that gels synthesised through RAFT polymerisation exhibited a higher swelling ratio than gels made via FRP, which was attributed to less highly crosslinked nanogel domains in the RAFT-mediated network.

Another important advantage of networks formed via RAFT polymerisation is the retention of the thiocarbonylthio polymer chain-end throughout the polymerisation. The dormant chain-end can be repeatedly activated by external stimuli, such as heat or light, to enable post-modification of the pre-formed network. One post-modification approach is to reactivate the chain-end for the subsequent addition of new monomers or crosslinkers to functionalise the polymeric materials. This has been widely used to produce structurally tailored and engineered macromolecular (STEM) gels, which are polymer networks containing latent active sites available for post-modification.¹²⁹⁻¹³⁴ STEM gels incorporated with functional groups in the primary network can be easily post-modified into materials with various properties.^{130, 134} For example, Johnson and co-workers demonstrated modification of “parent” polymer networks containing trithiocarbonate (TTC) units within the polymer backbone. Irradiated by blue light with the addition of a photocatalyst (PC) (10-phenylphenothiazine, PTH) and monomers (*N*-isopropylacrylamide, NIPAAM) in acetonitrile, the TTC units can be activated, leading to subsequent polymerisation and modification of the primary network (**Figure 2.7**).¹³⁰ This network post-functionalization enabled the production of a wide range of daughter gels with differentiated chemical and mechanical properties.

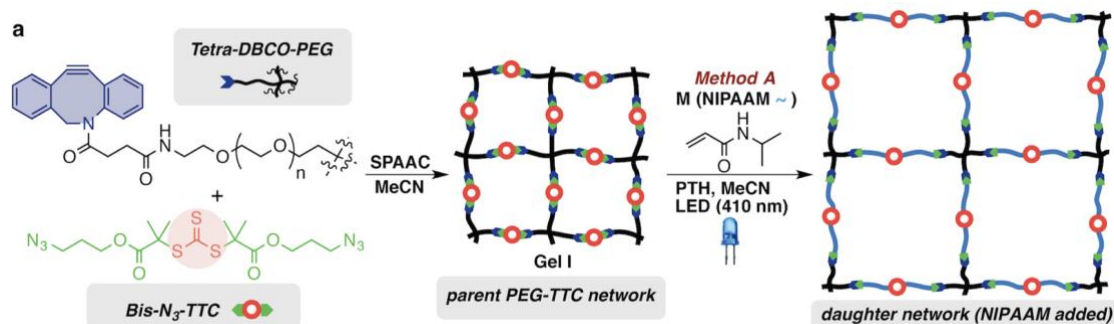


Figure 2.7 Demonstration of the modification of parent gels with the TTC units in the network in the presence of a photocatalyst (10-phenylphenothiazine, PTH) and monomers (*N*-isopropylacrylamide, NIPAAM) under blue light irradiation.¹³⁰

Another post-modification method is to reactivate thiocarbonylthio compounds in the network to undergo reversible covalent bond rearrangement between network strands.¹³⁵⁻¹³⁸ For instance, Matyjaszewski and co-workers exploited TTC units in a crosslinked butyl acrylate (BA) network to re-heal gels via reshuffling reactions.¹³⁷ They proposed that the weak C-S bonds of TTC units can undergo homolytic cleavage under UV light irradiation to generate a reactive carbon radical which can subsequently react with other TTC units by degenerative exchange reactions (reshuffling reactions) to promote network rearrangement and recombination (**Figure 2.8**). Moreover, the low glass transition temperature (T_g below room temperature) of the crosslinked polymers enables high chain mobility, which facilitates efficient reshuffling reactions and therefore facilitates self-healing process. In their work, a gel sample was firstly cut into three pieces which were subsequently fused into a cured single object under 4 h UV light irradiation in acetonitrile and nitrogen. To demonstrate the repetitive healing capability, the once healed sample was re-cut into three pieces and underwent a second self-healing reaction under the same conditions. After 12 h of photoirradiation, the cut pieces were re-healed and can be swollen in anisole for 6 h without breaking.

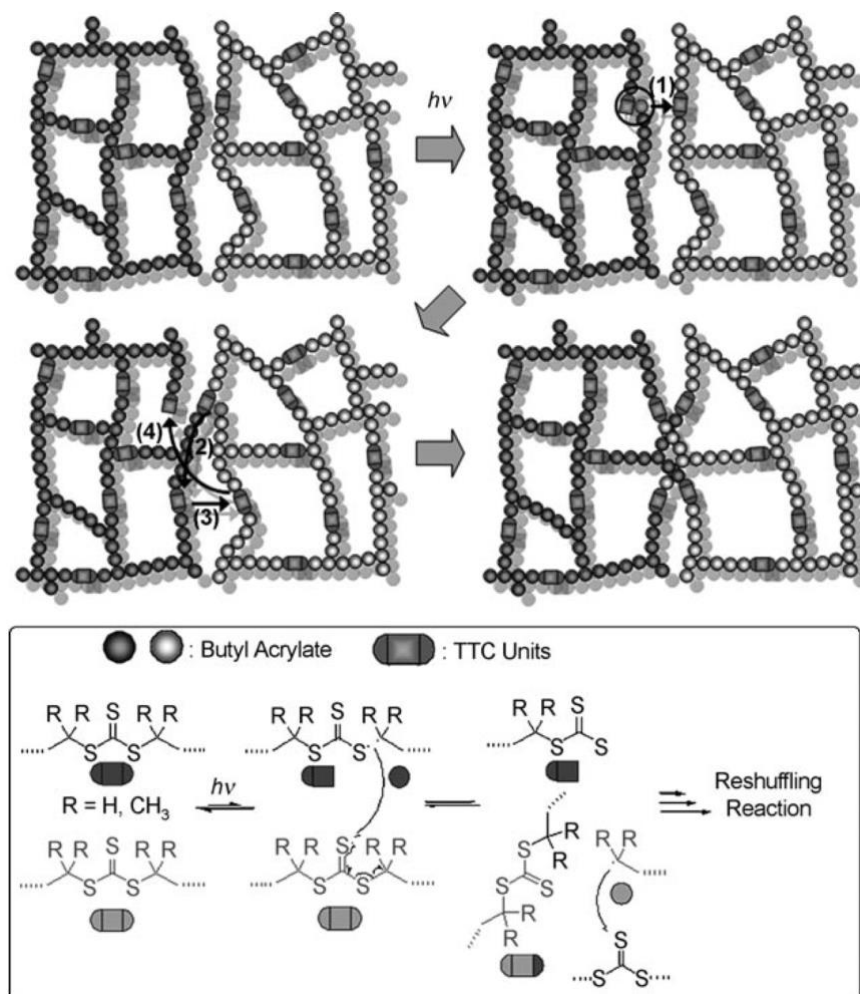


Figure 2.8 Proposed mechanism of self-healing process via reshuffling reaction of TTC units between network strands under UV light irradiation.¹³⁷

2.1.2.4 RAFT end-group functionalisation

Due to the versatility of the thiocarbonylthio group, RAFT polymer chain-ends can be functionalised via ω -end modification approaches, such as reaction with nucleophiles or aminolysis, radical induced reduction, hetero-Diels-Alder reactions, thermolysis, and other reactions (**Figure 2.9**).¹³⁹⁻¹⁴¹ Thiocarbonylthio compounds reacting with nucleophiles and ionic reducing agents is one of the most versatile and widely reported methods of RAFT end group transformation. The thiocarbonyl group can be easily transformed into a thiol group to allow for facile thiol-ene and other thiol modifications.^{140, 142-150} For example, Winnik and Qiu demonstrated that the thiocarbonylthio end group of polymers prepared by RAFT polymerisation of NIPAAm can be easily transformed into a stable thioether group via a mild one-pot process of thiocarbonylthio aminolysis and Michael addition of acrylate derivatives.¹⁴² Moreover, a number of examples have shown

that the thiocarbonylthio groups bearing electron-withdrawing Z groups facilitate their use as a dienophile in a hetero-Diels-Alder cycloaddition with an appropriate diene.¹⁴⁰ This method has been used in the synthesis of diblock copolymers and complex macromolecular structures, like stars.¹⁵¹ Stenzel and co-workers employed RAFT polymerisation to produce PSt by using dithioesters as RAFT agents. Subsequently, star polymers with up to 4 arms were synthesised via coupling reactions of PSt with multi-diene coupling agents in chloroform at 50 °C.¹⁵² Thermolysis is commonly used for thiocarbonylthio group removal. It provides an effective and simple method to yield a sulfur-free unsaturated end group with no chemical additions.¹⁴¹ However, one drawback of thermal elimination process is the release of toxic and odorous thermolysis by-products such as thiols and CS₂ released during the thermolysis of trithiocarbonates.^{140, 153}

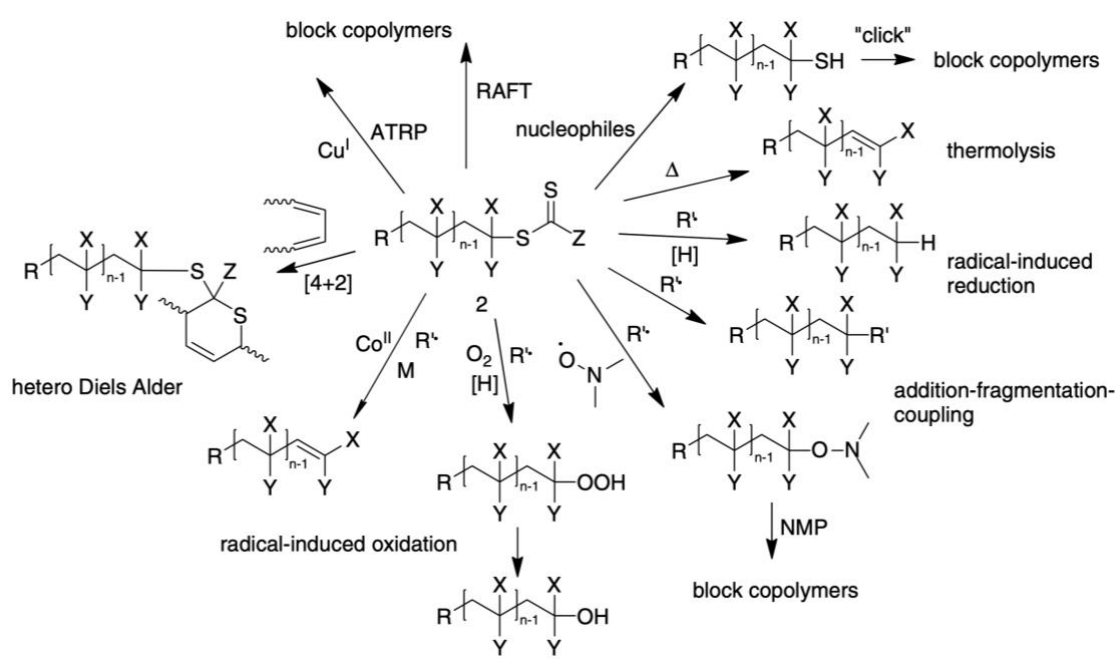


Figure 2.9 Processes of RAFT end-group transformation via ω -end modification approaches (R^\bullet = radical; $[H]$ = hydrogen donor; M = monomer).¹⁴¹

2.2 Photomediated RAFT Polymerisation

So far, there have been two main types of initiation methods utilised to trigger RAFT polymerisation: thermal-initiation^{7, 22, 78, 104, 113} and photo-initiation,^{40, 61, 154-160}. Photo-initiation processes have attracted great attention, largely due to the intrinsic benefits of light as an external stimulus, such as low cost and ubiquity, environmentally friendly nature, spatiotemporal control, temperature independence, various light source selections with specific intensity and wavelength. As a result, a wide range of photomediated RAFT techniques have been developed based on distinct photoinitiating systems. This section will focus on the advantages of using light in RAFT photopolymerisation, and will also illustrate three main photomediated RAFT mechanisms, including RAFT polymerisation initiated by conventional photoinitiators, RAFT polymerisation via iniferter polymerisation mechanism, and photoinduced electron/energy transfer-reversible addition-fragmentation chain transfer (PET-RAFT) polymerisation.

2.2.1 Benefits of light verses heat

2.2.1.1 Temporal control

One of the most attractive advantages of using light over heat to trigger polymerisation is temporal control.^{61, 161-162} In an ideal situation, the polymerisation can be readily stopped once light is off, and then restarted when light is reintroduced. However, in some reported photoinduced RDRP systems, a small amount of polymer growth can still be observed when light is off, which could be attributed to many factors, such as experimental errors or extended lifetime of residual active catalyst.¹⁶³⁻¹⁶⁵ This problem can be mitigated by changing reaction solvents, PCs, or switching to a different photo-polymerisation techniques.¹⁶⁶ A good example to demonstrate temporal control was demonstrated by Boyer and co-workers, employing chlorophyll *a* as the PC to initiate polymerisation under visible light irradiation ($\lambda_{\text{max}} = 461$ and 635 nm) via PET-RAFT polymerisation.¹⁵⁸ This efficient photoinitiation system provided excellent control over a broad range of monomers with or without functional groups, resulting in controlled molecular weights and low dispersities. More importantly, temporal control by changing the light between “on” and “off” was demonstrated. As shown in **Figure 2.10**, in the absence of light, no monomer conversion was observed; however, the reaction progressed when light was reintroduced.

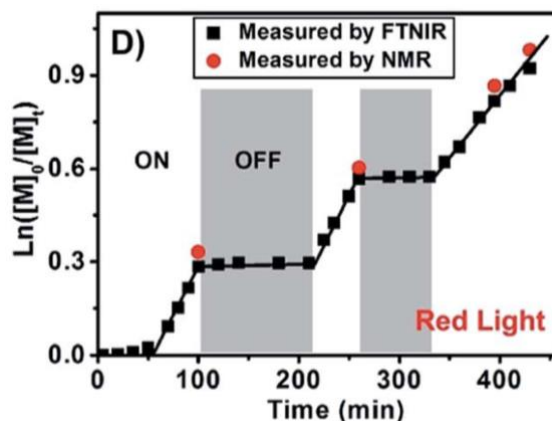


Figure 2.10 RAFT polymerisation of MA using chlorophyll a as photocatalyst in the presence (“ON”) or in the absence (“OFF”) of light.¹⁵⁸

2.2.1.2 Spatial control

Another benefit of using light over heat to trigger polymerisation is that the former can provide a precise activation of polymerisation in a target region in an easy and simplified way. This selective and customizable polymerisation enables the synthesis of materials with regionally differentiated functions and properties as needed.

Photomask technology is a featured photocontrolled method which has been used for spatial patterning in photopolymerisation.¹⁶⁷⁻¹⁷⁰ Light can only pass through the transparent region, while the opaque region stops light to pass through. One typical application of photomask technology in polymer chemistry is to synthesise three-dimensional (3D) polymer brushes.^{20, 171-172} By setting a specific pattern on the mask, brushes can only grow in exposed regions, leaving the unexposed regions unreacted. Moreover, through modulation of light exposure time and intensity, brush heights can be adjusted. As a result, polymer brushes with complex and arbitrary structures can be achieved. For example, Pester and co-workers introduced surface-initiated (SI) PET-RAFT polymerisation in combination with photomasks for patterned polymer brushes under visible light ($\lambda_{\max} = 405 \text{ nm}$) (**Figure 2.11(a)**).¹⁷³ In this work, the polymerisation of *N,N*-dimethylacrylamide (DMAm) was conducted on a RAFT agent (*S*-1-dodecyl-*S'*-(α,α' -dimethyl- α'' -acetic acid) trithiocarbonate, DDMAT) functionalised silica wafer, using 5,10,15,20-tetraphenyl-21H,23H-porphine zinc (ZnTPP) as the PC in conjunction with dimethyl sulfoxide (DMSO) which provides significant oxygen tolerance and allows the reaction to proceed in air.⁴⁰ By using an array of optical lenses, a grayscale photomask

image was projected onto the wafer. Subsequently, SI-PET-RAFT polymerisation of DMAM proceeded, resulting in the polymer brush reproduction of the original photograph (**Figure 2.11(b)**). The optical contrast was attributed to different heights of the polymer brush which was caused by distinct levels of the penetration of light through the mask.

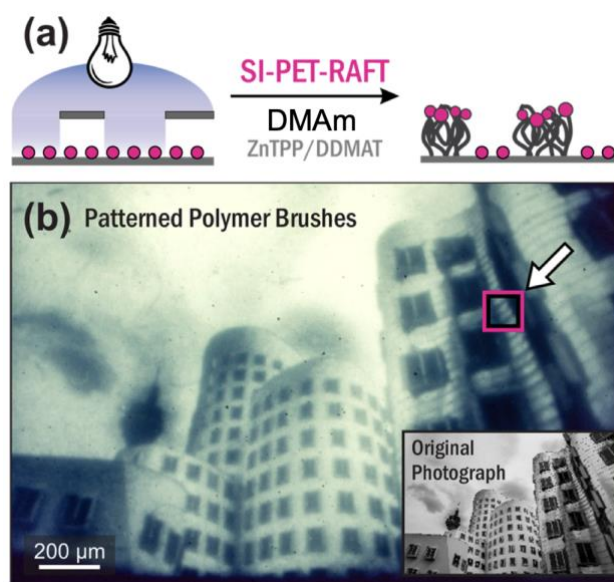


Figure 2.11 Demonstration of the formation of patterned polymer brushes via SI-PET-RAFT process. (a) Schematic of spatial control via SI-PET-RAFT in the polymerisation of DMAM on a DDMAT-functionalised substrate; (b) Optical micrograph of DMAM polymer brush (light) reproduction of an original photomask (inset) on silica (dark).¹⁷³

Another remarkable application of photochemistry is photoinduced 3D printing, widely known as vat photopolymerisation (VP). Generally, VP adopts a layer-by-layer curing procedure to transform a liquid photocurable resin into customised objects. For each layer printing, the light exposure will be confined to a precisely defined region in XY plane to initiate the photopolymerisation.¹⁷⁴ Also, the printing thickness per layer and curing time per layer can be changed to achieve adjustable Z-direction resolution as needed. There have been many VP technologies developed since 1980s, such as stereolithography (SLA), digital light processing (DLP), continuous liquid interface production (CLIP), volumetric stereolithography, and others.¹⁷⁵⁻¹⁷⁸ More information regarding to VP technologies will be detailed in **Section 2.3**.

2.2.1.3 Light intensity and wavelength variation

In general, extrinsic rate control for thermal polymerisation processes mainly relies on the change of reaction temperature. In comparison, photopolymerisation performs rate control via not only temperature, but more importantly light intensity and wavelength selection, which are more easily adjusted and can offer more instantaneous control.

At a given irradiation wavelength, the light intensity determines the number of photons irradiated from the light source. By increasing the light intensity, the photon flux increases, which then facilitates photoexcitation. As such, more propagating radicals can be generated, eventually leading to a faster polymerisation rate.¹⁷⁹ Notably, this process is temperature independent. Bai and co-workers successfully demonstrated polymerisation rate control via the manipulation of light intensity in photomediated RAFT polymerisation.¹⁸⁰ Using long-wave UV irradiation ($\lambda > 320$ nm) enabled direct photolysis of a trithiocarbonate compound to trigger RAFT polymerisation of MA. Moreover, with an increasing light intensity from 3 to 48 mW/cm², the induction period was dramatically reduced, and the polymerisation rate was promoted significantly (**Figure 2.12**). The result indicated that higher UV light intensity accelerated the decomposition of the trithiocarbonate compound.

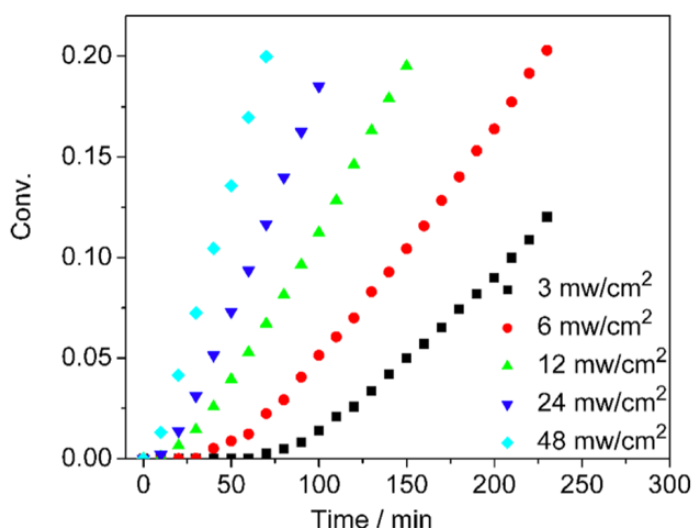


Figure 2.12 The effect of UV light intensity on polymerisation rates.¹⁸⁰

Light wavelength selection plays an important role in affecting the photoinitiation efficiency and reaction rate in photopolymerisation, as photoinitiators or PCs have

different light absorption at different wavelengths. Short wavelength ($\lambda < 350$ nm) UV irradiation was commonly used in early living photopolymerisation systems.^{2, 73, 181} Although these systems offered good control, there are many disadvantages of using high energy UV light, such as reactant and product degradation caused by prolonged UV exposure time, low light penetration depth and potential harm to long-term operation users.¹⁸²⁻¹⁸³ Therefore, photoinitiation systems have been shifting to employ longer wavelength irradiation. So far, a wide variety of chromophores which can be excited under long wavelength irradiation have been employed in many studies (**Figure 2.13**).¹⁸³ For instance, Boyer and co-workers compared five different porphyrin based PCs in RAFT polymerisation under both blue ($\lambda = 435$ -480 nm) and red light irradiation ($\lambda = 610$ -655 nm).¹⁵⁷ Among them, ZnTPP exhibited the best control over the polymerisation of MA. Moreover, as ZnTPP presents several absorption peaks from 435 to 655 nm, the polymerisation kinetics of MA were further investigated in the presence of ZnTPP under green ($\lambda_{\text{max}} = 522$ nm), yellow ($\lambda_{\text{max}} = 565$ nm), and orange ($\lambda_{\text{max}} = 595$ nm) lights. The kinetic results showed that the polymerisation rate relied on the light source, with the fastest to slowest polymerisation in the sequence of yellow > green > orange > red > blue light; the differences in polymerisation rates were mainly due to the different catalyst absorption under each wavelength range. Therefore, it demonstrates that polymerisation rates can be easily tuned via light wavelength manipulation.

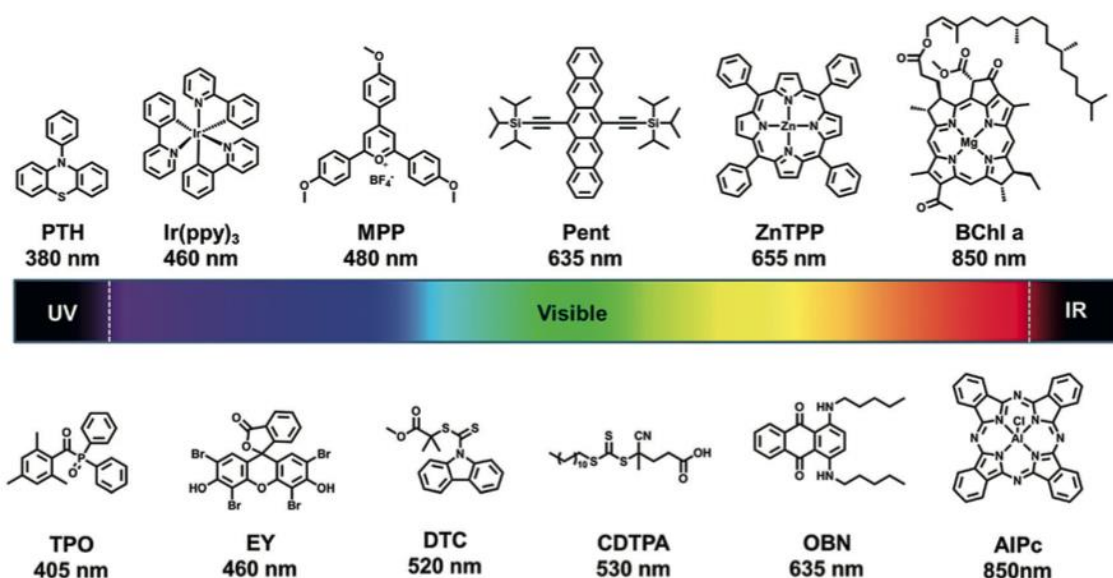


Figure 2.13 Examples of chromophores used in photopolymerisation. PTH: 10-phenylpheothiazine, Ir(ppy)₃: tris[2-phenylpyridinato-C2,N]iridium(III), MPP: 2,4,6-tris(*p*-methoxyphenyl)pyrylium tetrafluoroborate, Pent: 6,13-bis(triisopropylsilylethynyl)pentacene, ZnTPP: 5,10,15,20-tetraphenyl-21H,23H-porphine zinc, BChl *a*: bacteriochlorophyll *a*, TPO: (2,4,6-trimethylbenzoyl)diphenylphosphine oxide, EY: eosin Y, DTC: methyl 2-((9H-carbazole-9-carbonothioyl)thio)-2-methylpropanoate, CDTPA: 4-cyano-4-[(dodecylsulfanylthiocarbonyl)sulfanyl]pentanoic acid, OBN: oil blue N, AlPc: aluminium phthalocyanine.¹⁸³

Moreover, using different wavelengths to activate and control polymerisation enables chromic orthogonal reactions; one wavelength irradiation process can proceed independently of another to fabricate materials with various functions or properties.¹⁸⁴⁻¹⁸⁷ For instance, Boyer and co-workers employed an orthogonal reaction route to synthesise graft copolymers via the selective photoactivation of two PCs, pheophorbide *a* (PheoA) and ZnTPP, under different irradiation wavelengths (**Figure 2.14**).¹⁸⁸ PheoA was initially activated under red light ($\lambda_{\text{max}} = 635 \text{ nm}$) to produce PMMA homopolymers in the presence of a dithiobenzoate; subsequently, green light was used ($\lambda_{\text{max}} = 530 \text{ nm}$) to activate ZnTPP for the polymerisation of acrylate side chains in the presence of a trithiocarbonate. As such, a graft copolymer was successfully synthesised in one pot by simply switching the light from red to green.

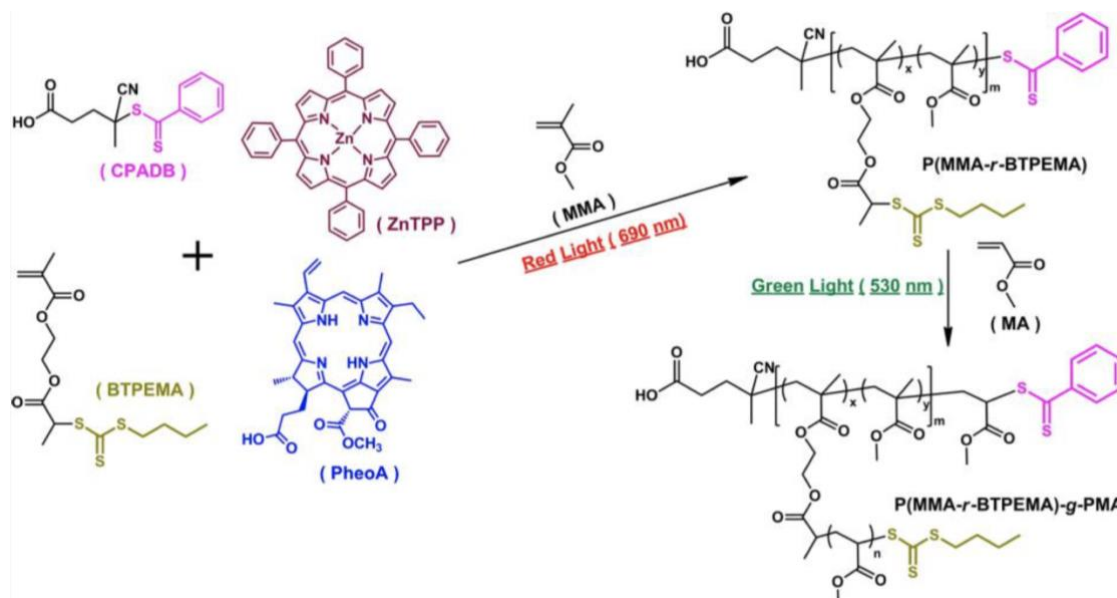


Figure 2.14 Reaction route for the synthesis of graft copolymers via the selective photoactivation of two PCs, PheoA and ZnTPP, in a one-pot, two-step process.¹⁸⁸

Multiple wavelength irradiation approaches can also be utilised for post-modification of pre-formed polymeric materials; two or more distinct wavelengths can be employed in one pot to activate polymerisation and subsequent post-modification.¹⁸⁹⁻¹⁹² Matyjaszewski and co-workers demonstrated a metal-free approach for the preparation of STEM gels by selectively activating trithiocarbonate compounds under different visible light irradiation coupled with RAFT process.¹³⁴ In Step 1, three types of primary PMMA STEM-0 gels were initially formed under green light irradiation with 4-cyano-4-[(dodecylsulfanylthiocarbonyl)sulfanyl]pentanoic acid (CDTPA) as the RAFT agent in the presence of crosslinker poly(ethylene glycol) dimethacrylate ($M_n = 750$) (PEGDMA₇₅₀) or bis[(2-propionate)ethyl methacrylate] trithiocarbonate (bisPEMAT)) and/or trithiocarbonate inimer (2-(2-(n-butyltrithiocarbonate)-propionate)ethyl methacrylate (BTPEMA)) (**Figure 2.15**). During this step, CDTPA was activated under green light, undergoing β -scission of the weak C-S bond to generate a tertiary carbon radical R^\bullet for the RAFT polymerisation of MMA. However, trithiocarbonate compound (bisPEMAT or BTPEMA) with R group composed of secondary carbon radical leaving group remained inert and was not involved in chain transfer reactions with tertiary carbon radicals. In Step 2, three STEM-0 gels were firstly infiltrated with a second monomer (MA or DMAm) and then irradiated under blue light which was able to activate both CDTPA and bisPEMAT or BTPEMA in the pre-formed networks to start a secondary

polymerisation. Therefore, STEM-1 gels with different mechanical properties and polarity (hydrophilicity/hydrophobicity) were finally synthesised.

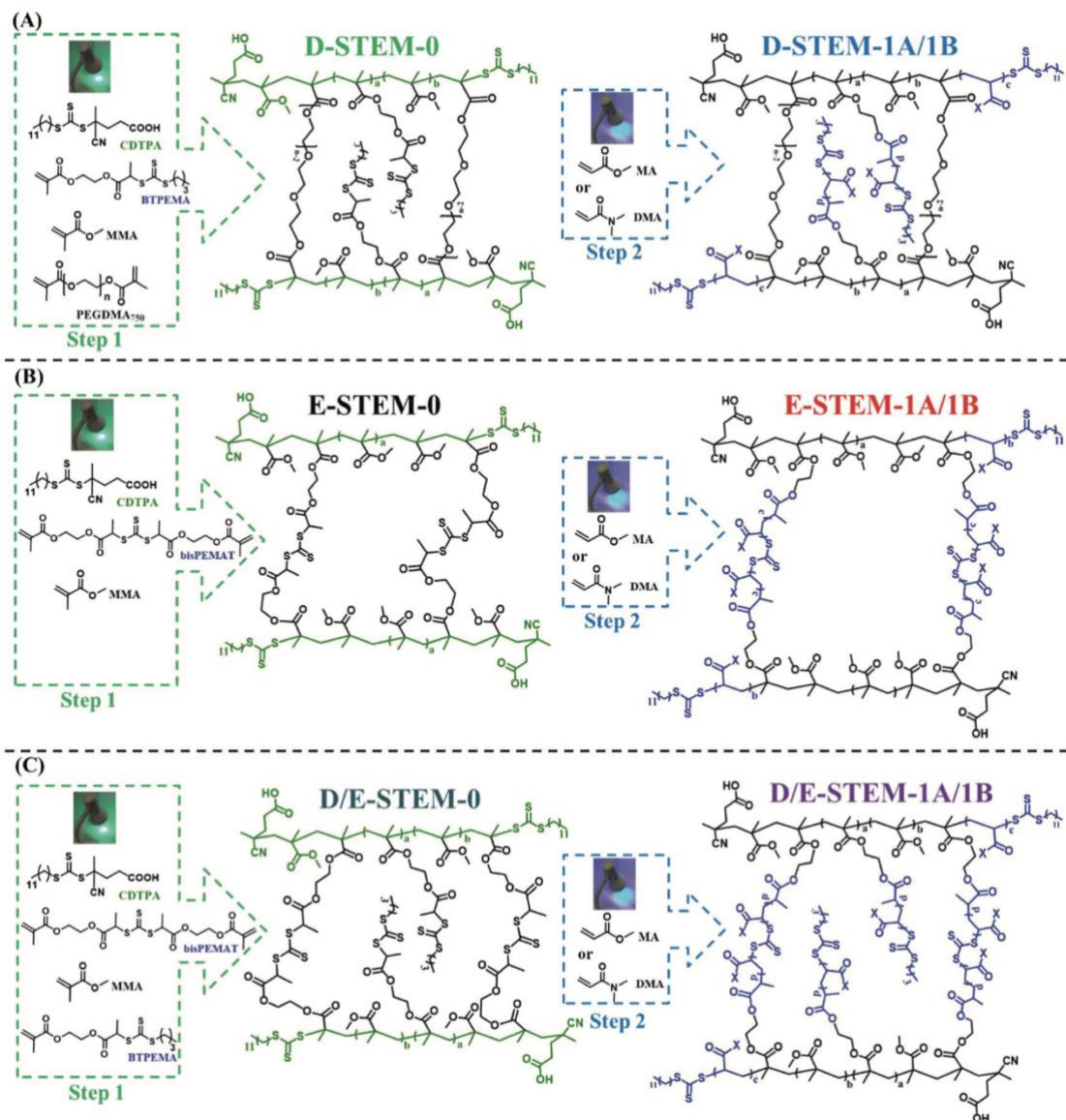


Figure 2.15 Synthesis of three types of STEM-0 networks (A–C, Step 1) under green light irradiation followed by post-modification in the presence of new monomers under blue light to generate STEM-1 gels (A–C, Step 2).¹³⁴

2.2.2 RAFT polymerisation initiated by conventional photoinitiators

Photoinduced RAFT polymerisation in the presence of external photoinitiators adopts a similar degenerative chain transfer mechanism to that of thermally initiated RAFT polymerisation. The photoinitiators are typically classified into two categories of Type I that generates radicals directly via bond homolytic cleavage upon absorption of light and Type II that generates radicals in conjunction with a co-initiator, such as an amine or thiol.¹⁹³⁻¹⁹⁴ Therefore, in a general photoinduced RAFT polymerisation process, photoinitiators are activated by light to generate initiating radicals, which can add to monomers as per the standard RAFT polymerisation process. As for an efficient photoinduced RAFT polymerisation, the selection of light sources, photoinitiators, and RAFT agents are of great significance.

In 2005, Cai and co-workers employed DDMAT in the polymerisation of MA in the presence and absence of photoinitiators.¹⁹⁵ To suppress the short-wavelength ($\lambda_{\text{max}} \leq 313$ nm) UV irradiation incurred severe photodegradation of RAFT agents which undermined the living character of polymerisation,¹⁸² long-wavelength ($\lambda_{\text{max}} \geq 365$ nm) UV irradiation was used. Initially, no polymerisation was observed in 6 hours in the absence of photoinitiators. As such, (2,4,6-trimethylbenzoyl)diphenylphosphine oxide (TPO) as the photoinitiator that has strong absorption from 365 to 405 nm was added, which efficiently initiated the polymerisation. A low dispersity ($\bar{D} = 1.09$) was finally achieved at high monomer conversions ($> 80\%$). Built on this work, the impacts of various UV wave range irradiations on living behaviour of RAFT polymerisation mediated by trithiocarbonates or dithioesters in the presence of TPO were further investigated in another report.¹⁹⁶ The results showed dithioesters decomposed more significantly than trithiocarbonates under full-wave UV irradiation ($\lambda = 254\text{-}405$ nm), due to the stronger absorption in the wave range 280-360 nm. By cutting off the short-wave range (below 320 nm), the undesired decomposition of trithiocarbonates was significantly suppressed from 9% to 4% under long-wave irradiation ($\lambda = 365\text{-}405$ nm), leading to a good control over the polymerisation of MA with a low dispersity ($\bar{D} < 1.1$) at 90% monomer conversion. By contrast, over 20% decomposition of dithioesters under long-wave irradiation was observed, resulting in a higher dispersity of polymerisation of MMA.

Later, Kwark and co-workers employed the xanthate methyl (ethoxycarbonothioyl)sulfanyl acetate to polymerise VAc in the presence of the photoinitiator bis(2,4,6-trimethylbenzoyl)phenylphosphine oxide under UV irradiation ($\lambda_{\text{max}} = 365 \text{ nm}$).¹⁹⁷ A rapid polymerisation with well-controlled molecular weights and low dispersities at high monomer conversions were achieved. However, the authors also claimed that the PVAc chain ends containing xanthate groups were not stable but can be decomposed under UV light irradiation.

Considering above findings, more attention has been drawn to use visible light to initiate the polymerisation. For instance, in the polymerisation of glycidyl methacrylate (GMA), visible light ($\lambda = 405\text{-}577 \text{ nm}$) was employed in the presence of 2-cyanoprop-2-yl(4-fluoro)dithiobenzoate (CPFDB) with the addition of TPO as the photoinitiator.¹⁹⁸ The photolysis of CPFDB was significant under UV irradiation, but was substantially suppressed under visible light. As a result, PGMA with a low dispersity ($\bar{D} = 1.2$) was synthesised. Moreover, ultrafast aqueous RAFT polymerisation in the presence of trithiocarbonates and TPO was demonstrated under visible light irradiation.¹⁹⁹⁻²⁰⁰ Except for obtaining well-controlled low dispersity polymers, a periodic light on and off process was also performed to reveal the temporal controllability of the photoinitiation systems.²⁰⁰

Inspired by these studies, the group of Cai firstly reported the visible light initiated polymerisation-induced self-assembly (PISA) of diacetone acrylamide (DAAm), using sodium phenyl-2,4,6-trimethylbenzoylphosphinate (SPTP) as a water-soluble photoinitiator under visible light irradiation at 25°C .²⁰¹ It was demonstrated that the insolubility of the PDAAm block effectively led to the *in situ* formation of spherical micelles. By using the same photoinitiator SPTP, Zhang and co-workers reported an aqueous photoinitiated PISA of 2-hydroxy-propyl methacrylate in the presence of a poly(ethylene glycol) (PEG) based macroRAFT agent under visible light at room temperature.²⁰² Remarkably, a broad range of polymer nanoparticle morphologies (e.g., spheres, worms, vesicles) were readily obtained by varying the degree of polymerisation (DP) and solids content.

Photoinduced RAFT polymerisation was also applied via photo-flow processing techniques, which is highly efficient for the synthesis of polymers in quantities that might be difficult to obtain via batch reactions. In 2016, Guthrie and co-workers firstly

demonstrated photoinduced RAFT polymerisation using a tubular continuous flow reactor in the presence of CDTPA as the RAFT agent and two different conventional photo-initiators.²⁰³ Under UV light irradiation ($\lambda = 310\text{-}380\text{ nm}$), the polymerisation of DMAM resulted in a good control, with a low dispersity ($\mathcal{D} < 1.3$) at high monomer conversions. Further, high loadings of photoinitiators and RAFT agent significantly increased the polymerisation kinetics, with approximately full monomer conversions after only 5 min irradiation at 30 °C. However, the dispersity was also slightly increased to around 1.6, which could be attributed to the increased chain termination under the forcing conditions.

Instead of using UV light, Boyer and co-workers utilised continuous flow reactors for the synthesis of nanoparticles with varied morphologies via alcoholic RAFT dispersion PISA under blue light ($\lambda_{\text{max}} = 460\text{ nm}$) irradiation.²⁰⁴ By varying the DP of the second block copolymer, diverse morphologies from spheres, to worms and vesicles can be formed. Moreover, it was also found that the impacts of photoinitiators on polymerisation rates were more crucial in the case of using acrylate-based macroRAFT agent than that of using methacrylate-based macroRAFT agent.

More information of photoinduced RAFT polymerisation in the presence of photoinitiators will not be detailed here but can be found elsewhere.²⁰⁵⁻²⁰⁸

2.2.3 RAFT polymerisation via iniferter polymerisation mechanism

The iniferter (referring to initiator-transfer-agent-terminator) polymerisation which was actually discovered before RAFT polymerisation was firstly employed by Otsu and co-workers in 1982.^{2, 73} Although it was proposed that photoiniferter polymerisation proceeds via a degenerative chain transfer process, unlike conventional photo-induced RAFT polymerisation, no exogenous radical initiators are needed in photoiniferter polymerisation (**Figure 2.16**). Irradiated by UV light, thiocarbonylthio compounds undergo β -scission of the weak C-S bond to generate a stabilised thiocarbonylthio radical and an active carbon-centered radical capable of adding across monomer vinyl bonds to initiate polymerisation. Subsequently, degenerative chain transfer process occurs between propagating radicals and iniferters which are not cleaved by photolysis which is similar to the RAFT equilibrium process. Finally, the stabilised thiocarbonylthio radical can recap a growing polymer chain to produce a dormant macroiniferter, which can be reactivated again upon further irradiation.^{42, 209-211}

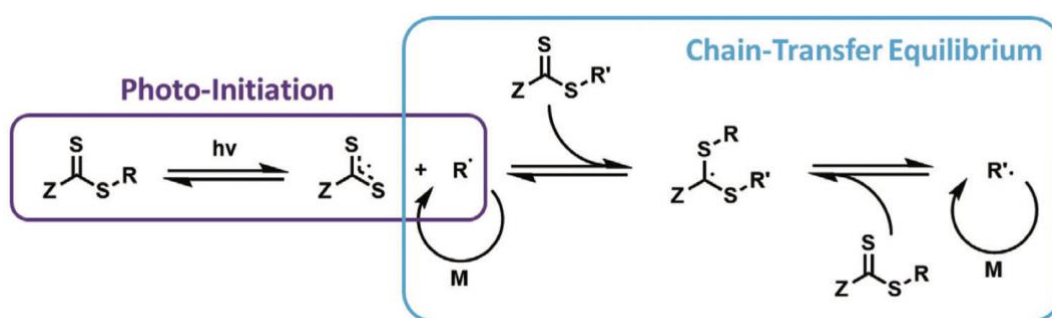


Figure 2.16 Schematic process of RAFT photoiniferter polymerisation.²¹¹

UV-light induced photoiniferter polymerisation has drawn great attention in early investigations. However, long-term UV irradiation inevitably led to side reactions, such as the direct photolytic degradation or termination reactions of iniferters, finally resulting in poor control over the polymerisation at high monomer conversions and limiting the overall livingness.²¹² For instance, Tardi and co-workers employed *p*-xylylene bis-(*N,N*-diethyldithiocarbamate) as photoiniferter in the polymerisation of BA.²¹³ A dramatic loss of active end group during polymerisation was found, which was partially attributed to the recombination of two dithiocarbamyl radicals to form tetraethylthiuram disulfide. Also, evidence has shown that the dithiocarbamate groups were degraded during the polymerisation, even though the mechanism could not be verified. As a result, it was

claimed that the polymerisation process was not truly living, and full control of the molar mass of the polymers was problematic. In a different report, Turner and Blevins demonstrated that under UV light, the dithiocarbamate irreversibly degraded to form CS₂ during the polymerisation, leading to the loss of the living nature of the functional chain-end and a high dispersity.²¹⁴ To suppress the side reactions and improve the control of the polymerisation, long-wavelength light irradiation is preferable.

In 2013, Bai and co-workers conducted a systematic study of the influence of light intensity, wavelength, and iniferter concentration on the photo-iniferter polymerisation under long-wavelength UV irradiation ($\lambda_{\text{max}} > 320 \text{ nm}$).¹⁸⁰ In this work, a narrow dispersity ($\mathcal{D} = 1.09$) of the linear PMA at a relatively high monomer conversion was obtained in the presence of DDMAT. It was reported that the rate of polymerisation was strongly dependent on both the concentration of DDMAT and the light intensity. Also, a high concentration of DDMAT was the key to the good control of the polymerisation. However, a low concentration of DDMAT led to poor control and a broad molecular weight distribution, which was due to the irreversible degradation of DDMAT at the low concentration. The authors also claimed that the structure of the iniferter can affect the living behaviour of the photo-iniferter polymerisation. In comparison with the polymerisation mediated by dithioesters,^{182, 196} high concentrations of trithiocarbonates can provide a better control at a high monomer conversion and maintain the livingness of the polymerisation.^{154, 215-216}

Later, Johnson and co-workers employed a bis-norbornene trithiocarbonate in the polymerisation of NIPAAM under long-wavelength UV irradiation ($\lambda_{\text{max}} = 352 \text{ nm}$).²¹⁷ Temporal control was demonstrated by switching the light “on” and “off”. As shown in **Figure 2.17**, a linear relationship between the molar mass and monomer conversion was observed across several irradiation cycles, with the final dispersity close to 1.1 at a high monomer conversion ($> 80\%$). Interestingly, sunlight was also used to initiate the polymerisation of NIPAAM in the presence of the bis-norbornene trithiocarbonate, obtaining the polymer with a lower dispersity ($\mathcal{D} = 1.09$) at monomer conversion over 70% in 5 h. This implies the potential of using visible light to initiate RAFT iniferter polymerisation.

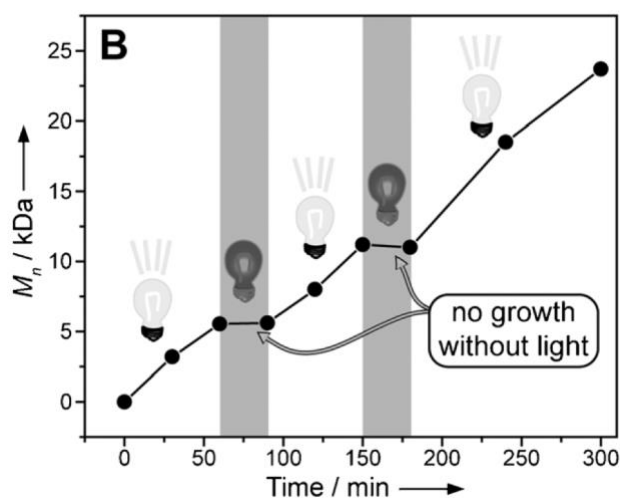


Figure 2.17 Temporal control over the polymerisation of NIPAAM in the presence of bis-norbornene trithiocarbonate under UV light irradiation.²¹⁷

In 2015, Boyer and co-workers pioneered the iniferter-mediated polymerisation of MMA and MA in the presence of four different thiocarbonylthio compounds under blue, green and red lights.¹⁵⁵ They found the structure of the RAFT agents played a vital role in controlling the polymerisation. Dithiobenzoate (4-cyano-4-(phenylcarbonothioylthio) pentanoic acid, CPADB) and trithiocarbonate (2-(butylthiocarbonothioylthio) propanoic acid, BTPA) with a secondary R group failed to initiate the polymerisation of MA or MMA, whereas trithiocarbonates (CDTPA, and DDMAT) with a tertiary R group can be used under blue and green light. Moreover, in the polymerisation of MMA, CDTPA offered a better control over the molecular weight distribution ($\bar{D} = 1.1$) under green light than that ($\bar{D} > 1.2$) of blue light. This could be explained as the higher energy of blue light leading to the photolytic degradation of CDTPA. The influence of RAFT agent and monomer structure on visible light induced photoiniferter polymerisation was also extensively investigated in Qiao's work.^{156, 218-219} Later, the influence of Z group with different electron withdrawing substituents on the initiation efficiency of iniferter polymerisation was explored by Konkolewicz's group.²²⁰ They concluded that electron donating groups can facilitate carbon-sulfur bond homolysis, in turn accelerating fragmentation procedure. By contrast, electron withdrawing groups inhibit homolytic cleavage, leading to a retarded reaction.

So far, RAFT photo-iniferter polymerisation has been applied in many different fields, as the controlled polymerisation without adding exogenous initiators, the high livingness of

the polymer chain end, multi-selection of various light sources, and the spatial and temporal control offer great benefits. One of the most important applications of this technique is to synthesise ultrahigh molecular weight (UHMW) polymers. Although UHMW polymers have been achieved via some RDRP techniques, specialised reaction conditions, such as high pressures or heterogeneous reactions were required.²²¹⁻²²³ In comparison, the preparation of UHMW polymers via photo-iniferter polymerisation can be performed in a mild condition. For instance, Sumerlin and co-workers have demonstrated the synthesis of UHMW polymers under long-wavelength UV irradiation ($\lambda_{\text{max}} = 365 \text{ nm}$) using thiocarbonylthio compounds in water at 35 °C.²²⁴ A rapid polymerisation was observed by using xanthate, obtaining an M_n of $2.47 \times 10^6 \text{ g/mol}$ in just 5 min. Extending the reaction time to 2 h, a UHMW polymer of $8.57 \times 10^6 \text{ g/mol}$ with a low dispersity ($\mathcal{D} = 1.17$) was finally obtained. In another report, the authors used benzyl maleimide (BzMIIm) as a comonomer to synthesise functional P(St-*alt*- BzMIIm) under blue light irradiation ($\lambda_{\text{max}} = 450 \text{ nm}$) in dioxane, obtaining the M_n of $2.4 \times 10^6 \text{ g/mol}$ at low dispersity ($\mathcal{D} = 1.10$).²²⁵

Another interesting application of this technique is to produce expandable networks which can be post-modified with desired properties and functions with the incorporation of iniferters in the primary networks.^{129, 226} The research work of Johnson's group in 2013 was possibly the first example to demonstrate the expandable network via RAFT photo-iniferter polymerisation.²¹⁷ Initially, a crosslinked gel incorporated with the TTC units in the primary network was prepared. By exposure to sunlight, the TTC units were reactivated and allowed the addition of new monomers into the network, obtaining a new gel with an increased swelling ratio in DMSO (**Figure 2.18**). Moreover, numerous studies have been performed to produce nanostructured materials with precise architectures via iniferter polymerisation,²²⁷⁻²²⁹ including bottlebrush and comb-like polymers by Matyjaszewski and co-workers.¹³³ More applications of RAFT photo-iniferter polymerisation will not be detailed here but can be found elsewhere.²³⁰⁻²³²

2.2.4 Photoinduced electron/energy transfer (PET)-RAFT polymerisation

The concept of PET-RAFT polymerisation was firstly introduced by Boyer and co-workers in 2014.⁶¹ The mechanism was proposed to undergo an electron transfer process between a PC and a thiocarbonylthio compound, followed by a RAFT polymerisation process (**Figure 2.19(A)**). Under light irradiation, the PC was excited to a higher energy level which was subsequently able to reduce the thiocarbonylthio compounds to generate thiocarbonylthio anion and radical species (R^{\bullet} or P_n^{\bullet}). The radical species can initiate polymerisation of monomers or be deactivated by the oxidated PC^+ to reform the dormant species. An alternative proposed mechanism for PET-RAFT involves the energy transfer from the excited PC^* to the thiocarbonylthio compound to generate radical species to initiate the subsequent RAFT polymerisation (**Figure 2.19(B)**).²³³⁻²³⁵

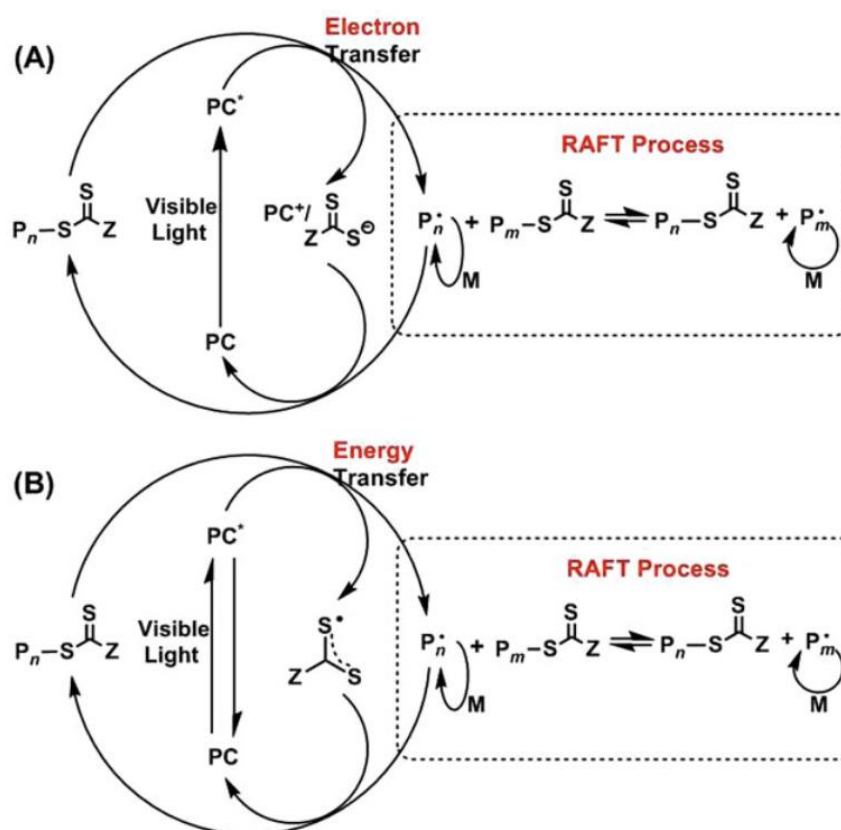


Figure 2.19 Proposed mechanism of PET-RAFT polymerisation in the presence of photocatalyst: (A) electron transfer and (B) energy transfer mechanism. PC: photocatalyst.²³⁵

PET-RAFT polymerisation has been demonstrated to be highly versatile in the first research work. By using an iridium-based PC, i.e., tris[2-phenylpyridinato-C2,N]iridium(III) (*fac*-[Ir(ppy)₃]), under blue light irradiation ($\lambda_{\text{max}} = 435 \text{ nm}$), a wide variety of monomers (both MAMs and LAMs) were successfully polymerised with a good dispersity control in the presence of different RAFT agents including dithiobenzoate, trithiocarbonate and xanthate.⁶¹ Remarkably, UHMW homopolymer of PMA with M_n over $2 \times 10^6 \text{ g/mol}$ at a low dispersity ($D = 1.08$) was synthesised by using BTPA as the RAFT agent. The BTPA end-group was subsequently confirmed by ¹H NMR and UV-Vis spectroscopy. Moreover, successive chain extensions of PMA were performed, obtaining a decablock P(MA)₁₀ copolymer with a high molecular weight ($M_n \approx 82\,000 \text{ g/mol}$). Temporal control was also demonstrated in the polymerisation of MMA. The polymerisation paused in the absence of light while continued when light was reintroduced.

Another important finding during their research was that PET-RAFT polymerisation can proceed in the air without degassing, but with some inhibition periods when (*fac*-[Ir(ppy)₃]) was employed. Oxygen is an excellent radical scavenger which can quench propagating radicals and inhibit the polymerisation. Deoxygenation procedure is therefore a necessity in conventional free radical polymerisation and RDRP process. However, in this work, it was found that the PC has strong reductive qualities to reduce oxygen into inactive species (such as superoxide). As such, an inhibition period of 3-4 h was observed in the polymerisation of MMA and MA, which was due to the reduction of oxygen by the PC. After the inhibition period, the polymerisation can proceed in a similar rate as that of the degassed reactions. The tris(bipyridine) ruthenium(II) chloride (Ru(bpy)₃Cl₂, Ru^(II)) was also employed to catalyse PET-RAFT polymerisation in the presence of oxygen. Although Ir(ppy)₃ was more efficient in giving higher monomer conversions under identical reaction conditions, Ru(bpy)₃Cl₂ was much less expensive and still provided good control.²³⁶ Also, the greater solubility of Ru(bpy)₃Cl₂ enabled PET-RAFT polymerisation to be performed in a wide range of reaction media, including DMSO, acetonitrile, methanol, toluene and water.²³⁷

Despite the highly efficient performance of these transition metal complexes in PET-RAFT polymerisation, the high cost and potential toxicity limits their implementation. The emergence of (metallo) organo-photocatalysts was expected to overcome these

shortcomings. Porphyrins and metalloporphyrins are important functional molecules which have strong absorption of visible light, widely existing in the form of chlorophyll, heme, and VB₁₂ on Earth.²³⁸ Chlorophyll *a* was reported as the first porphyrin-based structure employed as a PC to catalyse PET-RAFT polymerisation under visible LED light (λ_{max} = 461 and 635 nm) irradiation.¹⁵⁸ In this work, a broad range of functional and non-functional monomers were efficiently polymerised, obtaining polymers with controlled molecular weights at low dispersities. Later, bacteriochlorophyll *a* was utilised as the PC which enabled the PET-RAFT polymerisation to be performed under long wavelength irradiation from far-red (λ_{max} = 780 nm) to near-infrared (NIR) (λ_{max} = 850 nm).¹⁵⁹ Interestingly, polymerisation proceeded smoothly when the light passed through paper barriers before reaching the reaction vessel, which was mainly attributed to the deep penetration of NIR light.

Non-toxic and low cost metalloporphyrins were also employed in PET-RAFT polymerisation. During the investigation of metalloporphyrins to access their suitability as PC to catalyse PET-RAFT polymerisation, Boyer and co-workers found that ZnTPP was able to selectively activate trithiocarbonates under a broad range of wavelengths (from 435 to 655), but less effectively to activate other thiocarbonylthio compounds (dithiobenzoate, dithiocarbamate and xanthate).¹⁵⁷ Moreover, to compare with the polymerisation mediated by Ir(ppy)₃ or Ru(bpy)₃Cl₂, very little inhibition was observed in the presence of ZnTPP in the air. Further study of the oxygen tolerance mechanism was conducted by the same group in another report.⁴⁰ Briefly, it was claimed that the reactive triplet oxygen can be rapidly deactivated by the excited state ZnTPP into singlet oxygen through triplet-triplet annihilation (TTA), subsequently reacting with the solvent DMSO to form dimethylsulfone (DMSO₂) as a by-product (**Figure 2.20**).

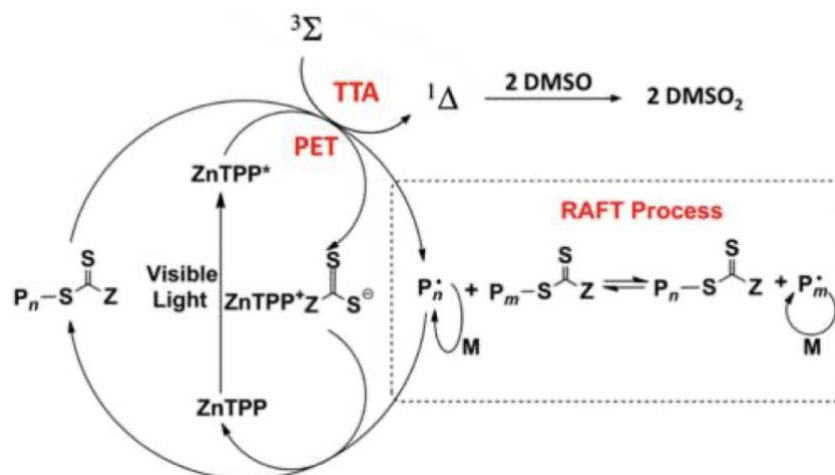


Figure 2.20 Proposed mechanism for PET-RAFT polymerisation mediated by ZnTPP in DMSO in the presence of oxygen. $^3\Sigma$ = ground state oxygen, $^1\Delta$ = singlet oxygen, TTA = triplet-triplet annihilation, DMSO₂ = dimethyl sulfone.⁴⁰

A series of organo-dyes including methylene blue, fluorescein, rhodamine 6G, Nile red and eosin Y (EY) was investigated in the polymerisation of MMA under blue light irradiation ($\lambda_{\text{max}} = 461 \text{ nm}$) via PET-RAFT process.²³⁹ EY was found to be the most effective PC to activate PET-RAFT polymerisation, due to its lower reduction potential, longer excitation lifetime and lower fluorescence quantum yield compared with other PCs.²³⁹ Moreover, the results for polymerisation in the air suggested that EY was able to quench oxygen to form superoxide anions (**Figure 2.21A**). The group also employed triethylamine (TEA) as an electron donor which was expected to improve the reaction yield in conjunction with EY. It was reported that in the presence of oxygen, the polymerisation rate of the TEA engaged reaction was doubled that of the reaction in the absence of TEA. In addition, the induction period was dramatically reduced, indicating that TEA improved the effectiveness of oxygen consumption. It was proposed that EY was reduced to form radical anion ($\text{EY}^{\bullet-}$) via an electron transfer from the electron donor (TEA). Subsequently, one part of $\text{EY}^{\bullet-}$ played a role in reducing oxygen into inactive species, whereas the other part transferred an electron to the RAFT agent to generate an anionic group and a propagating radical for chain growth (**Figure 2.21B**). Another oxygen consumption mechanism demonstrated by the group of Qiao was that the anionic RAFT group reduced by tertiary amine can also convert oxygen into inactive superoxide anion.²⁴⁰ Finally, well-defined polymers were synthesised by optimising the concentration of EY and TEA under air.

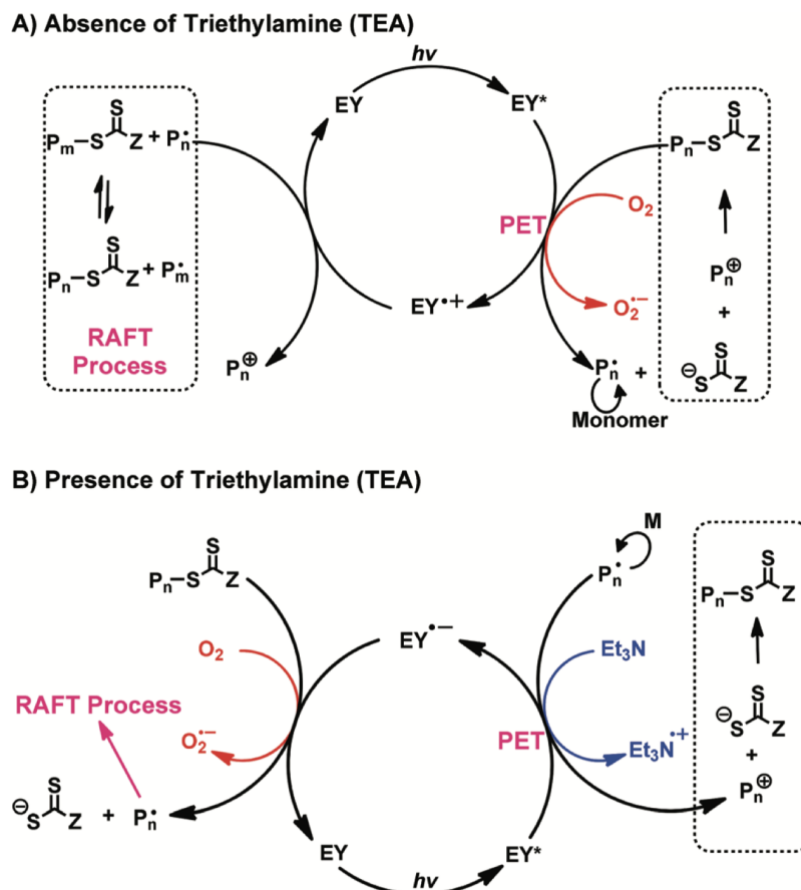


Figure 2.21 Proposed mechanisms for PET-RAFT polymerisation mediated by eosin Y in the absence (A) and presence (B) of triethylamine (TEA) and their oxygen tolerance.²³⁹

Upon this work, the catalytic performance of four different xanthene-based organic dyes including EY, erythrosin B (EB), rose bengal (RB) and phloxine B (PB) were further investigated.²⁴¹⁻²⁴² It was demonstrated that EB exhibited a higher efficiency than other catalysts in activating PET-RAFT polymerisation. Moreover, semiconductors, such as TiO_2 ,²⁴³⁻²⁴⁴ ZnO ²⁴⁵ or graphitic carbon nitride ($\text{g-C}_3\text{N}_4$),²⁴⁶ have also been utilised as PC for PET-RAFT polymerisation. The photocatalytic system mediated by semiconductors provides great benefits of excellent physicochemical stability, high oxidative capacity, low cost, and low toxicity, drawing great attention in recent years. **Table 2.2** provides a list of PCs which have been commonly used in PET-RAFT polymerisation. The PCs reported here are only a part of the broad classes of PCs employed for PET-RAFT polymerisation. More information can be found elsewhere.²⁴⁷⁻²⁵¹

Table 2.2 Examples of photocatalysts used in PET-RAFT polymerisations.

Photocatalyst	RAFT agents ^a	Oxygen tolerance	λ	ref.
Ir(ppy) ₃	CPADB, BTPA, BSTP, Xanthate	Non-degassed	B	61, 252-255
Ru(bpy) ₃ Cl ₂	CPADB, BTPA	Non-degassed	B	61, 236-237, 254
Chlorophyll <i>a</i>	CPADB, BTPA, BSTP, CDTPA, CDB, CPD	Non-degassed	B, R	158, 256
Bacteriochlorophyll <i>a</i>	CPADB	Degassed	R, FR, NIR	159
ZnTPP	CPADB, BTPA, BSTP, CDTPA, DTPA	Non-degassed	B, G, Y, R	40, 157, 188-189, 257-258
TPP	CPADB	Degassed	R	157
EY	CPADB, BTPA	Non-degassed	B, G	239, 241, 259-260
EB	BTPA, DTPA	Non-degassed	G	241-242
Fluorescein	CPADB, BTPA	Non-degassed	B	61
TiO ₂	CPADB	Degassed	UV	243-244
ZnO	CPADB	Degassed	UV	245
g-C ₃ N ₄	Benzyl dodecyl carbonotrithioate	Non-degassed	UV	246
PTH	Bis-azide TTC	Degassed	B	130

^aAbbreviations: BSTP: 3-(((benzylthio)carbonothioyl)thio)propionic acid; CDB: cumyl dithiobenzoate; CPD: 2-cyanopropan-2-yl benzodithioate; DTPA: 2-(((dodecylthio)carbonylthio)thio)propanoic acid; NIR: near infra-red; FR: far-red; R: red; Y: yellow; G: green; B: blue; UV: ultraviolet.

Overall, photomediated RAFT polymerisation is a versatile and robust technology for the synthesis of polymeric materials. Diverse photoinitiating systems and a wide range of light wavelength selections to activate polymerisation in combination with various

oxygen tolerance strategies enable this technology to be promisingly applied in many different fields.

2.3 Vat Photopolymerisation 3D printing

3D printing, also known as additive manufacturing, was firstly introduced in 1980s with the aim of producing customised objects which display high levels of complexity in geometry and function.^{178, 261} In contrast to conventional fabrication which needs complicated procedures of moulding, forging or machining, 3D printing allows faster transformation on computer-assisted designs (CAD) and manufacturing of customised products tailored to meet individual demands and other specific applications.¹⁷⁸ With the rapid development and innovations in material and machine design, 3D printing techniques have been widely employed in many different fields including dentistry,²⁶²⁻²⁶³ aerospace,²⁶⁴⁻²⁶⁵ automotive industry,²⁶⁶ electronics,²⁶⁷ medicine,²⁶⁸⁻²⁶⁹ and food industry²⁷⁰ by using a broad range of printing materials such as ceramics, metals and alloys, polymers, glass and bio-based materials.^{177, 271-272}

The American Society for Testing and Materials (ASTM) International has classified 3D printing technologies into seven main categories, including binder jetting, directed energy deposition, material extrusion, material jetting, VP, powder bed fusion and sheet lamination.²⁷³ Among these 3D printing techniques, VP has drawn special attention from material and polymer scientists due to the versatility of photochemistry.^{174, 274} The photocuring strategy behind VP is to use light to trigger polymerisation reaction in the presence of photoinitiating species, converting photocurable resins into solid materials.^{174, 177} The resins used to form 3D printed objects are typically composed of multifunctional (meth)acrylate- or epoxide-based monomers and oligomers; this provides thermoset materials with excellent mechanical performance of high modulus.²⁷⁵⁻²⁷⁶ To compare with other 3D printing technologies, VP has demonstrated superior advantages in performing spatiotemporal control and providing fast build rates and high printing resolution.¹⁷⁶ Moreover, using light as the external stimuli, the polymerisation process becomes less temperature sensitive, and can be controlled by selecting specific wavelength and light intensity.

Therefore, the following sections will focus on introducing various VP techniques, such as SLA, DLP and many others as well as their applications.

2.3.1 Laser scanning stereolithography (SLA)

It is widely believed that the term “stereolithography” (SLA) was coined by Hull’s patent in 1980s.²⁷⁷ It was proposed that the generation of 3D objects was layer by layer. **Figure 2.22** demonstrates the main components of an SLA instrument based on Hull’s concept of design.²⁷⁸ A general process of SLA printing starts with the design of a 3D model with CAD software, which will be subsequently converted to a standard tessellation language (STL) file. By decoding the STL file, the 3D model is cut into horizontal 2D slices with the information of cross-sections.²⁷⁹ Based on these information, the 3D model can be generated layer by layer.

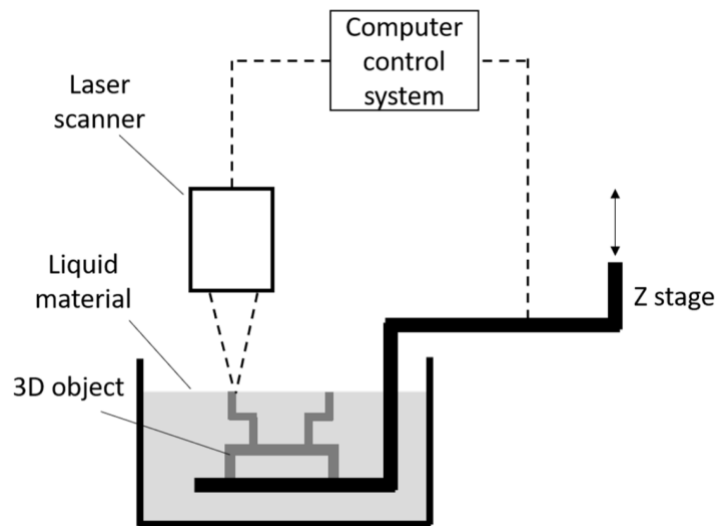


Figure 2.22 The concept of stereolithography.²⁷⁸

The principle behind SLA originates from the polymerisation and crosslinking reaction of the liquid resin in the vat induced by a focused laser beam scanning (usually in the UV-range).²⁸⁰ The spot size of the laser beam determines the accuracy of the print. The laser beam scanning is usually controlled by galvanometric mirrors, moving along the X-Y direction sequentially within the plane on the surface of photoresin. The curing time per layer therefore relies on the laser beam scanning speed and the dimension of the illuminated area.¹⁷⁸ The vertical resolution is determined by the light penetration depth, which can be improved by adding light absorbers to the photoresin. In a typical printing process, the platform of an SLA instrument is immersed in the vat. Once a layer is cured, the platform is lowered or raised in the Z direction with a fixed height of a layer. The curing process is repeated layer-by-layer until the whole object is printed.¹⁷⁷

SLA technology has been employed to investigate mechanical performance of materials 3D printed under different conditions. For instance, the study of mechanical properties of specimens 3D printed by using a Formlabs 'Form 2' SLA printer under different printing parameters was performed by the group of Qureshi.²⁸¹ It concluded that the layer thickness played a vital role in affecting both the material mechanical behaviour and the geometrical accuracy, due to its influence on the penetration of UV light through the layers. Moreover, the post-curing process had a significant impact on tensile properties of the 3D objects, with the samples exhibiting isotropic behaviour and obtaining dramatically increased elastic modulus and ultimate tensile stress. By using the same printer, Kiran and co-workers investigated the influence of build orientation, layer thickness, strain rate and size effect on mechanical properties of samples printed by using methacrylate-based photore sin.²⁸² Interestingly, it was found that the impact of different build orientations on mechanical properties of samples printed 'on edge' (0° - 90°) was not obvious (**Figure 2.23**). However, the 'FlatX' sample printed in a different plane exhibited reduced mechanical strength, which could be due to partial curing of larger cross-section areas.

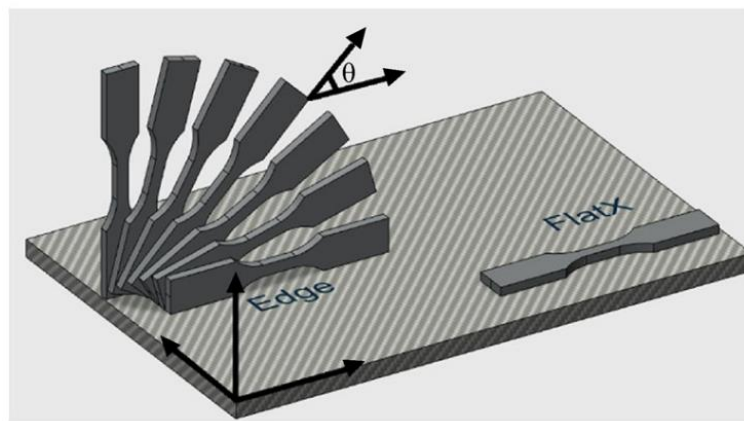


Figure 2.23 Different orientations of samples printed on platform (CAD representation).²⁸²

SLA technology has also gained great attention in biomedical applications and tissue engineering. In 2016, Minakuchi and co-workers printed dentures using methacrylate-based photore sin via SLA process. In this study, dentures were printed in three directions (0° , 45° , and 90°), with the highest trueness and precision occurred in the printing direction of 45° (**Figure 2.24**).²⁸³ Followed by this work, the same group also conducted the

investigation of the impact of printing direction on stress distribution on denture models.²⁸⁴ However, due to the cytotoxic nature of these photopolymers in the resin, recent research has moved on to synthesise biocompatible and biodegradable materials for 3D printing. For example, Akkus and co-workers printed ear-shaped scaffolds by using a hybrid biocompatible resin formulated with natural and synthetic polymers (chitosan and poly(ethylene glycol) diacrylate (PEGDA)).²⁸⁵ It was found that the mechanical properties, cell adhesion and printability were determined by the feed-ratio of chitosan and PEGDA.

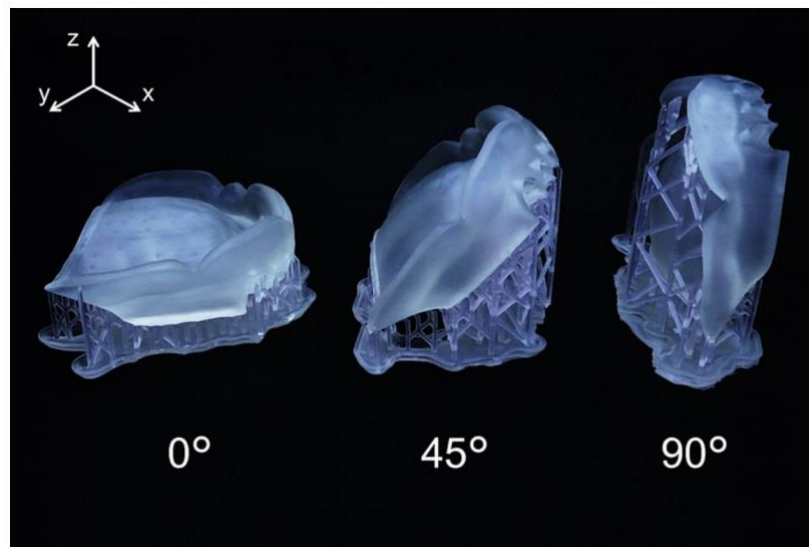


Figure 2.24 Dentures 3D printed via SLA process in three different directions (0°, 45°, and 90°).²⁸³

In addition, SLA technique has been extensively employed to produce smart materials via 4D printing, which enables 3D objects to transform into another structure over time under external stimuli.²⁸⁶ Shape memory materials are one of the main classes of smart materials. Tanarro and co-workers fabricated complex micro-vascular shape memory polymer actuators, such as microclaw and spring, via SLA-based printing process.²⁸⁷ Moreover, Magdassi and co-workers demonstrated the generation of shape memory-based 3D objects printed via SLA process, which can be used in flexible and responsible electrical circuits.²⁸⁸ Later, Huang and co-workers synthesised epoxy-acrylate hybrid photopolymer for the fabrication of shape memory polymers by using an SLA 3D printer. The 3D printed material demonstrated a rapid shape recovery rate, with the recovery process taking less than 20s.²⁸⁹

Overall, SLA technology is also progressing in many other fields, such as sensors, piezoelectric materials, soft actuators, which can be found in other reviews.^{175, 290-296}

2.3.2 Mask projection stereolithography (MPSL)

In contrast to laser scanning SLA which adopts a point-by-point printing method, mask projection stereolithography (MPSL) can print each layer of objects in one exposure by projecting mask images onto the resin surface. As such, MPSL provides a higher printing speed than SLA.^{176, 178} DLP is the most representative MPSL technique, which employs a digital light projector to generate dynamic mask images (**Figure 2.25**).²⁹⁵ The lateral resolution of DLP is usually in the range of 10-50 μm , greatly depending on the resolution of the digital projector. The vertical resolution is highly related to the light penetration and scattering, which can be improved with the addition of light absorbers and polymerisation facilitators.^{178, 295}

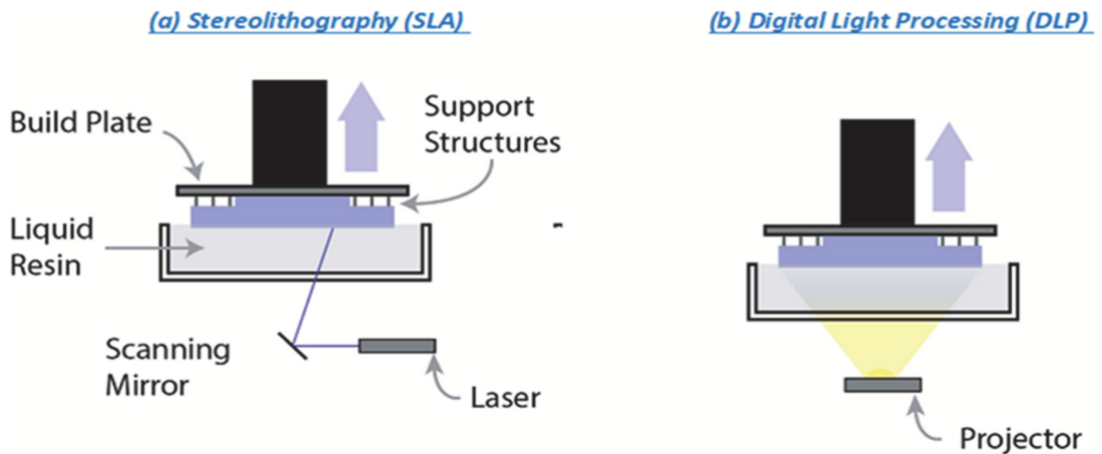


Figure 2.25 Comparison between the working principle of (a) SLA and (b) DLP 3D printers.²⁹⁵

DLP has been employed in many different applications, such as dentistry,²⁹⁷⁻²⁹⁸ biomedical applications and tissue engineering,²⁹⁹⁻³⁰¹ and production of shape memory materials and soft actuators.³⁰²⁻³⁰³ However, the light source of these applications is mainly reliant on UV light, which has many potential disadvantages, including low light penetration depth, threat to cellular photodamage and causing degradation of reactant and products.³⁰⁴⁻³⁰⁵ The progress in LED light-source technology in combination with a broad range of photoinitiators has facilitated the development of visible light initiating systems for photopolymerisation.³⁰⁶⁻³⁰⁸ Stampfl and co-workers demonstrated the fabrication of 3D objects in the presence of methacrylate-based photoresin, using DLP 3D printer equipped with 405 nm projector.³⁰⁹ Three visible light photoinitiators were employed,

with the ethyl(2,4,6-trimethylbenzoyl)phenylphosphinate offering the highest double-bond conversion and best mechanical properties. Surprisingly, the tensile strength and elongation at break of the objects 3D printed on this 405 nm DLP printer were even competitive with those printed with other 3D printing techniques. Followed by this work, visible light induced DLP 3D printing has developed rapidly and utilised in many applications, such as bioprinting and multimaterial fabrication.³¹⁰⁻³¹⁴ Recently, Page and co-workers demonstrated a rapid high-resolution DLP 3D printing (build speed up to 45 mm/h and feature size < 100 μm) activated by using four different visible light sources including violet, blue, green and red (**Figure 2.26**).³¹⁵ The addition of coinitiators and opaquing agents was critical to increase the printing speed and improve spatial resolution. Moreover, inert gas was also necessary for printing under green and red lights, due to the high oxygen sensitivity of the two PC (RB and ZnTPP). It was finally demonstrated that with optimised printing conditions, similar mechanical properties of the objects printed under different wavelengths can be achieved. This study was set as a good example to demonstrate the versatility of DLP printing technique which is compatible with a wide range of light sources and provides a high print speed.

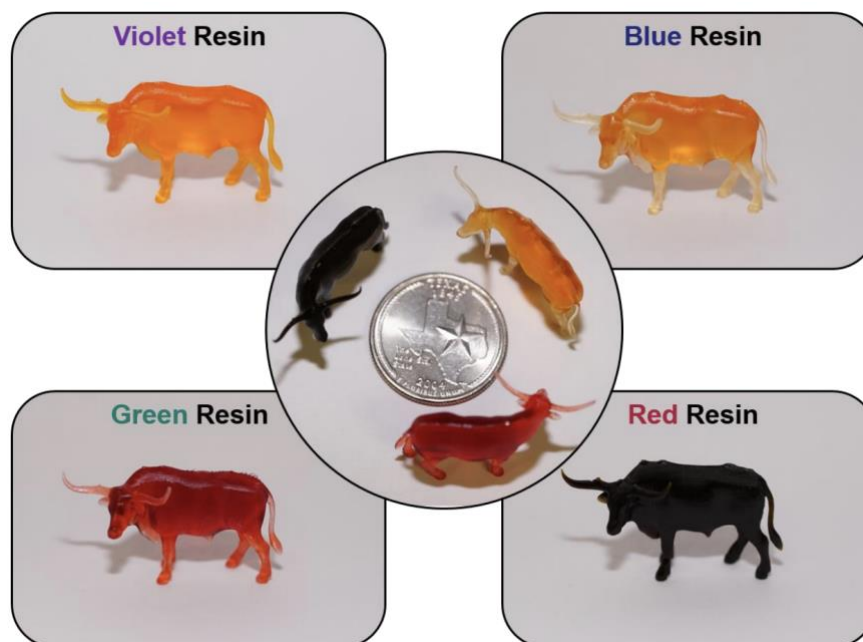


Figure 2.26 Optical images of 3D printed longhorns with corresponding resins indicated with the optimised resin composition and a slicing thickness of 100 μm .³¹⁵

An important extension of DLP technique is continuous liquid interface production (CLIP), which was introduced by DeSimone and co-workers in 2015 (**Figure 2.27**).³¹⁶

An oxygen-permeable “dead zone” which is a thin uncured resin interface between the UV-transparent window and the advancing part is introduced to maintain a continuous object production. Oxygen inhibition is inevitably encountered in free radical polymerisation in air, stopping chain propagation by combining with free radicals to form peroxides or quenching photoinitiator.⁶¹ However, CLIP takes the advantage of this feature to create an uncured liquid layer, in turn maintaining the cured part to be continuously exposed to the light to print while elevating. As for SLA or DLP printers, after printing each layer, the platform needs to be moved for the separation of cured parts from the surface of the vat and for the renewal of liquid resin, then repositions to continue printing. As a result, the printing speed of CLIP is up to two orders of magnitude faster compared to other MPSL techniques.³¹⁶

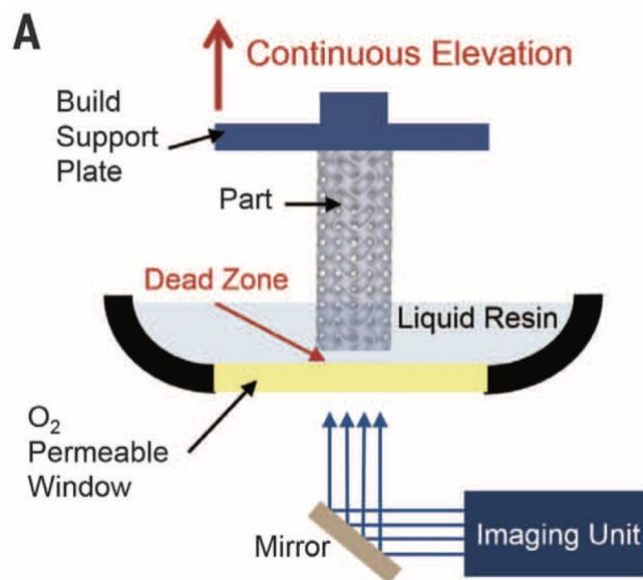


Figure 2.27 Demonstration of the working principle of CLIP 3D printer.³¹⁶

In 2016, DeSimone and co-workers further demonstrated the advantages of CLIP in the fabrication of layerless printing with advanced isotropic mechanical behaviour.³¹⁷ To compare with existing SLA or DLP 3D printing techniques, the staircasing effect on the objects 3D printed via CLIP process can be substantially controlled by decreasing slicing thickness without compromising on printing speed (40 mm/h) (**Figure 2.28**). Moreover, isotropic mechanical properties of the materials printed in the presence of acrylate-based photoresin were still achieved even with varied printing orientation and slicing thicknesses, which is always regarded as a challenge for other VP techniques.^{282, 318-319} Overall, the continuous fabrication of CLIP enables 3D printed materials with improved

surface properties without sacrificing on printing speed as well as isotropic mechanical properties.

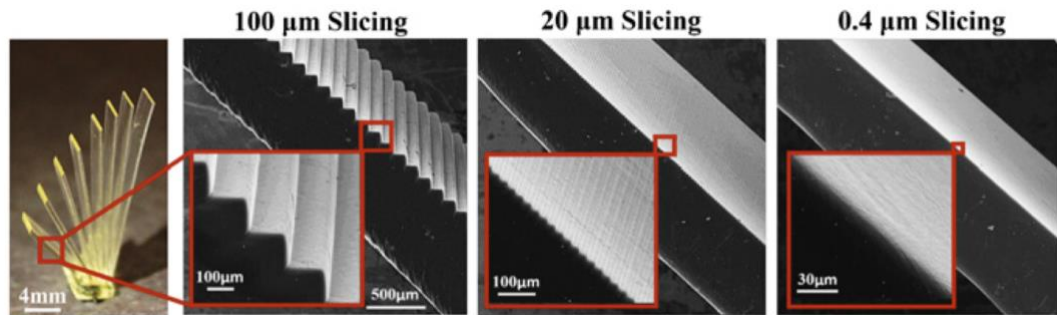


Figure 2.28 The slope feature of the open book fabricated with the same build speed of 40 mm/h but with different slicing thicknesses (100, 20 and 0.4 μm).³¹⁷

2.3.3 Volumetric stereolithography

Distinguishing from SLA and MPSL which adopt a layer-by-layer fabrication procedure, volumetric stereolithography is a new VP technique which can create an object directly in three dimensions. In 2017, inspired by the holographic lithography, Spadaccini and co-workers firstly implemented three orthogonal beams to project target patterns into a photoresin for the fabrication of complex 3D volumes as a unit operation.³²⁰ This technique significantly increased the build speed of 3D geometries on a time scale of seconds.

Followed by this work, a promising volumetric stereolithography technique realised by tomographic reconstruction was explored by Taylor and co-workers.³²¹ This technique was also named as computed axial lithography (CAL). It can selectively cure the liquid photoresin in a contained volume. As shown in **Figure 2.29A** and **B**, a container of liquid resin is rotated at a set rate in synchronisation with computed patterns of light irradiated from the projector. After the resin has been exposed from all angles, the accumulation of light dose is created. When the amount of absorbed light dose accumulates above a threshold value, the resin will be solidified, thus the object can be fabricated as a whole, without the presence of layer structures as observed in DLP (**Figure 2.29C** and **D**). However, the print feature size was limited to 300 μm .

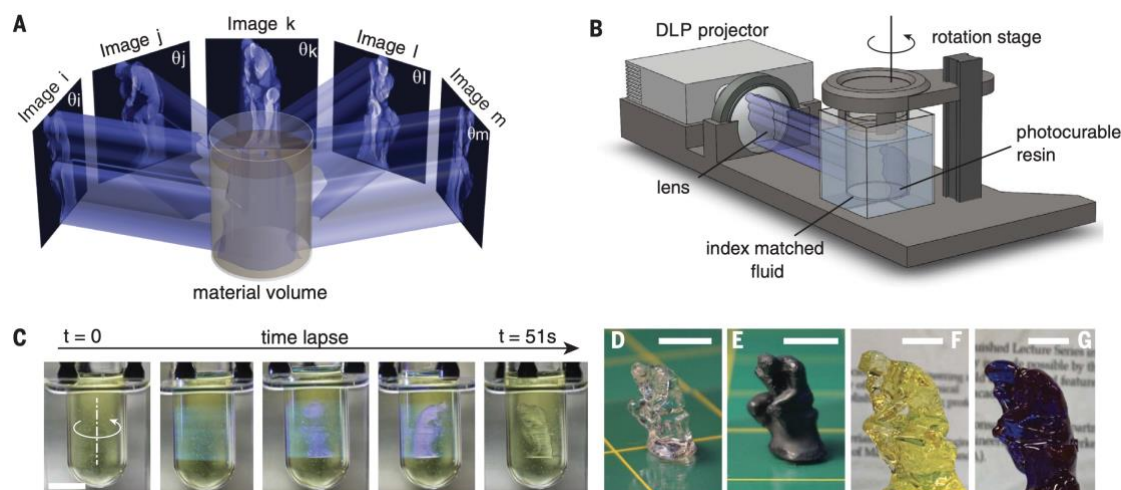


Figure 2.29 Demonstration of CAL volumetric fabrication. (A) the concept of CAL volumetric fabrication; (B) the components of CAL system; (C) time-sequenced views of the object during a CAL print; (D) the printed object after washing away uncured resin; (E) the object from (D) painted for clarity; (F) the same geometry of (D) in larger size; (G) opaque version of the geometry in (F) by using crystal violet dye in the resin. Scale bars: 10 mm.³²¹

Later, Moser and co-workers explored a low-extendue illumination system which improved the resolution of tomographic volumetric stereolithography to 80 μm . Moreover, a feedback-enhanced system was integrated to precisely control the photopolymerisation kinetics and improve the geometric accuracy of the object solidification.³²² In another study, Hecht and co-workers reported an xolography for linear volumetric 3D printing.³²³ Without any computer-aided optimisation and feedback systems, this technique exhibited a resolution about ten times higher than previous known macroscopic volumetric stereolithography. The advancement of tomographic volumetric stereolithography paves the way of the production of objects on a microscopic and nanoscopic level.

Recently, Yang and co-workers employed a rapid dual colour tomographic volumetric 3D printing to realise internal mechanical property gradients with high precision.³²⁴ In this work, blue light was utilised to polymerise acrylate monomers, while UV light was utilised for the polymerisation of epoxy monomers. The orthogonal chemistry allowed the polymerisation of different monomers selectively, in turn creating a functionally graded material with an average modulus gradient of 5 MPa/ μm . This approach opens the

gate for the fabrication of materials with multiscale structures which is highly demanded in tissue engineering.³²⁵

In another work, Levato and co-workers successfully demonstrated fast fabrication of large, complex free-form living tissue constructs by using cell-friendly hydrogel-based bioresins via a visible light induced volumetric stereolithography process (**Figure 2.30**).³²⁶ A high cell viability (85%) was also achieved. It was claimed that volumetric bioprinting allows the generation of geometrically complex, centimetre-scale objects in a time frame from seconds to tens of seconds, which has great potential for upscaling the production of hydrogel-based materials that can be widely used in clinically relevant grafts, regenerative medicine and soft robotics.

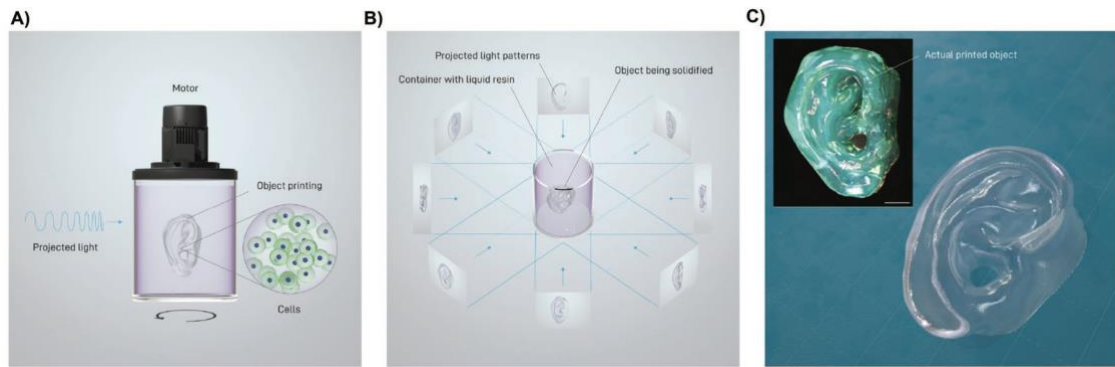


Figure 2.30 Demonstration of the volumetric bioprinting process. (A) the cell-laden gel resin container connected to a rotating platform; (B) the schematic of volumetric fabrication; (C) the final printed hydrogel-based human auricle model. Printing time = 22.7 s; scale bar = 2 mm.³²⁶

2.4 Summary

To summarise, the rapid development of RDRP techniques has provided chemists and scientists with powerful tools for polymer syntheses. In particular, RAFT polymerisation techniques have attracted great attention due to their ability to produce well-defined macromolecules with diverse architectures and chemical functionalities under various reaction conditions. Also, RAFT crosslinking polymerisation provides great benefits in preparing homogeneous networks. More significantly, the retention of the thiocarbonylthio polymer chain-ends throughout the RAFT polymerisation can be repeatedly activated by external stimuli to enable post-modification of the pre-formed polymers with desired properties and functionalities. Among various RAFT polymerisation techniques, photomediated RAFT polymerisation has been extensively employed due to the intrinsic benefits of light as an external stimulus, such as low cost and ubiquity, environmentally friendly nature, spatiotemporal control, and temperature independence. Also, various photoinitiating systems enable RAFT polymerisation to be performed in a broad range of light wavelengths. Additionally, attributed to diverse oxygen tolerance techniques, RAFT polymerisation can proceed in the open air without the complex procedure of deoxygenation.

Concurrently with the evolution of RDRP, VP 3D printing technology has developed promptly in the past few decades. VP techniques, such as SLA, DLP or CLIP have demonstrated superior advantages in performing spatiotemporal control and providing fast build rates and high printing resolution. However, these techniques currently adopt conventional photocuring method which is primarily reliant on non-living free radical or cationic polymerisation. Although this photocuring pathway has demonstrated the effectiveness and efficiency in 3D printing, it leads to limited control over polymer chain growth, crosslinked network architecture, and the final properties of polymeric materials. More importantly, the dead polymer chains produced via this process are unable to be reactivated for further chain growth, which prevents post-functionalisation of printed materials.

In this regard, the application of photomediated RAFT polymerisation in VP is expected to solve these problems to make functional polymeric materials. RAFT polymerisation performs control over polymer chain growth and network formation, allowing the tuning

of material properties. More importantly, the retention of the thiocarbonylthio polymer chain-ends in the network impart potential living characteristics to 3D printed materials, which can be reactivated by an external stimulus to enable post-functionalisation of the pre-formed networks. Further, due to the high compatibility of a broad scope of monomers in RAFT polymerisation, materials with selective functions and properties could be generated. Moreover, the high tolerance of oxygen and multiple photoinitiating system choices of photomediated RAFT polymerisation facilitates its application in 3D printing environment. Consequently, the application of photomediated RAFT polymerisation in VP appears to be a promising approach in the production of polymeric materials with advanced properties and diverse functionalities.

2.5 Reference

1. Szwarc, M., 'Living' Polymers. *Nature* **1956**, 178(4543), 1168-1169.
2. Otsu, T.; Yoshida, M., Role of initiator-transfer agent-terminator (iniferter) in radical polymerizations: Polymer design by organic disulfides as iniferters. *Die Makromolekulare Chemie, Rapid Communications* **1982**, 3(2), 127-132.
3. Matyjaszewski, K.; Gaynor, S.; Greszta, D.; Mardare, D.; Shigemoto, T., 'Living' and controlled radical polymerization. *Journal of Physical Organic Chemistry* **1995**, 8(4), 306-315.
4. Georges, M. K.; Veregin, R. P. N.; Kazmaier, P. M.; Hamer, G. K., Narrow molecular weight resins by a free-radical polymerization process. *Macromolecules* **1993**, 26(11), 2987-2988.
5. Wang, J.-S.; Matyjaszewski, K., Controlled/"living" radical polymerization. atom transfer radical polymerization in the presence of transition-metal complexes. *Journal of the American Chemical Society* **1995**, 117(20), 5614-5615.
6. Kato, M.; Kamigaito, M.; Sawamoto, M.; Higashimura, T., Polymerization of Methyl Methacrylate with the Carbon Tetrachloride/Dichlorotris-(triphenylphosphine)ruthenium(II)/Methylaluminum Bis(2,6-di-tert-butylphenoxide) Initiating System: Possibility of Living Radical Polymerization. *Macromolecules* **1995**, 28(5), 1721-1723.
7. Chiefari, J.; Chong, Y.; Ercole, F.; Krstina, J.; Jeffery, J.; Le, T. P.; Mayadunne, R. T.; Meijs, G. F.; Moad, C. L.; Moad, G., Living free-radical polymerization by reversible addition-fragmentation chain transfer: the RAFT process. *Macromolecules* **1998**, 31(16), 5559-5562.
8. Gaynor, S. G.; Wang, J.-S.; Matyjaszewski, K., Controlled Radical Polymerization by Degenerative Transfer: Effect of the Structure of the Transfer Agent. *Macromolecules* **1995**, 28(24), 8051-8056.
9. Percec, V.; Barboiu, B., "Living" Radical Polymerization of Styrene Initiated by Arenesulfonyl Chlorides and CuI(bpy)_nCl. *Macromolecules* **1995**, 28(23), 7970-7972.
10. Moad, C. L.; Moad, G., Fundamentals of reversible addition-fragmentation chain transfer (RAFT). *Chemistry Teacher International* **2021**, 3(2), 3-17.
11. Shipp, D. A., Reversible-Deactivation Radical Polymerizations. *Polymer Reviews* **2011**, 51(2), 99-103.
12. Corrigan, N.; Jung, K.; Moad, G.; Hawker, C. J.; Matyjaszewski, K.; Boyer, C., Reversible-deactivation radical polymerization (Controlled/living radical polymerization): From discovery to materials design and applications. *Progress in Polymer Science* **2020**, 111, 101311.
13. Braunecker, W. A.; Matyjaszewski, K., Controlled/living radical polymerization: Features, developments, and perspectives. *Progress in Polymer Science* **2007**, 32(1), 93-146.
14. Shanmugam, S.; Matyjaszewski, K., Reversible Deactivation Radical Polymerization: State-of-the-Art in 2017. In *Reversible Deactivation Radical Polymerization: Mechanisms and Synthetic Methodologies*, American Chemical Society: 2018; pp 1-39.
15. Jenkins, A. D.; Jones, R. G.; Moad, G., Terminology for reversible-deactivation radical polymerization previously called "controlled" radical or "living" radical polymerization (IUPAC Recommendations 2010). *Pure and Applied Chemistry* **2009**, 82(2), 483-491.
16. Matyjaszewski, K.; Müller, A. H. E., *Controlled and Living Polymerizations: From Mechanisms to Applications*. John Wiley & Sons: 2009.

17. Moad, G.; Rizzardo, E.; Thang, S. H., RAFT Polymerization and Some of its Applications. *Chemistry – An Asian Journal* **2013**, 8(8), 1634-1644.
18. Stuart, M. A. C.; Huck, W. T. S.; Genzer, J.; Müller, M.; Ober, C.; Stamm, M.; Sukhorukov, G. B.; Szleifer, I.; Tsukruk, V. V.; Urban, M.; Winnik, F.; Zauscher, S.; Luzinov, I.; Minko, S., Emerging applications of stimuli-responsive polymer materials. *Nature Materials* **2010**, 9(2), 101-113.
19. Matyjaszewski, K., Introduction to living polymeriz. Living and/or controlled polymerization. *Journal of Physical Organic Chemistry* **1995**, 8(4), 197-207.
20. Poelma, J. E.; Fors, B. P.; Meyers, G. F.; Kramer, J. W.; Hawker, C. J., Fabrication of complex three-dimensional polymer brush nanostructures through light-mediated living radical polymerization. *Angewandte Chemie International Edition* **2013**, 52(27), 6844-8.
21. Rowe-Konopacki, M. D.; Boyes, S. G., Synthesis of Surface Initiated Diblock Copolymer Brushes from Flat Silicon Substrates Utilizing the RAFT Polymerization Technique. *Macromolecules* **2007**, 40(4), 879-888.
22. Mayadunne, R. T. A.; Rizzardo, E.; Chiefari, J.; Krstina, J.; Moad, G.; Postma, A.; Thang, S. H., Living Polymers by the Use of Trithiocarbonates as Reversible Addition–Fragmentation Chain Transfer (RAFT) Agents: ABA Triblock Copolymers by Radical Polymerization in Two Steps. *Macromolecules* **2000**, 33(2), 243-245.
23. Benaglia, M.; Chen, M.; Chong, Y. K.; Moad, G.; Rizzardo, E.; Thang, S. H., Polystyrene-block-poly(vinyl acetate) through the Use of a Switchable RAFT Agent. *Macromolecules* **2009**, 42(24), 9384-9386.
24. Tsarevsky, N. V.; Sarbu, T.; Göbelt, B.; Matyjaszewski, K., Synthesis of Styrene–Acrylonitrile Copolymers and Related Block Copolymers by Atom Transfer Radical Polymerization. *Macromolecules* **2002**, 35(16), 6142-6148.
25. Chong, Y. K.; Le, T. P. T.; Moad, G.; Rizzardo, E.; Thang, S. H., A More Versatile Route to Block Copolymers and Other Polymers of Complex Architecture by Living Radical Polymerization: The RAFT Process. *Macromolecules* **1999**, 32(6), 2071-2074.
26. Clothier, G. K. K.; Guimarães, T. R.; Khan, M.; Moad, G.; Perrier, S.; Zetterlund, P. B., Exploitation of the Nanoreactor Concept for Efficient Synthesis of Multiblock Copolymers via MacroRAFT-Mediated Emulsion Polymerization. *ACS Macro Letters* **2019**, 8(8), 989-995.
27. Danielson, A. P.; Van Kuren, D. B.; Lucius, M. E.; Makaroff, K.; Williams, C.; Page, R. C.; Berberich, J. A.; Konkolewicz, D., Well-Defined Macromolecules Using Horseradish Peroxidase as a RAFT Initiase. *Macromolecular Rapid Communications* **2016**, 37(4), 362-367.
28. Yan, J.; Bockstaller, M. R.; Matyjaszewski, K., Brush-modified materials: Control of molecular architecture, assembly behavior, properties and applications. *Progress in Polymer Science* **2020**, 100, 101180.
29. Voit, B. I.; Lederer, A., Hyperbranched and Highly Branched Polymer Architectures—Synthetic Strategies and Major Characterization Aspects. *Chemical Reviews* **2009**, 109(11), 5924-5973.
30. Sun, Z.; Wang, M.; Li, Z.; Choi, B.; Mulder, R. J.; Feng, A.; Moad, G.; Thang, S. H., Versatile Approach for Preparing PVC-Based Mikto-Arm Star Additives Based on RAFT Polymerization. *Macromolecules* **2020**, 53(11), 4465-4479.
31. Xu, B.; Feng, C.; Huang, X., A versatile platform for precise synthesis of asymmetric molecular brush in one shot. *Nature Communications* **2017**, 8(1), 333.
32. Gao, H.; Matyjaszewski, K., Synthesis of functional polymers with controlled architecture by CRP of monomers in the presence of cross-linkers: From stars to gels. *Progress in Polymer Science* **2009**, 34(4), 317-350.

33. Moad, G., RAFT (Reversible addition-fragmentation chain transfer) crosslinking (co)polymerization of multi-olefinic monomers to form polymer networks. *Polymer International* **2015**, 64(1), 15-24.
34. Lowe, A. B.; McCormick, C. L., Homogeneous Controlled Free Radical Polymerization in Aqueous Media. *Australian journal of chemistry* **2002**, 55(7), 367-379.
35. McCormick, C. L.; Lowe, A. B., Aqueous RAFT Polymerization: Recent Developments in Synthesis of Functional Water-Soluble (Co)polymers with Controlled Structures. *Accounts of Chemical Research* **2004**, 37(5), 312-325.
36. Perrier, S.; Davis, T. P.; Carmichael, A. J.; Haddleton, D. M., First report of reversible addition-fragmentation chain transfer (RAFT) polymerisation in room temperature ionic liquids. *Chemical communications* **2002**, (19), 2226-2227.
37. Arita, T.; Beuermann, S.; Buback, M.; Vana, P., Reversible addition fragmentation chain transfer (RAFT) polymerization of styrene in fluid CO₂. *e-Polymers* **2004**, 4(1).
38. Sarbu, T.; Matyjaszewski, K., ATRP of Methyl Methacrylate in the Presence of Ionic Liquids with Ferrous and Cuprous Anions. *Macromolecular Chemistry and Physics* **2001**, 202(17), 3379-3391.
39. Xia, J.; Johnson, T.; Gaynor, S. G.; Matyjaszewski, K.; DeSimone, J., Atom Transfer Radical Polymerization in Supercritical Carbon Dioxide. *Macromolecules* **1999**, 32(15), 4802-4805.
40. Corrigan, N.; Rosli, D.; Jones, J. W. J.; Xu, J.; Boyer, C., Oxygen Tolerance in Living Radical Polymerization: Investigation of Mechanism and Implementation in Continuous Flow Polymerization. *Macromolecules* **2016**, 49(18), 6779-6789.
41. Pan, X.; Tasdelen, M. A.; Laun, J.; Junkers, T.; Yagci, Y.; Matyjaszewski, K., Photomediated controlled radical polymerization. *Progress in Polymer Science* **2016**, 62, 73-125.
42. Chen, M.; Zhong, M.; Johnson, J. A., Light-Controlled Radical Polymerization: Mechanisms, Methods, and Applications. *Chemical Reviews* **2016**, 116(17), 10167-10211.
43. Magenau Andrew, J. D.; Strandwitz Nicholas, C.; Gennaro, A.; Matyjaszewski, K., Electrochemically Mediated Atom Transfer Radical Polymerization. *Science* **2011**, 332(6025), 81-84.
44. Lorandi, F.; Fantin, M.; Shanmugam, S.; Wang, Y.; Isse, A. A.; Gennaro, A.; Matyjaszewski, K., Toward Electrochemically Mediated Reversible Addition-Fragmentation Chain-Transfer (eRAFT) Polymerization: Can Propagating Radicals Be Efficiently Electrogenenerated from RAFT Agents? *Macromolecules* **2019**, 52(4), 1479-1488.
45. Mohapatra, H.; Kleiman, M.; Esser-Kahn, A. P., Mechanically controlled radical polymerization initiated by ultrasound. *Nature Chemistry* **2017**, 9(2), 135-139.
46. Wang, Z.; Pan, X.; Li, L.; Fantin, M.; Yan, J.; Wang, Z.; Wang, Z.; Xia, H.; Matyjaszewski, K., Enhancing Mechanically Induced ATRP by Promoting Interfacial Electron Transfer from Piezoelectric Nanoparticles to Cu Catalysts. *Macromolecules* **2017**, 50(20), 7940-7948.
47. Zhang, B.; Wang, X.; Zhu, A.; Ma, K.; Lv, Y.; Wang, X.; An, Z., Enzyme-Initiated Reversible Addition-Fragmentation Chain Transfer Polymerization. *Macromolecules* **2015**, 48(21), 7792-7802.
48. Zhou, F.; Li, R.; Wang, X.; Du, S.; An, Z., Non-natural Photoenzymatic Controlled Radical Polymerization Inspired by DNA Photolyase. *Angewandte Chemie International Edition* **2019**, 58(28), 9479-9484.

49. Nicolas, J.; Guillaneuf, Y.; Lefay, C.; Bertin, D.; Gigmes, D.; Charleux, B., Nitroxide-mediated polymerization. *Progress in Polymer Science* **2013**, 38(1), 63-235.
50. Matyjaszewski, K.; Xia, J., Atom transfer radical polymerization. *Chemical Reviews* **2001**, 101(9), 2921-2990.
51. Moad, G.; Rizzardo, E.; Thang, S. H., Living Radical Polymerization by the RAFT Process – A Third Update. *Australian journal of chemistry* **2012**, 65(8), 985-1076.
52. Moad, G.; Rizzardo, E.; Thang, S. H., Living Radical Polymerization by the RAFT Process. *Australian journal of chemistry* **2005**, 58(6), 379-410.
53. Moad, G.; Rizzardo, E.; Thang, S. H., Living Radical Polymerization by the RAFT Process A First Update. *Australian journal of chemistry* **2006**, 59(10), 669-692.
54. Moad, G.; Rizzardo, E.; Thang, S. H., Radical addition–fragmentation chemistry in polymer synthesis. *Polymer* **2008**, 49(5), 1079-1131.
55. Moad, G.; Rizzardo, E.; Thang, S. H., Toward Living Radical Polymerization. *Accounts of Chemical Research* **2008**, 41(9), 1133-1142.
56. Moad, G.; Rizzardo, E.; Thang, S. H., Living Radical Polymerization by the RAFT Process A Second Update. *Australian journal of chemistry* **2009**, 62(11), 1402-1472.
57. Rizzardo, E.; Chiefari, J.; Mayadunne, R. T. A.; Moad, G.; Thang, S. H., Synthesis of Defined Polymers by Reversible Addition—Fragmentation Chain Transfer: The RAFT Process. In *Controlled/Living Radical Polymerization*, American Chemical Society: 2000; pp 278-296.
58. Truong, N. P.; Jones, G. R.; Bradford, K. G. E.; Konkolewicz, D.; Anastasaki, A., A comparison of RAFT and ATRP methods for controlled radical polymerization. *Nature Reviews Chemistry* **2021**, 5(12), 859-869.
59. Ding, C.; Fan, C.; Jiang, G.; Pan, X.; Zhang, Z.; Zhu, J.; Zhu, X., Photocatalyst-Free and Blue Light-Induced RAFT Polymerization of Vinyl Acetate at Ambient Temperature. *Macromolecular Rapid Communications* **2015**, 36(24), 2181-2185.
60. Stace, S. J.; Moad, G.; Fellows, C. M.; Keddie, D. J., The effect of Z-group modification on the RAFT polymerization of N-vinylpyrrolidone controlled by “switchable” N-pyridyl-functional dithiocarbamates. *Polymer Chemistry* **2015**, 6(40), 7119-7126.
61. Xu, J.; Jung, K.; Atme, A.; Shanmugam, S.; Boyer, C., A robust and versatile photoinduced living polymerization of conjugated and unconjugated monomers and its oxygen tolerance. *Journal of the American Chemical Society* **2014**, 136(14), 5508-5519.
62. Hawker, C. J.; Bosman, A. W.; Harth, E., New polymer synthesis by nitroxide mediated living radical polymerizations. *Chemical Reviews* **2001**, 101(12), 3661-3688.
63. Moad, G.; Rizzardo, E., Chapter 1 The History of Nitroxide-mediated Polymerization. In *Nitroxide Mediated Polymerization: From Fundamentals to Applications in Materials Science*, The Royal Society of Chemistry: 2016; pp 1-44.
64. Solomon, D. H., Genesis of the CSIRO polymer group and the discovery and significance of nitroxide-mediated living radical polymerization. *Journal of Polymer Science Part A: Polymer Chemistry* **2005**, 43(23), 5748-5764.
65. Rizzardo, E.; Solomon, D. H., On the Origins of Nitroxide Mediated Polymerization (NMP) and Reversible Addition–Fragmentation Chain Transfer (RAFT)*. *Australian journal of chemistry* **2012**, 65(8), 945-969.
66. Tang, W.; Kwak, Y.; Braunecker, W.; Tsarevsky, N. V.; Coote, M. L.; Matyjaszewski, K., Understanding Atom Transfer Radical Polymerization: Effect of Ligand and Initiator Structures on the Equilibrium Constants. *Journal of the American Chemical Society* **2008**, 130(32), 10702-10713.

67. Boyer, C.; Corrigan, N. A.; Jung, K.; Nguyen, D.; Nguyen, T.-K.; Adnan, N. N. M.; Oliver, S.; Shanmugam, S.; Yeow, J., Copper-Mediated Living Radical Polymerization (Atom Transfer Radical Polymerization and Copper(0) Mediated Polymerization): From Fundamentals to Bioapplications. *Chemical Reviews* **2016**, *116*(4), 1803-1949.
68. Patten, T. E.; Matyjaszewski, K., Atom Transfer Radical Polymerization and the Synthesis of Polymeric Materials. *Advanced Materials* **1998**, *10*(12), 901-915.
69. Matyjaszewski, K., Atom Transfer Radical Polymerization (ATRP): Current Status and Future Perspectives. *Macromolecules* **2012**, *45*(10), 4015-4039.
70. Cacioli, P.; Hawthorne, D. G.; Laslett, R. L.; Rizzardo, E.; Solomon, D. H., Copolymerization of ω -Unsaturated Oligo(Methyl Methacrylate): New Macromonomers. *Journal of Macromolecular Science: Part A - Chemistry* **1986**, *23*(7), 839-852.
71. Meijs, G. F.; Rizzardo, E.; Thang, S. H., Preparation of controlled-molecular-weight, olefin-terminated polymers by free radical methods. Chain transfer using allylic sulfides. *Macromolecules* **1988**, *21*(10), 3122-3124.
72. Meijs, G. F.; Rizzardo, E., Chain transfer by an addition-fragmentation mechanism. The use of α -benzyloxystyrene for the preparation of low-molecular-weight poly(methyl methacrylate) and polystyrene. *Die Makromolekulare Chemie, Rapid Communications* **1988**, *9*(8), 547-551.
73. Otsu, T.; Yoshida, M.; Tazaki, T., A model for living radical polymerization. *Die Makromolekulare Chemie, Rapid Communications* **1982**, *3*(2), 133-140.
74. Krstina, J.; Moad, C. L.; Moad, G.; Rizzardo, E.; Berge, C. T.; Fryd, M., A new form of controlled growth free radical polymerization. *Macromolecular Symposia* **1996**, *111*(1), 13-23.
75. Krstina, J.; Moad, G.; Rizzardo, E.; Winzor, C. L.; Berge, C. T.; Fryd, M., Narrow Polydispersity Block Copolymers by Free-Radical Polymerization in the Presence of Macromonomers. *Macromolecules* **1995**, *28*(15), 5381-5385.
76. Matyjaszewski, K.; Gaynor, S.; Wang, J.-S., Controlled Radical Polymerizations: The Use of Alkyl Iodides in Degenerative Transfer. *Macromolecules* **1995**, *28*(6), 2093-2095.
77. Barner-Kowollik, C.; Buback, M.; Charleux, B.; Coote, M. L.; Drache, M.; Fukuda, T.; Goto, A.; Klumperman, B.; Lowe, A. B.; McLeary, J. B.; Moad, G.; Monteiro, M. J.; Sanderson, R. D.; Tonge, M. P.; Vana, P., Mechanism and kinetics of dithiobenzoate-mediated RAFT polymerization. I. The current situation. *Journal of Polymer Science Part A: Polymer Chemistry* **2006**, *44*(20), 5809-5831.
78. Mayadunne, R. T. A.; Rizzardo, E.; Chiefari, J.; Chong, Y. K.; Moad, G.; Thang, S. H., Living Radical Polymerization with Reversible Addition-Fragmentation Chain Transfer (RAFT Polymerization) Using Dithiocarbamates as Chain Transfer Agents. *Macromolecules* **1999**, *32*(21), 6977-6980.
79. Destarac, M.; Charnot, D.; Franck, X.; Zard, S. Z., Dithiocarbamates as universal reversible addition-fragmentation chain transfer agents. *Macromolecular Rapid Communications* **2000**, *21*(15), 1035-1039.
80. Moad, G., A Critical Survey of Dithiocarbamate Reversible Addition-Fragmentation Chain Transfer (RAFT) Agents in Radical Polymerization. *Journal of Polymer Science Part A: Polymer Chemistry* **2019**, *57*(3), 216-227.
81. Benaglia, M.; Chiefari, J.; Chong, Y. K.; Moad, G.; Rizzardo, E.; Thang, S. H., Universal (Switchable) RAFT Agents. *Journal of the American Chemical Society* **2009**, *131*(20), 6914-6915.

82. Perrier, S.; Takolpuckdee, P., Macromolecular design via reversible addition–fragmentation chain transfer (RAFT)/xanthates (MADIX) polymerization. *Journal of Polymer Science Part A: Polymer Chemistry* **2005**, *43*(22), 5347-5393.
83. Charmot, D.; Corpart, P.; Adam, H.; Zard, S. Z.; Biadatti, T.; Bouhadir, G., Controlled radical polymerization in dispersed media. *Macromolecular Symposia* **2000**, 23-32.
84. Keddie, D. J.; Moad, G.; Rizzardo, E.; Thang, S. H., RAFT Agent Design and Synthesis. *Macromolecules* **2012**, *45*(13), 5321-5342.
85. Russum, J. P.; Barbre, N. D.; Jones, C. W.; Schork, F. J., Miniemulsion reversible addition fragmentation chain transfer polymerization of vinyl acetate. *Journal of Polymer Science Part A: Polymer Chemistry* **2005**, *43*(10), 2188-2193.
86. McLeary, J. B.; Klumperman, B., RAFT mediated polymerisation in heterogeneous media. *Soft Matter* **2006**, *2*(1), 45-53.
87. Lokitz, B. S.; Lowe, A. B.; McCormick, C. L., Reversible Addition Fragmentation Chain Transfer Polymerization of Water-Soluble, Ion-Containing Monomers. In *Polyelectrolytes and Polyzwitterions*, American Chemical Society: 2006; pp 95-115.
88. Ray, B.; Okamoto, Y.; Kamigaito, M.; Sawamoto, M.; Seno, K.-i.; Kanaoka, S.; Aoshima, S., Effect of Tacticity of Poly(N-isopropylacrylamide) on the Phase Separation Temperature of Its Aqueous Solutions. *Polymer Journal* **2005**, *37*(3), 234-237.
89. Mori, H.; Sutoh, K.; Endo, T., Controlled Radical Polymerization of an Acrylamide Containing 1-Phenylalanine Moiety via RAFT. *Macromolecules* **2005**, *38*(22), 9055-9065.
90. Lutz, J.-F.; Jakubowski, W.; Matyjaszewski, K., Controlled/Living Radical Polymerization of Methacrylic Monomers in the Presence of Lewis Acids: Influence on Tacticity. *Macromolecular Rapid Communications* **2004**, *25*(3), 486-492.
91. Arita, T.; Buback, M.; Janssen, O.; Vana, P., RAFT-Polymerization of Styrene up to High Pressure: Rate Enhancement and Improved Control. *Macromolecular Rapid Communications* **2004**, *25*(15), 1376-1381.
92. Rzaev, J.; Penelle, J., HP-RAFT: A Free-Radical Polymerization Technique for Obtaining Living Polymers of Ultrahigh Molecular Weights. *Angewandte Chemie International Edition* **2004**, *43*(13), 1691-1694.
93. Monteiro, M. J.; Bussels, R.; Beuermann, S.; Buback, M., High Pressure 'Living' Free-Radical Polymerization of Styrene in the Presence of RAFT. *Australian journal of chemistry* **2002**, *55*(7), 433-437.
94. Arita, T.; Buback, M.; Vana, P., Cumyl Dithiobenzoate Mediated RAFT Polymerization of Styrene at High Temperatures. *Macromolecules* **2005**, *38*(19), 7935-7943.
95. Xu, J.; He, J.; Fan, D.; Tang, W.; Yang, Y., Thermal Decomposition of Dithioesters and Its Effect on RAFT Polymerization. *Macromolecules* **2006**, *39*(11), 3753-3759.
96. Martin, L.; Gody, G.; Perrier, S., Preparation of complex multiblock copolymers via aqueous RAFT polymerization at room temperature. *Polymer Chemistry* **2015**, *6*(27), 4875-4886.
97. Boyer, C.; Bulmus, V.; Davis, T. P.; Ladmiral, V.; Liu, J.; Perrier, S., Bioapplications of RAFT Polymerization. *Chemical Reviews* **2009**, *109*(11), 5402-5436.
98. Moad, G.; Chen, M.; Häussler, M.; Postma, A.; Rizzardo, E.; Thang, S. H., Functional polymers for optoelectronic applications by RAFT polymerization. *Polymer Chemistry* **2011**, *2*(3), 492-519.
99. Moad, G., An Industrial History of RAFT Polymerization. In *RAFT Polymerization*, 2021; pp 1077-1169.

100. Moad, G.; Rizzardo, E., Overview of RAFT Polymerization. In *RAFT Polymerization*, 2021; pp 1-13.
101. Fairbanks, B. D.; Gunatillake, P. A.; Meagher, L., Biomedical applications of polymers derived by reversible addition-fragmentation chain-transfer (RAFT). *Advanced Drug Delivery Reviews* **2015**, *91*, 141-152.
102. Barner-Kowollik, C., *Handbook of RAFT polymerization*. John Wiley & Sons: 2008.
103. Vana, P.; Quinn, J. F.; Davis, T. P.; Barner-Kowollik, C., Recent advances in the kinetics of reversible addition fragmentation chain-transfer polymerization. *Australian journal of chemistry* **2002**, *55*(6-7 SPEC.).
104. Chiefari, J.; Mayadunne, R. T. A.; Moad, C. L.; Moad, G.; Rizzardo, E.; Postma, A.; Thang, S. H., Thiocarbonylthio Compounds (SC(Z)S-R) in Free Radical Polymerization with Reversible Addition-Fragmentation Chain Transfer (RAFT Polymerization). Effect of the Activating Group Z. *Macromolecules* **2003**, *36*(7), 2273-2283.
105. Moad, G.; Chiefari, J.; Chong, Y. K.; Krstina, J.; Mayadunne, R. T. A.; Postma, A.; Rizzardo, E.; Thang, S. H., Living free radical polymerization with reversible addition-fragmentation chain transfer (the life of RAFT). *Polymer International* **2000**, *49*(9), 993-1001.
106. Destarac, M.; Bzducha, W.; Taton, D.; Gauthier-Gillaizeau, I.; Zard, S. Z., Xanthates as Chain-Transfer Agents in Controlled Radical Polymerization (MADIX): Structural Effect of the O-Alkyl Group. *Macromolecular Rapid Communications* **2002**, *23*(17), 1049-1054.
107. Perrier, S.; Barner-Kowollik, C.; Quinn, J. F.; Vana, P.; Davis, T. P., Origin of Inhibition Effects in the Reversible Addition Fragmentation Chain Transfer (RAFT) Polymerization of Methyl Acrylate. *Macromolecules* **2002**, *35*(22), 8300-8306.
108. Monteiro, M. J.; de Brouwer, H., Intermediate Radical Termination as the Mechanism for Retardation in Reversible Addition-Fragmentation Chain Transfer Polymerization. *Macromolecules* **2001**, *34*(3), 349-352.
109. Kwak, Y.; Goto, A.; Tsujii, Y.; Murata, Y.; Komatsu, K.; Fukuda, T., A Kinetic Study on the Rate Retardation in Radical Polymerization of Styrene with Addition-Fragmentation Chain Transfer. *Macromolecules* **2002**, *35*(8), 3026-3029.
110. Calitz, F. M.; McLeary, J. B.; McKenzie, J. M.; Tonge, M. P.; Klumperman, B.; Sanderson, R. D., Evidence for Termination of Intermediate Radical Species in RAFT-Mediated Polymerization. *Macromolecules* **2003**, *36*(26), 9687-9690.
111. Hua, D.; Xiao, J.; Bai, R.; Lu, W.; Pan, C., Xanthate-Mediated Controlled/Living Free-Radical Polymerization under ^{60}Co γ -Ray Irradiation: Structure Effect of O-Group. *Macromolecular Chemistry and Physics* **2004**, *205*(13), 1793-1799.
112. Stenzel, M. H.; Cummins, L.; Roberts, G. E.; Davis, T. P.; Vana, P.; Barner-Kowollik, C., Xanthate Mediated Living Polymerization of Vinyl Acetate: A Systematic Variation in MADIX/RAFT Agent Structure. *Macromolecular Chemistry and Physics* **2003**, *204*(9), 1160-1168.
113. Chong, Y. K.; Krstina, J.; Le, T. P. T.; Moad, G.; Postma, A.; Rizzardo, E.; Thang, S. H., Thiocarbonylthio Compounds [SC(Ph)S-R] in Free Radical Polymerization with Reversible Addition-Fragmentation Chain Transfer (RAFT Polymerization). Role of the Free-Radical Leaving Group (R). *Macromolecules* **2003**, *36*(7), 2256-2272.
114. Bowman, C. N.; Carver, A. L.; Kennett, S. N.; Williams, M. M.; Peppas, N. A., Polymers for information storage systems III. Crosslinked structure of polydimethacrylates. *Polymer* **1990**, *31*(1), 135-139.

115. Patrickios, C. S., Polymer Networks: Recent Developments. *Macromolecular Symposia* **2010**, 291-292(1), 1-11.
116. Kausar, N.; Chowdhry, B. Z.; Snowden, M., *Microgels from smart polymers*. CRC Press: 2007; p 138-169.
117. Rey, L.; Duchet, J.; Galy, J.; Sautereau, H.; Vouagner, D.; Carrion, L., Structural heterogeneities and mechanical properties of vinyl/dimethacrylate networks synthesized by thermal free radical polymerisation. *Polymer* **2002**, 43(16), 4375-4384.
118. Zhuo, D.; Ruan, Y.; Zhao, X.; Ran, R., Kinetics of UV-initiated RAFT crosslinking polymerization of dimethacrylates. *Journal of applied polymer science* **2011**, 121(2), 660-665.
119. Gu, Y.; Zhao, J.; Johnson, J. A., Polymer Networks: From Plastics and Gels to Porous Frameworks. *Angewandte Chemie International Edition* **2020**, 59(13), 5022-5049.
120. Tobita, H.; Hamielec, A., Modeling of network formation in free radical polymerization. *Macromolecules* **1989**, 22(7), 3098-3105.
121. Zhu, S.; Hamielec, A., Influence of cross-link density distribution on network formation in free-radical copolymerization of vinyl/divinyl monomers. *Macromolecules* **1992**, 25(20), 5457-5464.
122. Matsumoto, A., Free-radical crosslinking polymerization and copolymerization of multivinyl compounds. In *Synthesis and Photosynthesis*, Springer Berlin Heidelberg: 1995; pp 41-80.
123. Kannurpatti, A. R.; Anseth, J. W.; Bowman, C. N., A study of the evolution of mechanical properties and structural heterogeneity of polymer networks formed by photopolymerizations of multifunctional (meth)acrylates. *Polymer* **1998**, 39(12), 2507-2513.
124. Roy, S. G.; Haldar, U.; De, P., Remarkable swelling capability of amino acid based cross-linked polymer networks in organic and aqueous medium. *ACS Applied Materials & Interfaces* **2014**, 6(6), 4233-4241.
125. Yu, Q.; Zhu, Y.; Ding, Y.; Zhu, S., Reaction behavior and network development in raft radical polymerization of dimethacrylates. *Macromolecular Chemistry and Physics* **2008**, 209(5), 551-556.
126. Norisuye, T.; Morinaga, T.; Tran-Cong-Miyata, Q.; Goto, A.; Fukuda, T.; Shibayama, M., Comparison of the gelation dynamics for polystyrenes prepared by conventional and living radical polymerizations: a time-resolved dynamic light scattering study. *Polymer* **2005**, 46(6), 1982-1994.
127. Yu, Q.; Xu, S.; Zhang, H.; Ding, Y.; Zhu, S., Comparison of reaction kinetics and gelation behaviors in atom transfer, reversible addition-fragmentation chain transfer and conventional free radical copolymerization of oligo(ethylene glycol) methyl ether methacrylate and oligo(ethylene glycol) dimethacrylate. *Polymer* **2009**, 50(15), 3488-3494.
128. Bünsow, J.; Mänz, M.; Vana, P.; Johannsmann, D., Electrochemically Induced RAFT Polymerization of Thermoresponsive Hydrogel Films: Impact on Film Thickness and Surface Morphology. *Macromolecular Chemistry and Physics* **2010**, 211(7), 761-767.
129. Cuthbert, J.; Balazs, A. C.; Kowalewski, T.; Matyjaszewski, K., STEM Gels by Controlled Radical Polymerization. *Trends in Chemistry* **2020**, 2(4), 341-353.
130. Chen, M.; Gu, Y.; Singh, A.; Zhong, M.; Jordan, A. M.; Biswas, S.; Korley, L. T.; Balazs, A. C.; Johnson, J. A., Living Additive Manufacturing: Transformation of Parent Gels into Diversely Functionalized Daughter Gels Made Possible by Visible Light Photoredox Catalysis. *ACS Central Science* **2017**, 3(2), 124-134.
131. Cuthbert, J.; Beziau, A.; Gottlieb, E.; Fu, L.; Yuan, R.; Balazs, A. C.; Kowalewski, T.; Matyjaszewski, K., Transformable Materials: Structurally Tailored and Engineered

- Macromolecular (STEM) Gels by Controlled Radical Polymerization. *Macromolecules* **2018**, *51*(10), 3808-3817.
132. Cuthbert, J.; Zhang, T.; Biswas, S.; Olszewski, M.; Shanmugam, S.; Fu, T.; Gottlieb, E.; Kowalewski, T.; Balazs, A. C.; Matyjaszewski, K., Structurally Tailored and Engineered Macromolecular (STEM) Gels as Soft Elastomers and Hard/Soft Interfaces. *Macromolecules* **2018**, *51*(22), 9184-9191.
 133. Shanmugam, S.; Cuthbert, J.; Kowalewski, T.; Boyer, C.; Matyjaszewski, K., Catalyst-Free Selective Photoactivation of RAFT Polymerization: A Facile Route for Preparation of Comblike and Bottlebrush Polymers. *Macromolecules* **2018**, *51*(19), 7776-7784.
 134. Shanmugam, S.; Cuthbert, J.; Flum, J.; Fantin, M.; Boyer, C.; Kowalewski, T.; Matyjaszewski, K., Transformation of gels via catalyst-free selective RAFT photoactivation. *Polymer Chemistry* **2019**, *10*(19), 2477-2483.
 135. Leung, D.; Bowman, C. N., Reducing Shrinkage Stress of Dimethacrylate Networks by Reversible Addition-Fragmentation Chain Transfer. *Macromolecular Chemistry and Physics* **2012**, *213*(2), 198-204.
 136. Amamoto, Y.; Otsuka, H.; Takahara, A.; Matyjaszewski, K., Changes in Network Structure of Chemical Gels Controlled by Solvent Quality through Photoinduced Radical Reshuffling Reactions of Trithiocarbonate Units. *ACS Macro Letters* **2012**, *1*(4), 478-481.
 137. Amamoto, Y.; Kamada, J.; Otsuka, H.; Takahara, A.; Matyjaszewski, K., Repeatable photoinduced self-healing of covalently cross-linked polymers through reshuffling of trithiocarbonate units. *Angewandte Chemie International Edition* **2011**, *50*(7), 1660-1663.
 138. Kloxin, C. J.; Bowman, C. N., Covalent adaptable networks: smart, reconfigurable and responsive network systems. *Chemical Society Reviews* **2013**, *42*(17), 7161-73.
 139. Chong, Y. K.; Moad, G.; Rizzardo, E.; Thang, S. H., Thiocarbonylthio End Group Removal from RAFT-Synthesized Polymers by Radical-Induced Reduction. *Macromolecules* **2007**, *40*(13), 4446-4455.
 140. Willcock, H.; O'Reilly, R. K., End group removal and modification of RAFT polymers. *Polymer Chemistry* **2010**, *1*(2), 149-157.
 141. Moad, G.; Rizzardo, E.; Thang, S. H., End-functional polymers, thiocarbonylthio group removal/transformation and reversible addition-fragmentation-chain transfer (RAFT) polymerization. *Polymer International* **2011**, *60*(1), 9-25.
 142. Qiu, X.-P.; Winnik, F. M., Facile and Efficient One-Pot Transformation of RAFT Polymer End Groups via a Mild Aminolysis/Michael Addition Sequence. *Macromolecular Rapid Communications* **2006**, *27*(19), 1648-1653.
 143. Spruell, J. M.; Levy, B. A.; Sutherland, A.; Dichtel, W. R.; Cheng, J. Y.; Stoddart, J. F.; Nelson, A., Facile postpolymerization end-modification of RAFT polymers. *Journal of Polymer Science Part A: Polymer Chemistry* **2009**, *47*(2), 346-356.
 144. Lima, V.; Jiang, X.; Brokken-Zijp, J.; Schoenmakers, P. J.; Klumperman, B.; Van Der Linde, R., Synthesis and characterization of telechelic polymethacrylates via RAFT polymerization. *Journal of Polymer Science Part A: Polymer Chemistry* **2005**, *43*(5), 959-973.
 145. Chan, J. W.; Yu, B.; Hoyle, C. E.; Lowe, A. B., Convergent synthesis of 3-arm star polymers from RAFT-prepared poly (N, N-diethylacrylamide) via a thiol-ene click reaction. *Chemical communications* **2008**, (40), 4959-4961.
 146. Nakayama, M.; Okano, T., Polymer Terminal Group Effects on Properties of Thermoresponsive Polymeric Micelles with Controlled Outer-Shell Chain Lengths. *Biomacromolecules* **2005**, *6*(4), 2320-2327.

147. Hoyle, C. E.; Bowman, C. N., Thiol–Ene Click Chemistry. *Angewandte Chemie International Edition* **2010**, 49(9), 1540-1573.
148. Boyer, C.; Granville, A.; Davis, T. P.; Bulmus, V., Modification of RAFT-polymers via thiol-ene reactions: A general route to functional polymers and new architectures. *Journal of Polymer Science Part A: Polymer Chemistry* **2009**, 47(15), 3773-3794.
149. Shen, W.; Qiu, Q.; Wang, Y.; Miao, M.; Li, B.; Zhang, T.; Cao, A.; An, Z., Hydrazine as a Nucleophile and Antioxidant for Fast Aminolysis of RAFT Polymers in Air. *Macromolecular Rapid Communications* **2010**, 31(16), 1444-1448.
150. Hornung, C. H.; von Känel, K.; Martinez-Botella, I.; Espiritu, M.; Nguyen, X.; Postma, A.; Saubern, S.; Chiefari, J.; Thang, S. H., Continuous Flow Aminolysis of RAFT Polymers Using Multistep Processing and Inline Analysis. *Macromolecules* **2014**, 47(23), 8203-8213.
151. Sinnwell, S.; Inglis, A. J.; Davis, T. P.; Stenzel, M. H.; Barner-Kowollik, C., An atom-efficient conjugation approach to well-defined block copolymers using RAFT chemistry and hetero Diels–Alder cycloaddition. *Chemical communications* **2008**, (17), 2052-2054.
152. Inglis, A. J.; Sinnwell, S.; Davis, T. P.; Barner-Kowollik, C.; Stenzel, M. H., Reversible Addition Fragmentation Chain Transfer (RAFT) and Hetero-Diels–Alder Chemistry as a Convenient Conjugation Tool for Access to Complex Macromolecular Designs. *Macromolecules* **2008**, 41(12), 4120-4126.
153. Chong, B.; Moad, G.; Rizzardo, E.; Skidmore, M.; Thang, S. H., Thermolysis of RAFT-Synthesized Poly(Methyl Methacrylate). *Australian journal of chemistry* **2006**, 59(10), 755-762.
154. You, Y.-Z.; Hong, C.-Y.; Bai, R.-K.; Pan, C.-Y.; Wang, J., Photo-Initiated Living Free Radical Polymerization in the Presence of Dibenzyl Trithiocarbonate. *Macromolecular Chemistry and Physics* **2002**, 203(3), 477-483.
155. Xu, J.; Shanmugam, S.; Corrigan, N. A.; Boyer, C., Catalyst-Free Visible Light-Induced RAFT Photopolymerization. In *Controlled Radical Polymerization: Mechanisms*, American Chemical Society: 2015; pp 247-267.
156. McKenzie, T. G.; Fu, Q.; Wong, E. H. H.; Dunstan, D. E.; Qiao, G. G., Visible Light Mediated Controlled Radical Polymerization in the Absence of Exogenous Radical Sources or Catalysts. *Macromolecules* **2015**, 48(12), 3864-3872.
157. Shanmugam, S.; Xu, J.; Boyer, C., Exploiting Metalloporphyrins for Selective Living Radical Polymerization Tunable over Visible Wavelengths. *Journal of the American Chemical Society* **2015**, 137(28), 9174-9185.
158. Shanmugam, S.; Xu, J.; Boyer, C., Utilizing the electron transfer mechanism of chlorophyll a under light for controlled radical polymerization. *Chemical Science* **2015**, 6(2), 1341-1349.
159. Shanmugam, S.; Xu, J.; Boyer, C., Light-Regulated Polymerization under Near-Infrared/Far-Red Irradiation Catalyzed by Bacteriochlorophyll a. *Angewandte Chemie International Edition* **2016**, 55(3), 1036-1040.
160. Corrigan, N.; Xu, J.; Boyer, C.; Allonas, X., Exploration of the PET-RAFT Initiation Mechanism for Two Commonly Used Photocatalysts. *ChemPhotoChem* **2019**, 3(11), 1193-1199.
161. Wu, Z.; Jung, K.; Boyer, C., Effective Utilization of NIR Wavelengths for Photo-Controlled Polymerization: Penetration Through Thick Barriers and Parallel Solar Syntheses. *Angewandte Chemie International Edition* **2020**, 59(5), 2013-2017.

162. Zhang, L.; Wu, C.; Jung, K.; Ng, Y. H.; Boyer, C., An Oxygen Paradox: Catalytic Use of Oxygen in Radical Photopolymerization. *Angewandte Chemie International Edition* **2019**, 58(47), 16811-16814.
163. Discekici, E. H.; Anastasaki, A.; Kaminker, R.; Willenbacher, J.; Truong, N. P.; Fleischmann, C.; Oschmann, B.; Lunn, D. J.; Read de Alaniz, J.; Davis, T. P.; Bates, C. M.; Hawker, C. J., Light-Mediated Atom Transfer Radical Polymerization of Semi-Fluorinated (Meth)acrylates: Facile Access to Functional Materials. *Journal of the American Chemical Society* **2017**, 139(16), 5939-5945.
164. Pearson, R. M.; Lim, C.-H.; McCarthy, B. G.; Musgrave, C. B.; Miyake, G. M., Organocatalyzed Atom Transfer Radical Polymerization Using N-Aryl Phenoxazines as Photoredox Catalysts. *Journal of the American Chemical Society* **2016**, 138(35), 11399-11407.
165. Anastasaki, A.; Nikolaou, V.; Zhang, Q.; Burns, J.; Samanta, S. R.; Waldron, C.; Haddleton, A. J.; McHale, R.; Fox, D.; Percec, V.; Wilson, P.; Haddleton, D. M., Copper(II)/Tertiary Amine Synergy in Photoinduced Living Radical Polymerization: Accelerated Synthesis of ω -Functional and α,ω -Heterofunctional Poly(acrylates). *Journal of the American Chemical Society* **2014**, 136(3), 1141-1149.
166. Dolinski, N. D.; Page, Z. A.; Discekici, E. H.; Meis, D.; Lee, I.-H.; Jones, G. R.; Whitfield, R.; Pan, X.; McCarthy, B. G.; Shanmugam, S.; Kottisch, V.; Fors, B. P.; Boyer, C.; Miyake, G. M.; Matyjaszewski, K.; Haddleton, D. M.; de Alaniz, J. R.; Anastasaki, A.; Hawker, C. J., What happens in the dark? Assessing the temporal control of photo-mediated controlled radical polymerizations. *Journal of Polymer Science Part A: Polymer Chemistry* **2019**, 57(3), 268-273.
167. Fromel, M.; Li, M.; Pester, C. W., Surface Engineering with Polymer Brush Photolithography. *Macromolecular Rapid Communications* **2020**, 41(18), 2000177.
168. Ramakers, G.; Krivcov, A.; Trouillet, V.; Welle, A.; Möbius, H.; Junkers, T., Organocatalyzed Photo-Atom Transfer Radical Polymerization of Methacrylic Acid in Continuous Flow and Surface Grafting. *Macromolecular Rapid Communications* **2017**, 38(21), 1700423.
169. Kabb, C. P.; O'Bryan, C. S.; Deng, C. C.; Angelini, T. E.; Sumerlin, B. S., Photoreversible Covalent Hydrogels for Soft-Matter Additive Manufacturing. *ACS Applied Materials & Interfaces* **2018**, 10(19), 16793-16801.
170. Zhou, X.; Liu, X.; Xie, Z.; Zheng, Z., 3D-patterned polymer brush surfaces. *Nanoscale* **2011**, 3(12), 4929-4939.
171. Discekici, E. H.; Pester, C. W.; Treat, N. J.; Lawrence, J.; Mattson, K. M.; Narupai, B.; Toumayan, E. P.; Luo, Y.; McGrath, A. J.; Clark, P. G.; Read de Alaniz, J.; Hawker, C. J., Simple Benchtop Approach to Polymer Brush Nanostructures Using Visible-Light-Mediated Metal-Free Atom Transfer Radical Polymerization. *ACS Macro Letters* **2016**, 5(2), 258-262.
172. Pester, C. W.; Narupai, B.; Mattson, K. M.; Bothman, D. P.; Klinger, D.; Lee, K. W.; Discekici, E. H.; Hawker, C. J., Engineering Surfaces through Sequential Stop-Flow Photopatterning. *Advanced Materials* **2016**, 28(42), 9292-9300.
173. Li, M.; Fromel, M.; Ranaweera, D.; Rocha, S.; Boyer, C.; Pester, C. W., SI-PET-RAFT: Surface-Initiated Photoinduced Electron Transfer-Reversible Addition-Fragmentation Chain Transfer Polymerization. *ACS Macro Letters* **2019**, 8(4), 374-380.
174. Layani, M.; Wang, X.; Magdassi, S., Novel Materials for 3D Printing by Photopolymerization. *Advanced Materials* **2018**, 30(41), 1706344.
175. Appuhamillage, G. A.; Chartrain, N.; Meenakshisundaram, V.; Feller, K. D.; Williams, C. B.; Long, T. E., 110th Anniversary: Vat Photopolymerization-Based

Additive Manufacturing: Current Trends and Future Directions in Materials Design. *Industrial & Engineering Chemistry Research* **2019**, 58(33), 15109-15118.

176. Zhang, F.; Zhu, L.; Li, Z.; Wang, S.; Shi, J.; Tang, W.; Li, N.; Yang, J., The recent development of vat photopolymerization: A review. *Additive Manufacturing* **2021**, 48, 102423.

177. Pagac, M.; Hajnys, J.; Ma, Q.-P.; Jancar, L.; Jansa, J.; Stefek, P.; Mesicek, J., A Review of Vat Photopolymerization Technology: Materials, Applications, Challenges, and Future Trends of 3D Printing. *Polymers* **2021**, 13(4), 598.

178. Ligon, S. C.; Liska, R.; Stampfl, J.; Gurr, M.; Mulhaupt, R., Polymers for 3D Printing and Customized Additive Manufacturing. *Chemical Reviews* **2017**, 117(15), 10212-10290.

179. Kurek, P. N.; Kloster, A. J.; Weaver, K. A.; Manahan, R.; Allegrezza, M. L.; De Alwis Watuthanthrige, N.; Boyer, C.; Reeves, J. A.; Konkolewicz, D., How Do Reaction and Reactor Conditions Affect Photoinduced Electron/Energy Transfer Reversible Addition–Fragmentation Transfer Polymerization? *Industrial & Engineering Chemistry Research* **2018**, 57(12), 4203-4213.

180. Wang, H.; Li, Q.; Dai, J.; Du, F.; Zheng, H.; Bai, R., Real-Time and in Situ Investigation of “Living”/Controlled Photopolymerization in the Presence of a Trithiocarbonate. *Macromolecules* **2013**, 46(7), 2576-2582.

181. Otsu, T.; Yamashita, K.; Tsuda, K., Synthesis, reactivity, and role of 4-vinylbenzyl N,N-diethyldithiocarbamate as a monomer-iniferter in radical polymerization. *Macromolecules* **1986**, 19(2), 287-290.

182. Quinn, J. F.; Barner, L.; Barner-Kowollik, C.; Rizzardo, E.; Davis, T. P., Reversible Addition–Fragmentation Chain Transfer Polymerization Initiated with Ultraviolet Radiation. *Macromolecules* **2002**, 35(20), 7620-7627.

183. Corrigan, N.; Yeow, J.; Judzewitsch, P.; Xu, J.; Boyer, C., Seeing the Light: Advancing Materials Chemistry through Photopolymerization. *Angewandte Chemie International Edition* **2019**, 58(16), 5170-5189.

184. Blanc, A.; Bochet, C. G., Wavelength-Controlled Orthogonal Photolysis of Protecting Groups. *The Journal of Organic Chemistry* **2002**, 67(16), 5567-5577.

185. Houck, H. A.; Du Prez, F. E.; Barner-Kowollik, C., Controlling thermal reactivity with different colors of light. *Nature Communications* **2017**, 8(1), 1869.

186. Fu, C.; Xu, J.; Boyer, C., Photoacid-mediated ring opening polymerization driven by visible light. *Chemical communications* **2016**, 52(44), 7126-7129.

187. Kottisch, V.; Michaudel, Q.; Fors, B. P., Photocontrolled Interconversion of Cationic and Radical Polymerizations. *Journal of the American Chemical Society* **2017**, 139(31), 10665-10668.

188. Xu, J.; Shanmugam, S.; Fu, C.; Aguey-Zinsou, K. F.; Boyer, C., Selective Photoactivation: From a Single Unit Monomer Insertion Reaction to Controlled Polymer Architectures. *Journal of the American Chemical Society* **2016**, 138(9), 3094-106.

189. Bagheri, A.; Yeow, J.; Arandiyani, H.; Xu, J.; Boyer, C.; Lim, M., Polymerization of a Photocleavable Monomer Using Visible Light. *Macromolecular Rapid Communications* **2016**, 37(11), 905-910.

190. Goldmann, A. S.; Glassner, M.; Inglis, A. J.; Barner-Kowollik, C., Post-Functionalization of Polymers via Orthogonal Ligation Chemistry. *Macromolecular Rapid Communications* **2013**, 34(10), 810-849.

191. Xiong, X.; Xue, L.; Cui, J., Phototriggered Growth and Detachment of Polymer Brushes with Wavelength Selectivity. *ACS Macro Letters* **2018**, 7(2), 239-243.

192. Hurrel, S.; Lauer, A.; Gliemann, H.; Mutlu, H.; Wöll, C.; Goldmann, A. S.; Barner-Kowollik, C., Two-in-One: λ -Orthogonal Photochemistry on a Radical Photoinitiating System. *Macromolecular Rapid Communications* **2017**, 38(13), 1600598.
193. Davidson, R. S., The chemistry of photoinitiators-some recent developments. *Journal of Photochemistry and Photobiology A: Chemistry* **1993**, 73(2), 81-96.
194. Gruber, H. F., Photoinitiators for free radical polymerization. *Progress in Polymer Science* **1992**, 17(6), 953-1044.
195. Lu, L.; Yang, N.; Cai, Y., Well-controlled reversible addition-fragmentation chain transfer radical polymerisation under ultraviolet radiation at ambient temperature. *Chemical communications* **2005**, (42), 5287-5288.
196. Lu, L.; Zhang, H.; Yang, N.; Cai, Y., Toward Rapid and Well-Controlled Ambient Temperature RAFT Polymerization under UV-Vis Radiation: Effect of Radiation Wave Range. *Macromolecules* **2006**, 39(11), 3770-3776.
197. Ham, M.-k.; HoYouk, J.; Kwon, Y.-K.; Kwark, Y.-J., Photoinitiated RAFT polymerization of vinyl acetate. *Journal of Polymer Science Part A: Polymer Chemistry* **2012**, 50(12), 2389-2397.
198. Yin, H.; Zheng, H.; Lu, L.; Liu, P.; Cai, Y., Highly efficient and well-controlled ambient temperature RAFT polymerization of glycidyl methacrylate under visible light radiation. *Journal of Polymer Science Part A: Polymer Chemistry* **2007**, 45(22), 5091-5102.
199. Shi, Y.; Gao, H.; Lu, L.; Cai, Y., Ultra-fast RAFT polymerisation of poly(ethylene glycol) acrylate in aqueous media under mild visible light radiation at 25 °C. *Chemical communications* **2009**, (11), 1368-1370.
200. Shi, Y.; Liu, G.; Gao, H.; Lu, L.; Cai, Y., Effect of Mild Visible Light on Rapid Aqueous RAFT Polymerization of Water-Soluble Acrylic Monomers at Ambient Temperature: Initiation and Activation. *Macromolecules* **2009**, 42(12), 3917-3926.
201. Jiang, Y.; Xu, N.; Han, J.; Yu, Q.; Guo, L.; Gao, P.; Lu, X.; Cai, Y., The direct synthesis of interface-decorated reactive block copolymer nanoparticles via polymerisation-induced self-assembly. *Polymer Chemistry* **2015**, 6(27), 4955-4965.
202. Tan, J.; Sun, H.; Yu, M.; Sumerlin, B. S.; Zhang, L., Photo-PISA: Shedding Light on Polymerization-Induced Self-Assembly. *ACS Macro Letters* **2015**, 4(11), 1249-1253.
203. Gardiner, J.; Hornung, C. H.; Tsanaktsidis, J.; Guthrie, D., Continuous flow photo-initiated RAFT polymerisation using a tubular photochemical reactor. *European Polymer Journal* **2016**, 80, 200-207.
204. Zaquen, N.; Azizi, W. A. A. W.; Yeow, J.; Kuchel, R. P.; Junkers, T.; Zetterlund, P. B.; Boyer, C., Alcohol-based PISA in batch and flow: exploring the role of photoinitiators. *Polymer Chemistry* **2019**, 10(19), 2406-2414.
205. Jiang, W.; Lu, L.; Cai, Y., Highly Efficient and Well-Controlled Ambient Temperature RAFT Polymerization under Solar Radiation. *Macromolecular Rapid Communications* **2007**, 28(6), 725-728.
206. Tan, J.; Bai, Y.; Zhang, X.; Huang, C.; Liu, D.; Zhang, L., Low-Temperature Synthesis of Thermoresponsive Diblock Copolymer Nano-Objects via Aqueous Photoinitiated Polymerization-Induced Self-Assembly (Photo-PISA) using Thermoresponsive Macro-RAFT Agents. *Macromolecular Rapid Communications* **2016**, 37(17), 1434-1440.
207. Tan, J.; Bai, Y.; Zhang, X.; Zhang, L., Room temperature synthesis of poly(poly(ethylene glycol) methyl ether methacrylate)-based diblock copolymer nano-objects via Photoinitiated Polymerization-Induced Self-Assembly (Photo-PISA). *Polymer Chemistry* **2016**, 7(13), 2372-2380.

208. Wenn, B.; Junkers, T., Continuous Microflow PhotoRAFT Polymerization. *Macromolecules* **2016**, *49*(18), 6888-6895.
209. Otsu, T., Iniferter concept and living radical polymerization. *Journal of Polymer Science Part A: Polymer Chemistry* **2000**, *38*(12), 2121-2136.
210. Otsu, T.; Matsumoto, A., Controlled Synthesis of Polymers Using the Iniferter Technique: Developments in Living Radical Polymerization. In *Microencapsulation Microgels Iniferters*, DiMari, S.; Funke, W.; Haralson, M. A.; Hunkeler, D.; Joos-Müller, B.; Matsumoto, A.; Okay, O.; Otsu, T.; Powers, A. C.; Prokop, A.; Wang, T. G.; Whitesell, R. R., Eds. Springer Berlin Heidelberg: 1998; pp 75-137.
211. Hartlieb, M., Photo-Iniferter RAFT Polymerization. *Macromolecular Rapid Communications* **2022**, *43*(1), 2100514.
212. Kannurpatti, A. R.; Lu, S.; Bunker, G. M.; Bowman, C. N., Kinetic and Mechanistic Studies of Iniferter Photopolymerizations. *Macromolecules* **1996**, *29*(23), 7310-7315.
213. Lambrinos, P.; Tardi, M.; Polton, A.; Sigwalt, P., The mechanism of the polymerization of n.butyl acrylate initiated with N,N-diethyl dithiocarbamate derivatives. *European Polymer Journal* **1990**, *26*(10), 1125-1135.
214. Turner, S. R.; Blevins, R. W., Photoinitiated block copolymer formation using dithiocarbamate free radical chemistry. *Macromolecules* **1990**, *23*(6), 1856-1859.
215. Tazhe Veetil, A.; Šolomek, T.; Ngoy, B. P.; Pavlíková, N.; Heger, D.; Klán, P., Photochemistry of S-Phenacyl Xanthates. *The Journal of Organic Chemistry* **2011**, *76*(20), 8232-8242.
216. Gruendling, T.; Kaupp, M.; Blinco, J. P.; Barner-Kowollik, C., Photoinduced Conjugation of Dithioester- and Trithiocarbonate-Functional RAFT Polymers with Alkenes. *Macromolecules* **2011**, *44*(1), 166-174.
217. Zhou, H.; Johnson, J. A., Photo-controlled Growth of Telechelic Polymers and End-linked Polymer Gels. *Angewandte Chemie International Edition* **2013**, *52*(8), 2235-2238.
218. McKenzie, T. G.; Wong, E. H. H.; Fu, Q.; Sulistio, A.; Dunstan, D. E.; Qiao, G. G., Controlled Formation of Star Polymer Nanoparticles via Visible Light Photopolymerization. *ACS Macro Letters* **2015**, *4*(9), 1012-1016.
219. Allison-Logan, S.; Karimi, F.; Sun, Y.; McKenzie, T. G.; Nothling, M. D.; Bryant, G.; Qiao, G. G., Highly Living Stars via Core-First Photo-RAFT Polymerization: Exploitation for Ultra-High Molecular Weight Star Synthesis. *ACS Macro Letters* **2019**, *8*(10), 1291-1295.
220. Allegrezza, M. L.; De Alwis Watuthanthrige, N.; Wang, Y.; Garcia, G. A.; Ren, H.; Konkolewicz, D., Substituent effects in iniferter photopolymerization: can bond homolysis be enhanced by electronics? *Polymer Chemistry* **2020**, *11*(38), 6129-6133.
221. Mueller, L.; Jakubowski, W.; Matyjaszewski, K.; Pietrasik, J.; Kwiatkowski, P.; Chaladaj, W.; Jurczak, J., Synthesis of high molecular weight polystyrene using AGET ATRP under high pressure. *European Polymer Journal* **2011**, *47*(4), 730-734.
222. Huang, Z.; Chen, J.; Zhang, L.; Cheng, Z.; Zhu, X., ICAR ATRP of Acrylonitrile under Ambient and High Pressure. *Polymers* **2016**, *8*(3), 59.
223. Truong, N. P.; Dussert, M. V.; Whittaker, M. R.; Quinn, J. F.; Davis, T. P., Rapid synthesis of ultrahigh molecular weight and low polydispersity polystyrene diblock copolymers by RAFT-mediated emulsion polymerization. *Polymer Chemistry* **2015**, *6*(20), 3865-3874.
224. Carmean, R. N.; Becker, T. E.; Sims, M. B.; Sumerlin, B. S., Ultra-High Molecular Weights via Aqueous Reversible-Deactivation Radical Polymerization. *Chem* **2017**, *2*(1), 93-101.

225. Carmean, R. N.; Sims, M. B.; Figg, C. A.; Hurst, P. J.; Patterson, J. P.; Sumerlin, B. S., Ultrahigh Molecular Weight Hydrophobic Acrylic and Styrenic Polymers through Organic-Phase Photoiniferter-Mediated Polymerization. *ACS Macro Letters* **2020**, 9(4), 613-618.
226. Lampley, M. W.; Harth, E., Photocontrolled Growth of Cross-Linked Nanonetworks. *ACS Macro Letters* **2018**, 7(6), 745-750.
227. Arrington, K. J.; Matson, J. B., Assembly of a visible light photoreactor: an inexpensive tool for bottlebrush polymer synthesis via photoiniferter polymerization. *Polymer Chemistry* **2017**, 8(48), 7452-7456.
228. Corrigan, N.; Trujillo, F. J.; Xu, J.; Moad, G.; Hawker, C. J.; Boyer, C., Divergent Synthesis of Graft and Branched Copolymers through Spatially Controlled Photopolymerization in Flow Reactors. *Macromolecules* **2021**, 54(7), 3430-3446.
229. Yeow, J.; Sugita, O. R.; Boyer, C., Visible Light-Mediated Polymerization-Induced Self-Assembly in the Absence of External Catalyst or Initiator. *ACS Macro Letters* **2016**, 5(5), 558-564.
230. Xu, J., Single Unit Monomer Insertion: A Versatile Platform for Molecular Engineering through Radical Addition Reactions and Polymerization. *Macromolecules* **2019**, 52(23), 9068-9093.
231. Benetti, E. M.; Zapotoczny, S.; Vancso, G. J., Tunable Thermoresponsive Polymeric Platforms on Gold by "Photoiniferter"-Based Surface Grafting. *Advanced Materials* **2007**, 19(2), 268-271.
232. Krause, J. E.; Brault, N. D.; Li, Y.; Xue, H.; Zhou, Y.; Jiang, S., Photoiniferter-Mediated Polymerization of Zwitterionic Carboxybetaine Monomers for Low-Fouling and Functionalizable Surface Coatings. *Macromolecules* **2011**, 44(23), 9213-9220.
233. Christmann, J.; Ibrahim, A.; Charlot, V.; Croutxé-Barghorn, C.; Ley, C.; Allonas, X., Elucidation of the Key Role of [Ru(bpy)₃]²⁺ in Photocatalyzed RAFT Polymerization. *ChemPhysChem* **2016**, 17(15), 2309-2314.
234. Corrigan, N.; Xu, J.; Boyer, C.; Allonas, X., Exploration of the PET-RAFT Initiation Mechanism for Two Commonly Used Photocatalysts. *ChemPhotoChem* **2019**, 3(11), 1193-1199.
235. Seal, P.; Xu, J.; De Luca, S.; Boyer, C.; Smith, S. C., Unraveling Photocatalytic Mechanism and Selectivity in PET-RAFT Polymerization. *Advanced Theory and Simulations* **2019**, 2(6), 1900038.
236. Xu, J.; Jung, K.; Boyer, C., Oxygen Tolerance Study of Photoinduced Electron Transfer–Reversible Addition–Fragmentation Chain Transfer (PET-RAFT) Polymerization Mediated by Ru(bpy)₃Cl₂. *Macromolecules* **2014**, 47(13), 4217-4229.
237. Xu, J.; Jung, K.; Corrigan, N. A.; Boyer, C., Aqueous photoinduced living/controlled polymerization: tailoring for bioconjugation. *Chemical Science* **2014**, 5(9), 3568-3575.
238. Bellotti, V.; Simonutti, R., New Light in Polymer Science: Photoinduced Reversible Addition-Fragmentation Chain Transfer Polymerization (PET-RAFT) as Innovative Strategy for the Synthesis of Advanced Materials. *Polymers* **2021**, 13(7), 1119.
239. Xu, J.; Shanmugam, S.; Duong, H. T.; Boyer, C., Organo-photocatalysts for photoinduced electron transfer-reversible addition–fragmentation chain transfer (PET-RAFT) polymerization. *Polymer Chemistry* **2015**, 6(31), 5615-5624.
240. Fu, Q.; Xie, K.; McKenzie, T. G.; Qiao, G. G., Trithiocarbonates as intrinsic photoredox catalysts and RAFT agents for oxygen tolerant controlled radical polymerization. *Polymer Chemistry* **2017**, 8(9), 1519-1526.

241. Wu, C.; Corrigan, N.; Lim, C. H.; Jung, K.; Zhu, J.; Miyake, G.; Xu, J.; Boyer, C., Guiding the Design of Organic Photocatalyst for PET-RAFT Polymerization: Halogenated Xanthene Dyes. *Macromolecules* **2019**, *52*(1), 236-248.
242. Corrigan, N.; Zhernakov, L.; Hashim, M. H.; Xu, J.; Boyer, C., Flow mediated metal-free PET-RAFT polymerisation for upscaled and consistent polymer production. *Reaction Chemistry & Engineering* **2019**, *4*(7), 1216-1228.
243. He, J.-Y.; Lu, M., Photoinduced electron transfer-reversible addition-fragmentation chain transfer (PET-RAFT) polymerization of acrylonitrile in miniemulsion. *Journal of Macromolecular Science, Part A* **2019**, *56*(5), 443-449.
244. Cheng, B.-F.; Wang, L.-H.; You, Y.-Z., Photoinduced electron transfer-reversible addition-fragmentation chain transfer (PET-RAFT) polymerization using titanium dioxide. *Macromolecular Research* **2016**, *24*(9), 811-815.
245. Liang, E.; Liu, M.-s.; He, B.; Wang, G.-X., ZnO as photocatalyst for photoinduced electron transfer–reversible addition–fragmentation chain transfer of methyl methacrylate. *Advances in Polymer Technology* **2018**, *37*(8), 2879-2884.
246. Fu, Q.; Ruan, Q.; McKenzie, T. G.; Reyhani, A.; Tang, J.; Qiao, G. G., Development of a Robust PET-RAFT Polymerization Using Graphitic Carbon Nitride (g-C₃N₄). *Macromolecules* **2017**, *50*(19), 7509-7516.
247. Zhu, Y.; Liu, Y.; Miller, K. A.; Zhu, H.; Egap, E., Lead Halide Perovskite Nanocrystals as Photocatalysts for PET-RAFT Polymerization under Visible and Near-Infrared Irradiation. *ACS Macro Letters* **2020**, *9*(5), 725-730.
248. Zhu, Y.; Egap, E., PET-RAFT polymerization catalyzed by cadmium selenide quantum dots (QDs): Grafting-from QDs photocatalysts to make polymer nanocomposites. *Polymer Chemistry* **2020**, *11*(5), 1018-1024.
249. Liang, Y.; Ma, H.; Zhang, W.; Cui, Z.; Fu, P.; Liu, M.; Qiao, X.; Pang, X., Size effect of semiconductor quantum dots as photocatalysts for PET-RAFT polymerization. *Polymer Chemistry* **2020**, *11*(31), 4961-4967.
250. Zhang, L.; Shi, X.; Zhang, Z.; Kuchel, R. P.; Namivandi-Zangeneh, R.; Corrigan, N.; Jung, K.; Liang, K.; Boyer, C., Porphyrinic Zirconium Metal–Organic Frameworks (MOFs) as Heterogeneous Photocatalysts for PET-RAFT Polymerization and Stereolithography. *Angewandte Chemie International Edition* **2021**, *60*(10), 5489-5496.
251. Hakobyan, K.; Gegenhuber, T.; McErlean, C. S. P.; Müllner, M., Visible-Light-Driven MADIX Polymerisation via a Reusable, Low-Cost, and Non-Toxic Bismuth Oxide Photocatalyst. *Angewandte Chemie International Edition* **2019**, *58*(6), 1828-1832.
252. Fu, C.; Xu, J.; Kokotovic, M.; Boyer, C., One-Pot Synthesis of Block Copolymers by Orthogonal Ring-Opening Polymerization and PET-RAFT Polymerization at Ambient Temperature. *ACS Macro Letters* **2016**, *5*(4), 444-449.
253. Shanmugam, S.; Xu, J.; Boyer, C., Photoinduced Electron Transfer–Reversible Addition–Fragmentation Chain Transfer (PET-RAFT) Polymerization of Vinyl Acetate and N-Vinylpyrrolidinone: Kinetic and Oxygen Tolerance Study. *Macromolecules* **2014**, *47*(15), 4930-4942.
254. Shanmugam, S.; Boyer, C., Stereo-, Temporal and Chemical Control through Photoactivation of Living Radical Polymerization: Synthesis of Block and Gradient Copolymers. *Journal of the American Chemical Society* **2015**, *137*(31), 9988-9999.
255. Jung, K.; Xu, J.; Zetterlund, P. B.; Boyer, C., Visible-Light-Regulated Controlled/Living Radical Polymerization in Miniemulsion. *ACS Macro Letters* **2015**, *4*(10), 1139-1143.
256. Wu, C.; Shanmugam, S.; Xu, J.; Zhu, J.; Boyer, C., Chlorophyll a crude extract: efficient photo-degradable photocatalyst for PET-RAFT polymerization. *Chemical communications* **2017**, *53*(93), 12560-12563.

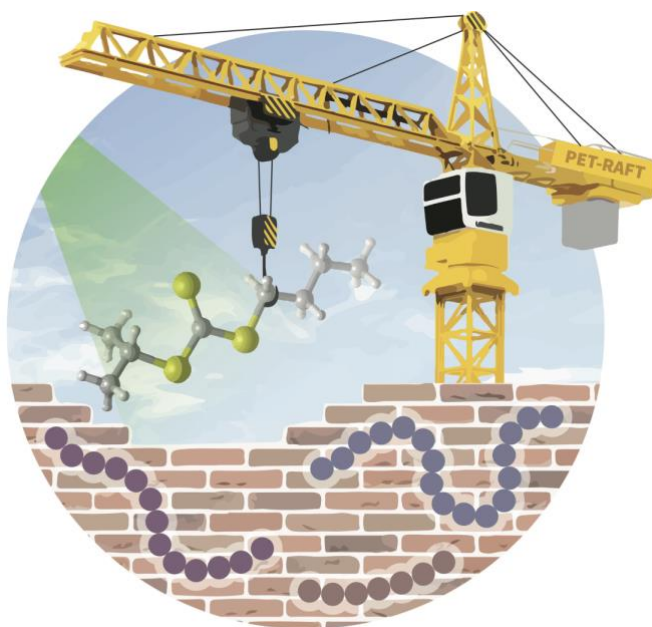
257. Gormley, A. J.; Yeow, J.; Ng, G.; Conway, Ó.; Boyer, C.; Chapman, R., An Oxygen-Tolerant PET-RAFT Polymerization for Screening Structure–Activity Relationships. *Angewandte Chemie International Edition* **2018**, 57(6), 1557-1562.
258. Ng, G.; Yeow, J.; Xu, J.; Boyer, C., Application of oxygen tolerant PET-RAFT to polymerization-induced self-assembly. *Polymer Chemistry* **2017**, 8(18), 2841-2851.
259. Yeow, J.; Chapman, R.; Xu, J.; Boyer, C., Oxygen tolerant photopolymerization for ultralow volumes. *Polymer Chemistry* **2017**, 8(34), 5012-5022.
260. Figg, C. A.; Hickman, J. D.; Scheutz, G. M.; Shanmugam, S.; Carmean, R. N.; Tucker, B. S.; Boyer, C.; Sumerlin, B. S., Color-Coding Visible Light Polymerizations To Elucidate the Activation of Trithiocarbonates Using Eosin Y. *Macromolecules* **2018**, 51(4), 1370-1376.
261. Gao, W.; Zhang, Y.; Ramanujan, D.; Ramani, K.; Chen, Y.; Williams, C. B.; Wang, C. C. L.; Shin, Y. C.; Zhang, S.; Zavattieri, P. D., The status, challenges, and future of additive manufacturing in engineering. *Computer-Aided Design* **2015**, 69, 65-89.
262. Prasad, S.; Kader, N. A.; Sujatha, G.; Raj, T.; Patil, S., 3D printing in dentistry. *Journal of 3D Printing in Medicine* **2018**, 2(3), 89-91.
263. Tian, Y.; Chen, C.; Xu, X.; Wang, J.; Hou, X.; Li, K.; Lu, X.; Shi, H.; Lee, E.-S.; Jiang, H. B., A Review of 3D Printing in Dentistry: Technologies, Affecting Factors, and Applications. *Scanning* **2021**, 2021, 9950131.
264. Joshi, S. C.; Sheikh, A. A., 3D printing in aerospace and its long-term sustainability. *Virtual and Physical Prototyping* **2015**, 10(4), 175-185.
265. Wang, Y.-C.; Chen, T.; Yeh, Y.-L., Advanced 3D printing technologies for the aircraft industry: a fuzzy systematic approach for assessing the critical factors. *The International Journal of Advanced Manufacturing Technology* **2019**, 105(10), 4059-4069.
266. Ahmed, N. A.; Page, J. R., Manufacture of an Unmanned Aerial Vehicle (UAV) for Advanced Project Design Using 3D Printing Technology. *Applied Mechanics and Materials* **2013**, 397-400, 970-980.
267. Foo, C. Y.; Lim, H. N.; Mahdi, M. A.; Wahid, M. H.; Huang, N. M., Three-Dimensional Printed Electrode and Its Novel Applications in Electronic Devices. *Scientific Reports* **2018**, 8(1), 7399.
268. Liaw, C.-Y.; Guvendiren, M., Current and emerging applications of 3D printing in medicine. *Biofabrication* **2017**, 9(2), 024102.
269. Chung, P.; Heller, J. A.; Etemadi, M.; Ottoson, P. E.; Liu, J. A.; Rand, L.; Roy, S., Rapid and Low-cost Prototyping of Medical Devices Using 3D Printed Molds for Liquid Injection Molding. *The Journal of Visualized Experiments* **2014**, (88), e51745.
270. Liu, Z.; Zhang, M.; Bhandari, B.; Wang, Y., 3D printing: Printing precision and application in food sector. *Trends in Food Science & Technology* **2017**, 69, 83-94.
271. Xu, X.; Awad, A.; Robles-Martinez, P.; Gaisford, S.; Goyanes, A.; Basit, A. W., Vat photopolymerization 3D printing for advanced drug delivery and medical device applications. *Journal of Controlled Release* **2021**, 329, 743-757.
272. Shahrubudin, N.; Lee, T. C.; Ramlan, R., An Overview on 3D Printing Technology: Technological, Materials, and Applications. *Procedia Manufacturing* **2019**, 35, 1286-1296.
273. ASTM International F2792-12a. Standard terminology for additive manufacturing technologies. ASTM International: West Conshohocken, PA, 2012.
274. Zhang, J.; Xiao, P., 3D printing of photopolymers. *Polymer Chemistry* **2018**, 9(13), 1530-1540.
275. Kaiser, T., Highly crosslinked polymers. *Progress in Polymer Science* **1989**, 14(3), 373-450.

276. Wendel, B.; Rietzel, D.; Kühnlein, F.; Feulner, R.; Hülder, G.; Schmachtenberg, E., Additive Processing of Polymers. *Macromolecular Materials and Engineering* **2008**, 293(10), 799-809.
277. Hull, C. W. Apparatus for production of three-dimensional objects by stereolithography. U.S. Patent 4575330, 1986.
278. Huang, J.; Qin, Q.; Wang, J., A Review of Stereolithography: Processes and Systems. *Processes* **2020**, 8(9).
279. Dolenc, A.; Mäkelä, I., Slicing procedures for layered manufacturing techniques. *Computer-Aided Design* **1994**, 26(2), 119-126.
280. Bártolo, P., *Stereolithography: Materials, Processes and Applications*. Springer Science & Business Media: Berlin, Germany, 2011.
281. Garcia, E. A.; Ayranci, C.; Qureshi, A. J., Material Property-Manufacturing Process Optimization for Form 2 Vat-Photo Polymerization 3D Printers. *Journal of Manufacturing and Materials Processing* **2020**, 4(1), 12.
282. Naik, D. L.; Kiran, R., On anisotropy, strain rate and size effects in vat photopolymerization based specimens. *Additive Manufacturing* **2018**, 23, 181-196.
283. Hada, T.; Kanazawa, M.; Iwaki, M.; Arakida, T.; Soeda, Y.; Katheng, A.; Otake, R.; Minakuchi, S., Effect of Printing Direction on the Accuracy of 3D-Printed Dentures Using Stereolithography Technology. *Materials* **2020**, 13(15), 3405.
284. Hada, T.; Kanazawa, M.; Iwaki, M.; Arakida, T.; Minakuchi, S., Effect of printing direction on stress distortion of three-dimensional printed dentures using stereolithography technology. *Journal of the Mechanical Behavior of Biomedical Materials* **2020**, 110, 103949.
285. Morris, V. B.; Nimbalkar, S.; Younesi, M.; McClellan, P.; Akkus, O., Mechanical Properties, Cytocompatibility and Manufacturability of Chitosan:PEGDA Hybrid-Gel Scaffolds by Stereolithography. *Annals of Biomedical Engineering* **2017**, 45(1), 286-296.
286. Momeni, F.; M.Mehdi Hassani, N. S.; Liu, X.; Ni, J., A review of 4D printing. *Materials & Design* **2017**, 122, 42-79.
287. Lantada, A. D.; de Blas Romero, A.; Tanarro, E. C., Micro-vascular shape-memory polymer actuators with complex geometries obtained by laser stereolithography. *Smart Materials and Structures* **2016**, 25(6), 065018.
288. Zarek, M.; Layani, M.; Cooperstein, I.; Sachyani, E.; Cohn, D.; Magdassi, S., 3D Printing of Shape Memory Polymers for Flexible Electronic Devices. *Advanced Materials* **2016**, 28(22), 4449-4454.
289. Yu, R.; Yang, X.; Zhang, Y.; Zhao, X.; Wu, X.; Zhao, T.; Zhao, Y.; Huang, W., Three-Dimensional Printing of Shape Memory Composites with Epoxy-Acrylate Hybrid Photopolymer. *ACS Applied Materials & Interfaces* **2017**, 9(2), 1820-1829.
290. Wang, W.; Sun, J.; Guo, B.; Chen, X.; Ananth, K. P.; Bai, J., Fabrication of piezoelectric nano-ceramics via stereolithography of low viscous and non-aqueous suspensions. *Journal of the European Ceramic Society* **2020**, 40(3), 682-688.
291. Chan, V.; Park, K.; Collens, M. B.; Kong, H.; Saif, T. A.; Bashir, R., Development of Miniaturized Walking Biological Machines. *Scientific Reports* **2012**, 2(1), 857.
292. Chan, V.; Jeong, J. H.; Bajaj, P.; Collens, M.; Saif, T.; Kong, H.; Bashir, R., Multi-material bio-fabrication of hydrogel cantilevers and actuators with stereolithography. *Lab on a Chip* **2012**, 12(1), 88-98.
293. Zolfagharian, A.; Kouzani, A. Z.; Khoo, S. Y.; Moghadam, A. A. A.; Gibson, I.; Kaynak, A., Evolution of 3D printed soft actuators. *Sensors and Actuators A: Physical* **2016**, 250, 258-272.

294. Gul, J. Z.; Sajid, M.; Rehman, M. M.; Siddiqui, G. U.; Shah, I.; Kim, K.-H.; Lee, J.-W.; Choi, K. H., 3D printing for soft robotics – a review. *Science and Technology of Advanced Materials* **2018**, *19*(1), 243-262.
295. Al Rashid, A.; Ahmed, W.; Khalid, M. Y.; Koç, M., Vat photopolymerization of polymers and polymer composites: Processes and applications. *Additive Manufacturing* **2021**, *47*, 102279.
296. Zhao, W.; Wang, Z.; Zhang, J.; Wang, X.; Xu, Y.; Ding, N.; Peng, Z., Vat Photopolymerization 3D Printing of Advanced Soft Sensors and Actuators: From Architecture to Function. *Advanced Materials Technologies* **2021**, *6*(8), 2001218.
297. Barone, S.; Neri, P.; Paoli, A.; Razonale, A. V.; Tamburrino, F., Development of a DLP 3D printer for orthodontic applications. *Procedia Manufacturing* **2019**, *38*, 1017-1025.
298. Yousef, H.; Harris, B. T.; Elathamna, E. N.; Morton, D.; Lin, W.-S., Effect of additive manufacturing process and storage condition on the dimensional accuracy and stability of 3D-printed dental casts. *The Journal of Prosthetic Dentistry* **2021**.
299. Wu, Y. L.; D'Amato, A. R.; Yan, A. M.; Wang, R. Q.; Ding, X.; Wang, Y., Three-Dimensional Printing of Poly(glycerol sebacate) Acrylate Scaffolds via Digital Light Processing. *ACS Applied Bio Materials* **2020**, *3*(11), 7575-7588.
300. Chen, H.; Lee, S. Y.; Lin, Y. M., Synthesis and Formulation of PCL-Based Urethane Acrylates for DLP 3D Printers. *Polymers* **2020**, *12*(7), 1500.
301. Xue, D.; Zhang, J.; Wang, Y.; Mei, D., Digital Light Processing-Based 3D Printing of Cell-Seeding Hydrogel Scaffolds with Regionally Varied Stiffness. *ACS Biomaterials Science & Engineering* **2019**, *5*(9), 4825-4833.
302. Patel, D. K.; Sakhaei, A. H.; Layani, M.; Zhang, B.; Ge, Q.; Magdassi, S., Highly Stretchable and UV Curable Elastomers for Digital Light Processing Based 3D Printing. *Advanced Materials* **2017**, *29*(15), 1606000.
303. Keshavarzan, M.; Kadkhodaei, M.; Forooghi, F., An investigation into compressive responses of shape memory polymeric cellular lattice structures fabricated by vat polymerization additive manufacturing. *Polymer Testing* **2020**, *91*, 106832.
304. Bagheri, A.; Jin, J., Photopolymerization in 3D Printing. *ACS Applied Polymer Materials* **2019**, *1*(4), 593-611.
305. Zheng, Z.; Eglin, D.; Alini, M.; Richards, G. R.; Qin, L.; Lai, Y., Visible Light-Induced 3D Bioprinting Technologies and Corresponding Bioink Materials for Tissue Engineering: A Review. *Engineering* **2021**, *7*(7), 966-978.
306. Xiao, P.; Zhang, J.; Dumur, F.; Tehfe, M. A.; Morlet-Savary, F.; Graff, B.; Gigmes, D.; Fouassier, J. P.; Lalevée, J., Visible light sensitive photoinitiating systems: Recent progress in cationic and radical photopolymerization reactions under soft conditions. *Progress in Polymer Science* **2015**, *41*, 32-66.
307. Shao, J.; Huang, Y.; Fan, Q., Visible light initiating systems for photopolymerization: status, development and challenges. *Polymer Chemistry* **2014**, *5*(14), 4195-4210.
308. Neumann, M. G.; Schmitt, C. C.; Ferreira, G. C.; Corrêa, I. C., The initiating radical yields and the efficiency of polymerization for various dental photoinitiators excited by different light curing units. *Dental Materials* **2006**, *22*(6), 576-584.
309. Steyrer, B.; Neubauer, P.; Liska, R.; Stampfl, J., Visible Light Photoinitiator for 3D-Printing of Tough Methacrylate Resins. *Materials* **2017**, *10*(12), 1445.
310. Lim, K. S.; Levato, R.; Costa, P. F.; Castilho, M. D.; Alcala-Orozco, C. R.; van Dorenmalen, K. M. A.; Melchels, F. P. W.; Gawlitta, D.; Hooper, G. J.; Malda, J.; Woodfield, T. B. F., Bio-resin for high resolution lithography-based biofabrication of complex cell-laden constructs. *Biofabrication* **2018**, *10*(3), 034101.

311. Schwartz, J. J.; Boydston, A. J., Multimaterial actinic spatial control 3D and 4D printing. *Nature Communications* **2019**, *10*(1), 791.
312. Kwak, H.; Shin, S.; Lee, H.; Hyun, J., Formation of a keratin layer with silk fibroin-polyethylene glycol composite hydrogel fabricated by digital light processing 3D printing. *Journal of Industrial and Engineering Chemistry* **2019**, *72*, 232-240.
313. Maturi, M.; Pulignani, C.; Locatelli, E.; Vetri Buratti, V.; Tortorella, S.; Sambri, L.; Comes Franchini, M., Phosphorescent bio-based resin for digital light processing (DLP) 3D-printing. *Green Chemistry* **2020**, *22*(18), 6212-6224.
314. Zanon, M.; Baruffaldi, D.; Sangermano, M.; Pirri, C. F.; Frascella, F.; Chiappone, A., Visible light-induced crosslinking of unmodified gelatin with PEGDA for DLP-3D printable hydrogels. *European Polymer Journal* **2021**, *160*, 110813.
315. Ahn, D.; Stevens, L. M.; Zhou, K.; Page, Z. A., Rapid High-Resolution Visible Light 3D Printing. *ACS Central Science* **2020**, *6*(9), 1555-1563.
316. Tumbleston, J. R.; Shirvanyants, D.; Ermoshkin, N.; Januszewicz, R.; Johnson, A. R.; Kelly, D.; Chen, K.; Pinschmidt, R.; Rolland, J. P.; Ermoshkin, A.; Samulski, E. T.; DeSimone, J. M., Additive manufacturing. Continuous liquid interface production of 3D objects. *Science* **2015**, *347*(6228), 1349-1352.
317. Januszewicz, R.; Tumbleston John, R.; Quintanilla Adam, L.; Mecham Sue, J.; DeSimone Joseph, M., Layerless fabrication with continuous liquid interface production. *Proceedings of the National Academy of Sciences* **2016**, *113*(42), 11703-11708.
318. Chockalingam, K.; Jawahar, N.; Chandrasekhar, U., Influence of layer thickness on mechanical properties in stereolithography. *Rapid Prototyping Journal* **2006**, *12*(2), 106-113.
319. Garcia, E.; Ayranci, C.; Qureshi, A. In *Digital light processing (DLP): anisotropic tensile considerations*, Proceedings of the 28th Annual International Solid Freeform Fabrication Symposium, 2017; pp 413-425.
320. Shusteff, M.; Browar Allison, E. M.; Kelly Brett, E.; Henriksson, J.; Weisgraber Todd, H.; Panas Robert, M.; Fang Nicholas, X.; Spadaccini Christopher, M., One-step volumetric additive manufacturing of complex polymer structures. *Science Advances* **2017**, *3*(12), eaao5496.
321. Kelly Brett, E.; Bhattacharya, I.; Heidari, H.; Shusteff, M.; Spadaccini Christopher, M.; Taylor Hayden, K., Volumetric additive manufacturing via tomographic reconstruction. *Science* **2019**, *363*(6431), 1075-1079.
322. Loterie, D.; Delrot, P.; Moser, C., High-resolution tomographic volumetric additive manufacturing. *Nature Communications* **2020**, *11*(1), 852.
323. Regehly, M.; Garmshausen, Y.; Reuter, M.; König, N. F.; Israel, E.; Kelly, D. P.; Chou, C.-Y.; Koch, K.; Asfari, B.; Hecht, S., Xolography for linear volumetric 3D printing. *Nature* **2020**, *588*(7839), 620-624.
324. Wang, B.; Engay, E.; Stubbe, P. R.; Moghaddam, S. Z.; Thormann, E.; Almdal, K.; Islam, A.; Yang, Y., Stiffness control in dual color tomographic volumetric 3D printing. *Nature Communications* **2022**, *13*(1), 367.
325. Shapira, A.; Dvir, T., 3D Tissue and Organ Printing—Hope and Reality. *Advanced Science* **2021**, *8*(10), 2003751.
326. Bernal, P. N.; Delrot, P.; Loterie, D.; Li, Y.; Malda, J.; Moser, C.; Levato, R., Volumetric Bioprinting of Complex Living-Tissue Constructs within Seconds. *Advanced Materials* **2019**, *31*(42), 1904209.
327. Hudson, D. E.; Hudson, D. O.; Wininger, J. M.; Richardson, B. D., Penetration of Laser Light at 808 and 980 nm in Bovine Tissue Samples. *Photomedicine and Laser Surgery* **2013**, *31*(4), 163-168.

Chapter 3. A Versatile 3D and 4D Printing System through Photocontrolled RAFT Polymerisation



The contents of this chapter were published in: Zhang, Z.; Corrigan, N.; Bagheri, A.; Jin, J.; Boyer, C. A Versatile 3D and 4D Printing System through Photocontrolled RAFT Polymerisation. *Angewandte Chemie International Edition* **2019**, 58(50), 17954-17963.

3.1 Introduction

The development of additive manufacturing techniques over the past 30 years has had an immeasurable impact on materials science.¹⁻⁵ Compared to traditional subtractive manufacturing, additive manufacturing has allowed the production of materials with arbitrary geometries while minimizing waste, and has provided non-experts access to complex materials. Among the most common 3D printing techniques (fused filament fabrication, 3D inkjet printing, etc.) photoinduced processes have garnered significant attention, largely due to the inherent benefits of light as an external stimuli, including temperature insensitivity, high biocompatibility, and spatiotemporal control; 3D printing via stereolithography (SLA), projection microstereolithography, and digital light processing (DLP) techniques all exploit the ability for light to be constrained in a well-defined region to produce geometrically complex objects.⁶⁻¹⁴ Moreover, the extensive range of photochemistry available to perform photoinduced polymerisation has provided materials with diverse physical and chemical properties.

Recently, some interesting 3D and 4D printing techniques have been developed by several research groups that exploit the unique attributes of light to produce complex materials.¹⁵⁻²⁹ For instance, Hawker and co-workers developed a new approach for visible light controlled 3D printing based on the bleaching of photochromic molecules, which allowed large cure depths and printed materials devoid of layer defects.¹⁷ Notably, the use of a single resin formulation containing both cationic and radically sensitive components enabled one step printing of multimaterial objects. Schwartz and Boydston have also demonstrated a dual wavelength 3D and 4D printing approach that activated dual cationic and radical polymerisations under UV and visible irradiation wavelengths, respectively.¹⁸ The use of a multi-wavelength DLP system provided 4D printed materials with tailored anisotropic properties that showed swelling induced actuation based on the spatial confinement of each wavelength during the one-pass layer-by-layer printing process. In other works by Dunn, Ge and co-workers, the independence of thermal and photo-induced chemistry was utilised for 3D printed multimaterial, shape memory, and reprocessable polymers.^{20, 30} In these examples, the use of light to 3D print the initial objects enabled the secondary material transformations to be independently activated.

Concurrently with the expansion of 3D and 4D printing techniques, the development of reversible deactivation radical polymerisation (RDRP) and other controlled polymerisation techniques over the past 20 years has provided polymer chemists with new tools to enact macromolecular syntheses.³¹⁻³⁷ Particularly, reversible addition-fragmentation chain transfer (RAFT) polymerisation techniques have been extensively studied due to their ability to produce well-defined macromolecules with diverse architectures and chemical functionalities under a wide range of conditions.³⁸⁻⁴¹ RAFT polymerisation utilises a degenerative chain transfer process between propagating radicals and thiocarbonylthio species (RAFT agents),^{32,40,42} which allows a large fraction of the growing polymer chains to remain dormant. The key for synthesizing architecturally diverse polymers via these approaches lies in the retention of the thiocarbonylthio polymer chain-end throughout the polymerisation; repeated activation of the dormant thiocarbonylthio-capped polymer chain via transfer reactions, and subsequent monomer additions allow the formation of all manner of block, graft, and branched copolymers.

More recently, photocontrolled RAFT polymerisation processes have been developed that display the favourable properties of RAFT polymerisation while being activated with benign, low energy visible light.⁴³⁻⁴⁴ Notably, our group developed a photocatalyzed polymerisation process termed photoinduced electron/energy transfer-RAFT (PET-RAFT) polymerisation.⁴⁵⁻⁵⁰ In PET-RAFT polymerisation, a photocatalyst (PC) is excited under visible or near-infrared light irradiation, and subsequently transfers an electron or energy to a thiocarbonylthio species. The thiocarbonylthio species can then fragment to produce a radical capable of initiating radical polymerisation.⁵¹⁻⁵² PET-RAFT polymerisation exhibits outstanding tolerance to molecular oxygen and can produce polymers under a broad range of conditions with high retention of the thiocarbonylthio chain-end. The high chain-end fidelity of polymeric networks synthesised through these and other photoinduced RAFT processes have also been exploited to expand the functionality of pre-formed materials.⁵³⁻⁵⁹ For instance, Johnson and co-workers presented an elegant strategy for modifying “parent” polymer networks containing trithiocarbonate units within the polymer backbone.⁵³ Under blue light irradiation in the presence of solutions containing a PC and monomer, the trithiocarbonate units were able to be activated, leading to polymerisation and modification of the original network. This network post-functionalisation provided “daughter” gels with variable properties.

Additionally, other thiocarbonylthio functional groups capable of degenerative chain transfer have been used in polymeric materials to modify the as-formed network structures. Matyjaszewski and co-workers showed an early example of a trithiocarbonate mediated network rearrangement process.⁶⁰ Remarkably, the butyl acrylate (BA) networks were able to be cut and subsequently fused together under UV light irradiation via photoinduced degenerative transfer between the trithiocarbonate functionalities in each network fragment. Similarly, dithiocarbamates have been used by Kloxin and co-workers to relieve stress, and induce self-healing behaviour within networks via bond rearrangement processes under UV light.⁶¹ Notably, this example utilised the spatial control possible with light to induce a secondary photopatterning of the original material. Although these methods demonstrate that RAFT agents can be incorporated into networks for rich post-modification procedures, the slow polymerisation rate for typical RAFT polymerisation (and other RDRP) processes has precluded their direct application to 3D printing processes. As 3D printing processes require a rapid cure time for practical applications, 3D printing of polymeric materials is generally conducted using comparatively rapid free-radical or cationic polymerisations. As such, 3D printing via RAFT polymerisation has remained a great challenge.

Herein, we investigate 3D and 4D printing via photoinduced RAFT polymerisation (PET-RAFT 3D and 4D printing using an organic PC) activated under visible light ($\lambda_{\text{max}} = 525$ nm, intensity = 0.32 mW/cm²). The photocatalytic system featured an organic dye (Erythrosin B, EB) and a tertiary amine co-catalyst (triethanolamine, TEtOHA), which allowed 3D printing to be conducted in aqueous solutions without prior deoxygenation. Following fabrication and mechanical testing of the 3D printed materials, the trithiocarbonate groups incorporated in the networks were activated under visible light for post-modification processes. The dormant RAFT-capped polymer chains were able to be reinitiated in the presence of EB under green light irradiation, which enabled surface modification of the printed objects. Additionally, the use of light allowed the formation of materials with spatially tailored properties to be printed in a single step, which provided an avenue to print 4D materials through swelling and dehydration induced actuation.

3.2 Experimental Section

3.2.1 Materials

Triethanolamine (TEtOHA, Sigma-Aldrich, 99%), dimethylsulfoxide (DMSO, chem-supply), basic aluminium oxide (Al_2O_3 , Sigma-Aldrich, 99.9%), 2-(butylthiocarbonothioylthio) propanoic acid (BTPA, Boron Molecular), absolute ethanol AR (chem supply), 1-pyrenemethyl methacrylate (pyrene-MMA, Sigma-Aldrich, 99%), Eosin Y disodium salt (EY, Sigma-Aldrich, >85%) and Erythrosin B (EB, dye content 90%, Sigma-Aldrich) were used as received. Poly(ethylene glycol) diacrylate average M_n 250 (PEGDA, Sigma-Aldrich, >92%), butyl acrylate (BA, Sigma > 99 %) and *N,N*-dimethylacrylamide (DMAM, Sigma-Aldrich, 99%) were deinhibited by percolation through basic alumina column before use.

3.2.2 Instrumentation

Attenuated total reflectance-fourier-transform infrared (ATR-FTIR) spectroscopy was employed to monitor vinyl bond conversions, using an approach similar to Magdassi, Banin, and co-workers.⁶² A Bruker Alpha FT-IR equipped with room temperature DTGS detectors was used for measurement. Each spectrum composed of 16 scans with a resolution of 4 cm^{-1} was collected in the spectral region between $4000\text{--}500\text{ cm}^{-1}$. Analysis was performed using OPUS software.

A TA instruments Q800 dynamic mechanical analyser (DMA) was used to obtain mechanical property measurements on the 3D printed materials. The Q800 DMA was equipped with a TA instruments liquid nitrogen gas cooling accessory (GCA) for temperature control.

Micromake L4, the LCD digitally masked DLP 3D printer modified with a green LED light board ($\lambda_{\text{max}} = 525\text{ nm}$, $I_0 = 0.32\text{ mW/cm}^2$) was employed to print rectangular samples for DMA analysis. The light intensity was measured using a Newport 843-R power meter. The targeted material geometries and .stl files were generated using Autodesk Fusion 360, and printing parameters (slicing thickness and layer cure times) were generated using Micromake L4 software.

UV–Vis spectroscopy spectra were recorded using a CARY 300 spectrophotometer (Varian) equipped with a temperature controller. All measurements were obtained by placing the 3D printed film in a 1 cm × 1 cm glass cuvette. The spectra were baseline corrected against the empty cuvette.

Contact angle measurements were performed using Motic live imaging module, a Moticam 5.0 MP camera, a KSV instruments Cam 200 backlight. The photographs were processed using Microsoft powerpoint, and the contact angle was determined using Fiji imageJ software.

3.2.3 Experimental procedure

Polymerisation for determination of reaction kinetics

A typical polymerisation solution was prepared as follows: to a 4 mL glass vial was added 0.53 mg (2.2 μ mol, 1 equiv) of BTPA, followed by 222.0 mg (2.2 mmol, 1000 equiv) of DMAM and 27.99 mg (0.11 mmol, 50 equiv) of PEGDA. 84.09 μ L (27.8 mmol) distilled water was then added, followed by 98.5 mL of a stock solution of EB in distilled water at 0.2 mg/mL (0.022 μ mol EB, 0.01 equiv), and 66.82 mL of a stock solution of TtOHA in water at 100 mg/mL (0.045 mmol, 20 equiv) to make the total reaction mixture 50 wt% monomer and crosslinker (DMAM and PEGDA). If the reaction was performed in bulk, the EB stock solution was prepared with DMAM as solvent. The reaction mixture was then covered with foil, vortexed for ~10 s, sonicated for 20 s, prior to the irradiation. A 20 μ L aliquot of the reaction mixture was then pipetted onto the ATR crystal plate and irradiated with a household LED lamp emitting green light ($\lambda_{\text{max}} = 525$ nm) with an intensity at the polymerisation surface, $I_0 = 4.3$ mW/cm² as measured using a Newport 843-R power meter.

Vinyl bond conversion was calculated based on the disappearance of the methylene group vibrations at 981 cm⁻¹ assigned to the out of plane bending mode of the =C-H group. The integral under this peak in the range of 935-1000 cm⁻¹ was evaluated after increasing irradiation times and compared to the peak in the range of 1236-1268 cm⁻¹ assigned to the amide C-N stretching mode for solution polymerisation. The vinyl bond conversion for polymerisation performed in bulk was calculated based on the disappearance of the methylene group vibrations at 981 cm⁻¹ assigned to the out of plane bending mode of the =C-H group. The integral under this peak in the range of 935-1000 cm⁻¹ was evaluated

after increasing irradiation times and compared to the peak in the range of 1685-1760 cm⁻¹ assigned to the acryl C=O stretching mode. The vinyl bond conversion was calculated from **Equation 1**, where std_0 is the integral under the curve in the range of 1236-1268 cm⁻¹ for solution polymerisation and 1685-1760 cm⁻¹ for polymerisation in bulk before irradiation, std_x is the integral under the curve in the range of 1236-1268 cm⁻¹ for solution polymerisation and 1685-1760 cm⁻¹ for polymerisation in bulk after x mins irradiation, int_0 is the integral under the curve in the range of 935-1000 cm⁻¹ before irradiation, and int_x is the integral under the curve in the range of 935-1000 cm⁻¹ after irradiation for x mins. All FTIR measurements were performed in triplicate.

$$\text{Vinyl bond conversion} = 1 - (int_x / std_x) / (int_0 / std_0) \quad \text{Eq. 1}$$

3D printing procedures of rectangular samples

A typical procedure for 3D printing is as follows: to a 20 mL glass vial was added 32.03 mg (0.134 mmol, 1 equiv) of BTPA, followed by 1.89 g (19.1 mmol, 142 equiv) of DMAM and 12.82 g (51.28 mmol, 382 equiv) of PEGDA. 295.5 µL of a stock solution of EB in DMAM at 4.0 mg/mL (1.3 µmol EB, 0.01 equiv and 2.87 mmol DMAM, 22 equiv) and 400.9 mg TEtOHA (2.69 mmol, 20 equiv) was then added to make a total equivalents of DMAM = 164, and [DMAM] : [PEGDA] = 30 : 70. The total mass for all reaction mixtures used for polymerisation in bulk was 15 g, and the molality of BTPA, EB, and TEtOHA was fixed. The reaction mixture was then covered with foil, vortexed for ~10 s, sonicated for 20 s, prior to addition to the 3D printer vat (vat dimensions 60 mm × 60 mm × 20 mm), and subsequently irradiated with spatially controlled green light during the 3D printing process. The targeted material geometries (40 × 13 × 1.6 mm (l, w, t)) and .stl files were generated using Autodesk Fusion 360. The sample printing parameters (slicing thickness and layer cure times) were generated using Micromake L4 software. The sample was then printed by using Micromake L4 DLP 3D printer. To ensure adhesion between the 3D printed material and the build stage, the first two (bottom) layers of the material were irradiated for 150 s, after which the regular cure time per layer was 13 s/layer with a layer thickness of 20 µm. The Z lift distance was 1 mm, the Z lift speed was 30 mm/min, and the Z retract speed was 300 mm/min. After the object was printed, the build stage was removed, and the residual polymerisation surface was briefly washed with ethanol. The material was allowed to dry for 5 mins then analysed by DMA.

3D printing procedures of the cross-shaped sample

The resin formulation of [EB] : [DMAm] : [PEGDA] : [BTPA] : [TEtOHA] = 0.01 : 1000 : 50 : 1 : 20 in a 50 wt% solution of water was used to print the cross-shaped sample. The sample geometries ($25 \times 5 \times 2$ mm (l, w, t)) and .stl files were generated using Autodesk Fusion 360. The sample printing parameters (slicing thickness and layer cure times) were generated using Micromake L4 software. The sample was then printed by using Micromake L4 DLP 3D printer. The first layer was printed with a layer slicing thickness of 20 μ m and a cure time 150 s, while the subsequent 20 μ m layers (99 layers) were exposed to green light for only 13 s. The Z lift distance was 1 mm, the Z lift speed was 30 mm/min, and the Z retract speed was 300 mm/min. After the object was printed, the build stage was removed, and the residual polymerisation surface was briefly washed with ethanol.

Calculation of light dose per layer in 3D printing

The light source produces 0.32 mW/cm² at the polymerisation surface (3.2 W/m²). The surface of the cross is 2.25 cm², i.e. 0.000225 m². As such the light dose on the cross is 0.00072 J/s. Now, the bottom layer experiences 150 s irradiation = 0.1080 J, while the subsequent layers receive 13 s irradiation = 0.0094 J per layer.

3D printing procedures of films

The resin formulations of [EB] : [DMAm] : [PEGDA] : [BTPA] : [TEtOHA] = 0.01 : 164 : 382 : 1 : 20 and [EB] : [DMAm] : [PEGDA] : [BTPA] : [TEtOHA] = 0.01 : 164 : 382 : 0 : 20 in bulk were used to print films. The sample geometries ($35 \times 7 \times 1$ mm (l, w, t)) and .stl files were generated using Autodesk Fusion 360. The sample printing parameters (slicing thickness and layer cure times) were generated using Micromake L4 software. The sample was then printed by using Micromake L4 DLP 3D printer. To ensure adhesion between the 3D printed material and the build stage, the first two (bottom) layers of the material were irradiated for 150 s, after which the regular cure time per layer was 20 s/layer with a layer thickness of 20 μ m. The Z lift distance was 1 mm, the Z lift speed was 30 mm/min, and the Z retract speed was 300 mm/min. After the object was printed, the build stage was removed, and the residual polymerisation surface was briefly washed with ethanol.

3D printing procedures of samples for post-modification

The resin formulation of [EB] : [DMAm] : [PEGDA] : [BTPA] : [TEtOHA] = 0.01 : 164 : 382 : 5 : 20 in bulk was used to print rectangular samples. The sample geometries ($50 \times 30 \times 2$ mm (l, w, t)) and .stl files were generated using Autodesk Fusion 360. The sample printing parameters (slicing thickness and layer cure times) were generated using Micromake L4 software. The sample was then printed by using Micromake L4 DLP 3D printer. To ensure adhesion between the 3D printed material and the build stage, the first two (bottom) layers of the material were irradiated for 150 s, after which the regular cure time per layer was 25 s/layer with a layer thickness of 20 μ m. The Z lift distance was 1 mm, the Z lift speed was 30 mm/min, and the Z retract speed was 300 mm/min. After the object was printed, the build stage was removed, and the residual polymerisation surface was briefly washed with ethanol.

DMA test of 3D printed rectangular samples

In DMA test, a 3D printed sample was measured with digital callipers, placed into the calibrated single cantilever clamp, and fixed into place with a torque wrench operated at a force of 5 in lb. The GCA was used to adjust the temperature to -25 $^{\circ}$ C and subsequently hold isothermal conditions for 2 minutes. The temperature was then ramped to 100 $^{\circ}$ C at a rate of 2 $^{\circ}$ C/min while the frequency was held constant at 1 Hz, using a displacement of 30 μ m. The storage modulus was determined around room temperature (specifically at the closest temperature to 20 $^{\circ}$ C) and 1 Hz, while the glass transition temperature (T_g) was calculated as the temperature at which the 1 Hz Tan δ curve peaked. All DMA results were performed using duplicate samples.

Contact angle measurements on 3D printed samples

The 3D printed material surface was washed with a solution of ethanol prior to contact angle measurements. A 20 μ L droplet of water was then pipetted onto the surface and left for 1 min prior to measurement of the contact angle. The photographs were processed using Microsoft powerpoint, and the contact angle was determined using Fiji imageJ software.

3.3 Results and Discussion

3.3.1 Optimisation of resin formulations

In the development of our RAFT mediated photopolymerisation process, we initially prioritised increasing the polymerisation rate such that application to open-air vat 3D printing systems would provide practical printing speeds. Based on our previous experience with organic dyes as PCs for PET-RAFT polymerisation, we initially tested two xanthene based dyes, namely eosin Y (EY) and erythrosin B (EB), for their ability to mediate rapid polymerisation under green light in the presence of air.⁶³⁻⁶⁹ EY is frequently used as a biological stain, and has also previously been used to initiate free-radical polymerisation in the presence of tertiary amines as co-catalysts via a type II photoinitiation mechanism, as well as other organic synthetic transformations.⁷⁰⁻⁷⁶ The structurally similar EB has been used by our group for PET-RAFT polymerisation, where it was determined to be a more effective PC compared to EY and similar halogenated xanthene dyes, such as phloxine B and rose bengal, due to its favourable photophysical and electrochemical properties, including a higher triplet quantum yield (Φ_T), decreased fluorescence quantum yield (Φ_F), and a higher excited state reduction potential ($E^0(\text{PC}^{\bullet+}/\text{PC}^*)$).⁶⁴⁻⁶⁵ In addition to the organic dye as PC, we also included a tertiary amine as co-catalyst in this system as these formulation have previously shown the ability to mediate rapid PET-RAFT polymerisation.⁶⁷ The inclusion of tertiary amines increases the polymerisation rate by providing more energetically favourable photoinduced electron transfer (PET) processes under green light irradiation.^{66, 77}

The reaction components and proposed mechanism of this photopolymerisation process are shown in **Figure 3.1**; after excitation by visible light, the PC can be reduced by tertiary amines, generating a reduced PC and a corresponding tertiary amine radical cation (**Figure 3.1B**). The reduced PC can then transfer an electron to the RAFT agent, returning the PC to the ground state. The reduced RAFT species subsequently undergoes β -scission of the weak C-S bond to generate a thiocarbonylthio stabilised anion species and a radical propagating species (P_n^{\bullet}) capable of adding across monomer vinyl bonds. The propagating radical species can interact with other thiocarbonylthio species and chain growth is regulated by the regular RAFT mechanism.³⁹ Recombination of the propagating radical with the anionic thiocarbonylthio species and further electron transfer to oxygen

or tertiary amine radical cations closes the catalytic cycle. Notably, molecular oxygen present in the reaction mixture can be consumed by electron transfer reactions from the reduced PC species or the anionic RAFT agent, as was proposed by Qiao and co-workers.^{63, 78} Although another mechanism involving direct electron transfer from the excited state PC to the RAFT agent is possible, the inclusion of tertiary amines in these mixtures favours the reductive PET-RAFT process shown in **Figure 3.1B**.⁶⁶

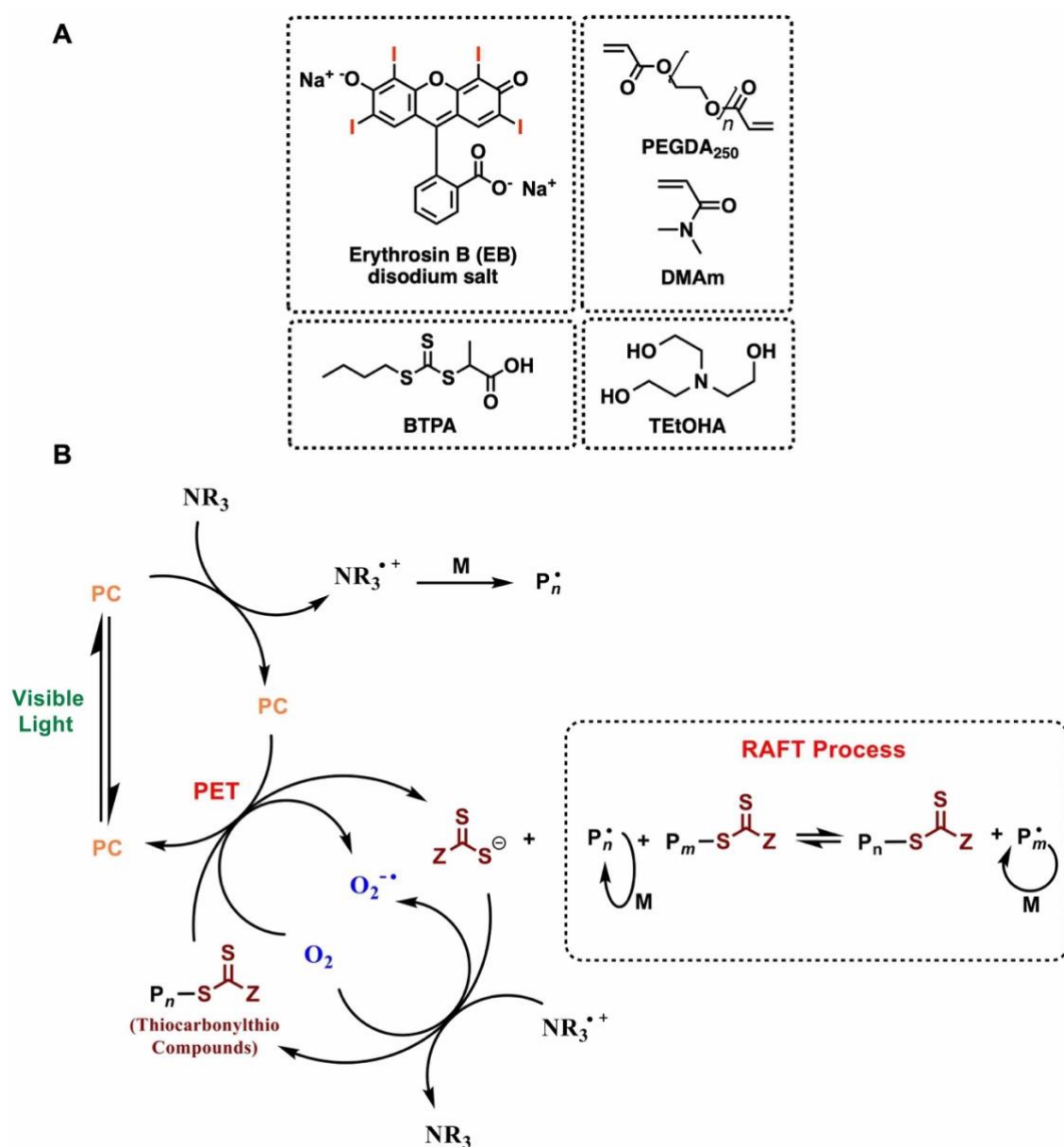


Figure 3.1 Thiocarbonylthio containing photopolymerisation resins. (A) reaction components; (B) proposed PET-RAFT mechanism. PC: photocatalyst; NR₃: tertiary amine; PET: photoinduced electron transfer.

For the initial model polymerisations, *N,N*-dimethylacrylamide (DMAm) and poly(ethylene glycol) diacrylate (PEGDA, average $M_n = 250$ g/mol) were used as monomer and crosslinker, respectively. 2-(Butylthiocarbonothioylthio) propanoic acid (BTPA) was selected as RAFT agent and triethanolamine (TEtOHA) was used as a tertiary amine co-catalyst, and the reaction was performed in water at a total solids content of 50 wt%. The initial ratio of [DMAm] : [PEGDA] : [BTPA] : [TEtOHA] was 1000 : 50 : 1 : 20 and the ratio of catalyst (EY or EB) to BTPA was either 0.1 : 1 or 0.1 : 0. The model polymerisations were conducted in open-air droplets (20 μ L) under 4.3 mW/cm² green light ($\lambda_{\text{max}} = 530$ nm) irradiation. We monitored the polymerisation kinetics of these systems under different conditions by following the disappearance of the peak assigned to the vinylic =C-H out of plane bending mode in ATR-FTIR spectroscopy. Particularly, the vinyl bond conversions after 1 min ($\alpha_{1\text{min}}$) and 4 mins ($\alpha_{4\text{min}}$) were used as a comparative guide; we reasoned those systems that present faster rates in the early stages of the polymerisation (i.e., high $\alpha_{4\text{min}}$ values), and those that present negligible induction periods ($\alpha_{1\text{min}}$), would be more suitable for implementation in 3D printing processes. This is particularly pertinent in 3D printing conducted in open-air vats, where the concentration of molecular oxygen is required to be reduced to a critical concentration prior to the onset of polymerisation.^{23, 25, 79-82}

The evolutions of vinyl bond conversions with time for the initial reactions, as determined by online ATR-FTIR spectroscopy, are shown in **Figure 3.2**. The catalytic system using EB provided faster polymerisation rates compared to EY for analogous recipes due to its favourable photocatalytic properties. Unexpectedly, however, the presence of BTPA in both systems provided a noticeable rate increase compared to systems that did not include the thiocarbonylthio species. The rate increase observed with the addition of RAFT agent can be attributed to an additional reaction pathway, that is, reduction of the RAFT agent by the radical anion PC species formed after photoreduction by the tertiary amine. Recently, Sikes and co-workers proposed a photochemical mechanism for the regeneration of ground state EY based on oxidation of the EY radical anion by molecular oxygen;⁸³ as the thiocarbonylthio species is also capable of oxidizing the dye radical anion species, the regeneration of the ground state PC for further catalytic cycles should also be present in our system.

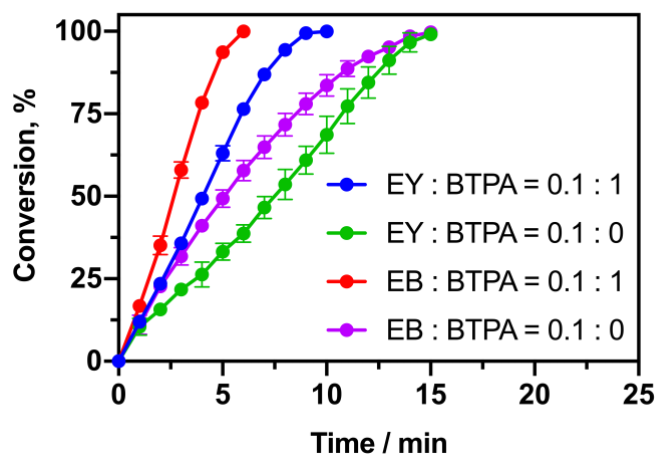


Figure 3.2 Kinetics of polymerisation for DMAM / PEGDA mixtures in the presence of EY or EB as PC, with varied molar ratios of BTPA as RAFT agent at a molar concentration of [DMAM] : [PEGDA] : [TetOHA] : [PC] : [BTPA] = 1000 : 50 : 20 : 0.1 : variable. Note: All reactions were performed using a solids content of 50 wt% under green light ($\lambda_{\text{max}} = 525 \text{ nm}$ and $I_0 = 4.3 \text{ mW/cm}^2$).

Given that EB provided faster polymerisation kinetics compared to EY in the model reactions, we subsequently investigated the effect of altering the other reaction components on the polymerisation rate. The initial experiments performed with varying concentrations of TetOHA showed that for analogous recipes, the polymerisation rates of EB catalysed systems were faster than those of EY catalysed systems (**Figure 3.3 and Table 3.1**). Therefore, EB was selected as the PC for further experiments. Interestingly, in the absence of BTPA and TetOHA the polymerisation still proceeded, albeit it at a much slower rate compared to the other systems.

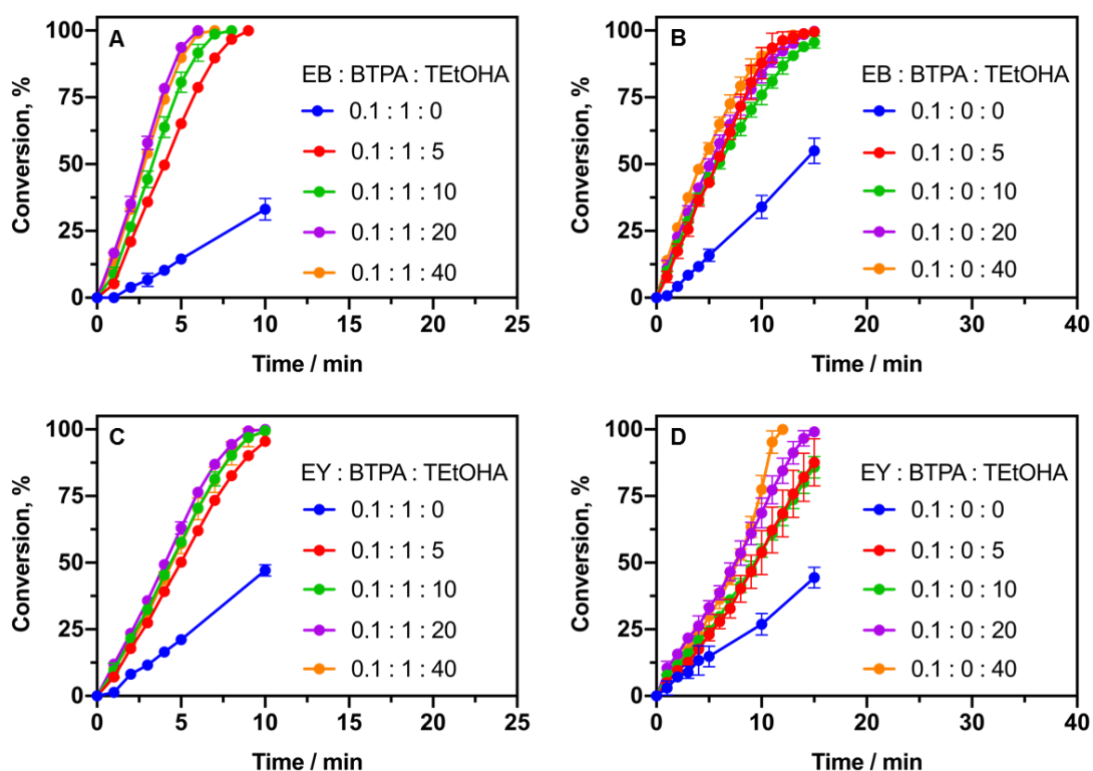


Figure 3.3 Kinetics of polymerisation for DMAM / PEGDA mixtures using EB or EY as catalyst and varied concentrations of BTPA and TEtOHA. (A) [EB] : [DMAM] : [PEGDA] : [BTPA] : [TEtOHA] = 0.1 : 1000 : 50 : 1 : variable; (B) [EB] : [DMAM] : [PEGDA] : [BTPA] : [TEtOHA] = 0.1 : 1000 : 50 : 0 : variable. (C) [EY] : [DMAM] : [PEGDA] : [BTPA] : [TEtOHA] = 0.1 : 1000 : 50 : 1 : variable; (D) [EY] : [DMAM] : [PEGDA] : [BTPA] : [TEtOHA] = 0.1 : 1000 : 50 : 0 : variable. Note: All reactions were performed using a solids content of 50 wt% under green light ($\lambda_{\text{max}} = 525 \text{ nm}$ and $I_0 = 4.3 \text{ mW/cm}^2$).

Table 3.1 Effect of changing catalyst and concentrations of TtEtOHA and BTPA on the polymerisation kinetics of DMAm / PEGDA mixtures performed in 50 wt% solutions of water.^a

#	PC	[PC]	[DMAm]	[PEGDA]	[BTPA]	[TtEtOHA]	$\alpha_{4\text{min}}$ (%) ^b	$\alpha_{1\text{min}}$ (%) ^b
1	EY	0.1	1000	50	1	0	16.5	1.4
2	EY	0.1	1000	50	1	5	39.2	7.2
3	EY	0.1	1000	50	1	10	45.3	9.6
4	EY	0.1	1000	50	1	20	49.3	12.0
5	EY	0.1	1000	50	1	40	44.1	10.3
6	EY	0.1	1000	50	0	0	13.3	3.0
7	EY	0.1	1000	50	0	5	17.5	5.0
8	EY	0.1	1000	50	0	10	20.9	7.9
9	EY	0.1	1000	50	0	20	26.3	10.5
10	EY	0.1	1000	50	0	40	22.9	7.7
11	EB	0.1	1000	50	1	0	10.3	0.0
12	EB	0.1	1000	50	1	5	49.7	5.2
13	EB	0.1	1000	50	1	10	63.9	8.8
14	EB	0.1	1000	50	1	20	78.3	16.7
15	EB	0.1	1000	50	1	40	74.3	13.9
16	EB	0.1	1000	50	0	0	11.7	0.8
17	EB	0.1	1000	50	0	5	36.3	7.8
18	EB	0.1	1000	50	0	10	37.1	10.0
19	EB	0.1	1000	50	0	20	41.1	11.1
20	EB	0.1	1000	50	0	40	48.1	13.9

^aConditions: reaction was performed using a solids content of 50 wt% monomer and crosslinker, with water as solvent. Polymerisation was performed under 4.3 mW/cm² green light ($\lambda_{\text{max}} = 525 \text{ nm}$), using a droplet (20 μL) of reaction mixture. ^bConversion determined by ATR-FTIR spectroscopy.

As the initial experiments performed with varying concentrations of TtEtOHA showed that the ratio of [EB] : [BTPA] : [TtEtOHA] of 0.1 : 1 : 20 provided the fastest polymerisation after 4 mins irradiation with vinyl bond conversion reaching 78.3%

(**Table 3.1**), the ratio of [BTPA] : [TEtOHA] = 1 : 20 was fixed while the catalyst concentration was varied. As shown in **Figure 3.4**, the polymerisation proceeded efficiently with EB : BTPA ratios between 0.1 and 0.005, and the fastest polymerisation occurred with a ratio of 0.025 : 1. Additionally, there was only a modest rate difference between this system and the system containing 2.5 times less EB ([EB] : [BTPA] = 0.01 : 1).

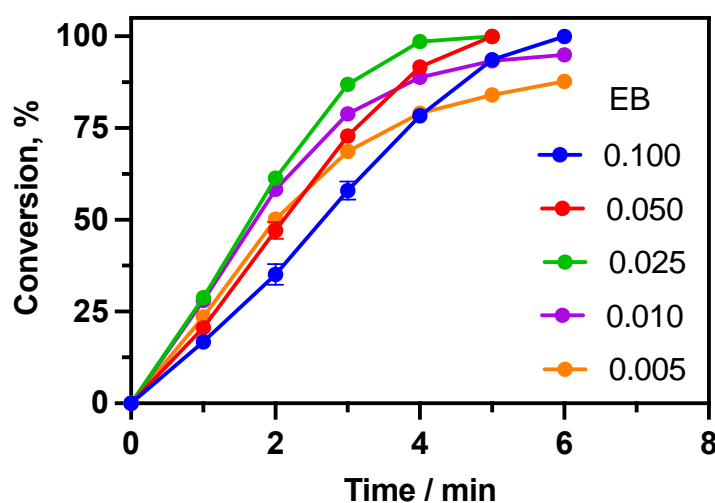


Figure 3.4 Kinetics of polymerisation for DMAM / PEGDA mixtures with varied molar ratio of EB as PC at a fixed molar concentration of [DMAM] : [PEGDA] : [TEtOHA] : [BTPA] = 1000 : 50 : 20 : 1. Note: All reactions were performed using a solids content of 50 wt% under green light ($\lambda_{\text{max}} = 525 \text{ nm}$ and $I_0 = 4.3 \text{ mW/cm}^2$).

The solids content in these model reactions was also varied between 25, 50, and 75 wt% while changing the TEtOHA ratio and EB ratio relative to RAFT agent; polymerisation proceeded in all cases with the 50 wt% system providing the fastest rates (**Figure 3.5** and **Table 3.2**).

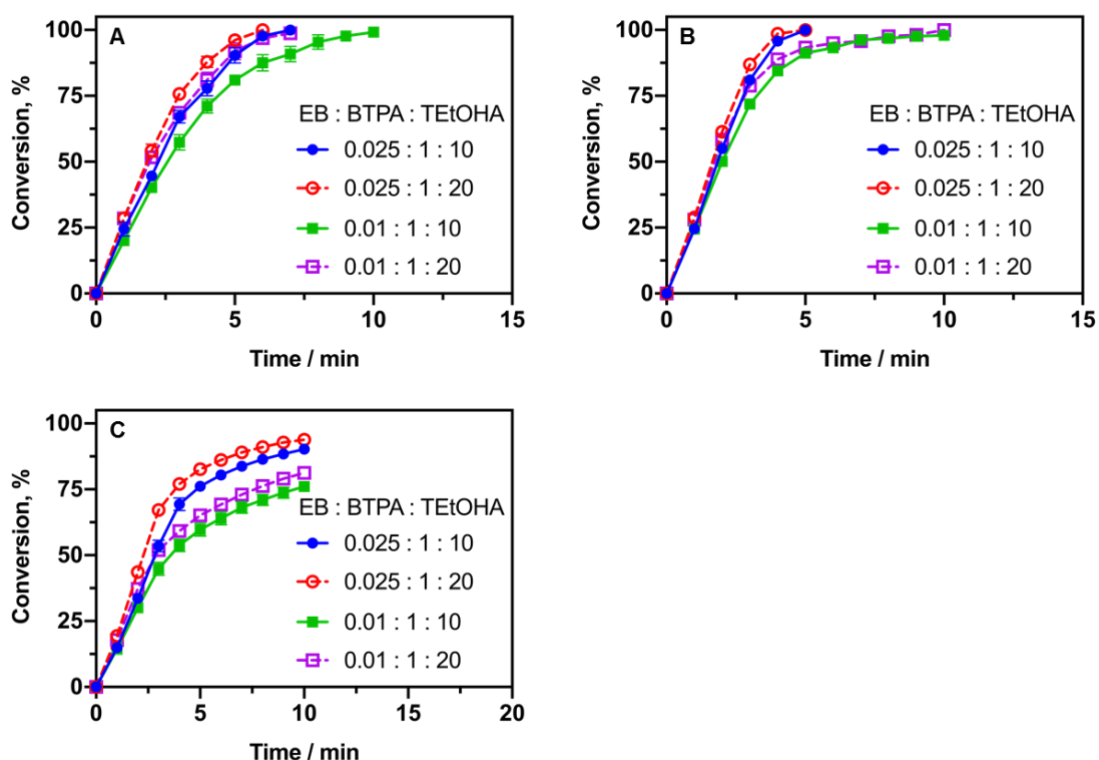


Figure 3.5 Kinetics of polymerisation for DMAM / PEGDA mixtures using BTPA as RAFT agent at different concentrations of EB and TetOHA and different total solids content. (A) solid content = 25%; (B) solid content = 50%; (C) solid content = 75%. Conditions: [EB] : [DMAM] : [PEGDA] : [BTPA] : [TetOHA] = 0.01/0.025 : 1000 : 50 : 1 : 10/20. Polymerisation was performed under 4.3 mW/cm² green light ($\lambda_{\text{max}} = 525$ nm), using a droplet (20 μL) of reaction mixture. Vinyl bond conversion over time was quantified by ATR-FTIR spectroscopy.

Table 3.2 Effect of changing catalyst and TEtOHA molar ratios, and the solids content of monomer and crosslinker on the polymerization kinetics of DMAm / PEGDA mixtures.^a

Weight ratio (%)	[EB]	[DMAm]	[PEGDA]	[BTPA]	[TEtOHA]	$\alpha_{4\text{min}}$ (%) ^b	$\alpha_{1\text{min}}$ (%) ^b
25	0.01	1000	50	1	10	71.1	20.1
25	0.01	1000	50	1	20	81.1	28.5
25	0.025	1000	50	1	10	77.9	24.5
25	0.025	1000	50	1	20	87.9	28.5
50	0.01	1000	50	1	10	84.5	24.5
50	0.01	1000	50	1	20	88.9	28.0
50	0.025	1000	50	1	10	95.8	24.5
50	0.025	1000	50	1	20	98.6	28.8
75	0.01	1000	50	1	10	53.7	14.3
75	0.01	1000	50	1	20	59.2	17.8
75	0.025	1000	50	1	10	69.4	14.9
75	0.025	1000	50	1	20	77.1	19.3

^aConditions: reaction was performed using a solids content of 25 wt%, 50 wt% and 75 wt% monomer and crosslinker, respectively, with water as solvent. Polymerisation was performed under 4.3 mW/cm² green light ($\lambda_{\text{max}} = 525$ nm), using a droplet (20 μL) of reaction mixture. ^bConversion determined by ATR-FTIR spectroscopy.

Encouragingly, these green light mediated model photopolymerisations presented rapid cure times under low energy ($I_0 = 4.3$ mW/cm²) green light. Prior to implementation in the 3D printing setup, we altered the ratio of monomer to crosslinker to tailor toward high modulus, free-standing materials once printed. **Figure 3.6A** shows the polymerisation rate under various ratios of [DMAm] : [PEGDA], using constant concentrations and ratios of [EB] : [BTPA] : [TEtOHA] = [0.01] : [1] : [20]. These reactions were performed in bulk to more closely match the prospective 3D printing conditions. Interestingly, the monomer conversions in these polymerisations did not surpass 70 %; this may be due to the formation of a rigid network in the early stages of polymerisation, and the inability of the pendent double bonds from PEGDA to participate in further reaction on the time scales investigated.⁸⁴ Regardless, we noticed that the polymers produced with higher

concentrations of PEGDA were free standing after the droplet polymerisation, which is to be expected given the higher network connectivity compared to the systems with higher molar fractions of DMAM. The polymerisation performed in bulk presented relatively slow rates when the [DMAM]: [PEGDA] ratio was above 70 : 30 and there was solubility issues below a ratio of 30 : 70 (**Table 3.3**). Comparatively, polymerisation using a 50 wt% formulation presented fast polymerisation rates with the vinyl bond conversion surpassing 88% after 4 minutes for ratios of DMAM: PEGDA between 95 : 5 and 70 : 30 (**Figure 3.6B**). Higher concentrations of PEGDA resulted in solubility issues in the 50 wt% system.

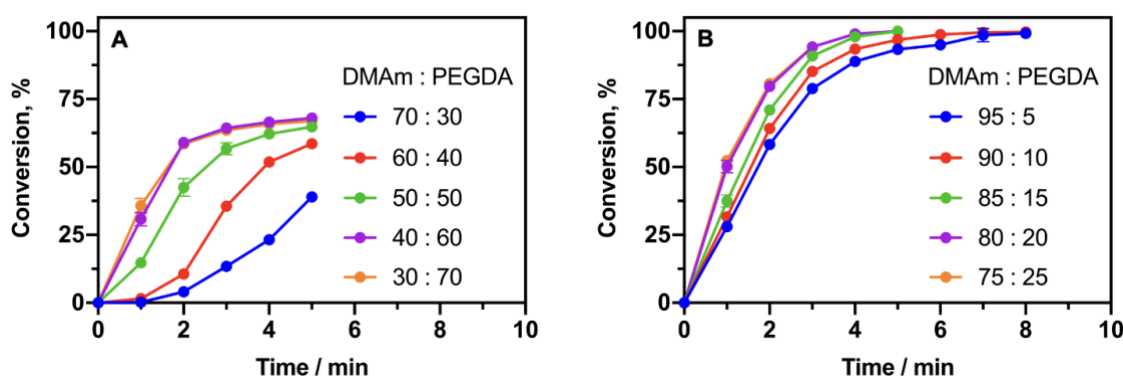


Figure 3.6 Kinetics of polymerisation for DMAM / PEGDA mixtures using BTPA as RAFT agent at different total solids content of DMAM and PEGDA and varied DMAM / PEGDA ratios. (A) bulk (solvent free) reaction using a ratio of [EB] : [BTPA] : [TEtOHA] = 0.01 : 1 : 20 and a constant BTPA molality of 8.96 mmol/kg; (B) solids content 50 wt% monomer and crosslinker using a ratio of [EB] : [BTPA] : [TETOHA] = 0.01 : 1 : 20 and a constant BTPA molality of 8.96 mmol/kg. *N.B.* DMAM : PEGDA ratio of 95 : 5 actually performed using a ratio of 1000 : 50 (approximately 95 : 5). Conditions: Polymerisation was performed under 4.3 mW/cm² green light ($\lambda_{\text{max}} = 525$ nm), using a droplet (20 μL) of reaction mixture. Vinyl bond conversion over time was quantified by ATR-FTIR spectroscopy.

Table 3.3 Effect of changing monomer and crosslinker molar ratios in an aqueous system (50 wt%) and in the absence of solvent (bulk) on the polymerisation kinetics of DMAM / PEGDA mixtures.^a

#	Weight ratio (wt %)	[DMAM]	[PEGDA]	$\alpha_{4\text{min}}$ (%) ^c	$\alpha_{1\text{min}}$ (%) ^c
1	50	95 ^b	5 ^b	88.9	28.0
2	50	90	10	93.4	31.6
3	50	85	15	97.9	37.5
4	50	80	20	99	50.1
5	50	75	25	99	52.4
6	50	70	30	– ^d	– ^d
7	Bulk	70	30	23.3	0.3
8	Bulk	60	40	51.8	1.5
9	Bulk	50	50	62.2	14.7
10	Bulk	40	60	66.5	30.8
11	Bulk	30	70	65.7	35.8
12	Bulk	10	90	– ^d	– ^d

^aConditions: reaction was performed both in aqueous solution with a solids content of 50 wt% monomer and crosslinker and in the absence of water as solvent (bulk). Polymerisation was performed under 4.3 mW/cm² green light ($\lambda_{\text{max}} = 525$ nm), using a droplet (20 μ L) of reaction mixtures. BTPA molality was 8.96 mmol/kg and the ratio of [EB] : [BTPA] : [TEtOHA] was fixed at 0.01 : 1 : 20. ^bRatio of DMAM : PEGDA was 1000 : 50 (approximately 95 : 5). ^cConversion determined by ATR-FTIR spectroscopy. ^dLow monomer to crosslinker molar ratios led to poor solubility of the reagents.

3.3.2 Controlling mechanical properties of RAFT containing 3D printed materials

Having established that photomediated polymerisation led to reasonable cure rates for our thiocarbonylthio containing resins, we then applied our resin to a 3D printing setup. For all 3D printing conducted in this work, a DLP 3D printer was used to spatially confine the material formation via digital masking of the green LED light source ($\lambda_{\text{max}} = 525$ nm, $I_0 = 0.32$ mW/cm²). Initially, three different resin formulations with varying ratios of [DMAM] : [PEGDA] and fixed concentrations of BTPA, EB, and TEtOHA were used to print a simple rectangular prism with dimensions $40 \times 13 \times 1.6$ mm (l, w, t) (**Figure 3.7C**).

These objects were printed using a layer slicing thickness of 20 μm and a layer cure time of 13 s. The storage modulus (E') and glass transition temperature (T_g) of the printed materials were then determined by dynamic mechanical analysis (DMA) by performing a temperature ramp from -50 $^{\circ}\text{C}$ to 100 $^{\circ}\text{C}$ at a frequency of 1 Hz (**Figure 3.7D**). E' was calculated at room temperature (≈ 20 $^{\circ}\text{C}$), while T_g was taken as the maximum of the $\tan \delta$ curve at a frequency of 1 Hz. As shown in **Figure 3.7A**, the samples printed in bulk with [DMAm] : [PEGDA] ratios of 30 : 70, 40 : 60, and 50 : 50, all showed similar E' values in the range of 250 MPa at 20 $^{\circ}\text{C}$. The T_g for the 30 : 70, 40 : 60, and 50 : 50 [DMAm] : [PEGDA] systems was 30, 31, and 33, respectively. This increase in T_g with the increase of DMAm concentration was expected given the relatively high T_g of DMAm (≈ 90 $^{\circ}\text{C}$) compared to typical PEG based acrylates (T_g typically less than 0 $^{\circ}\text{C}$).⁸⁵⁻⁸⁷ The samples printed with a higher mole fraction of PEGDA (i.e., 30 : 70 [DMAm] : [PEGDA]) resulted in 3D materials with slightly sharper features. Therefore, the [DMAm] : [PEGDA] ratio was then fixed at 30 : 70 for subsequent tests.

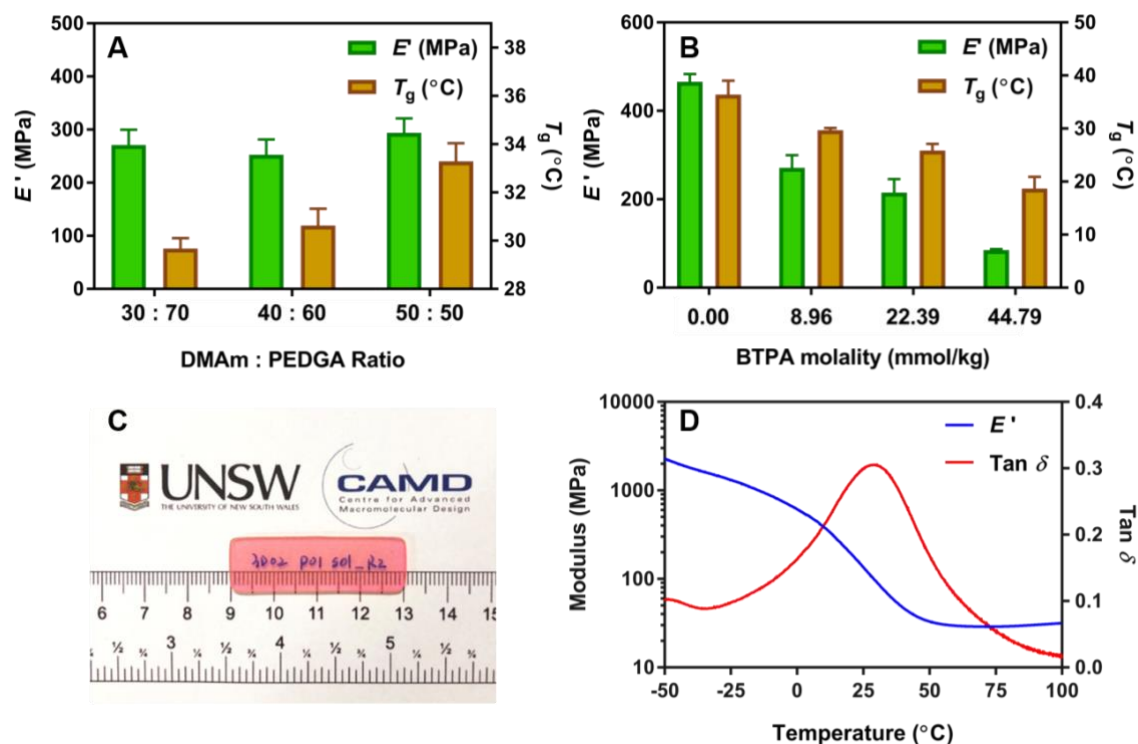


Figure 3.7 Samples 3D printed with photocontrolled RAFT polymerisation. (A) effect of changing the DMAM : PEGDA ratio on the storage modulus (E') and glass transition temperature (T_g), while holding the EB, BTPA, and TEtOHA concentrations constant; (B) effect of changing RAFT concentrations using a ratio [EB] : [DMAM] : [PEGDA] : [BTPA] : [TEtOHA] = 0.01 : 164 : 382 : variable : 20 in bulk; (C) sample printed with a layer thickness of 20 μm and cure time per layer of 13 s using a recipe of [EB] : [DMAM] : [PEGDA] : [BTPA] : [TEtOHA] = 0.01 : 164 : 382 : 1 : 20; (D) Storage modulus (E') and Tan δ for sample shown in **Figure 3.7C** at a frequency of 1 Hz determined by DMA. Error bars were calculated using duplicate samples.

We then examined the effect of the BTPA concentration of the mechanical properties of the 3D printed materials. As the thiocarbonylthio species plays a vital role in mediating the radical polymerisation process, we expected that altering its concentration would change the network structure, and in turn, the resultant material properties. As shown in **Figure 3.7B**, increasing the concentration of BTPA from 0, 8.96, 22.39, and 44.79 mmol per kg of resin (0, 100, 250, and 500 equivalents to EB) significantly reduced the E' as well as the T_g . The reduced stiffness in the materials containing a higher concentration of BTPA was ascribed to the correspondingly lower segmental molecular weight between crosslinks and higher concentration of chain ends; as described by Flory, Fox, and Stockmayer, these networks have a higher free volume, and thus lower modulus and T_g .⁸⁸⁻

⁹⁰ Notably, a range of functional groups, including trithiocarbonates, have been utilised for the formation and rearrangement of crosslinked networks, as well as for producing shape-memory and self-healing materials, and even to induce permanent phase changes of polymeric materials.⁹¹⁻¹⁰⁵ The inclusion of these trithiocarbonate species thus allows controlled tuning of the material mechanical properties based on their concentrations. We subsequently investigated the build rate of our 3D printed materials. The model system used to fabricate the 3D printed objects in the previous section used a layer slicing thickness of 20 μm and a total layer cure time of 13 s, resulting in a build rate of 0.55 cm/h. Using the same resin formulation, the slicing thickness was then increased to 100 μm and the cure time per layer was changed to 13, 20, 25, and 30 s, which led to ill-defined objects, except for the system that used a 30 s exposure time (**Figure 3.8**). Under these conditions, the build rate was increased to 1.2 cm/h.



Figure 3.8 3D printed object definition using a 100 μm layer slicing thickness and various layer cure times with the resin formulation of [EB] : [DMAM] : [PEGDA] : [BTPA] : [TEtOHA] = 0.01 : 164 : 382 : 1 : 20 in bulk. (A) 13 s exposure time per layer; (B) 20 s exposure time per layer; (C) 25 s exposure time per layer; (D) 30 s exposure time per layer.

Similarly, a layer cure time of 20 s was required to form well-defined objects when the slicing thickness per layer was reduced to 50 μm . As expected, changing the total light dose by altering the slicing thickness and cure time per layer affected the resulting E' and T_g of the 3D printed materials. For instance, increasing the layer cure time while holding the layer slicing thickness constant led to stiffer materials (**Figure 3.9A**). At a slicing thickness of 100 μm and layer cure time of 30 s the resulting E' was 100 MPa, while at a slicing thickness of 100 μm and layer cure time of 40 s the E' of the resulting material was 161 MPa. Additionally, printed materials that were post-cured through irradiation under green light ($\lambda_{\text{max}} = 525 \text{ nm}$, $I_0 = 4.3 \text{ mW/cm}^2$) showed increasing E' and T_g values up to 6 h post-cure time, which further demonstrated the ability for the mechanical properties of these materials to be manipulated via the irradiation parameters (**Figure 3.9B**).

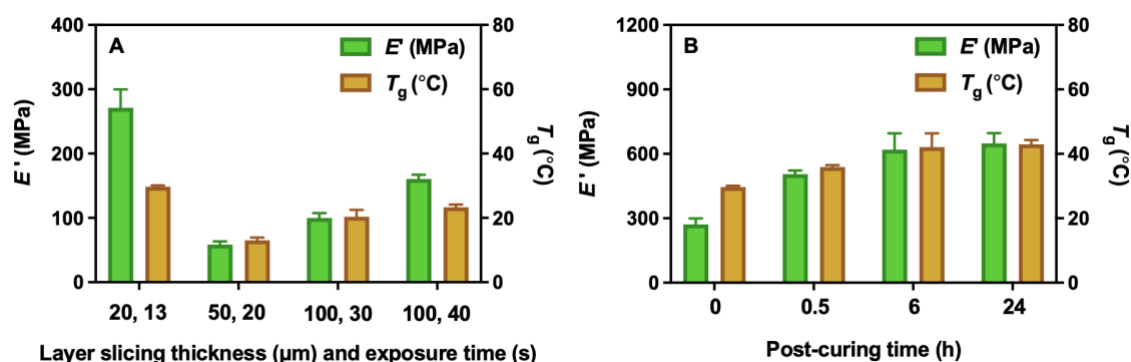


Figure 3.9 Mechanical properties of 3D printed materials by using the resin formulation of [EB] : [DMAm] : [PEGDA] : [BTPA] : [TEtOHA] = 0.01 : 164 : 382 : 1 : 20 in bulk. (A) effect of layer slicing thickness and irradiation time per layer on resulting storage modulus (E') and glass transition temperature (T_g). First number on x-axis label indicates layer thickness in μm and second number indicated exposure time per layer in seconds; (B) effect of post-curing times under 4.3 mW/cm^2 green light ($\lambda_{\text{max}} = 525 \text{ nm}$) irradiation on resulting storage modulus (E') and glass transition temperature (T_g).

3.3.3 4D printed materials through spatially controlled aqueous photopolymerisation

Spatially controlled light intensities have been previously explored by several groups for controlling the mechanical properties of 3D materials prepared by conventional photopolymerisation, and even for 4D printing via swelling and dehydration induced actuation.^{19, 106-109} As the mechanical properties of our 3D printed materials were

dependent on the light exposure, we decided to exploit these differences to print a material with spatially resolved properties. Furthermore, our resin formulations were water soluble, which allowed objects to be printed in aqueous solutions. To date, only a handful of aqueous 3D printing systems have been developed¹¹⁰⁻¹¹¹ due to the insolubility of typical photoinitiators and monomers in water, however, the current system tailors toward 3D bioprinting due to the high biocompatibility of aqueous systems.^{22, 27-28, 112} To demonstrate the utility of our formulation, a hydrogel with spatially resolved properties was 3D printed and subsequently dehydrated and re-swelled for actuation; as such, a 4D printed material was fabricated using our photosensitive resin. A cross shaped object with spatially resolved properties based on the light dose to each layer was designed as shown in **Figure 3.10A**, and printed using a ratio of [EB] : [DMAM] : [PEGDA] : [BTPA] : [TEtOHA] = 0.01 : 1000 : 50 : 1 : 20 in a 50 wt% solution of water. Using this geometry, the first layer was printed with a layer slicing thickness of 20 μm and a cure time 150 s, corresponding to a total dose of 108.0 mJ, while the subsequent 20 μm layers (99 layers) were exposed to green light for only 13 s, resulting in lower dose of light (9.4 mJ per layer) (**Figure 3.10B**). The cross was then placed in a water filled petri dish filled with the layer exposed to the higher light dose facing down; the cross started to deform as the layer with the higher cure time was swollen with water (**Figure 3.10C**). Subsequently, the cross was removed from the petri dish, flipped (**Figure 3.10D**), and exposed to a slow stream of compressed air to induce evaporation. Correspondingly, the arched cross flattened and then inverted its arch as the material dehydrated (**Figure 3.10E and F**).

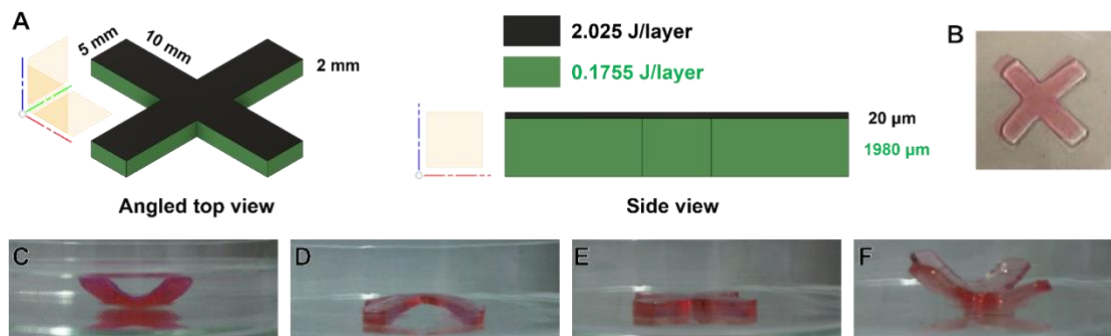


Figure 3.10 Swelling and desolvation induced actuation of a material 3D printed with spatially resolved light doses. (A) designed geometrical properties of cross; (B) top view of swollen cross geometry (layer exposed to higher light dose on bottom of object); (C) cross with layer exposed to higher light dose on the bottom, after 5 mins in water; (D) flipped swollen cross before dehydration (layer exposed to higher light dose on top); (E) cross after 80 seconds of dehydration; (F) cross after 7 mins of dehydration.

3.3.4 Reactivation of trithiocarbonate groups for post-modification of 3D printed materials

Interestingly, our pink coloured 3D printed materials changed colour after post-curing under green light irradiation, resulting in materials that displayed a yellow hue (**Figure 3.11A**). To verify that the yellow colour was the remaining RAFT agent in the 3D printed materials, UV-Vis spectroscopy was used to analyse films with dimensions $35 \times 7 \times 1$ mm (l, w, t) printed in both the absence and presence of BTPA using resin formulations of [EB] : [DMAm] : [PEGDA] : [BTPA] : [TEtOHA] = 0.01 : 164 : 382 : 1 : 20 and [EB] : [DMAm] : [PEGDA] : [BTPA] : [TEtOHA] = 0.01 : 164 : 382 : 0 : 20 in bulk. **Figure 3.11B** shows the UV-Vis spectra for films before and after a 45 min post-curing process under 4.3 mW/cm^2 green light irradiation. Both films printed in the presence and absence of BTPA displayed the typical EB absorption peak around 540 nm which disappeared after post-curing, however, only the film containing BTPA displayed an additional peak at 435 nm both before and after the photoinduced post-curing process.⁸³ This peak corresponds to the spin forbidden $n \rightarrow \pi^*$ transition of the thiocarbonyl group, and demonstrates the retention of the BTPA end group in our materials.⁴⁴

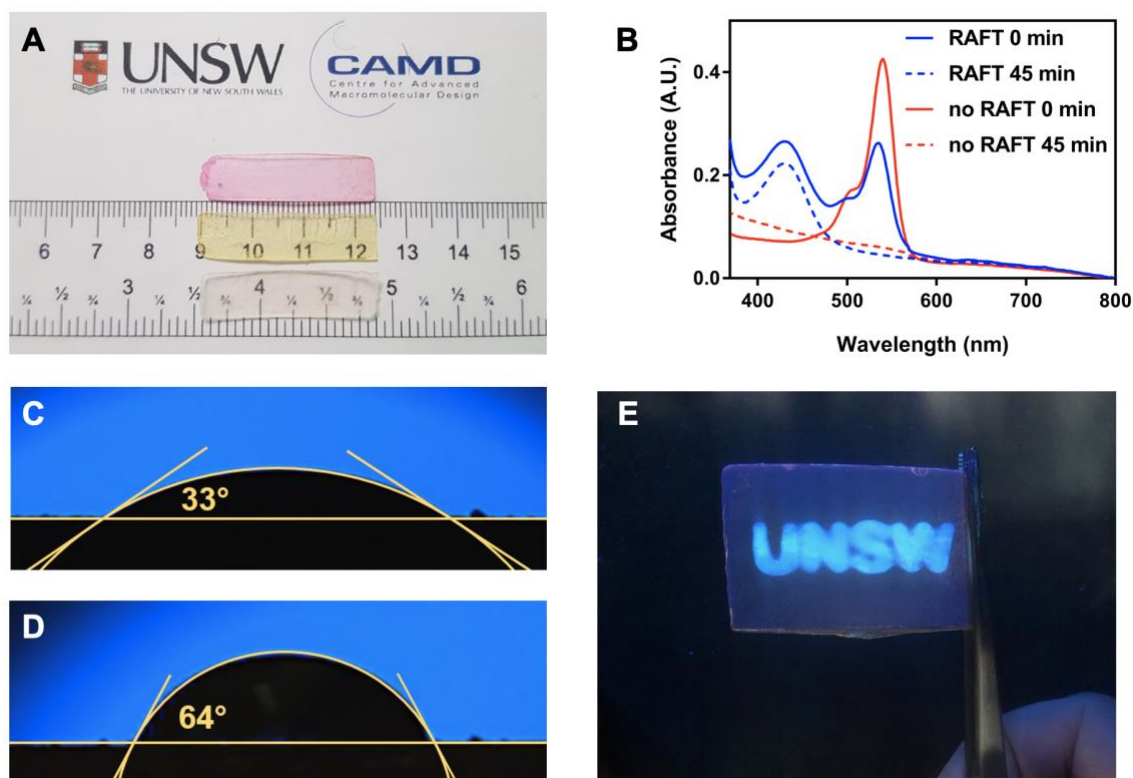


Figure 3.11 Secondary polymerisation from 3D printed materials to change the surface properties. (A) colour change in 3D printed films via post-curing under green light irradiation. From top: 3D printed film before post-curing, after post-curing for BTPA containing resins, and after post-curing for RAFT agent-free resins; (B) absorbance spectra before and after post-curing for films 3D printed in the presence and absence of RAFT agents; (C) high surface wettability of 3D printed DMAm/PEDGA networks; (D) decreased surface wettability for BA functionalised material; (E) spatially resolved fluorescence of 3D printed materials containing RAFT agent through photoinduced surface-functionalisation in the presence of pyrene-MMA.

The ability to reinitiate polymerisation from dormant thiocarbonylthio end-groups in the presence of diverse monomers has allowed multifunctional polymeric materials with diverse architectures to be synthesised in a straightforward manner. Moreover, surface-initiated RAFT polymerisation enables facile manipulation of surface properties. Indeed, many groups have investigated the initiation of surface tethered thiocarbonylthio species to impart functionality on the surface of materials.¹¹³⁻¹¹⁶ As our 3D printed materials contained thiocarbonylthio species throughout the network as well as on the surface, we posited that we could post-functionalise our materials via a secondary photopolymerisation process to change the surface properties. To demonstrate this

concept, we 3D printed a rectangular prism with dimensions of $50 \times 30 \times 2$ mm (l, w, t) using a recipe of [EB] : [DMAm] : [PEGDA] : [BTPA] : [TEtOHA] = 0.01 : 164 : 382 : 5 : 20; the monomers used during the 3D printing process provided a hydrophilic surface with high wettability (contact angle = 33°), as shown in **Figure 3.11C**. Following fabrication, the 3D printed object was thoroughly washed with ethanol and the reaction mixture in the 3D printer vat was then switched to a butyl acrylate (BA) solution containing EB with a ratio of [EB] : [BA] = 0.01 : 1000 and a small amount of ethanol (1.2 vol%) to help solubilise the EB. The vat was then irradiated with 0.32 mW/cm^2 green light for 5 mins to induce polymerisation on the surface of the hydrophilic network and change the surface properties. As shown in **Figure 3.11D**, the 3D printed material displayed a lower surface wettability following the secondary polymerisation process, as demonstrated by a higher water contact angle (64°). As such, the surface properties of our 3D printed materials were altered after the secondary polymerisation process.

To further demonstrate the ability to change the surface properties of our RAFT containing 3D printed materials, a spatially controlled polymerisation process using fluorescent monomers was performed. A DMAm/PEGDA network was fabricated and subsequently exposed to green light irradiation in the presence of 1-pyrene methylmethacrylate (pyrene-MMA), DMAm, and EB ([EB] : [pyrene-MMA] : [DMAm] = 0.01 : 20 : 980). The spatially controlled irradiation was demonstrated in the form of letters spelling “UNSW” across the material surface. Following 10 min irradiation, the 3D printed material was removed from the build stage and carefully washed three times with a 1/1 volume mixture of DMSO/ethanol and irradiated with UV light ($\lambda = 312 \text{ nm}$) to determine if the pyrene-MMA was successfully attached to the surface of the 3D printed material. As shown in **Figure 3.11E**, the 3D printed material showed strong fluorescence only in the “UNSW” region that was exposed to light during the secondary photopolymerisation, thus indicating a spatially controlled functionalisation from the RAFT agent on the surface of our 3D printed materials.

3.4 Conclusion

In summary, a water soluble and environmentally friendly photocurable resin containing thiocarbonylthio compounds for application to 3D and 4D printing processes was developed. The use of the organic dye EB in conjunction with triethanolamine as co-catalyst and BTPA as RAFT agent allowed build speeds up to 1.2 cm/h, and provided a platform for photoinduced 3D printing in aqueous solutions under benign, low energy green light irradiation; these systems thus tailor toward 3D-bioprinting applications. Remarkably, the ability to spatially control the dose of light applied during the 3D printing process provided stimuli-responsive materials in a one-pass fabrication process, as demonstrated by swelling and dehydration induced actuation of a 4D printed hydrogel. The spatially controlled properties conferred on these hydrogels demonstrate the first 4D printing using a RDRP process. More importantly, the retention of the RAFT functionality during the 3D printing process allowed the 3D printed materials to be easily post-modified after printing. The reinitiation of dormant RAFT agents on the surface of the 3D printed hydrophilic network structure was demonstrated by chain extension with a hydrophobic monomer, which resulted in an increase in surface hydrophobicity. Surface functionalisation of the 3D printed material was also able to be spatially confined through selected irradiation during the post-functionalisation. The versatility of this photomediated RAFT polymerisation process provides access to a range of new functional and stimuli-responsive materials which can be applied for the design of biocompatible materials.

3.5 Reference

1. Hartings, M. R.; Ahmed, Z., Chemistry from 3D printed objects. *Nature Reviews Chemistry* **2019**, 3(5), 305-314.
2. Huang, S. H.; Liu, P.; Mokasdar, A.; Hou, L., Additive manufacturing and its societal impact: a literature review. *The International Journal of Advanced Manufacturing Technology* **2013**, 67(5), 1191-1203.
3. Gross, B. C.; Erkal, J. L.; Lockwood, S. Y.; Chen, C.; Spence, D. M., Evaluation of 3D Printing and Its Potential Impact on Biotechnology and the Chemical Sciences. *Analytical Chemistry* **2014**, 86(7), 3240-3253.
4. Stansbury, J. W.; Idacavage, M. J., 3D printing with polymers: Challenges among expanding options and opportunities. *Dental Materials* **2016**, 32(1), 54-64.
5. Ligon, S. C.; Liska, R.; Stampfl, J.; Gurr, M.; Mülhaupt, R., Polymers for 3D Printing and Customized Additive Manufacturing. *Chemical Reviews* **2017**, 117(15), 10212-10290.
6. Barner-Kowollik, C.; Bastmeyer, M.; Blasco, E.; Delaittre, G.; Müller, P.; Richter, B.; Wegener, M., 3D Laser Micro- and Nanoprinting: Challenges for Chemistry. *Angewandte Chemie International Edition* **2017**, 56(50), 15828-15845.
7. Zhang, J.; Xiao, P., 3D printing of photopolymers. *Polymer Chemistry* **2018**, 9(13), 1530-1540.
8. Boydston, A. J.; Cao, B.; Nelson, A.; Ono, R. J.; Saha, A.; Schwartz, J. J.; Thrasher, C. J., Additive manufacturing with stimuli-responsive materials. *Journal of Materials Chemistry A* **2018**, 6(42), 20621-20645.
9. Kuang, X.; Roach, D. J.; Wu, J.; Hamel, C. M.; Ding, Z.; Wang, T.; Dunn, M. L.; Qi, H. J., Advances in 4D Printing: Materials and Applications. *Advanced Functional Materials* **2019**, 29(2), 1805290.
10. Hull, C. W. Apparatus for production of three-dimensional objects by stereolithography. 11 March 1986, 1986.
11. Bagheri, A.; Jin, J., Photopolymerization in 3D Printing. *ACS Applied Polymer Materials* **2019**, 1(4), 593-611.
12. Chatani, S.; Kloxin, C. J.; Bowman, C. N., The power of light in polymer science: photochemical processes to manipulate polymer formation, structure, and properties. *Polymer Chemistry* **2014**, 5(7), 2187-2201.
13. Corrigan, N.; Yeow, J.; Judzewitsch, P.; Xu, J.; Boyer, C., Seeing the Light: Advancing Materials Chemistry through Photopolymerization. *Angewandte Chemie International Edition* **2019**, 58(16), 5170-5189.
14. Mu, Q.; Wang, L.; Dunn, C. K.; Kuang, X.; Duan, F.; Zhang, Z.; Qi, H. J.; Wang, T., Digital light processing 3D printing of conductive complex structures. *Additive Manufacturing* **2017**, 18, 74-83.
15. Zieger, M. M.; Müller, P.; Blasco, E.; Petit, C.; Hahn, V.; Michalek, L.; Mutlu, H.; Wegener, M.; Barner-Kowollik, C., A Subtractive Photoresist Platform for Micro- and Macroscopic 3D Printed Structures. *Advanced Functional Materials* **2018**, 28(29), 1801405.
16. Gräfe, D.; Wickberg, A.; Zieger, M. M.; Wegener, M.; Blasco, E.; Barner-Kowollik, C., Adding chemically selective subtraction to multi-material 3D additive manufacturing. *Nature Communications* **2018**, 9(1), 2788.
17. Dolinski, N. D.; Page, Z. A.; Callaway, E. B.; Eisenreich, F.; Garcia, R. V.; Chavez, R.; Bothman, D. P.; Hecht, S.; Zok, F. W.; Hawker, C. J., Solution Mask Liquid Lithography (SMaLL) for One-Step, Multimaterial 3D Printing. *Advanced Materials* **2018**, 30(31), 1800364.

18. Schwartz, J. J.; Boydston, A. J., Multimaterial actinic spatial control 3D and 4D printing. *Nature Communications* **2019**, *10*(1), 791.
19. Peterson, G. I.; Schwartz, J. J.; Zhang, D.; Weiss, B. M.; Ganter, M. A.; Storti, D. W.; Boydston, A. J., Production of Materials with Spatially-Controlled Cross-Link Density via Vat Photopolymerization. *ACS Applied Materials & Interfaces* **2016**, *8*(42), 29037-29043.
20. Zhang, B.; Kowsari, K.; Serjouei, A.; Dunn, M. L.; Ge, Q., Reprocessable thermosets for sustainable three-dimensional printing. *Nature Communications* **2018**, *9*(1), 1831.
21. Adzima, B. J.; Kloxin, C. J.; DeForest, C. A.; Anseth, K. S.; Bowman, C. N., 3D Photofixation Lithography in Diels–Alder Networks. *Macromolecular Rapid Communications* **2012**, *33*(24), 2092-2096.
22. Kim, S. H.; Yeon, Y. K.; Lee, J. M.; Chao, J. R.; Lee, Y. J.; Seo, Y. B.; Sultan, M. T.; Lee, O. J.; Lee, J. S.; Yoon, S.-i.; Hong, I.-S.; Khang, G.; Lee, S. J.; Yoo, J. J.; Park, C. H., Precisely printable and biocompatible silk fibroin bioink for digital light processing 3D printing. *Nature Communications* **2018**, *9*(1), 1620.
23. Kelly, B. E.; Bhattacharya, I.; Heidari, H.; Shusteff, M.; Spadaccini, C. M.; Taylor, H. K., Volumetric additive manufacturing via tomographic reconstruction. *Science* **2019**, eaau7114.
24. Shusteff, M.; Browar, A. E. M.; Kelly, B. E.; Henriksson, J.; Weisgraber, T. H.; Panas, R. M.; Fang, N. X.; Spadaccini, C. M., One-step volumetric additive manufacturing of complex polymer structures. *Science Advances* **2017**, *3*(12), eaao5496.
25. Tumbleston, J. R.; Shirvanyants, D.; Ermoshkin, N.; Januszewicz, R.; Johnson, A. R.; Kelly, D.; Chen, K.; Pinschmidt, R.; Rolland, J. P.; Ermoshkin, A.; Samulski, E. T.; DeSimone, J. M., Continuous liquid interface production of 3D objects. *Science* **2015**, *347*(6228), 1349.
26. Eckel, Z. C.; Zhou, C.; Martin, J. H.; Jacobsen, A. J.; Carter, W. B.; Schaedler, T. A., Additive manufacturing of polymer-derived ceramics. *Science* **2016**, *351*(6268), 58.
27. Yin, H.; Ding, Y.; Zhai, Y.; Tan, W.; Yin, X., Orthogonal programming of heterogeneous micro-mechano-environments and geometries in three-dimensional biostereolithography. *Nature Communications* **2018**, *9*(1), 4096.
28. Mondschein, R. J.; Kanitkar, A.; Williams, C. B.; Verbridge, S. S.; Long, T. E., Polymer structure-property requirements for stereolithographic 3D printing of soft tissue engineering scaffolds. *Biomaterials* **2017**, *140*, 170-188.
29. Kotz, F.; Arnold, K.; Bauer, W.; Schild, D.; Keller, N.; Sachsenheimer, K.; Nargang, T. M.; Richter, C.; Helmer, D.; Rapp, B. E., Three-dimensional printing of transparent fused silica glass. *Nature* **2017**, *544*(7650), 337-339.
30. Ge, Q.; Sakhaei, A. H.; Lee, H.; Dunn, C. K.; Fang, N. X.; Dunn, M. L., Multimaterial 4D Printing with Tailorable Shape Memory Polymers. *Scientific Reports* **2016**, *6*, 31110.
31. Boyer, C.; Corrigan, N. A.; Jung, K.; Nguyen, D.; Nguyen, T.-K.; Adnan, N. N. M.; Oliver, S.; Shanmugam, S.; Yeow, J., Copper-Mediated Living Radical Polymerization (Atom Transfer Radical Polymerization and Copper(0) Mediated Polymerization): From Fundamentals to Bioapplications. *Chemical Reviews* **2016**, *116*(4), 1803-1949.
32. Moad, G.; Rizzardo, E.; Thang, S. H., Living Radical Polymerization by the RAFT Process – A Third Update. *Australian journal of chemistry* **2012**, *65*(8), 985-1076.
33. Hawker, C. J., Molecular Weight Control by a "Living" Free-Radical Polymerization Process. *Journal of the American Chemical Society* **1994**, *116*(24), 11185-11186.

34. Wang, J.-S.; Matyjaszewski, K., Controlled/"living" radical polymerization. atom transfer radical polymerization in the presence of transition-metal complexes. *Journal of the American Chemical Society* **1995**, *117*(20), 5614-5615.
35. Braunecker, W. A.; Matyjaszewski, K., Controlled/living radical polymerization: Features, developments, and perspectives. *Progress in Polymer Science* **2007**, *32*(1), 93-146.
36. Perrier, S.; Takolpuckdee, P., Macromolecular design via reversible addition–fragmentation chain transfer (RAFT)/xanthates (MADIX) polymerization. *Journal of Polymer Science Part A: Polymer Chemistry* **2005**, *43*(22), 5347-5393.
37. Shanmugam, S.; Matyjaszewski, K., Reversible Deactivation Radical Polymerization: State-of-the-Art in 2017. In *Reversible Deactivation Radical Polymerization: Mechanisms and Synthetic Methodologies*, American Chemical Society: 2018; pp 1-39.
38. Barner-Kowollik, C., *Handbook of RAFT polymerization*. John Wiley & Sons: 2008.
39. Chiefari, J.; Chong, Y.; Ercole, F.; Krstina, J.; Jeffery, J.; Le, T. P.; Mayadunne, R. T.; Meijs, G. F.; Moad, C. L.; Moad, G., Living free-radical polymerization by reversible addition– fragmentation chain transfer: the RAFT process. *Macromolecules* **1998**, *31*(16), 5559-5562.
40. Perrier, S., 50th Anniversary Perspective: RAFT Polymerization—A User Guide. *Macromolecules* **2017**, *50*(19), 7433-7447.
41. Hawker, C. J.; Bosman, A. W.; Harth, E., New Polymer Synthesis by Nitroxide Mediated Living Radical Polymerizations. *Chemical Reviews* **2001**, *101*(12), 3661-3688.
42. Hill, M. R.; Carmean, R. N.; Sumerlin, B. S., Expanding the Scope of RAFT Polymerization: Recent Advances and New Horizons. *Macromolecules* **2015**, *48*(16), 5459-5469.
43. Xu, J.; Shanmugam, S.; Corrigan, N. A.; Boyer, C., Catalyst-Free Visible Light-Induced RAFT Photopolymerization. In *Controlled Radical Polymerization: Mechanisms*, American Chemical Society: 2015; pp 247-267.
44. McKenzie, T. G.; Fu, Q.; Wong, E. H. H.; Dunstan, D. E.; Qiao, G. G., Visible Light Mediated Controlled Radical Polymerization in the Absence of Exogenous Radical Sources or Catalysts. *Macromolecules* **2015**, *48*(12), 3864-3872.
45. Shanmugam, S.; Xu, J.; Boyer, C., Exploiting Metalloporphyrins for Selective Living Radical Polymerization Tunable over Visible Wavelengths. *Journal of the American Chemical Society* **2015**, *137*(28), 9174-9185.
46. Corrigan, N.; Rosli, D.; Jones, J. W. J.; Xu, J.; Boyer, C., Oxygen Tolerance in Living Radical Polymerization: Investigation of Mechanism and Implementation in Continuous Flow Polymerization. *Macromolecules* **2016**, *49*(18), 6779-6789.
47. Xu, J.; Jung, K.; Atme, A.; Shanmugam, S.; Boyer, C., A Robust and Versatile Photoinduced Living Polymerization of Conjugated and Unconjugated Monomers and Its Oxygen Tolerance. *Journal of the American Chemical Society* **2014**, *136*(14), 5508-5519.
48. Shanmugam, S.; Xu, J.; Boyer, C., Utilizing the electron transfer mechanism of chlorophyll a under light for controlled radical polymerization. *Chemical Science* **2015**, *6*(2), 1341-1349.
49. Shanmugam, S.; Xu, J.; Boyer, C., Light-Regulated Polymerization under Near-Infrared/Far-Red Irradiation Catalyzed by Bacteriochlorophyll a. *Angewandte Chemie International Edition* **2016**, *55*(3), 1036-1040.
50. Zhang, L.; Wu, C.; Jung, K.; Ng, Y. H.; Boyer, C., An Oxygen Paradox: Catalytic Use of Oxygen in Radical Photopolymerization. *Angew Chem Int Ed Engl* **2019**, *58*(47), 16811-16814.

51. Corrigan, N.; Xu, J.; Boyer, C.; Allonas, X., Exploration of the PET-RAFT Initiation Mechanism for Two Commonly Used Photocatalysts. *ChemPhotoChem* **2019**, 3(11), 1193-1199.
52. Seal, P.; Xu, J.; De Luca, S.; Boyer, C.; Smith, S. C., Unraveling Photocatalytic Mechanism and Selectivity in PET-RAFT Polymerization. *Advanced Theory and Simulations* **2019**, 2(6), 1900038.
53. Chen, M.; Gu, Y.; Singh, A.; Zhong, M.; Jordan, A. M.; Biswas, S.; Korley, L. T. J.; Balazs, A. C.; Johnson, J. A., Living Additive Manufacturing: Transformation of Parent Gels into Diversely Functionalized Daughter Gels Made Possible by Visible Light Photoredox Catalysis. *ACS Central Science* **2017**, 3(2), 124-134.
54. Zhou, H.; Johnson, J. A., Photo-controlled Growth of Telechelic Polymers and End-linked Polymer Gels. *Angewandte Chemie International Edition* **2013**, 52(8), 2235-2238.
55. Cuthbert, J.; Beziau, A.; Gottlieb, E.; Fu, L.; Yuan, R.; Balazs, A. C.; Kowalewski, T.; Matyjaszewski, K., Transformable Materials: Structurally Tailored and Engineered Macromolecular (STEM) Gels by Controlled Radical Polymerization. *Macromolecules* **2018**, 51(10), 3808-3817.
56. Shanmugam, S.; Cuthbert, J.; Flum, J.; Fantin, M.; Boyer, C.; Kowalewski, T.; Matyjaszewski, K., Transformation of gels via catalyst-free selective RAFT photoactivation. *Polymer Chemistry* **2019**, 10(19), 2477-2483.
57. Bagheri, A.; Bainbridge, C.; Jin, J., Visible Light-Induced Transformation of Polymer Networks. *ACS Applied Polymer Materials* **2019**, 1(7), 1896-1904.
58. Lampley, M. W.; Tsogtgerel, E.; Harth, E., Nanonetwork photogrowth expansion: Tailoring nanoparticle networks' chemical structure and local topology. *Polymer Chemistry* **2019**, 10(28), 3841-3850.
59. Shanmugam, S.; Xu, J.; Boyer, C., Living Additive Manufacturing. *ACS Central Science* **2017**, 3(2), 95-96.
60. Amamoto, Y.; Kamada, J.; Otsuka, H.; Takahara, A.; Matyjaszewski, K., Repeatable Photoinduced Self-Healing of Covalently Cross-Linked Polymers through Reshuffling of Trithiocarbonate Units. *Angewandte Chemie International Edition* **2011**, 50(7), 1660-1663.
61. Gordon, M. B.; French, J. M.; Wagner, N. J.; Kloxin, C. J., Dynamic Bonds in Covalently Crosslinked Polymer Networks for Photoactivated Strengthening and Healing. *Advanced Materials* **2015**, 27(48), 8007-8010.
62. Pawar, A. A.; Halivni, S.; Waiskopf, N.; Ben-Shahar, Y.; Soreni-Harari, M.; Bergbreiter, S.; Banin, U.; Magdassi, S., Rapid Three-Dimensional Printing in Water Using Semiconductor-Metal Hybrid Nanoparticles as Photoinitiators. *Nano letters* **2017**, 17(7), 4497-4501.
63. Xu, J.; Shanmugam, S.; Duong, H. T.; Boyer, C., Organo-photocatalysts for photoinduced electron transfer-reversible addition-fragmentation chain transfer (PET-RAFT) polymerization. *Polymer Chemistry* **2015**, 6(31), 5615-5624.
64. Wu, C.; Corrigan, N.; Lim, C.-H.; Jung, K.; Zhu, J.; Miyake, G.; Xu, J.; Boyer, C., Guiding the Design of Organic Photocatalyst for PET-RAFT Polymerization: Halogenated Xanthene Dyes. *Macromolecules* **2019**, 52(1), 236-248.
65. Corrigan, N.; Zhernakov, L.; Hashim, M. H.; Xu, J.; Boyer, C., Flow mediated metal-free PET-RAFT polymerisation for upscaled and consistent polymer production. *Reaction Chemistry & Engineering* **2019**, 4(7), 1216-1228.
66. Figg, C. A.; Hickman, J. D.; Scheutz, G. M.; Shanmugam, S.; Carmean, R. N.; Tucker, B. S.; Boyer, C.; Sumerlin, B. S., Color-Coding Visible Light Polymerizations

To Elucidate the Activation of Trithiocarbonates Using Eosin Y. *Macromolecules* **2018**, *51*(4), 1370-1376.

67. Zaquen, N.; Kadir, A. M. N. B. P. H. A.; Iasa, A.; Corrigan, N.; Junkers, T.; Zetterlund, P. B.; Boyer, C., Rapid Oxygen Tolerant Aqueous RAFT Photopolymerization in Continuous Flow Reactors. *Macromolecules* **2019**, *52*(4), 1609-1619.

68. Shanmugam, S.; Xu, S.; Adnan, N. N. M.; Boyer, C., Heterogeneous Photocatalysis as a Means for Improving Recyclability of Organocatalyst in “Living” Radical Polymerization. *Macromolecules* **2018**, *51*(3), 779-790.

69. Jin, J.; Bagheri, A., *Submitted*.

70. Avens, H. J.; Chang, E. L.; May, A. M.; Berron, B. J.; Seedorf, G. J.; Balasubramaniam, V.; Bowman, C. N., Fluorescent polymeric nanocomposite films generated by surface-mediated photoinitiation of polymerization. *Journal of Nanoparticle Research* **2011**, *13*(1), 331-346.

71. Avens, H. J.; Bowman, C. N., Development of fluorescent polymerization-based signal amplification for sensitive and non-enzymatic biodetection in antibody microarrays. *Acta Biomaterialia* **2010**, *6*(1), 83-89.

72. Avens, H. J.; Bowman, C. N., Mechanism of cyclic dye regeneration during eosin-sensitized photoinitiation in the presence of polymerization inhibitors. *Journal of Polymer Science Part A: Polymer Chemistry* **2009**, *47*(22), 6083-6094.

73. Avens, H. J.; Randle, T. J.; Bowman, C. N., Polymerization behavior and polymer properties of eosin-mediated surface modification reactions. *Polymer* **2008**, *49*(22), 4762-4768.

74. Hu, J.; Wang, J.; Nguyen, T. H.; Zheng, N., The chemistry of amine radical cations produced by visible light photoredox catalysis. *Beilstein Journal of Organic Chemistry* **2013**, *9*, 1977-2001.

75. Kızılel, S.; Pérez-Luna, V. H.; Teymour, F., Photopolymerization of Poly(Ethylene Glycol) Diacrylate on Eosin-Functionalized Surfaces. *Langmuir* **2004**, *20*(20), 8652-8658.

76. Hari, D. P.; König, B., Synthetic applications of eosin Y in photoredox catalysis. *Chemical Communications* **2014**, *50*(51), 6688-6699.

77. Nomeir, B.; Fabre, O.; Ferji, K., Effect of Tertiary Amines on the Photoinduced Electron Transfer-Reversible Addition-Fragmentation Chain Transfer (PET-RAFT) Polymerization. *Macromolecules* **2019**, *52*(18), 6898-6903.

78. Fu, Q.; Xie, K.; McKenzie, T. G.; Qiao, G. G., Trithiocarbonates as intrinsic photoredox catalysts and RAFT agents for oxygen tolerant controlled radical polymerization. *Polymer Chemistry* **2017**, *8*(9), 1519-1526.

79. Yeow, J.; Chapman, R.; Gormley, A. J.; Boyer, C., Up in the air: oxygen tolerance in controlled/living radical polymerisation. *Chemical Society Reviews* **2018**, *47*(12), 4357-4387.

80. Ligon, S. C.; Husár, B.; Wutzel, H.; Holman, R.; Liska, R., Strategies to Reduce Oxygen Inhibition in Photoinduced Polymerization. *Chemical Reviews* **2014**, *114*(1), 557-589.

81. Bowman, C. N.; Kloxin, C. J., Toward an enhanced understanding and implementation of photopolymerization reactions. *AIChE Journal* **2008**, *54*(11), 2775-2795.

82. Childress, K. K.; Kim, K.; Glugla, D. J.; Musgrave, C. B.; Bowman, C. N.; Stansbury, J. W., Independent Control of Singlet Oxygen and Radical Generation via Irradiation of a Two-Color Photosensitive Molecule. *Macromolecules* **2019**, *52*(13), 4968-4978.

83. Aguirre-Soto, A.; Kaastrup, K.; Kim, S.; Ugo-Beke, K.; Sikes, H. D., Excitation of Metastable Intermediates in Organic Photoredox Catalysis: Z-Scheme Approach Decreases Catalyst Inactivation. *ACS Catalysis* **2018**, 8(7), 6394-6400.
84. Ligon-Auer, S. C.; Schwentenwein, M.; Gorsche, C.; Stampfl, J.; Liska, R., Toughening of photo-curable polymer networks: a review. *Polymer Chemistry* **2016**, 7(2), 257-286.
85. Brandrup, J.; Immergut, E. H.; Grulke, E. A.; Abe, A.; Bloch, D. R., *Polymer handbook*. Wiley New York: 1999; Vol. 89.
86. Krause, S.; Gormley, J. J.; Roman, N.; Shetter, J. A.; Watanabe, W. H., Glass temperatures of some acrylic polymers. *Journal of Polymer Science Part A: General Papers* **1965**, 3(10), 3573-3586.
87. Ju, H.; McCloskey, B. D.; Sagle, A. C.; Kusuma, V. A.; Freeman, B. D., Preparation and characterization of crosslinked poly(ethylene glycol) diacrylate hydrogels as fouling-resistant membrane coating materials. *Journal of Membrane Science* **2009**, 330(1), 180-188.
88. Fox, T. G.; Flory, P. J., Second-Order Transition Temperatures and Related Properties of Polystyrene. I. Influence of Molecular Weight. *Journal of Applied Physics* **1950**, 21(6), 581-591.
89. Stockmayer, W. H., Theory of Molecular Size Distribution and Gel Formation in Branched-Chain Polymers. *The Journal of Chemical Physics* **1943**, 11(2), 45-55.
90. Flory, P. J., *Principles of polymer chemistry*. Cornell university press: 1953.
91. Kloxin, C. J.; Bowman, C. N., Covalent adaptable networks: smart, reconfigurable and responsive network systems. *Chemical Society Reviews* **2013**, 42(17), 7161-7173.
92. Chakma, P.; Konkolewicz, D., Dynamic Covalent Bonds in Polymeric Materials. *Angewandte Chemie International Edition* **2019**, 58(29), 9682-9695.
93. Meng, Y.; Fenoli, C. R.; Aguirre-Soto, A.; Bowman, C. N.; Anthamatten, M., Photoinduced Diffusion Through Polymer Networks. *Advanced Materials* **2014**, 26(37), 6497-6502.
94. Yakacki, C. M.; Shandas, R.; Safranski, D.; Ortega, A. M.; Sassaman, K.; Gall, K., Strong, Tailored, Biocompatible Shape-Memory Polymer Networks. *Advanced Functional Materials* **2008**, 18(16), 2428-2435.
95. Park, H. Y.; Kloxin, C. J.; Scott, T. F.; Bowman, C. N., Stress Relaxation by Addition-Fragmentation Chain Transfer in Highly Cross-Linked Thiol-Yne Networks. *Macromolecules* **2010**, 43(24), 10188-10190.
96. Lendlein, A.; Jiang, H.; Jünger, O.; Langer, R., Light-induced shape-memory polymers. *Nature* **2005**, 434(7035), 879-882.
97. Kloxin, C. J.; Scott, T. F.; Park, H. Y.; Bowman, C. N., Mechanophotopatterning on a Photoresponsive Elastomer. *Advanced Materials* **2011**, 23(17), 1977-1981.
98. Kloxin, C. J.; Scott, T. F.; Bowman, C. N., Stress Relaxation via Addition-Fragmentation Chain Transfer in a Thiol-ene Photopolymerization. *Macromolecules* **2009**, 42(7), 2551-2556.
99. Scott, T. F.; Schneider, A. D.; Cook, W. D.; Bowman, C. N., Photoinduced Plasticity in Cross-Linked Polymers. *Science* **2005**, 308(5728), 1615.
100. Telitel, S.; Amamoto, Y.; Poly, J.; Morlet-Savary, F.; Soppera, O.; Lalevée, J.; Matyjaszewski, K., Introduction of self-healing properties into covalent polymer networks via the photodissociation of alkoxyamine junctions. *Polymer Chemistry* **2014**, 5(3), 921-930.
101. Amamoto, Y.; Otsuka, H.; Takahara, A.; Matyjaszewski, K., Self-Healing of Covalently Cross-Linked Polymers by Reshuffling Thiuram Disulfide Moieties in Air under Visible Light. *Advanced Materials* **2012**, 24(29), 3975-3980.

102. Amamoto, Y.; Otsuka, H.; Takahara, A.; Matyjaszewski, K., Changes in Network Structure of Chemical Gels Controlled by Solvent Quality through Photoinduced Radical Reshuffling Reactions of Trithiocarbonate Units. *ACS Macro Letters* **2012**, *1*(4), 478-481.
103. McBride, M. K.; Hendrikx, M.; Liu, D.; Worrell, B. T.; Broer, D. J.; Bowman, C. N., Photoinduced Plasticity in Cross-Linked Liquid Crystalline Networks. *Advanced Materials* **2017**, *29*(17), 1606509.
104. Worrell, B. T.; McBride, M. K.; Lyon, G. B.; Cox, L. M.; Wang, C.; Mavila, S.; Lim, C.-H.; Coley, H. M.; Musgrave, C. B.; Ding, Y.; Bowman, C. N., Bistable and photoswitchable states of matter. *Nature Communications* **2018**, *9*(1), 2804.
105. Gernhardt, M.; Blasco, E.; Hippler, M.; Blinco, J.; Bastmeyer, M.; Wegener, M.; Frisch, H.; Barner-Kowollik, C., Tailoring the Mechanical Properties of 3D Microstructures Using Visible Light Post-Manufacturing. *Advanced Materials* **2019**, *31*(30), 1901269.
106. Kuang, X.; Wu, J.; Chen, K.; Zhao, Z.; Ding, Z.; Hu, F.; Fang, D.; Qi, H. J., Grayscale digital light processing 3D printing for highly functionally graded materials. *Science Advances* **2019**, *5*(5), eaav5790.
107. Wiley, K. L.; Ovadia, E. M.; Calo, C. J.; Huber, R. E.; Kloxin, A. M., Rate-based approach for controlling the mechanical properties of 'thiol-ene' hydrogels formed with visible light. *Polymer Chemistry* **2019**, *10*(32), 4428-4440.
108. Huang, L.; Jiang, R.; Wu, J.; Song, J.; Bai, H.; Li, B.; Zhao, Q.; Xie, T., Ultrafast Digital Printing toward 4D Shape Changing Materials. *Advanced Materials* **2017**, *29*(7), 1605390.
109. Zhao, Z.; Wu, J.; Mu, X.; Chen, H.; Qi, H. J.; Fang, D., Desolvation Induced Origami of Photocurable Polymers by Digit Light Processing. *Macromolecular Rapid Communications* **2017**, *38*(13), 1600625.
110. Pawar, A. A.; Saada, G.; Cooperstein, I.; Larush, L.; Jackman, J. A.; Tabaei, S. R.; Cho, N.-J.; Magdassi, S., High-performance 3D printing of hydrogels by water-dispersible photoinitiator nanoparticles. *Science Advances* **2016**, *2*(4), e1501381.
111. Pawar, A. A.; Halivni, S.; Waiskopf, N.; Ben-Shahar, Y.; Soreni-Harari, M.; Bergbreiter, S.; Banin, U.; Magdassi, S., Rapid Three-Dimensional Printing in Water Using Semiconductor-Metal Hybrid Nanoparticles as Photoinitiators. *Nano Letters* **2017**, *17*(7), 4497-4501.
112. Niu, J.; Lunn, D. J.; Pusuluri, A.; Yoo, J. I.; O'Malley, M. A.; Mitragotri, S.; Soh, H. T.; Hawker, C. J., Engineering live cell surfaces with functional polymers via cytocompatible controlled radical polymerization. *Nature Chemistry* **2017**, *9*(6), 537-545.
113. Rowe-Konopacki, M. D.; Boyes, S. G., Synthesis of Surface Initiated Diblock Copolymer Brushes from Flat Silicon Substrates Utilizing the RAFT Polymerization Technique. *Macromolecules* **2007**, *40*(4), 879-888.
114. Barbey, R.; Lavanant, L.; Paripovic, D.; Schüwer, N.; Sugnaux, C.; Tugulu, S.; Klok, H.-A., Polymer Brushes via Surface-Initiated Controlled Radical Polymerization: Synthesis, Characterization, Properties, and Applications. *Chemical Reviews* **2009**, *109*(11), 5437-5527.
115. Luo, N.; Hutchison, J. B.; Anseth, K. S.; Bowman, C. N., Synthesis of a novel methacrylic monomer iniferter and its application in surface photografting on crosslinked polymer substrates. *Journal of Polymer Science Part A: Polymer Chemistry* **2002**, *40*(11), 1885-1891.
116. Li, M.; Fromel, M.; Ranaweera, D.; Rocha, S.; Boyer, C.; Pester, C. W., SI-PET-RAFT: Surface-Initiated Photoinduced Electron Transfer-Reversible Addition-Fragmentation Chain Transfer Polymerization. *ACS Macro Letters* **2019**, *8*(4), 374-380.

Chapter 4. Effect of Thiocarbonylthio Compounds on Visible Light Mediated 3D Printing



The contents of this chapter were published in: Zhang, Z.; Corrigan, N.; Boyer, C. Effect of Thiocarbonylthio Compounds on Visible-Light-Mediated 3D Printing. *Macromolecules* **2021**, 54(3), 1170-1182.

4.1 Introduction

3D printing is an additive manufacturing (AM) technology that has been developed to fabricate advanced materials with complex geometries and functions. In comparison to conventional fabrication, 3D printing allows faster transformation of computer-assisted designs into customised objects engineered to meet specific demands.¹ Among the various 3D printing approaches, photoinduced techniques such as stereolithography (SLA) or digital light processing (DLP) have attracted significant attention due to the versatility of photochemistry and high printing resolution and speed.²⁻⁹ Moreover, temperature independent photoinduced 3D printing processes are more suitable for bioengineering applications.¹⁰⁻¹² However, current photoinduced 3D printing is primarily based on nonliving radical and cationic polymerisation, which produces ‘dead’ polymers that are inactive to further chain growth processes, thus impeding controlled post-functionalisation of the printed objects. Furthermore, using such non-living polymerisations leads to heterogeneous polymer networks due to the lack of control over the chain growth processes.¹³⁻¹⁴ Indeed, in free radical polymerisation systems, polymer chains grow rapidly after initiation and undergo intramolecular cyclisation and significant termination in the early stages of the reaction, generating nanogels with high crosslink densities.¹⁵⁻¹⁶ These nanogels are loosely connected towards the later stages of the reaction to form networks with highly variable crosslink densities.

As an alternative to photoinduced free radical polymerisation (FRP), photoinduced reversible deactivation radical polymerisation (RDRP) systems, particularly atom transfer radical polymerisation (ATRP) and reversible addition-fragmentation chain transfer polymerisation (RAFT) polymerisation, have been extensively studied due to their ability to impart living characteristics to radical polymerisation processes.¹⁷⁻²⁶ For RAFT polymerisation, the thiocarbonylthio species (RAFT agents) play a critical role by providing an equilibrium between dormant RAFT agent capped polymer chains and active propagating species via degenerate chain transfer.²⁷⁻³² As a result, the growth of all chains in the reaction mixture is more even, and well-defined polymers with various architectures and chemical functionalities can be synthesised. Similarly, the formation of polymer networks through RAFT and other RDRP processes occurs in a more controlled manner; lower molecular weight chains formed during the initial stages of the polymerisation have sufficient time to relax and diffuse, significantly reducing nanogel

formation and facilitating intermolecular crosslinking reactions to produce more homogeneous networks in the later stages of the reaction.³³⁻³⁵

Notably, using RDRP for polymer network synthesis has been shown to provide advantages compared to uncontrolled FRP systems. For instance, Zhu, Yu and co-workers investigated the homogeneity of networks formed via free radical polymerisation and RAFT polymerisation of oligo(ethylene glycol) dimethacrylates. Remarkably, the addition of dithobenzoate RAFT agents resulted in a less crosslinked and more homogeneous network.³⁴ In addition, De and co-workers synthesised crosslinked polymer gels in the presence of a trithiocarbonate RAFT agent in organic and aqueous solvents.³³ They found that gels synthesised through RAFT polymerisation exhibited a higher swelling ratio than gels made via FRP, which was attributed to less highly crosslinked nanogel domains in the RAFT-mediated network. Despite these findings, the typically slow polymerisation rate of RDRP systems has largely limited their direct application in 3D printing.

To overcome these limitations, our group applied photoinduced electron/energy transfer-RAFT (PET-RAFT) polymerisation³⁶⁻³⁹ to visible light mediated 3D printing.⁴⁰ In the PET-RAFT process, polymerisation is conducted under visible or near-infrared light irradiation in the presence of a photocatalyst (PC), which is photoexcited to induce an electron or energy transfer to RAFT agents. The reduced or excited RAFT agent species subsequently fragments to produce an initiating radical for polymerisation.⁴¹ Moreover, the excited state PC species provide outstanding oxygen tolerance,⁴²⁻⁴⁶ which facilitates application to open to air 3D printing systems. Indeed, **Chapter 3** demonstrated a versatile 3D and 4D printing system via PET-RAFT polymerisation under green light irradiation and open to air conditions.⁴⁰ The use of an organic dye in conjunction with a tertiary amine as cocatalyst and a trithiocarbonate RAFT agent allowed build speeds of up to 1.2 cm/h and provided control over the mechanical properties of the 3D printed materials. Furthermore, light dose dependent printing provided 4D printed materials that displayed swelling and dehydration induced actuation. In collaboration with our group, Bagheri, Jin and co-workers have also applied PET-RAFT polymerisation to 3D printing, similarly employing trithiocarbonate RAFT agents under blue light and green light irradiation.⁴⁷⁻⁴⁸ While these works have collectively demonstrated the ability to induce RDRP in photoinduced 3D printing systems, more thorough investigation into the RAFT

agents used has not been performed. As RAFT agent structures plays a crucial role in the ability to mediate successful RDRP, understanding their effects on 3D printing is critical for the future design of advanced polymeric materials.

In this chapter, 3D printing via PET-RAFT polymerisation was applied under visible light irradiation ($\lambda_{\text{max}} = 525 \text{ nm}$, intensity = 0.32 mW/cm^2). The kinetics of various thiocarbonylthio species with different activating Z groups and homolytic leaving R groups in the resin formulations were investigated to predict their feasibility in 3D printing, followed by mechanical testing of the 3D printed materials. The impact of the addition of different RAFT agents in the resin formulations was also explored. Finally, the post-modification of the 3D printed objects with RAFT agents in the resin was achieved via a one-pot transformation of thiocarbonylthio groups through aminolysis and thiol-Michael addition to introduce a fluorescent functionality in the 3D printed polymer network.

4.2 Experimental Section

4.2.1 Materials

Triethanolamine (TEtOHA, Sigma-Aldrich, 99%), hexylamine (Sigma-Aldrich, 99%), dimethyl sulfoxide (DMSO, chem-supply), dimethylformamide (DMF, chem-supply), basic aluminium oxide (Al_2O_3 , Sigma-Aldrich, 99.9%), 2-(butylthiocarbonothioylthio) propanoic acid (BTPA, Boron Molecular), 4-cyano-4-[(dodecylsulfanylthiocarbonyl)sulfanyl]pentanoic acid (CDTPA, Boron Molecular), dibenzyl trithiocarbonate (DBTTC, Boron Molecular), 4-cyano-4-(phenylcarbonothioylthio) pentanoic acid (CPADB, Boron Molecular), cyanomethyl (3,5-dimethyl-1H-pyrazole)-carbodithioate (DTC1, Boron Molecular) and 2-cyanobutan-2-yl 4-chloro-3,5-dimethyl-1H-pyrazole-1-carbodithioate (DTC2, Boron Molecular), absolute ethanol AR (chem supply), 1-pyrenemethyl methacrylate (pyrene-MMA, Sigma-Aldrich, 99%) and Erythrosin B (EB, dye content 90%, Sigma-Aldrich) were used as received. Poly(ethylene glycol) diacrylate average M_n 250 (PEGDA, Sigma-Aldrich, >92%) and poly(ethylene glycol) methyl ether acrylate average M_n 480 (PEGA, Sigma-Aldrich) were deinhibited by percolation through basic alumina column before use. Methyl 2-((ethoxycarbonothioyl)thio) propanoate (Xanthate) was synthesised by literature protocols.⁴⁹

4.2.2 Instrumentation

Attenuated total reflectance-fourier-transform infrared (ATR-FTIR) spectroscopy was employed to monitor vinyl bond conversions, using an approach similar to Magdassi, Banin, and co-workers.⁵⁰ A Bruker Alpha FT-IR equipped with room temperature DTGS detectors was used for measurement. Each spectrum composed of 16 scans with a resolution of 4 cm^{-1} was collected in the spectral region between $4000\text{--}500\text{ cm}^{-1}$. Analysis was performed using OPUS software.

A TA instruments Q800 dynamic mechanical analyser (DMA) was used to obtain mechanical property measurements on the 3D printed materials. The Q800 DMA was equipped with a TA instruments liquid nitrogen gas cooling accessory (GCA) for temperature control.

Micromake L4, the LCD digitally masked DLP 3D printer modified with a green LED light board ($\lambda_{\text{max}} = 525 \text{ nm}$, $I_0 = 0.32 \text{ mW/cm}^2$) was employed to print rectangular samples for DMA analysis. The light intensity was measured using a Newport 843-R power meter. The targeted material geometries and .stl files were generated using Autodesk Fusion 360, and printing parameters (slicing thickness and layer cure times) were generated using Micromake L4 software.

Anycubic Photon S, the LCD digitally masked DLP 3D printer modified with a green LED light board ($\lambda_{\text{max}} = 525 \text{ nm}$, $I_0 = 0.32 \text{ mW/cm}^2$) was employed to print complex objects. The light intensity was measured using a Newport 843-R power meter. Printing parameters (slicing thickness and layer cure times) were generated using Photon WorkShop software.

UV–Vis spectroscopy spectra were recorded using a CARY 300 spectrophotometer (Varian) equipped with a temperature controller. All measurements were obtained by placing the 3D printed samples or reaction mixtures in a $1 \text{ cm} \times 1 \text{ cm}$ glass cuvette. The spectra were baseline corrected against the empty cuvette.

4.2.3 Experimental procedure

Polymerisation for determination of reaction kinetics

A typical polymerisation solution with the recipe of [PEGA] : [PEGDA] : [BTPA] : [EB] : [TtOHA] = 571 : 1333 : 5 : 0.2 : 40 was prepared as follows: to a 4 mL glass vial was added 0.54 mg (2.27 μmol , 5 equiv) of BTPA, followed by 68.56 mg (0.14 mmol, 315 equiv) of PEGA and 150.98 mg (0.6 mmol, 1333 equiv) of PEGDA. 26.5 μL of a stock solution of EB in PEGA at 3 mg/mL (0.091 μmol EB, 0.2 equiv and 0.06 mmol PEGA, 133 equiv) was then added, followed by 26.98 μL of a stock solution of TtOHA in PEGA at 100 mg/mL (0.018 mmol, 40 equiv and 0.056 mmol PEGA, 123 equiv) to make a total equivalents of PEGA = 571, and [PEGA] : [PEGADA] = 30 : 70. The reaction mixture was then covered with foil, vortexed for $\sim 10 \text{ s}$, sonicated for 20 s, prior to the irradiation. A 20 μL aliquot of the reaction mixture was then pipetted onto the ATR crystal plate and irradiated with a household LED lamp emitting green light ($\lambda_{\text{max}} = 525 \text{ nm}$) with an intensity at the polymerisation surface, $I_0 = 4.3 \text{ mW/cm}^2$ as measured using a Newport 843-R power meter.

Vinyl bond conversion was calculated based on the disappearance of the methylene group vibrations in the range of 1590-1655 cm⁻¹ assigned to the stretching mode of the =C-H group. The integral under this peak in the range of 1590-1655 cm⁻¹ was evaluated after increasing irradiation times and compared to the peak in the range of 1660-1800 cm⁻¹ assigned to the acrylate C=O stretching mode. The vinyl bond conversion was calculated from **Equation 1**, where *std₀* is the integral under the curve in the range of 1660-1800 cm⁻¹ before irradiation, *std_x* is the integral under the curve in the range of 1660-1800 cm⁻¹ after *x* mins irradiation, *int₀* is the integral under the curve in the range of 1590-1655 cm⁻¹ before irradiation, and *int_x* is the integral under the curve in the range of 1590-1655 cm⁻¹ after irradiation for *x* mins. All FTIR measurements were performed in triplicate.

$$\text{Vinyl bond conversion} = 1 - (int_x / std_x) / (int_0 / std_0) \quad \text{Eq. 1}$$

Vinyl bond conversions of 3D printed samples

The vinyl bond conversions of 3D printed samples were obtained by placing the ground sample powder on the ATR crystal plate, and then compressed by lowering the testing arm. The vinyl bond conversion was calculated from **Equation 1**, where *std₀* is the integral under the curve in the range of 1660-1800 cm⁻¹ of the resin before printing, *std_x* is the integral under the curve in the range of 1660-1800 cm⁻¹ of the 3D sample powder, *int₀* is the integral under the curve in the range of 1590-1655 cm⁻¹ of the resin before printing, and *int_x* is the integral under the curve in the range of 1590-1655 cm⁻¹ of the 3D sample powder. All FTIR measurements were performed in triplicate.

3D printing procedures of rectangular samples

A typical procedure for 3D printing a rectangular sample is as follows: to a 20 mL glass vial was added 21.6 mg (0.0906 mmol, 5 equiv) of BTPA, followed by 4.28 g (8.91 mmol, 491 equiv) of PEGA and 6.04 g (24.16 mmol, 1333 equiv) of PEGDA. 636.5 µL of a stock solution of EB in PEGA at 5.0 mg/mL (3.6 µmol EB, 0.2 equiv and 1.45 mmol PEGA, 80 equiv) and 107.9 mg TEtOHA (0.72 mmol, 40 equiv) was then added to make a total equivalents of PEGA = 571, and [PEGA] : [PEGDA] = 30 : 70. The total volume for all reaction mixtures used for polymerisation in bulk was 10 ml. The reaction mixture was then covered with foil, vortexed for ~10 s, sonicated for 20 s, prior to addition to the 3D printer vat (vat dimensions 60 mm × 60 mm × 20 mm), and subsequently irradiated with spatially controlled green light during the 3D printing process. The rectangular

sample geometries ($40 \times 12 \times 2$ mm (l, w, t)) and .stl files were generated using Autodesk Fusion 360. The sample printing parameters (slicing thickness and layer cure times) were generated using Micromake L4 software. The sample was then printed by using Micromake L4 DLP 3D printer. To ensure adhesion between the 3D printed material and the build stage, the first two (bottom) layers of the material were irradiated for 150 s/layer, after which the regular cure time per layer was 20 s/layer or 40 s/layer with a layer thickness of 20 μ m. The Z lift distance was 1 mm, the Z lift speed was 30 mm/min, and the Z retract speed was 300 mm/min. After the object was printed, the build stage was removed, and the residual polymerisation surface was briefly washed with ethanol. The material was allowed to dry for 5 mins then analysed by DMA.

3D printing procedures of the theatre complex

The resin formulation of [PEGA] : [PEGDA] : [RAFT] : [EB] : [TEtOHA] = 571 : 1333 : 5 : 0.2 : 40 was used to print a theatre complex. The theatre complex .stl file was downloaded from the internet.⁵¹ The dimensions of the object were $45.9 \times 45.99 \times 29$ mm (x, y, z). The printing parameters (slicing thickness and layer cure times) were generated using Photon WorkShop software and the object was printed by using Anycubic Photon S DLP 3D printer. To ensure adhesion between the 3D printed material and the build stage, the first 10 (bottom) layers of the material were irradiated for 150 s/layer, after which the regular cure time per layer was 30 s/layer with a layer thickness of 20 μ m. The Z lift distance was 1 mm, the Z lift speed was 360 mm/min, and the Z retract speed was 360 mm/min.

DMA test of 3D printed rectangular samples

In DMA test, a 3D printed rectangular sample was measured with digital callipers, placed into the calibrated single cantilever clamp, and fixed into place with a torque wrench operated at a force of 1 in·lb. The GCA was used to adjust the temperature to -50 °C and subsequently hold isothermal conditions for 3 minutes. The temperature was then ramped to 100 °C at a rate of 2 °C/min while the frequency was held constant at 1 Hz, using a displacement of 30 μ m. The storage modulus was determined at glassy state (specifically at the closest temperature to -45 °C) and rubbery plateau region (specifically at the closest temperature to 50 °C) and 1 Hz, while the glass transition temperature (T_g) was calculated as the temperature at which the 1 Hz Tan δ curve peaked. All DMA results were performed using duplicate samples.

Aminolysis of 3D printed samples

A typical aminolysis procedure of 3D printed samples is as follows: a rectangular sample with dimensions of $30 \times 8 \times 1.5$ mm (l, w, t) was printed using the resin formulation of [BTPA] : [PEGA] : [PEGDA] : [EB] : [TetOHA] = 25 : 571 : 1333 : 0.2 : 40. After printing, the sample was post-cured under green light ($\lambda_{\text{max}} = 525$ nm, 7.1 mW/ cm²) for 10 min, and then was submerged in DMF solution containing hexylamine with a molar ratio of [hexylamine] : [BTPA] = 100 : 1 at room temperature. The amount of BTPA contained in the 3D printed sample was calculated assuming a constant weight percentage of BTPA in both the resin and the 3D printed materials. The concentration of BTPA in the resin was 0.96 wt%. Therefore, 10 mL DMF solution containing hexylamine (~2 vol%) was employed to aminolyse the sample.

Aminolysis of BTPA in DMF solution containing hexylamine

The aminolysis solution was prepared as follows: to a 20 mL glass vial was added 3.9 mg (0.0163 mmol, 1 equiv) of BTPA, followed by 3784 μ L of DMF. As a baseline measurement, the UV-Vis spectrum was measured prior to the addition of hexylamine in a 1 cm \times 1 cm glass cuvette. Subsequently, 216 μ L hexylamine (1.63 mmol, 100 equiv) was added to make the ratio of [BTPA] : [hexylamine] = 1 : 100. The total volume for all reaction mixtures used for aminolysis was 4 mL.

4.3 Results and Discussion

4.3.1 Optimisation of resin formulations

In the previous chapter, a rapid RAFT-mediated 3D and 4D printing process was demonstrated under visible light, however, a single RAFT agent, 2-(butylthiocarbonothioylthio) propanoic acid (BTPA), was used in relatively low concentrations.⁴⁰ To elicit more thorough details on the effects of RAFT agents in such 3D printing processes, different RAFT agents were applied to a model 3D printing system at higher concentrations. Initially, the photopolymerisation conditions were optimised to achieve fast polymerisation rates and enable practical 3D printing speeds. For these model polymerisations, poly(ethylene glycol) methyl ether acrylate (PEGA, average $M_n = 480 \text{ g mol}^{-1}$) and poly(ethylene glycol) diacrylate (PEGDA, average $M_n = 250 \text{ g mol}^{-1}$) were used as monomer and crosslinker, respectively. PEG oligomers and PEG-based monomers are widely considered as non-toxic and have been applied in various fields, such as medicine,⁵²⁻⁵³ self-healing materials,⁵⁴ drug delivery,⁵⁵ and tissue engineering.⁵⁶ Erythrosin B (EB) was selected as PC in conjunction with triethanolamine (TEtOHA) as co-catalyst, and the reaction was performed in the absence of solvent (bulk) to match prospective 3D printing conditions. The initial ratio of [PEGA] : [PEGDA] : [EB] : [TEtOHA] was 1000 : 500 : 0.025 : 20 and the ratios of [BTPA] : [EB] were varied between 0 : 0.025 and 50 : 0.025. The model reactions were performed in open-air droplets (20 μL) under green light ($\lambda_{\text{max}} = 525 \text{ nm}$, $I_0 = 4.3 \text{ mW/cm}^2$). The polymerisation kinetics of these systems under different concentrations of BTPA were monitored by following the decrease of the ATR-FTIR absorption peak assigned to the stretching mode of the vinylic group =C-H unit.

The change in vinyl bond conversion with time for the initial polymerisations are shown in **Figure 4.1A**. Based on previous work, the vinyl bond conversions after 1 min and 4 min were used as an important guide; systems that present a high vinyl bond conversion after 4 min and exhibit a short induction period ($< 1 \text{ min}$) are more suitable for implementation in 3D printing processes.⁴⁰ After 4 min irradiation, the systems that contained 0, 5, and 10 equiv. of BTPA showed reasonable monomer conversions ($\alpha \approx 50\%$, **Figure 4.1A**). The system with [BTPA] : [EB] = 25 : 0.025 displayed a reduced vinyl bond conversion after 4 min ($\alpha = 23.2\%$), and critically showed negligible vinyl

bond conversion after 1 min due to a longer inhibition time. This result indicates a reduced likelihood of successful 3D printing at practical build speeds. Furthermore, increasing the BTPA ratio to 50 equiv relative to EB led to no observable vinyl bond conversion after 10 min irradiation. The inhibition effect in these RAFT polymerisations can be attributed to either the slow fragmentation of the initial intermediate RAFT radical or the insufficient re-initiation ability of the homolytic leaving group radical from the initial RAFT agent.⁵⁷⁻⁵⁹ Barlow, Moad and co-workers also showed that RAFT agent concentrations affect the inhibition time, with increasing concentrations of thiocarbonylthio compounds leading to increased inhibition time.⁶⁰

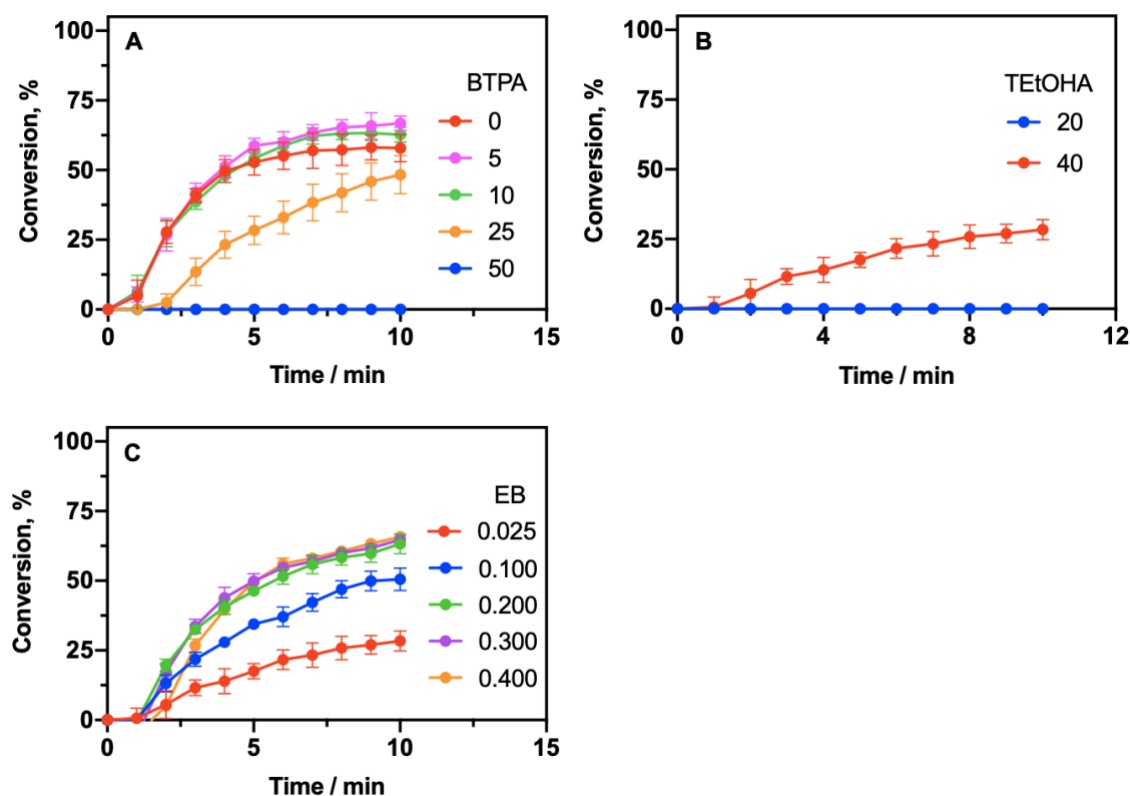


Figure 4.1 Kinetics of polymerisation for PEGA / PEGDA mixtures using BTPA as RAFT agent. (A) vinyl bond conversions *vs* time for varied molar ratios of BTPA as RAFT agent at molar concentrations of [PEGA] : [PEGDA] : [BTPA] : [EB] : [TEtOHA] = 1000 : 500 : [variable] : 0.025 : 20; (B) vinyl bond conversion *vs* time for varied TEtOHA molar ratios at molar concentrations of [PEGA] : [PEGDA] : [BTPA] : [EB] : [TEtOHA] = 1000 : 500 : 50 : 0.025 : [variable]; (C) vinyl bond conversion *vs* time for varied EB molar ratios at molar concentrations of [PEGA] : [PEGDA] : [BTPA] : [EB] : [TEtOHA] = 1000 : 500 : 50 : [variable] : 40. Note: All reactions were performed in bulk under green light ($\lambda_{\text{max}} = 525 \text{ nm}$ and $I_0 = 4.3 \text{ mW/cm}^2$).

To find suitable conditions for rapid polymerisation in the presence of higher concentrations of BTPA (50 equiv.), the concentrations of EB and TtOHA were altered to optimise the catalytic system. The polymerisation kinetics were monitored using an increased ratio of TtOHA, ([BTPA] : [EB] : [TtOHA] = 50 : 0.025 : 40), which led to an increase in monomer conversion at 4 min (α = 13.9%, **Figure 4.1B**). The concentration of TtOHA was not increased further to limit its effect as a plasticizing agent. Thus, the ratio of [BTPA] : [TtOHA] = 50 : 40 was fixed, while the EB concentration was varied between 0.025, 0.1, 0.2, 0.3, and 0.4 equiv. As shown in **Figure 4.1C**, the fastest polymerisation occurred with the ratio of [EB] : [BTPA] = 0.3 : 50 after 4 min irradiation, however, only slight differences in conversion were observed between this system and the system containing 1.5 times less EB (i.e., at a ratio of [EB] : [TtOHA] : [BTPA] = 0.2 : 40 : 50). As such, the ratio of catalyst and cocatalyst was fixed at [EB] : [TtOHA] = 0.2 : 40 for further experiments.

4.3.2 Kinetics comparison between different RAFT agents

To date, only three RAFT agents have been applied in DLP 3D printing, namely trithiocarbonates BTPA, 4-(((dodecylthio)carbonothioyl)thio) pentanoic acid (CDTPA), and dibenzyl trithiocarbonate (DBTTC).^{40, 47} However, a much larger pool of RAFT agents exists, which could be potentially employed in 3D printing. Thiocarbonylthio (RSC(Z)=S) RAFT agents include trithiocarbonates ($Z = SR'$), dithioesters ($Z = \text{alkyl or aryl}$), xanthates ($Z = OR'$), and dithiocarbamates ($Z = NR'R''$). Dithioesters, aromatic amine-based dithiocarbamates and trithiocarbonates are reactive RAFT agents with high transfer constants and suitable for controlling polymerisation of “more-activated” monomers (MAMs) where the vinyl bond is conjugated to an aromatic ring (e.g., styrene (St)), a carbonyl group (e.g., methyl acrylate (MA)) or a nitrile (e.g., acrylonitrile (AN)).^{49, 61} In comparison, xanthates and alkyl dithiocarbamates which have low transfer constants can be selected for controlling polymerisation of “less activated” monomers (LAMs) where the vinyl bond is adjacent to an oxygen or nitrogen lone pair (e.g., vinyl acetate (VAc) or N-vinylpyrrolidone (NVP)) or the heteroatom of a heteroaromatic ring (e.g., N-vinylcarbazole (NVC)).^{49, 61}

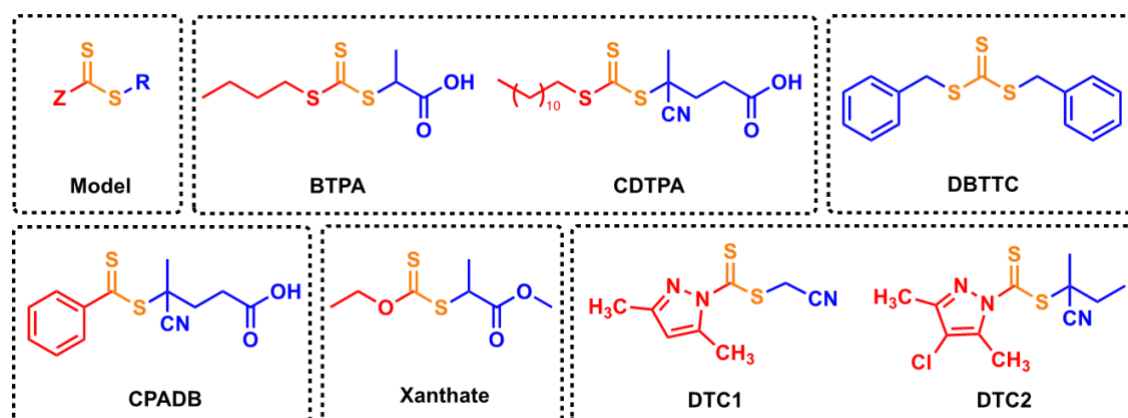


Figure 4.2 Various RAFT agents used in this work composed of thiocarbonylthio group (orange), activating Z group (red) and leaving R group (blue), 2-(butylthiocarbonothioylthio) propanoic acid (**BTPA**), 4-cyano-4-[(dodecylsulfanylthiocarbonyl)sulfanyl]pentanoic acid (**CDTPA**), dibenzyl trithiocarbonate (**DBTTC**), 4-cyano-4-(phenylcarbonothioylthio) pentanoic acid (**CPADB**), methyl 2-((ethoxycarbonothioyl)thio) propanoate (**Xanthate**), cyanomethyl (3,5-dimethyl-1H-pyrazole)-carbodithioate (**DTC1**) and 2-cyanobutan-2-yl 4-chloro-3,5-dimethyl-1H-pyrazole-1-carbodithioate (**DTC2**).

To investigate the effect of RAFT structures, several RAFT agents were selected, namely cyano-4-(phenylcarbonothioylthio) pentanoic acid (**CPADB**) as dithibenzoate, **CDTPA**, **DBTTC** and **BTPA** as trithiocarbonates, cyanomethyl (3,5-dimethyl-1H-pyrazole)-carbodithioate (**DTC1**) and 2-cyanobutan-2-yl 4-chloro-3,5-dimethyl-1H-pyrazole-1-carbodithioate (**DTC2**) as dithiocarbamates, and methyl 2-((ethoxycarbonothioyl)thio) propanoate (**Xanthate**) as a xanthate (**Figure 4.2**). Tailoring towards high modulus, free-standing 3D printed materials, ratios of [PEGA] : [PEGDA] : [EB] : [TEtOHA] : [RAFT]= 571 : 1333 : 0.2 : 40 : 5/50 were adopted. To clearly differentiate the inhibition period and subsequent polymerisation rate for systems mediated by different RAFT agents, vinyl bond conversions at each interval over the first 4 min of the reaction are reported in **Table 4.1**. As shown in **Figure 4.3A**, the formulation without RAFT agents presented a higher polymerisation rate than those containing RAFT agents,^{57, 60, 62} with the vinyl bond conversion reaching 60.0% after 1 min irradiation, and 89.8% after 4 min (**Table 4.1**). Critically, the differences in polymerisation behaviour in the presence of RAFT agents depend on the RAFT agent structure, and more precisely, on the structures of the activating Z groups and leaving R groups (**Figure 4.2**). Therefore, a more thorough analysis of the combined effects of the Z and R groups on the polymerisations was

considered to explain the polymerisation kinetics. Three thermodynamic descriptors, including RAFT agent stability (ΔH_{stab}), the fragmentation efficiency (ΔH_{frag}), and the radical stabilisation energies of leaving group radicals (RSE of R^\bullet), were employed to provide a semi-quantitative method of assessing the kinetic behaviour of the RAFT agents.⁶³⁻⁶⁴

Table 4.1 Kinetics of polymerisation for PEGA / PEGDA mixtures using various RAFT agents.^a

RAFT ^a	[RAFT] ^a	$\alpha_{1\text{min}}$ (%) ^b	$\alpha_{2\text{min}}$ (%) ^b	$\alpha_{3\text{min}}$ (%) ^b	$\alpha_{4\text{min}}$ (%) ^b
No RAFT	0	60.0	83.0	88.3	89.8
Xanthate	5	54.1	81.4	88.4	90.4
BTPA	5	37.3	73.6	84.5	88.1
DTC 1	5	6.4	49.3	71.1	79.7
DTC 2	5	0.0	58.5	76.3	80.4
CDTPA	5	0.0	61.6	78.8	82.8
DBTTC	5	1.3	37.8	60.3	70.5
CPADB	5	0.0	0.0	0.0	0.0
Xanthate	50	25.4	62.6	79.1	85.5
BTPA	50	0.6	25.9	43.1	56.1
DTC 1	50	1.9	15.5	28.3	38.6
DTC 2	50	0.2	0.9	0.9	0.9
CDTPA	50	0.0	0.0	0.0	0.0
DBTTC	50	0.0	0.0	0.0	0.0
CPADB	50	0.0	0.0	0.0	0.0

^aConditions: reaction was performed using molar concentrations of [RAFT] : [PEGA] : [PEGDA] : [EB] : [TEtOHA] = variable : 571 : 1333 : 0.2 : 40. Polymerisation was performed in bulk under 4.3 mW/cm² green light ($\lambda_{\text{max}} = 525$ nm), using a droplet (20 μ L) of reaction mixture. ^bVinyl bond conversion was determined by ATR-FTIR spectroscopy.

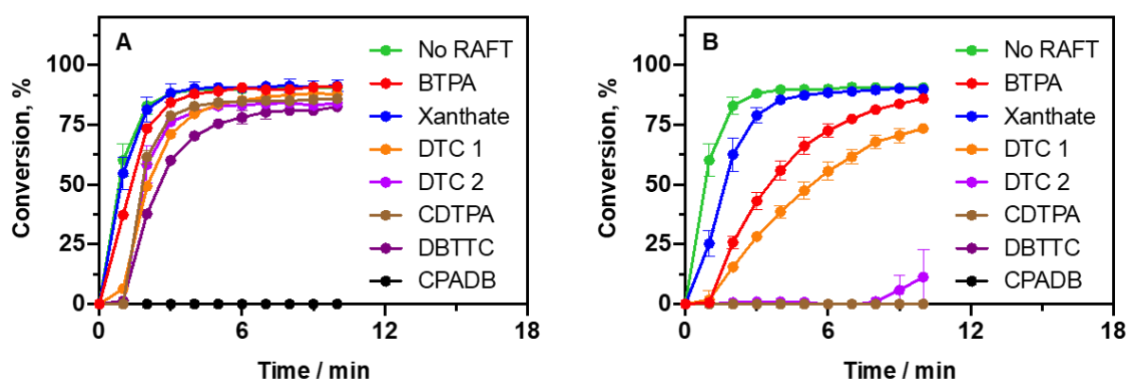


Figure 4.3 Kinetics of polymerisation for PEGA / PEGDA mixtures using various RAFT agents. (A) vinyl bond conversions *vs* time for varied RAFT agents at a fixed molar concentration of [PEGA] : [PEGDA] : [RAFT] : [EB] : [TEtOHA] = 571 : 1333 : 5 : 0.2 : 40; (B) vinyl bond conversions *vs* time for varied RAFT agents at a fixed molar concentration of [PEGA] : [PEGDA] : [RAFT] : [EB] : [TEtOHA] = 571 : 1333 : 50 : 0.2 : 40. Note: All reactions were performed in bulk under green light ($\lambda_{\text{max}} = 525 \text{ nm}$ and intensity = 4.3 mW/cm^2).

The fastest kinetics among all the formulations containing 5 equiv. RAFT agents was observed for the polymerisation using xanthate ($\alpha_{1\text{min}} = 54.1\%$ and $\alpha_{4\text{min}} = 90.4\%$, **Table 4.1**) and was closely aligned with the kinetics in the absence of RAFT agent. The fast polymerisation kinetics can be attributed to the low reactivity of the thiocarbonyl bond due to the interaction between the lone pair of the oxygen from the *O*-ethyl *Z* group and the thiocarbonyl bond of xanthate, which gives rise to zwitterionic canonical forms, in turn enhancing the stability of xanthate ($\Delta H_{\text{stab}} = 86.8 \text{ kJ/mol}$, **Figure 4.4**).⁶⁵ Although the fragmentation efficiency is high (as given by a very exothermic $\Delta H_{\text{frag}} = -44.3 \text{ kJ/mol}$, **Figure 4.4**), the stability of the starting RAFT agent is too high to allow efficient addition of the relatively stable secondary acrylic radical species to the thiocarbonyl bond, resulting in polymerisation behaviour similar to that of the free radical polymerisation. A decrease of polymerisation rate was observed when the xanthate ratio was increased from 5 to 50 equiv. and the vinyl bond conversion was $\alpha = 25.4\%$ at 1 min and $\alpha = 85.5\%$ at 4 min (**Figure 4.3B** and **Table 4.1**).

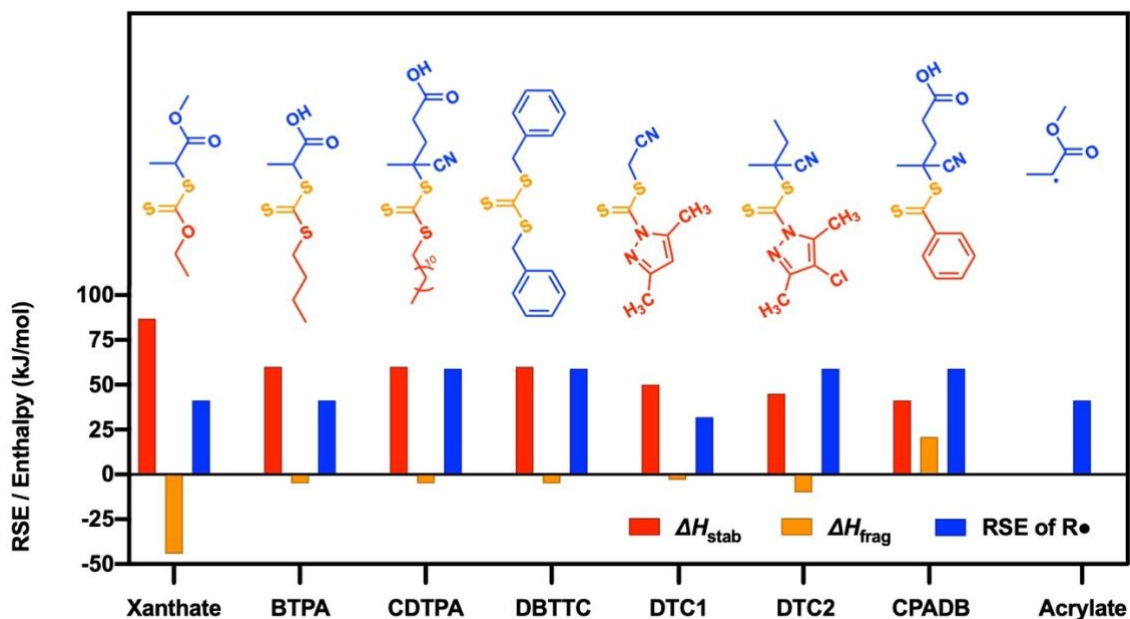


Figure 4.4 Values of ΔH_{stab} , ΔH_{frag} and RSE of R^\bullet (kJ/mol) for RAFT agents in the present work.⁶³⁻⁶⁴ The values of ΔH_{stab} and ΔH_{frag} are associated with the effect of Z group, while the value of RSE of R^\bullet is associated with the effect of R group. The value of RSE of R^\bullet of acrylate (assumed to have the structure $CH(CH_3)(CO)OCH_3$) was used as a reference for the secondary acrylic propagating radical species in the system.

Polymerisation using 5 equiv. of BTPA also led to slightly decreased vinyl bond conversions at 1 min ($\alpha = 37.3\%$) and 4 min ($\alpha = 88.1\%$) compared with the no RAFT system (**Figure 4.3A and Table 4.1**).⁶¹ The rate was further reduced for the system with 50 equiv. of BTPA, with an observed 1 min inhibition period and reduced conversion ($\alpha = 25.9\%$) after 2 min; the monomer conversion reached 56.1% after 4 min. The reduction in rate and increase in inhibition period with increasing BTPA concentration was expected in this system, as has been shown previously for other RAFT mediated polymerisations (**Figure 4.3B**).⁶⁰

For the formulation containing 5 equiv. of CDTPA, the induction period was prolonged to 1 min, however, the polymerisation then proceeded rapidly, with a vinyl bond conversion of 61.6% after 2 min and 82.8% after 4 min (**Figure 4.3A and Table 4.1**). The increased inhibition period compared to BTPA was attributed to two factors which have been discussed in the literature.⁵⁷⁻⁵⁹ Given that the propagating radical species are secondary acrylic radicals ($R \approx CH(CH_3)COOCH_3$), the RSE of polymeric propagating radical species will be roughly 41.3 kJ/mol (**Figure 4.4**). Consequently, although the Z

groups of BTPA and CDTPA are essentially the same, the tertiary carbon (4-cyanopentanoic acid) radical leaving group on CDTPA group is less efficient at reinitiating polymerisation of acrylates due to its increased stability (RSE of $R^{\bullet} \approx 59.0$ kJ/mol, **Figure 4.4**). As such, the higher concentration of these tertiary propagating species compared to acrylic propagating species is expected to reduce the polymerisation rate. Indeed, when increasing the CDTPA concentration to 50 equiv., no polymerisation was observed after 10 min irradiation due to a long inhibition period, as shown in **Figure 4.3B**.

For the formulation containing the symmetrical trithiocarbonate DBTTC at 5 equiv., a long induction period (1 min) was observed in **Figure 4.3A**, which can be rationalised in terms of the poor reinitiating abilities of the two identical benzyl leaving R groups with a high RSE of $R^{\bullet} = 58.9$ kJ/mol (**Figure 4.4**). Comparatively, no vinyl bond conversion was observed after 10 min at higher concentrations (50 equiv.) of DBTTC (**Figure 4.3B**). Similarly, for the formulations containing both low concentration and high concentration of CPADB, no polymerisation was observed after 10 min irradiation (**Figure 4.3A and B**). To compare with CDTPA which has the same homolytic leaving group as CPADB, the phenyl Z group of CPADB contributes more to stabilizing the initial intermediate RAFT radical, leading to much slower fragmentation in the pre-equilibrium (as given by a very endothermic $\Delta H_{\text{frag}} = 21.0$ kJ/mol, **Figure 4.4**), and significantly retarded polymerisation, as has been seen in previous works.^{57, 66-68}

For resins containing dithiocarbamates, two RAFT agents DTC1 and DTC2 with different pyrazole-based Z groups and different leaving R groups were selected.⁶¹ As shown in **Figure 4.3A and Table 4.1** for systems containing 5 equiv. of RAFT agent, the vinyl bond conversion of DTC1 formula reached 6.4% in 1 min and 79.7% in 4 min, while the polymerisation for the DTC2 system showed a 1 min inhibition period and a vinyl bond conversion of 80.4% after 4 min. As shown in **Figure 4.4**, the 3,5-dimethyl-1*H*-pyrazole Z group on DTC1 decreases its stability ($\Delta H_{\text{stab}} \approx 48.0$ kJ/mol) compared with BTPA ($\Delta H_{\text{stab}} \approx 59.4$ kJ/mol) and thus the addition of acrylic propagating radicals is more efficient to DTC1. However, the release of cyanomethyl radicals from DTC1 (RSE of $R^{\bullet} = 31.9$ kJ/mol) is energetically unfavorable compared to release of acrylic propagating radicals (RSE of $R^{\bullet} = 41.3$ kJ/mol), in turn reducing polymerisation rate. In contrast, BTPA will release energetically analogous radicals and the polymerisation will continue

as normal. As for DTC2, the varied polymerisation behaviour compared with DTC1 system can be primarily ascribed to differences in the structures of the leaving R groups. The high stability of tertiary nitrile substituted R group (RSE of $R^{\bullet} \approx 59.0$ kJ/mol, **Figure 4.4**) on DTC2 led to reduced efficiency in reinitiating polymerisation and caused slow polymerisation. This behaviour is in agreement with the BTPA and CDTPA systems. At higher concentrations (50 equiv.) of DTC1 the inhibition period remained at 1 min, however, the polymerisation rate was again reduced, reaching 38.6% conversion after 4 min (**Table 4.1**). Comparatively, the DTC2 formulation showed a very significant 8 min inhibition period and slow polymerisation thereafter, with the conversion reaching 11.3% after 10 min (**Figure 4.3B**).

4.3.3 3D printing and mechanical properties comparison with various RAFT agents

Based on the kinetics performance of the resins containing various thiocarbonylthio species, formulations containing xanthate, BTPA, CDTPA, DBTTC and DTC 2 were then applied to a 3D printing setup. A commercial DLP 3D printer modified with a green LED light board ($\lambda_{\text{max}} = 525$ nm, $I_0 = 0.32$ mW/cm²) was employed to spatially control the formation of the 3D objects. Initially, resin formulations with a ratio of [RAFT] : [PEGA] : [PEGDA] : [EB] : [TEtOHA] = 5 : 571 : 1333 : 0.2 : 40 were used to print simple rectangular samples with dimensions $40 \times 12 \times 2$ mm (l, w, t) (**Figure 4.5A**). These objects were printed using a fixed layer slicing thickness of 20 μm and a variable single layer cure time of 20 or 40 s/layer. The storage modulus (E') and glass transition temperature (T_g) of the printed objects were subsequently examined by dynamic mechanical analysis (DMA) by performing a temperature ramp from -50 °C to 100 °C at a frequency of 1 Hz. The E' was selected at -45 °C and 50 °C to provide mechanical property information in both the glassy and rubbery states, while T_g was determined from the peak of the Tan δ curve at a frequency of 1 Hz (**Figure 4.5B**). Additionally, the vinyl bond conversions of the 3D printed objects were determined by examining the ATR-FTIR absorption peak assigned to the stretching mode of the vinylic group.

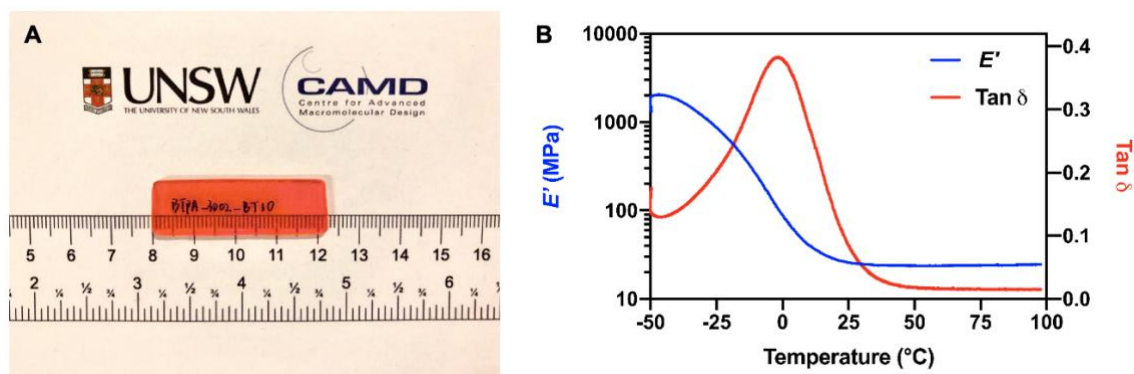


Figure 4.5 Rectangular sample 3D printed via PET-RAFT polymerisation. (A) sample 3D printed with a layer thickness of 20 μm and cure time per layer of 20 s using a recipe of [BTPA] : [PEGA] : [PEGDA] : [EB] : [TEtOHA] = 5 : 571 : 1333 : 0.2 : 40; (B) storage modulus (E') and $\text{Tan } \delta$ for the sample at a frequency of 1Hz determined by DMA.

As shown in **Table 4.2**, the vinyl bond conversions of the samples printed with various formulations under 20 s/layer cure time were between 69.0% and 82.9%. Specifically, the formulations containing no RAFT agent, BTPA, or Xanthate exhibited high vinyl bond conversions ($\alpha = 79.1\text{-}82.9\%$ at 20 s/layer cure time), while the DTC2, CDTPA, and DBTTC formulations displayed lower conversions ($\alpha = 69.0\text{-}76.5\%$ at 20s/layer). This behaviour was in alignment with the kinetics results obtained in the previous section and demonstrate that the choice of RAFT agent has a significant effect on the 3D printing process. In addition, as shown in **Table 4.2**, as the layer cure time was increased from 20 to 40 s/layer, both the E' (at 50 $^{\circ}\text{C}$ and -45 $^{\circ}\text{C}$) and the T_g increased for the samples printed in the presence or absence of RAFT agents. The extended layer cure time increased the vinyl bond conversion, resulting in the formation of a more highly crosslinked network and stiffer materials with a higher T_g .⁶⁹⁻⁷¹ The increases of E' in glassy state were more obvious, especially for the samples printed with the resins containing CDTPA, DTC2 or DBTTC. Under a cure time of 40 s/layer, the object printed with the resin having no RAFT agents had the highest E' of 31.9 ± 0.4 MPa at 50 $^{\circ}\text{C}$ and 2400 ± 70 MPa at -45 $^{\circ}\text{C}$. The addition of xanthate or BTPA in the resin slightly reduced the E' and caused minor changes to the T_g . Comparatively, the E' and T_g of the samples printed with the resin containing CDTPA, DTC2 or DBTTC were lower, as their slow polymerisation kinetics negatively affected the network formation.

Table 4.2 The mechanical properties of samples 3D printed with various RAFT agents.^a

RAFT ^a	Cure time / layer ^a	T_g	E' (MPa)		Vinyl bond conversion ^b
	(s)	(°C)	50 °C	-45 °C	(%)
No RAFT	20 s	-1.8	27.6 ± 2.1	2300 ± 30	82.4
	40 s	0.2	31.9 ± 0.4	2400 ± 70	87.0
Xanthate	20 s	-2.4	22.0 ± 0.6	1950 ± 80	79.1
	40 s	0.3	23.3 ± 1.7	2150 ± 60	84.2
BTPA	20 s	-1.5	25.2 ± 1.3	2050 ± 20	82.9
	40 s	0.0	28.9 ± 1.4	2050 ± 100	88.1
CDTPA	20 s	-3.9	19.6 ± 1.9	1750 ± 40	72.5
	40 s	-1.8	22.1 ± 1.7	1900 ± 60	80.7
DTC 2	20 s	-5.8	15.2 ± 0.8	1450 ± 70	76.5
	40 s	-5.7	15.7 ± 2.2	1600 ± 50	82.1
DBTTC	20 s	-5.7	8.6 ± 0.6	1100 ± 20	69.0
	40 s	-3.7	17.0 ± 0.8	1500 ± 60	81.8

^aSamples were 3D printed with a layer thickness of 20 µm and 20 s/layer and 40 s/layer in the presence of various RAFT agent using a recipe of [PEGA] : [PEGDA] : [RAFT] : [EB] : [TEtOHA] = 571 : 1333 : 5 : 0.2 : 40; ^bVinyl bond conversion was determined by ATR-FTIR spectroscopy. A commercial DLP 3D printer modified with a green LED light board ($\lambda_{\max} = 525$ nm, $I_0 = 0.32$ mW/cm²) was employed to spatially control the formation of the 3D printed samples.

As the resin formulations containing xanthate and BTPA provided a fast 3D printing build rate without compromising on material stiffness, they were selected for further investigation at higher concentrations. The minimum cure time needed for successful prints using resins containing 50 equiv. of xanthate and BPTA was 40 s/layer, under which the corresponding vinyl bond conversions were 79.3% and 76.2%, respectively (**Table 4.3**). As such, an obvious decrease of E' (at 50 °C and -45 °C) and the T_g of the two samples were observed. However, extending the cure time to 120 s/layer increased the E' and T_g of the sample printed with 50 equiv. of BTPA in the resin, especially at -45 °C, where the E' was 2700 ± 20 MPa which was higher compared to the objects printed in the absence of RAFT agents. Longer cure times were not suitable for samples printed

in the absence of RAFT agents, as overcuring of each layer caused ill-defined objects due to light scattering.⁷² In comparison to the BTPA system, increasing the cure time per layer for the system containing 50 equiv. xanthate led to negligible increases in E' both above and below the glass transition region (**Table 4.3**).

Table 4.3 Mechanical properties of 3D printed samples containing BTPA and Xanthate.^a

RAFT ^a	[RAFT]	Cure time / layer ^a	<i>T</i> _g	<i>E</i> ' (MPa)		Vinyl bond conversion ^b
		(s)	(°C)	50°C	-45°C	(%)
No RAFT	0	40 s	0.2	31.9 ± 0.4	2400 ± 70	87.0
BTPA	5	40 s	0.0	28.9 ± 1.4	2050 ± 100	88.1
	50	40 s	-2.2	12.7 ± 1.9	1750 ± 30	76.2
		80 s	2.0	24.1 ± 0.4	2350 ± 30	87.1
		120s	2.0	26.2 ± 2.8	2700 ± 20	89.1
Xanthate	5	40 s	0.3	23.3 ± 1.7	2150 ± 60	84.2
	50	40 s	-7.8	19.3 ± 0.2	1900 ± 80	79.3
		80 s	-5.1	19.0 ± 0.9	2050 ± 10	86.1
		120s	-4.4	20.0 ± 0.8	2000 ± 100	88.9

^aSamples were 3D printed with a layer thickness of 20 µm and varied cure time per layer using molar concentrations of [RAFT] : [PEGA] : [PEGDA] : [EB] : [TEtOHA] = variable : 571 : 1333 : 0.2 : 40; ^bVinyl bond conversion was determined by ATR-FTIR spectroscopy. A commercial DLP 3D printer modified with a green LED light board ($\lambda_{\max} = 525$ nm, $I_0 = 0.32$ mW/cm²) was employed to spatially control the formation of the 3D printed samples.

The differences in mechanical properties between the 3D printed objects in the absence or presence of RAFT agents may be a result of differences in the formation of the polymer networks. Indeed, the network developing processes in free radical polymerisation (FRP) and RAFT agents involved system have been investigated by many groups.^{33-35, 73-76} At the early stages of FRP, intermolecular crosslinking is limited due to the very low concentration of polymer chains. As a result, the pendent vinyl bonds are consumed rapidly by propagating radicals via intramolecular cyclisation reactions, yielding various nanogels with highly compact structures.⁷³⁻⁷⁵ As the reaction proceeds, the number of

these nanogels increases and intermolecular reactions occur, eventually forming a heterogeneous network. In contrast to the FRP technique, the RAFT polymerisation system establishes an equilibrium between propagating radicals and dormant chains, allowing all chains to grow more evenly throughout the polymerisation. An effective chain transfer process promotes chain relaxation and diffusion, favouring intermolecular crosslinking and reducing intramolecular cyclization, resulting in the production of more homogeneous networks.³³⁻³⁵ **Figure 4.6** compares the gelation process by free radical polymerisation versus RAFT polymerisation.

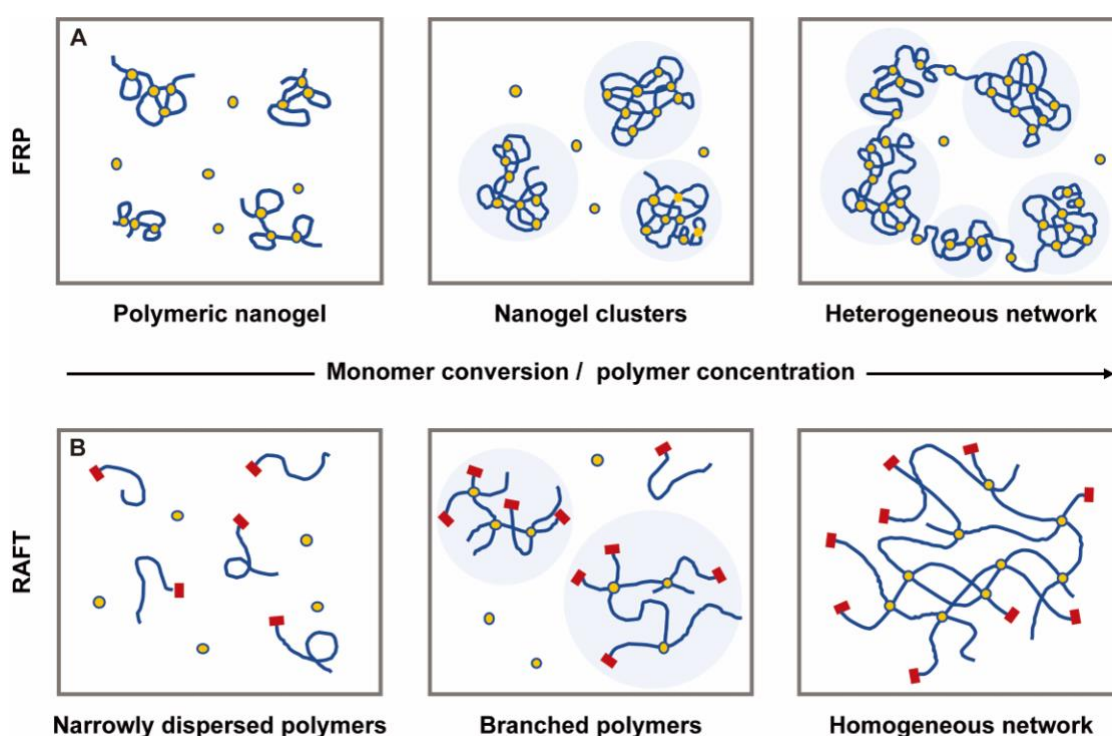


Figure 4.6 Schematic presentations of polymer network synthesis process: (A) highly crosslinked nanogels formation via free radical polymerisation (FRP) and the resulting heterogenous network structures; (B) RAFT polymerisation process leading to more homogeneous network structure via the formation of more highly branched polymers in the earlier stages of the polymerisation.

For the objects 3D printed in the presence of BTPA, an effective chain transfer process is likely to have resulted in the formation of networks with more homogeneous crosslink densities; however, the differences in the E' compared to the system without RAFT agents were still limited. At the rubbery plateau region (50 °C), the storage modulus of the sample printed with 50 equiv. BTPA ($E' = 26.2 \pm 2.8$ MPa) was lower than that of the

sample printed without RAFT agents ($E' = 31.9 \pm 0.4$ MPa), indicating that the network of the sample 3D printed with BTPA was less crosslinked (**Figure 4.6**). We propose that the reduced modulus may be due to an increased number of dangling chain-ends on the highly branched polymers formed during the RAFT mediated network formation.^{40, 69, 77-79} Further studies are needed to corroborate this behaviour. In the glassy state (-45 °C), the storage modulus of the sample printed with 50 equiv. BTPA ($E' = 2700 \pm 20$ MPa) was higher than the 3D printed sample without RAFT agents ($E' = 2400 \pm 70$ MPa, **Table 4.3**), which is consistent with a previous study.³⁴ It has been demonstrated that below the T_g , the storage modulus of the polymer is primarily controlled by the free volume.⁸⁰ Furthermore, according to the free volume theory, the stiffness increases as the fractional free volume decreases, which suggests that the sample printed with 50 equiv. BTPA had less free volume due to more limited nanogel formation during the early stages of the reaction.⁸¹

As previously mentioned, the performance of xanthate as a chain transfer agent for the polymerisation of more activated monomers is poor due to its high stability (ΔH_{stab}). Although the T_g of the objects printed with the resin containing 50 equiv. of xanthate increased under long layer cure time, they were still below 0 °C. Additionally, these objects showed an upper limit of storage modulus ($E' \approx 2000.0$ MPa at -45 °C) even at a high vinyl bond conversion ($\alpha = 88.9\%$, **Table 4.3**). As discussed regarding the kinetics performance of various RAFT agents, the high stability of xanthate ($\Delta H_{stab} = 86.8$ kJ/mol, **Figure 4.4**) significantly reduces the addition of secondary acrylic radical species to the thiocarbonyl bond. As a result, the xanthate formulations are likely to act similarly to the no RAFT systems at the early stage of the polymerisation, resulting in the formation of nanogels and thus less rigid materials below the T_g (**Figure 4.6**).⁷⁶

As BTPA provided a good balance of polymerisation rates and efficient chain transfer behaviour, further experiments were conducted to gain deeper insight into its effects and potential in 3D printing. Resin formulations containing 25 and 100 equiv. of BTPA were used to provide a broad concentration range for investigating the impacts of BTPA concentrations on the mechanical properties of 3D materials. As shown in **Figure 4.7**, a long inhibition period and significant polymerisation rate reduction were observed in the resin containing 100 equiv. of BTPA. Therefore, a layer cure time of 80 s was applied to obtain a complete 3D printed object. As expected, at a high vinyl bond conversion ($\alpha =$

88%) of the sample printed by using 25 equiv. of BTPA in the resin, as expected, the corresponding E' values and T_g were between that of the objects printed with the resin having 5 equiv. and 50 equiv. of BTPA (**Table 4.4**). However, the E' and T_g of the 3D objects containing 100 equiv. of BTPA was reduced, with the highest E' at $-45\text{ }^{\circ}\text{C}$ reaching $1900 \pm 160\text{ MPa}$ and T_g being $-1.9\text{ }^{\circ}\text{C}$ even under 160 s/per layer. This result was attributed to the slow polymerisation kinetics, which significantly reduced the degree of crosslinking and resulted in the incomplete formation of the network during 3D printing.⁶⁰

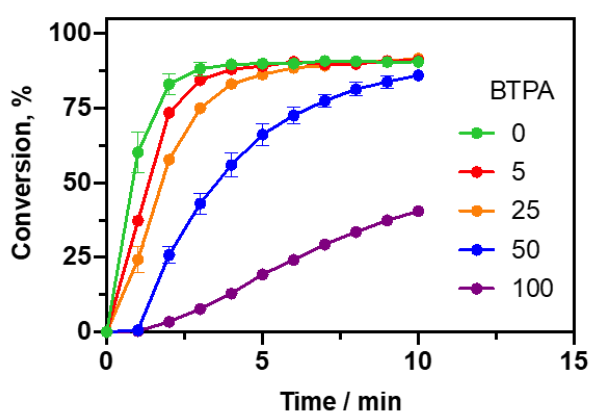


Figure 4.7 Kinetics of polymerisation for PEGA / PEGDA mixtures using varied molar ratios of BTPA as RAFT agent at a fixed molar concentration of [PEGA] : [PEGDA] : [EB] : [TEtOHA] = 571 : 1333 : 0.2 : 40, performed in bulk. Note: All reactions were performed under green light ($\lambda_{\text{max}} = 525\text{ nm}$ and intensity = 4.3 mW/cm^2).

Table 4.4 The mechanical properties of samples 3D printed with varied concentrations of BTPA.^a

[BTPA] ^a	Cure time / layer ^a	T_g	E' (MPa)		Vinyl bond conversion ^b
	(s)	(°C)	50 °C	-45 °C	(%)
0	20 s	-1.8	27.6 ± 2.1	2300 ± 30	82.4
	40 s	0.2	31.9 ± 0.4	2400 ± 70	87.0
5	20 s	-1.5	25.2 ± 1.3	2050 ± 20	82.9
	40 s	0.0	28.9 ± 1.4	2050 ± 100	88.1
25	20 s	-3.4	18.2 ± 0.3	1700 ± 90	74.8
	40 s	0.4	24.6 ± 0.0	2300 ± 40	82.5
	80s	1.9	27.9 ± 2.2	2400 ± 140	88.3
50	40 s	-2.2	12.7 ± 1.9	1750 ± 30	76.2
	80 s	2.0	24.1 ± 0.4	2350 ± 30	87.1
	120s	2.0	26.2 ± 2.8	2700 ± 20	89.1
100	80 s	-8.8	9.0 ± 0.6	1500 ± 50	72.1
	120 s	-2.0	9.8 ± 1.2	1800 ± 10	81.5
	160 s	-1.9	13.0 ± 2.0	1900 ± 160	82.7

^a Samples were 3D printed with a layer thickness of 20 µm and varied cure time per layer in the presence of varied molar ratios of BTPA using a recipe of a fixed molar concentration of [PEGA] : [PEGDA] : [EB] : [TEtOHA] = 571 : 1333 : 0.2 : 40; ^b Vinyl bond conversion was determined by ATR-FTIR spectroscopy. A commercial DLP 3D printer modified with a green LED light board ($\lambda_{\max} = 525$ nm, $I_0 = 0.32$ mW/cm²) was employed to spatially control the formation of the 3D printed samples.

Thereafter, a 3D theatre complex was printed using the recipe containing 5 equiv. of BTPA to demonstrate the ability to 3D print more complex objects. The slicing thickness was set as 20 µm per layer for the purpose of obtaining a 3D print with high resolution. Furthermore, to achieve a rigid object without compromising on printing speed, a 30 s/layer cure time was selected. As shown in **Figure 4.8**, to compare with the original .stl file image, the 3D printed object exhibited great printing details. The shell overhang curling outlines were sharply printed, with a clear shadow projecting on the wall. All

shells were also easily distinguished, and the theatre front face and stage were exquisitely printed with natural transitions.

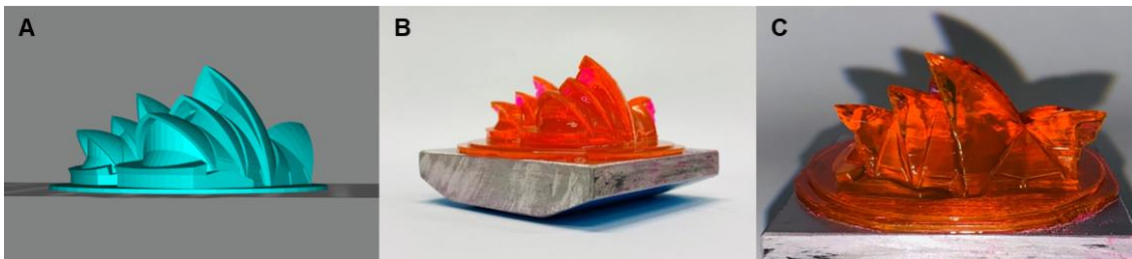


Figure 4.8 3D printed theatre complex. (A) original .stl file image; (B) the theatre complex printed using the resin formulation of [PEGA] : [PEGDA] : [RAFT] : [EB] : [TEtOHA] = 571 : 1333 : 5 : 0.2 : 40; (C) side view of the theatre complex.

4.3.4 Post-modification of 3D printed objects

Thiocarbonylthio groups offer further possibilities for post-functionalization. These end groups can be easily transformed into thiol groups via aminolysis, to allow for facile thiol-ene and other thiol-modifications.⁸²⁻⁹¹ Indeed, the robustness and high efficiency of thiol-ene chemistry have been exploited to introduce functional acrylates into aminolysed RAFT polymers in one-pot processes under mild conditions.⁸²⁻⁸³ As the thiocarbonylthio groups contained in the 3D printed objects were embedded throughout the network as well as on the surface, it was expected that the materials could be post-modified by aminolysis of the thiocarbonate functions and thiol-ene reactions to change the material properties in a one-pot process. Therefore, the aminolysis process of the 3D materials containing RAFT agents was examined. The resin formulation containing 25 equiv. of BTPA was selected, as the 3D printed object was rigid and was produced using reasonable printing speed. A rectangular sample with dimensions of $30 \times 8 \times 1.5$ mm (l , w , t) was printed at a layer slicing thickness of 20 μ m and a cure time of 40 s/layer.

As shown in **Figure 4.9C**, the orange coloured 3D printed sample (**Figure 4.9A**) displayed the typical EB and BTPA absorption peaks around 540 nm and 435 nm, respectively.^{42, 92} After post-curing under green light ($\lambda_{\text{max}} = 525$ nm, 7.1 mW/cm²) for 10 min, the sample displayed a yellow hue (**Figure 4.9B**), which was due to the remaining RAFT agent in the material; this was verified by the almost unchanged BTPA absorption peak in the UV-Vis spectroscopy (**Figure 4.9C**). Subsequently, aminolysis was

performed by submerging the post-cured 3D printed sample in 10 ml DMF solution containing hexylamine (~2 vol%) with a molar ratio of [hexylamine] : [BTPA] = 100 : 1 at room temperature. The samples were analysed using UV-Vis spectroscopy after treatment with hexylamine for 30, 60, 120, and 150 min (**Figure 4.9E**). The BTPA absorption signal at 435 nm reduced significantly after 30 min, but the change in colour of the sample was not obvious. However, after 120 min, the BTPA absorption peak was significantly reduced and the sample became obviously discoloured (**Figure 4.9D**). Interestingly, a peak around 540 nm appeared to increase with the decrease of BTPA absorption peak, which was ascribed to the reformation of strongly light absorbing EB species (**Figure 4.9E**).⁹³ To verify this was attributed to EB and not a RAFT agent-derived by-product, another experiment was performed with a ~5 vol% hexylamine solution containing [hexylamine] : [BTPA] = 100 : 1 in 4 ml DMF (**Figure 4.9F**) at room temperature. As expected, no absorption peak was observed around 540 nm after 10 min reaction, while the decreasing BTPA absorption peak around 435 nm was still clearly visible.

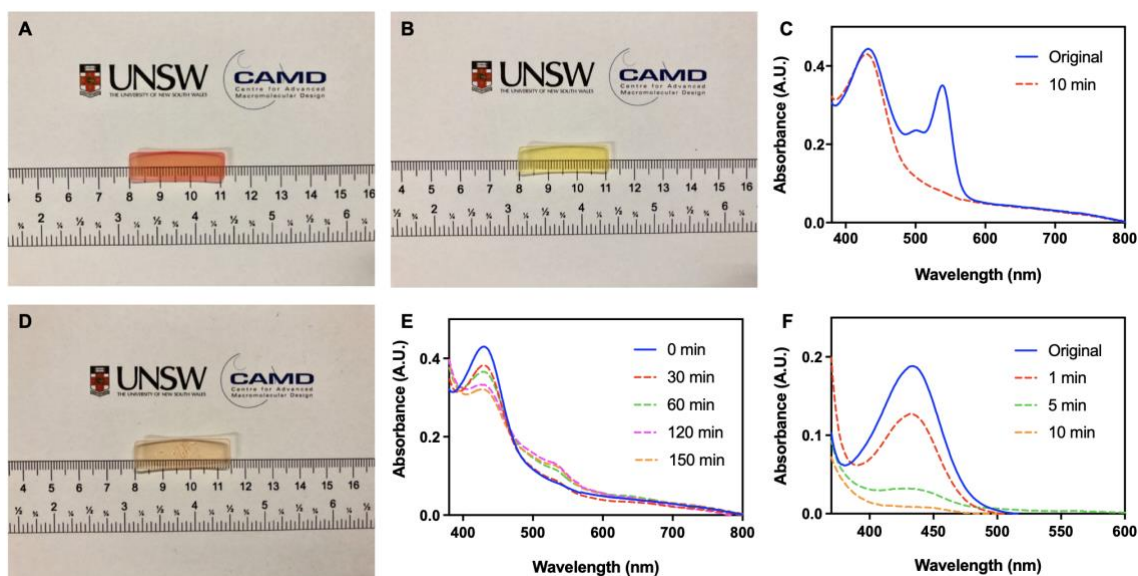


Figure 4.9 Aminolysis of 3D printed materials to change 3D printed material properties. (A) sample printed with a layer thickness of 20 μm and cure time per layer of 40 s using a recipe of [PEGA] : [PEGDA] : [BPTA] : [EB] : [TEtOHA] = 571 : 1333 : 25 : 0.2 : 40; (B) sample post-cured for 10 min under green light ($\lambda_{\text{max}} = 525 \text{ nm}$, 7.1 mW/cm^2); (C) absorbance spectra of the sample 3D printed in the presence of BTPA before and after post-curing for 10 min under green light ($\lambda_{\text{max}} = 525 \text{ nm}$, 7.1 mW/cm^2); (D) sample aminolysed for 120 min with a molar ratio of [hexylamine] : [BTPA] = 100 : 1 in 10 ml DMF solution at room temperature; (E) absorbance spectra before and after aminolysis for samples 3D printed in the presence of BTPA; (F) absorbance spectra before and after aminolysis of a mixture with a molar ratio of [BTPA] : [hexylamine] = 1 : 100 in a total volume of 4 ml DMF solution at room temperature.

Subsequently, a one-pot transformation of the RAFT agent end group was performed via aminolysis of thiocarbonylthio groups and introduction of a fluorescent functional group from 1-pyrene methyl methacrylate (PyMMA, **Figure 4.10A**). An object with dimensions of $40 \times 12 \times 2 \text{ mm}$ (l, w, t) was first 3D printed, then post-cured under green light (7.1 mW/cm^2) for 10 min, and finally submerged in a 5 ml DMF solution containing hexylamine ($\sim 12 \text{ vol\%}$) with a molar ratio of [BTPA] : [hexylamine] : [PyMMA] = 1 : 100 : 10 at room temperature in an orbital shaker. After 1 h reaction, the sample was carefully washed with a 1/1 volume mixture of DMSO/ethanol and irradiated with UV light ($\lambda = 312 \text{ nm}$). As shown in **Figure 4.10B, bottom**, PyMMA was successfully grafted to the surface of the aminolysed 3D printed sample, which showed strong fluorescence under 312 nm irradiation. For comparison, another experiment was conducted where the

further crosslinking of the polymer network through unreacted vinyl bonds. In the presence of PyMMA and hexylamine, further crosslinking via the thiol-Michael reaction with pendent vinyl groups may also have occurred to increase the material modulus due to the aminolysis of RAFT end groups into thiol. Pleasingly, however, the post-modification process did not degrade the 3D printed materials, as might have been expected upon swelling of the polymer networks and subsequent relaxation. To demonstrate the integrity of complex 3D printed objects after post-modification, the theatre complex 3D printed using the recipe containing 5 equiv. of BTPA was firstly post-cured for 10 min under green light ($\lambda_{\text{max}} = 525 \text{ nm}$, 7.1 mW/cm^2). Subsequently, the theatre complex was inverted and submerged halfway in a 60 ml DMF solution containing hexylamine (~4 vol%) with a molar ratio of [BTPA] : [hexylamine] : [PyMMA]= 1 : 100 : 10 at room temperature. After 1 h reaction, the sample was carefully washed with a 1/1 volume mixture of DMSO/ethanol and irradiated with UV light ($\lambda = 312 \text{ nm}$). As shown in **Figure 4.10C**, the object remained intact after functionalisation and displayed fluorescence on areas of the theatre complex that were exposed to the PyMMA solution.

4.4 Conclusion

In summary, resins containing various thiocarbonylthio species were investigated for their application in 3D printing. Both the activating Z groups and leaving R groups have a considerable impact on the polymerisation rate, which affects the 3D printing process and the resulting mechanical properties of 3D printed materials. The resins containing BTPA or xanthate produced rigid 3D printed objects. By contrast, the materials printed in the presence of trithiocarbonates such as CDTPA or pyrazole-based dithiocarbamates which demonstrated a slower polymerisation rate, were softer even under extended cure times per layer. The addition of BTPA in the 3D printing resins significantly affected the resulting mechanical behaviour of the 3D printed materials; the E' of materials printed in the presence of increasing concentrations of BTPA increased to a point, and reduced thereafter, which was ascribed to reduction in polymerisation rates at higher BTPA concentrations. The resins containing high concentrations of BTPA were still printable, however, long cure times per layer were required. The presence of thiocarbonylthio groups into the 3D materials also provided an easy route for the functionalisation of 3D printed objects. The thiocarbonylthio end groups were aminolysed to thiols, which were subsequently reacted via a thiol-Michael addition reaction, and functionalisation of the 3D printed objects was demonstrated via a one-pot aminolysis process and addition of fluorescent monomer. The RAFT mediated photopolymerisation process has become an important approach for producing new functional materials that can be utilised for various purposes.

4.5 Reference

1. Ligon, S. C.; Liska, R.; Stampfl, J.; Gurr, M.; Mulhaupt, R., Polymers for 3D Printing and Customized Additive Manufacturing. *Chemical Reviews* **2017**, *117*(15), 10212-10290.
2. Rogers, C. I.; Qaderi, K.; Woolley, A. T.; Nordin, G. P., 3D printed microfluidic devices with integrated valves. *Biomicrofluidics* **2015**, *9*(1), 016501.
3. Zarek, M.; Layani, M.; Cooperstein, I.; Sachyani, E.; Cohn, D.; Magdassi, S., 3D Printing of Shape Memory Polymers for Flexible Electronic Devices. *Advanced Materials* **2016**, *28*(22), 4449-54.
4. Schwartz, J. J.; Boydston, A. J., Multimaterial actinic spatial control 3D and 4D printing. *Nature Communications* **2019**, *10*(1), 791.
5. Dolinski, N. D.; Page, Z. A.; Callaway, E. B.; Eisenreich, F.; Garcia, R. V.; Chavez, R.; Bothman, D. P.; Hecht, S.; Zok, F. W.; Hawker, C. J., Solution Mask Liquid Lithography (SMaLL) for One-Step, Multimaterial 3D Printing. *Advanced Materials* **2018**, *30*(31), 1800364.
6. Zhang, B.; Kowsari, K.; Serjouei, A.; Dunn, M. L.; Ge, Q., Reprocessable thermosets for sustainable three-dimensional printing. *Nature Communications* **2018**, *9*(1), 1831.
7. Ge, Q.; Sakhaei, A. H.; Lee, H.; Dunn, C. K.; Fang, N. X.; Dunn, M. L., Multimaterial 4D Printing with Tailorable Shape Memory Polymers. *Scientific Reports* **2016**, *6*, 31110.
8. Zheng, X.; Lee, H.; Weisgraber, T. H.; Shusteff, M.; DeOtte, J.; Duoss, E. B.; Kuntz, J. D.; Biener, M. M.; Ge, Q.; Jackson, J. A.; Kucheyev, S. O.; Fang, N. X.; Spadaccini, C. M., Ultralight, ultrastiff mechanical metamaterials. *Science* **2014**, *344*(6190), 1373-1377.
9. Jung, K.; Corrigan, N.; Ciftci, M.; Xu, J.; Seo, S. E.; Hawker, C. J.; Boyer, C., Designing with Light: Advanced 2D, 3D, and 4D Materials. *Advanced Materials* **2020**, *32*(18), 1903850.
10. Hong, S.; Sycks, D.; Chan, H. F.; Lin, S.; Lopez, G. P.; Guilak, F.; Leong, K. W.; Zhao, X., 3D Printing of Highly Stretchable and Tough Hydrogels into Complex, Cellularized Structures. *Advanced Materials* **2015**, *27*(27), 4035-4040.
11. Kim, S. H.; Yeon, Y. K.; Lee, J. M.; Chao, J. R.; Lee, Y. J.; Seo, Y. B.; Sultan, M. T.; Lee, O. J.; Lee, J. S.; Yoon, S.-i.; Hong, I.-S.; Khang, G.; Lee, S. J.; Yoo, J. J.; Park, C. H., Precisely printable and biocompatible silk fibroin bioink for digital light processing 3D printing. *Nature Communications* **2018**, *9*(1), 1620.
12. Lim, K. S.; Galarraga, J. H.; Cui, X.; Lindberg, G. C. J.; Burdick, J. A.; Woodfield, T. B. F., Fundamentals and Applications of Photo-Cross-Linking in Bioprinting. *Chemical Reviews* **2020**, *120*(19), 10662-10694.
13. Gao, H.; Matyjaszewski, K., Synthesis of functional polymers with controlled architecture by CRP of monomers in the presence of cross-linkers: From stars to gels. *Progress in Polymer Science* **2009**, *34*(4), 317-350.
14. Moad, G., RAFT (Reversible addition-fragmentation chain transfer) crosslinking (co)polymerization of multi-olefinic monomers to form polymer networks. *Polymer International* **2015**, *64*(1), 15-24.
15. Rey, L.; Duchet, J.; Galy, J.; Sautereau, H.; Vouagner, D.; Carrion, L., Structural heterogeneities and mechanical properties of vinyl/dimethacrylate networks synthesized by thermal free radical polymerisation. *Polymer* **2002**, *43*(16), 4375-4384.
16. Kannurpatti, A. R.; Anseth, J. W.; Bowman, C. N., A study of the evolution of mechanical properties and structural heterogeneity of polymer networks formed by

- photopolymerizations of multifunctional (meth)acrylates. *Polymer* **1998**, 39(12), 2507-2513.
17. Corrigan, N.; Jung, K.; Moad, G.; Hawker, C. J.; Matyjaszewski, K.; Boyer, C., Reversible-deactivation radical polymerization (Controlled/living radical polymerization): From discovery to materials design and applications. *Progress in Polymer Science* **2020**, 111, 101311.
 18. Konkolewicz, D.; Schröder, K.; Buback, J.; Bernhard, S.; Matyjaszewski, K., Visible Light and Sunlight Photoinduced ATRP with ppm of Cu Catalyst. *ACS Macro Letters* **2012**, 1(10), 1219-1223.
 19. Kutahya, C.; Wang, P.; Li, S.; Liu, S.; Li, J.; Chen, Z.; Strehmel, B., Carbon Dots as a Promising Green Photocatalyst for Free Radical and ATRP-Based Radical Photopolymerization with Blue LEDs. *Angewandte Chemie International Edition* **2020**, 59(8), 3166-3171.
 20. Martinez, M. R.; Sobieski, J.; Lorandi, F.; Fantin, M.; Dadashi-Silab, S.; Xie, G.; Olszewski, M.; Pan, X.; Ribelli, T. G.; Matyjaszewski, K., Understanding the Relationship between Catalytic Activity and Termination in photoATRP: Synthesis of Linear and Bottlebrush Polyacrylates. *Macromolecules* **2019**, 53(1), 59-67.
 21. Yan, W.; Dadashi-Silab, S.; Matyjaszewski, K.; Spencer, N. D.; Benetti, E. M., Surface-Initiated Photoinduced ATRP: Mechanism, Oxygen Tolerance, and Temporal Control during the Synthesis of Polymer Brushes. *Macromolecules* **2020**, 53(8), 2801-2810.
 22. Yang, Q.; Lalevée, J.; Poly, J., Development of a Robust Photocatalyzed ATRP Mechanism Exhibiting Good Tolerance to Oxygen and Inhibitors. *Macromolecules* **2016**, 49(20), 7653-7666.
 23. Xu, J.; Shanmugam, S.; Corrigan, N. A.; Boyer, C., Catalyst-Free Visible Light-Induced RAFT Photopolymerization. In *Controlled Radical Polymerization: Mechanisms*, American Chemical Society: 2015; pp 247-267.
 24. McKenzie, T. G.; Fu, Q.; Wong, E. H.; Dunstan, D. E.; Qiao, G. G., Visible light mediated controlled radical polymerization in the absence of exogenous radical sources or catalysts. *Macromolecules* **2015**, 48(12), 3864-3872.
 25. Corrigan, N.; Yeow, J.; Judzewitsch, P.; Xu, J.; Boyer, C., Seeing the Light: Advancing Materials Chemistry through Photopolymerization. *Angewandte Chemie International Edition* **2019**, 58(16), 5170-5189.
 26. Chen, M.; Zhong, M.; Johnson, J. A., Light-Controlled Radical Polymerization: Mechanisms, Methods, and Applications. *Chem Rev* **2016**, 116(17), 10167-10211.
 27. Barner-Kowollik, C., *Handbook of RAFT polymerization*. John Wiley & Sons: 2008.
 28. Chiefari, J.; Chong, Y.; Ercole, F.; Krstina, J.; Jeffery, J.; Le, T. P.; Mayadunne, R. T.; Meijs, G. F.; Moad, C. L.; Moad, G., Living free-radical polymerization by reversible addition-fragmentation chain transfer: the RAFT process. *Macromolecules* **1998**, 31(16), 5559-5562.
 29. Perrier, S. b., 50th Anniversary Perspective: RAFT Polymerization-A User Guide. *Macromolecules* **2017**, 50(19), 7433-7447.
 30. Hawker, C. J.; Bosman, A. W.; Harth, E., New polymer synthesis by nitroxide mediated living radical polymerizations. *Chemical Reviews* **2001**, 101(12), 3661-88.
 31. Moad, G.; Rizzardo, E.; Thang, S. H., Living Radical Polymerization by the RAFT Process – A Third Update. *Australian journal of chemistry* **2012**, 65(8), 985-1076.
 32. Hill, M. R.; Carmean, R. N.; Sumerlin, B. S., Expanding the scope of RAFT polymerization: recent advances and new horizons. *Macromolecules* **2015**, 48(16), 5459-5469.

33. Roy, S. G.; Haldar, U.; De, P., Remarkable swelling capability of amino acid based cross-linked polymer networks in organic and aqueous medium. *ACS Applied Materials & Interfaces* **2014**, 6(6), 4233-4241.
34. Yu, Q.; Zhu, Y.; Ding, Y.; Zhu, S., Reaction behavior and network development in raft radical polymerization of dimethacrylates. *Macromolecular Chemistry and Physics* **2008**, 209(5), 551-556.
35. Norisuye, T.; Morinaga, T.; Tran-Cong-Miyata, Q.; Goto, A.; Fukuda, T.; Shibayama, M., Comparison of the gelation dynamics for polystyrenes prepared by conventional and living radical polymerizations: a time-resolved dynamic light scattering study. *Polymer* **2005**, 46(6), 1982-1994.
36. Shanmugam, S.; Xu, J.; Boyer, C., Exploiting Metalloporphyrins for Selective Living Radical Polymerization Tunable over Visible Wavelengths. *Journal of the American Chemical Society* **2015**, 137(28), 9174-9185.
37. Xu, J.; Jung, K.; Atme, A.; Shanmugam, S.; Boyer, C., A robust and versatile photoinduced living polymerization of conjugated and unconjugated monomers and its oxygen tolerance. *Journal of the American Chemical Society* **2014**, 136(14), 5508-5519.
38. Xu, J.; Shanmugam, S.; Duong, H. T.; Boyer, C., Organo-photocatalysts for photoinduced electron transfer-reversible addition-fragmentation chain transfer (PET-RAFT) polymerization. *Polymer Chemistry* **2015**, 6(31), 5615-5624.
39. Wu, Z.; Jung, K.; Boyer, C., Effective Utilization of NIR Wavelengths for Photo-Controlled Polymerization: Penetration Through Thick Barriers and Parallel Solar Syntheses. *Angewandte Chemie International Edition* **2020**, 59(5), 2013-2017.
40. Zhang, Z.; Corrigan, N.; Bagheri, A.; Jin, J.; Boyer, C., A Versatile 3D and 4D Printing System through Photocontrolled RAFT Polymerization. *Angewandte Chemie International Edition* **2019**, 131(50), 18122-18131.
41. Corrigan, N.; Xu, J.; Boyer, C.; Allonas, X., Exploration of the PET-RAFT Initiation Mechanism for Two Commonly Used Photocatalysts. *ChemPhotoChem* **2019**, 3(11), 1193-1199.
42. Wu, C.; Corrigan, N.; Lim, C. H.; Jung, K.; Zhu, J.; Miyake, G.; Xu, J.; Boyer, C., Guiding the Design of Organic Photocatalyst for PET-RAFT Polymerization: Halogenated Xanthene Dyes. *Macromolecules* **2019**, 52(1), 236-248.
43. Corrigan, N.; Rosli, D.; Jones, J. W. J.; Xu, J.; Boyer, C., Oxygen Tolerance in Living Radical Polymerization: Investigation of Mechanism and Implementation in Continuous Flow Polymerization. *Macromolecules* **2016**, 49(18), 6779-6789.
44. Zaquen, N.; Kadir, A. M. N. B. P. H. A.; Iasa, A.; Corrigan, N.; Junkers, T.; Zetterlund, P. B.; Boyer, C., Rapid Oxygen Tolerant Aqueous RAFT Photopolymerization in Continuous Flow Reactors. *Macromolecules* **2019**, 52(4), 1609-1619.
45. Corrigan, N.; Zhernakov, L.; Hashim, M. H.; Xu, J.; Boyer, C., Flow mediated metal-free PET-RAFT polymerisation for upscaled and consistent polymer production. *Reaction Chemistry & Engineering* **2019**, 4(7), 1216-1228.
46. Xu, J.; Jung, K.; Boyer, C., Oxygen Tolerance Study of Photoinduced Electron Transfer-Reversible Addition-Fragmentation Chain Transfer (PET-RAFT) Polymerization Mediated by Ru(bpy)₃Cl₂. *Macromolecules* **2014**, 47(13), 4217-4229.
47. Bagheri, A.; Bainbridge, C. W. A.; Engel, K. E.; Qiao, G. G.; Xu, J.; Boyer, C.; Jin, J., Oxygen Tolerant PET-RAFT Facilitated 3D Printing of Polymeric Materials under Visible LEDs. *ACS Applied Polymer Materials* **2020**, 2(2), 782-790.
48. Bainbridge, C. W. A.; Engel, K. E.; Jin, J., 3D printing and growth induced bending based on PET-RAFT polymerization. *Polymer Chemistry* **2020**, 11(25), 4084-4093.

49. Keddie, D. J.; Moad, G.; Rizzardo, E.; Thang, S. H., RAFT Agent Design and Synthesis. *Macromolecules* **2012**, *45*(13), 5321-5342.
50. Pawar, A. A.; Halivni, S.; Waiskopf, N.; Ben-Shahar, Y.; Soreni-Harari, M.; Bergbreiter, S.; Banin, U.; Magdassi, S., Rapid Three-Dimensional Printing in Water Using Semiconductor-Metal Hybrid Nanoparticles as Photoinitiators. *Nano letters* **2017**, *17*(7), 4497-4501.
51. Thingiverse, CLEAN Sydney Opera House - Easy Print. <https://www.thingiverse.com/thing:465989> (accessed 2/9/2020).
52. Liu, Z.; Robinson, J. T.; Sun, X.; Dai, H., PEGylated nanographene oxide for delivery of water-insoluble cancer drugs. *Journal of the American Chemical Society* **2008**, *130*(33), 10876-10877.
53. Cleland, J. L.; Builder, S. E.; Swartz, J. R.; Winkler, M.; Chang, J. Y.; Wang, D. I., Polyethylene glycol enhanced protein refolding. *Biotechnology (N Y)* **1992**, *10*(9), 1013-1019.
54. Zhang, Y.; Tao, L.; Li, S.; Wei, Y., Synthesis of multiresponsive and dynamic chitosan-based hydrogels for controlled release of bioactive molecules. *Biomacromolecules* **2011**, *12*(8), 2894-901.
55. Gittard, S. D.; Ovsianikov, A.; Akar, H.; Chichkov, B.; Monteiro-Riviere, N. A.; Stafslie, S.; Chisholm, B.; Shin, C. C.; Shih, C. M.; Lin, S. J.; Su, Y. Y.; Narayan, R. J., Two Photon Polymerization-Micromolding of Polyethylene Glycol-Gentamicin Sulfate Microneedles. *Advanced Engineering Materials* **2010**, *12*(4), B77-B82.
56. Bahney, C. S.; Lujan, T. J.; Hsu, C. W.; Bottlang, M.; West, J. L.; Johnstone, B., Visible light photoinitiation of mesenchymal stem cell-laden bioresponsive hydrogels. *European Cells and Materials* **2011**, *22*, 43-55; discussion 55.
57. Perrier, S.; Barner-Kowollik, C.; Quinn, J. F.; Vana, P.; Davis, T. P., Origin of Inhibition Effects in the Reversible Addition Fragmentation Chain Transfer (RAFT) Polymerization of Methyl Acrylate. *Macromolecules* **2002**, *35*(22), 8300-8306.
58. Vana, P.; Davis, T. P.; Barner-Kowollik, C., Kinetic Analysis of Reversible Addition Fragmentation Chain Transfer (RAFT) Polymerizations: Conditions for Inhibition, Retardation, and Optimum Living Polymerization. *Macromolecular Theory and Simulations* **2002**, *11*(8), 823-835.
59. Donovan, M. S.; Lowe, A. B.; Sumerlin, B. S.; McCormick, C. L., Raft Polymerization of N,N-Dimethylacrylamide Utilizing Novel Chain Transfer Agents Tailored for High Reinitiation Efficiency and Structural Control†. *Macromolecules* **2002**, *35*(10), 4123-4132.
60. Barlow, K. J.; Hao, X.; Hughes, T. C.; Hutt, O. E.; Polyzos, A.; Turner, K. A.; Moad, G., Porous, functional, poly(styrene-co-divinylbenzene) monoliths by RAFT polymerization. *Polymer Chemistry* **2014**, *5*(3), 722-732.
61. Moad, G.; Rizzardo, E.; Thang, S. H., Radical addition-fragmentation chemistry in polymer synthesis. *Polymer* **2008**, *49*(5), 1079-1131.
62. López-Domínguez, P.; Hernández-Ortiz, J. C.; Barlow, K. J.; Vivaldo-Lima, E.; Moad, G., Modeling the Kinetics of Monolith Formation by RAFT Copolymerization of Styrene and Divinylbenzene. *Macromolecular Reaction Engineering* **2014**, *8*(10), 706-722.
63. Krenske, E. H.; Izgorodina, E. I.; Coote, M. L., An Ab Initio Guide to Structure—Reactivity Trends in Reversible Addition Fragmentation Chain Transfer Polymerization. In *Controlled/Living Radical Polymerization*, American Chemical Society: 2006; pp 406-420.
64. Gardiner, J.; Martinez-Botella, I.; Kohl, T. M.; Krstina, J.; Moad, G.; Tyrell, J. H.; Coote, M. L.; Tsanaktsidis, J., 4-Halogeno-3,5-dimethyl-1H-pyrazole-1-carbodithioates:

versatile reversible addition fragmentation chain transfer agents with broad applicability. *Polymer International* **2017**, 66(11), 1438-1447.

65. Chiefari, J.; Mayadunne, R. T. A.; Moad, C. L.; Moad, G.; Rizzardo, E.; Postma, A.; Thang, S. H., Thiocarbonylthio Compounds (SC(Z)S-R) in Free Radical Polymerization with Reversible Addition-Fragmentation Chain Transfer (RAFT Polymerization). Effect of the Activating Group Z. *Macromolecules* **2003**, 36(7), 2273-2283.

66. Monteiro, M. J.; de Brouwer, H., Intermediate Radical Termination as the Mechanism for Retardation in Reversible Addition-Fragmentation Chain Transfer Polymerization. *Macromolecules* **2001**, 34(3), 349-352.

67. Kwak, Y.; Goto, A.; Tsujii, Y.; Murata, Y.; Komatsu, K.; Fukuda, T., A Kinetic Study on the Rate Retardation in Radical Polymerization of Styrene with Addition-Fragmentation Chain Transfer. *Macromolecules* **2002**, 35(8), 3026-3029.

68. Calitz, F. M.; McLeary, J. B.; McKenzie, J. M.; Tonge, M. P.; Klumperman, B.; Sanderson, R. D., Evidence for Termination of Intermediate Radical Species in RAFT-Mediated Polymerization. *Macromolecules* **2003**, 36(26), 9687-9690.

69. Charlesby, A., Elastic modulus formulae for a crosslinked network. *International Journal of Radiation Applications and Instrumentation, Part C* **1992**, 40(2), 117-120.

70. Ricciardi, M. R.; Papa, I.; Langella, A.; Langella, T.; Lopresto, V.; Antonucci, V., Mechanical properties of glass fibre composites based on nitrile rubber toughened modified epoxy resin. *Composites, Part B: Engineering* **2018**, 139, 259-267.

71. Cook, W. D.; Forsythe, J. S.; Irawati, N.; Scott, T. F.; Xia, W. Z., Cure kinetics and thermomechanical properties of thermally stable photopolymerized dimethacrylates. *Journal of applied polymer science* **2003**, 90(14), 3753-3766.

72. Gorsche, C.; Seidler, K.; Knaack, P.; Dorfinger, P.; Koch, T.; Stampfl, J.; Moszner, N.; Liska, R., Rapid formation of regulated methacrylate networks yielding tough materials for lithography-based 3D printing. *Polymer Chemistry* **2016**, 7(11), 2009-2014.

73. Tobita, H.; Hamielec, A., Modeling of network formation in free radical polymerization. *Macromolecules* **1989**, 22(7), 3098-3105.

74. Zhu, S.; Hamielec, A., Influence of cross-link density distribution on network formation in free-radical copolymerization of vinyl/divinyl monomers. *Macromolecules* **1992**, 25(20), 5457-5464.

75. Matsumoto, A., Free-radical crosslinking polymerization and copolymerization of multivinyl compounds. In *Synthesis and Photosynthesis*, Springer Berlin Heidelberg: 1995; pp 41-80.

76. Taton, D.; Baussard, J. F.; Dupayage, L.; Poly, J.; Gnanou, Y.; Ponsinet, V.; Destarac, M.; Mignaud, C.; Pitois, C., Water soluble polymeric nanogels by xanthate-mediated radical crosslinking copolymerisation. *Chemical communications* **2006**, (18), 1953-5.

77. Sheiko, S. S.; Dobrynin, A. V., Architectural Code for Rubber Elasticity: From Supersoft to Superfirm Materials. *Macromolecules* **2019**, 52(20), 7531-7546.

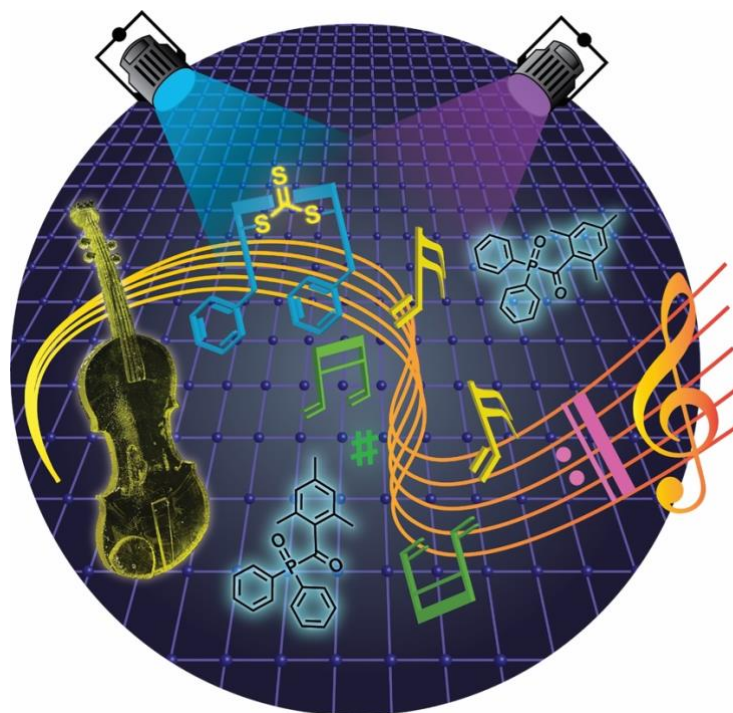
78. Zhong, M.; Wang, R.; Kawamoto, K.; Olsen, B. D.; Johnson, J. A., Quantifying the impact of molecular defects on polymer network elasticity. *Science* **2016**, 353(6305), 1264.

79. Lin, T.-S.; Wang, R.; Johnson, J. A.; Olsen, B. D., Revisiting the Elasticity Theory for Real Gaussian Phantom Networks. *Macromolecules* **2019**, 52(4), 1685-1694.

80. Menard, K. P., *Dynamic mechanical analysis: A Practical Introduction, 2nd Edition*. CRC Press: 2008.

81. Jean, Y. C.; Deng, Q.; Nguyen, T. T., Free-Volume Hole Properties in Thermosetting Plastics Probed by Positron Annihilation Spectroscopy: Chain Extension Chemistry. *Macromolecules* **1995**, 28(26), 8840-8844.
82. Qiu, X.-P.; Winnik, F. M., Facile and Efficient One-Pot Transformation of RAFT Polymer End Groups via a Mild Aminolysis/Michael Addition Sequence. *Macromolecular Rapid Communications* **2006**, 27(19), 1648-1653.
83. Spruell, J. M.; Levy, B. A.; Sutherland, A.; Dichtel, W. R.; Cheng, J. Y.; Stoddart, J. F.; Nelson, A., Facile postpolymerization end-modification of RAFT polymers. *Journal of Polymer Science Part A: Polymer Chemistry* **2009**, 47(2), 346-356.
84. Lima, V.; Jiang, X.; Brokken-Zijp, J.; Schoenmakers, P. J.; Klumperman, B.; Van Der Linde, R., Synthesis and characterization of telechelic polymethacrylates via RAFT polymerization. *Journal of Polymer Science Part A: Polymer Chemistry* **2005**, 43(5), 959-973.
85. Chan, J. W.; Yu, B.; Hoyle, C. E.; Lowe, A. B., Convergent synthesis of 3-arm star polymers from RAFT-prepared poly (N, N-diethylacrylamide) via a thiol-ene click reaction. *Chemical communications* **2008**, (40), 4959-4961.
86. Nakayama, M.; Okano, T., Polymer Terminal Group Effects on Properties of Thermoresponsive Polymeric Micelles with Controlled Outer-Shell Chain Lengths. *Biomacromolecules* **2005**, 6(4), 2320-2327.
87. Hoyle, C. E.; Bowman, C. N., Thiol-Ene Click Chemistry. *Angewandte Chemie International Edition* **2010**, 49(9), 1540-1573.
88. Boyer, C.; Granville, A.; Davis, T. P.; Bulmus, V., Modification of RAFT-polymers via thiol-ene reactions: A general route to functional polymers and new architectures. *Journal of Polymer Science Part A: Polymer Chemistry* **2009**, 47(15), 3773-3794.
89. Willcock, H.; O'Reilly, R. K., End group removal and modification of RAFT polymers. *Polymer Chemistry* **2010**, 1(2), 149-157.
90. Shen, W.; Qiu, Q.; Wang, Y.; Miao, M.; Li, B.; Zhang, T.; Cao, A.; An, Z., Hydrazine as a Nucleophile and Antioxidant for Fast Aminolysis of RAFT Polymers in Air. *Macromolecular Rapid Communications* **2010**, 31(16), 1444-1448.
91. Hornung, C. H.; von Känel, K.; Martinez-Botella, I.; Espiritu, M.; Nguyen, X.; Postma, A.; Saubern, S.; Chiefari, J.; Thang, S. H., Continuous Flow Aminolysis of RAFT Polymers Using Multistep Processing and Inline Analysis. *Macromolecules* **2014**, 47(23), 8203-8213.
92. McKenzie, T. G.; Fu, Q.; Wong, E. H. H.; Dunstan, D. E.; Qiao, G. G., Visible Light Mediated Controlled Radical Polymerization in the Absence of Exogenous Radical Sources or Catalysts. *Macromolecules* **2015**, 48(12), 3864-3872.
93. Aguirre-Soto, A.; Kaastrup, K.; Kim, S.; Ugo-Beke, K.; Sikes, H. D., Excitation of Metastable Intermediates in Organic Photoredox Catalysis: Z-Scheme Approach Decreases Catalyst Inactivation. *ACS Catalysis* **2018**, 8(7), 6394-6400.

Chapter 5. Effect of Thiocarbonylthio Compounds on Visible Light Mediated 3D Printing



The contents of this chapter were published in: Zhang, Z.; Corrigan, N.; Boyer, C. A Photoinduced Dual-Wavelength Approach for 3D Printing and Self-Healing of Thermosetting Materials. *Angewandte Chemie International Edition* **2022**, 61(11), e202114111.

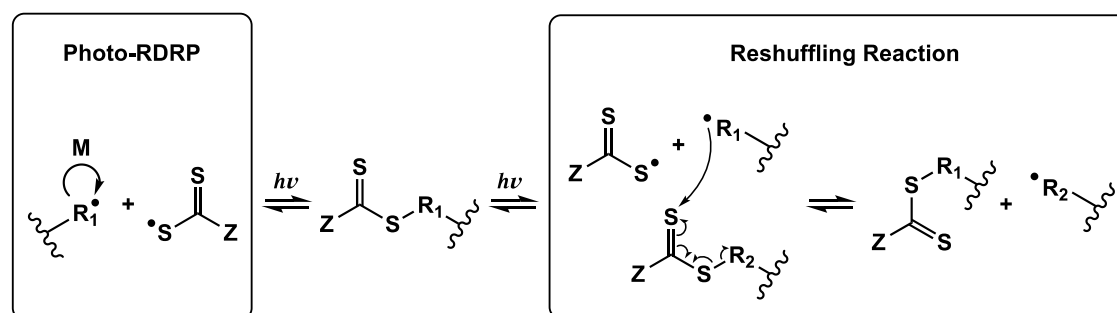
5.1 Introduction

Vat photopolymerisation has become a promising 3D printing technique which enables the fabrication of complex 3D objects with advantageous material properties via versatile photochemistries.¹⁻⁸ Among the various 3D printing approaches, photoinduced techniques such as stereolithography (SLA) and digital light processing (DLP) 3D printing present fast build rates and high printing resolution with low feature size.^{7, 9-13} The photocuring strategy behind the 3D photopolymerisation is based on using light as the stimulus in the presence of photoinitiating species, converting reactive liquid resins into solid materials.¹ The resins used to form 3D printed objects are typically composed of multifunctional (meth)acrylate- or epoxide-based monomers and oligomers; this provides thermoset materials which have excellent mechanical performance with high modulus, but lack repairability due to the irreversibly crosslinked polymer networks.¹⁴⁻¹⁶ As a result, these thermosets cannot be repaired after damage, leading to wasted resources and materials, and the production of environmental pollutants.¹⁷

Recently, researchers have incorporated dynamic covalent bonds in crosslinked polymer networks to enable reversible network rearrangement and reformation under external stimuli.^{16, 18-23} Importantly, dynamic covalent chemistry has been used to imbue 3D printed materials with self-healing properties, allowing these materials to self-repair cracks and other damage and thus recover material mechanical strength and functionality.²⁴⁻³³ As such, materials with dynamic covalent bonds can have extended lifespans, which helps to reduce plastic waste generation and create more sustainable 3D printing. The self-healing of materials with dynamic covalent bonds is typically induced either thermally or photochemically. Indeed, self-healing based on thermally reversible reactions such as Diels-Alder reactions or transesterification has been demonstrated for thermosets 3D printed via vat photopolymerisation.^{24, 26} Smaldone and co-workers successfully employed SLA 3D printing to print objects with self-healing properties provided via Diels-Alder chemistry.²⁶ After damage, the 3D printed objects recovered 99% of their original tensile strength under two sequential thermal treatments at 110°C for 24 h followed by 80°C for 24 h. In another example, Ge and co-workers repaired a 3D printed object by exploiting transesterification.²⁴ Upon heating to 180°C for 4 h, the damaged object regained its mechanical performance due to the reformation of ester bonds between the adjacent hydroxyl and ester functional groups present in the pre-formed network.

However, these thermally-triggered healing procedures demand temperatures over 100°C, which limit potential applications and practicality. In comparison, self-healing processes that use light can be performed at ambient temperatures in a spatially-controlled manner due to the ability to confine the light to specific, targeted areas.³⁴⁻³⁹

Photoinduced covalent bond rearrangement via reversible addition-fragmentation chain transfer (RAFT) chemistry has become an emerging approach for self-healing covalently crosslinked materials.^{35, 38, 40} In these systems, thiocarbonylthio compounds (RAFT agents) can play roles as both a chain transfer agent during formation of the polymer network, and also as an initiator-transfer-agent-terminator (iniferter)⁴¹⁻⁵⁵ under specific light irradiation to enable post-modification of the network.⁵⁶⁻⁶² According to previous studies, the RAFT agents incorporated in the network can facilitate self-healing via reshuffling reactions between network strands and via photo-reactivation of chains which can subsequently polymerise.^{35-38, 63} As shown in **Scheme 5.1**, the RAFT agent group within the network can undergo UV-induced photolysis to cleave the weak C-S bond and generate a thiocarbonylthio radical fragment and a reactive carbon-centered radical R^{\bullet} .⁵⁵ Subsequently, the radical R^{\bullet} can react with other thiocarbonylthio groups by degenerative exchange reactions (reshuffling reactions) to promote network rearrangement and recombination. Alternatively, the radical R^{\bullet} can initiate chain growth with monomers or/and crosslinkers via a photo-controlled RAFT process to extend or rebuild the network.^{54, 64-68} For instance, Matyjaszewski and co-workers exploited trithiocarbonate (TTC) units in a crosslinked butyl acrylate network to re-heal gels via degenerative reshuffling reactions under 4 h UV light irradiation in acetonitrile and nitrogen.^{35, 63, 69}



Scheme 5.1 Self-healing via photo-reversible deactivation radical polymerisation (photo-RDRP) and reshuffling reactions in the presence of photoiniferters.

However, in the absence of solvent, the healing time was extended to 48 h, resulting in an incompletely healed object as noted by the presence of small cracks on the surface.³⁵ Chen, Johnson and co-workers demonstrated self-healing behaviour by using TTC units incorporated in the network to grow polymer chains via photo-reversible deactivation radical polymerisation (photo-RDRP).³⁸ In the presence of deoxygenated solutions containing photocatalyst (PC), monomer and crosslinker, the TTC units were reactivated to mediate further polymerisation at the cut interfaces, yielding a healed material with no visible damage under 4 h blue light irradiation.³⁸ While these examples elegantly demonstrate the utility of photoinduced dynamic covalent bonds within network polymers, to the best of our knowledge, there are no 3D printed thermoset materials with self-healing capability triggered by light.

RAFT polymerisation has recently been applied to photoinduced 3D printing to produce materials with various functions and properties.^{11, 59-60, 70-71} In this chapter, we investigate the self-healing of thermosets obtained via a RAFT-mediated photoinduced 3D printing process. A Norrish type I photoinitiation system was adopted to facilitate RAFT photopolymerisation under violet light ($\lambda_{\text{max}} = 405 \text{ nm}$), using symmetric difunctional RAFT agents to mediate the network formation. The self-healing behaviour of the resulting materials was demonstrated under 365 nm irradiation at room temperature; critically, the distinct irradiation wavelengths allowed efficient photopolymerisation during 3D printing and subsequent network reformation of severed 3D printed thermosets. Furthermore, self-healing was performed under open-to-air conditions and did not require any specialised equipment. The impact of varying the concentration of RAFT agents in the resin on the healing efficiency was also explored. Finally, the healing ability of the 3D objects printed in the presence of difunctional RAFT agent and monofunctional RAFT agent was compared to demonstrate the significance of the RAFT agent structures on healing efficiency.

5.2 Experimental Section

5.2.1 Materials

2-hydroxyethyl acrylate (HEA, $M_n = 116.12 \text{ g mol}^{-1}$, Sigma-Aldrich, 96%), ethylene glycol dimethacrylate (EGDMA, $M_n = 198.22 \text{ g mol}^{-1}$, Sigma-Aldrich, 98%), (2,4,6-trimethylbenzoyl)diphenylphosphine oxide (TPO, Sigma-Aldrich, >97%), poly(ethylene glycol) diacrylate average M_n 250 (PEGDA, Sigma-Aldrich, >92%), acrylic acid (AA, Sigma-Aldrich, 99%), dimethylsulfoxide (DMSO, chem-supply), dibenzyl trithiocarbonate (DBTTC, Boron Molecular, 98%) and 3-(((benzylthio)carbonothioyl)thio)propionic acid (BSTP, Boron Molecular) were used as received. The double-side tape was purchased from X-Press IT.

5.2.2 Instrumentation

Attenuated total reflectance-fourier-transform infrared (ATR-FTIR) spectroscopy was employed to monitor vinyl bond conversions, using an approach similar to Magdassi, Banin, and co-workers.⁷² A Bruker Alpha FT-IR equipped with room temperature DTGS detectors was used for measurement. Each spectrum composed of 16 scans with a resolution of 4 cm^{-1} was collected in the spectral region between $4000\text{--}400 \text{ cm}^{-1}$. Analysis was performed using OPUS software.

Fourier Transform Near-Infrared (FTNIR) spectroscopy was performed using a Bruker Vertex 70 Fourier transform spectrometer. FTNIR spectroscopy was employed to determine vinyl bond conversion of 3D printed samples. Analysis was performed using OPUS software 7.5.

A TA instruments Q800 dynamic mechanical analyzer (DMA) was employed to obtain mechanical property measurements on the 3D printed objects. The Q800 DMA was equipped with a TA instruments liquid nitrogen gas cooling accessory (GCA) for temperature control.

Anycubic Photon S, the LCD digitally masked DLP 3D printer with an LED light array emitting 0.51 mW/cm^2 violet light ($\lambda_{\text{max}} = 405 \text{ nm}$) was employed. The light intensity was

measured using a Newport 843-R power meter. Printing parameters (slicing thickness and layer cure times) were generated using Photon WorkShop software.

A Mark-10 testing machine with a 25 N load cell or a 1000 N load cell was employed to measure tensile strength and elongation at break of 3D printed dumbbell-shaped samples.

Hitachi S-3400N Scanning electron microscopy (SEM) which is fitted with secondary and backscatter electron detectors was used to acquire SEM images at an accelerating voltage of 15 kV or 30 kV. Samples were mounted on aluminium stubs using double-sided adhesive tape and coated with 30 nm platinum nanoparticles using Quorum Q300T D Plus sputter coater.

An Oriel VeraSol LED solar simulator consisting of the LSS-7120 LED controller and LSH-7520 LED head was used as the light source to provide white light according to AM 1.5 Standard Spectral irradiance in the self-healing test.

5.2.3 Experimental procedure

Polymerisation for determination of reaction kinetics

A typical polymerisation solution with the recipe of [DBTTC] : [HEA] : [EGDMA] : [TPO] = 1 : 60 : 6 : 0.5 was prepared as follows: 11.7 mg (40.38 μmol , 1 equiv) of DBTTC, 7.0 mg (20.19 μmol , 0.5 equiv) of TPO, 254.3 μL (2.42 mmol, 60 equiv) of HEA, 45.7 μL (0.24 mmol, 6 equiv) of EGDMA was added to a 4 mL glass vial. The reaction mixture was then covered with foil, vortexed for ~ 10 s, sonicated for 20 s, prior to the irradiation. A 20 μL aliquot of the reaction mixture was then pipetted onto the ATR crystal plate and irradiated with a Thorlabs mounted LED with a collimation adapter ($\lambda_{\text{max}} = 405$ nm) with an intensity at the polymerisation surface, $I_0 = 3.6$ mW/cm² as measured using a Newport 843-R power meter. Gel formation of the droplet was confirmed by observation and finger touch, with the droplet being rigid and holding the shape to free stand. Vinyl bond conversion was calculated based on the disappearance of the methylene group vibrations in the range of 1590-1655 cm⁻¹ assigned to the stretching mode of the =C-H group. The integral under this peak in the range of 1590-1655 cm⁻¹ was evaluated after increasing irradiation times and compared to the peak in the range of 1660-1800 cm⁻¹ assigned to the acrylate C=O stretching mode. The vinyl bond conversion was calculated from **Equation 1**, where *stdo* is the integral under the curve in the range of 1660-1800 cm⁻¹

before irradiation, std_x is the integral under the curve in the range of 1660-1800 cm^{-1} after x mins irradiation, int_0 is the integral under the curve in the range of 1590-1655 cm^{-1} before irradiation, and int_x is the integral under the curve in the range of 1590-1655 cm^{-1} after irradiation for x mins. All FTIR measurements were performed in triplicate.

$$\text{Vinyl bond conversion} = 1 - (int_x / std_x) / (int_0 / std_0) \quad \text{Eq. 1}$$

Vinyl bond conversions of 3D printed samples

FTNIR spectroscopy was employed to determine vinyl bond conversion of 3D printed samples by comparing the integral of the C-H vinylic stretching overtone at 6120-6220 cm^{-1} between 3D printed samples and uncured resin.^{46, 73-74} Analysis was performed using OPUS software 7.5. 3 mL of uncured resin was placed in a 1×1 cm quartz cuvette to collect the absorption spectrum in the spectral region between 4000-8000 cm^{-1} . The thickness of the 3D printed sample was measured using a digital calliper. The 3D printed samples were placed in the cuvette to obtain absorption spectra. The final vinyl bond conversion was calculated from **Equation 2**, Where int_f is the integral under the curve in the range of 6120-6220 cm^{-1} for the 3D printed sample, int_0 is the integral under the curve in the range of 6120-6220 cm^{-1} for the uncured resin, t_{sample} is the thickness of the 3D printed sample, and $t_{cuvette}$ is the path length of the cuvette.

$$\text{Vinyl bond conversion} = 1 - (int_f / int_0) / (t_{sample} / t_{cuvette}) \quad \text{Eq. 2}$$

3D printing procedures of dumbbell-shaped samples

A typical procedure for 3D printing a dumbbell-shaped sample is as follows: 469.1 mg (1.61 mmol, 1 equiv) of DBTTC, 281.3 mg (0.81 mmol, 0.5 equiv) of TPO, 10.72 mL (102.11 mmol, 63.2 equiv) of HEA, 1.28 mL (6.79 mmol, 4.2 equiv) of EGDMA was added to a 20 mL glass vial. The total volume for all reaction mixtures used for polymerisation in bulk was 12 mL. The reaction mixture was then covered with foil, vortexed for ~10 s, sonicated for 20 s, prior to addition to the 3D printer vat (vat dimensions 60 mm × 60 mm × 20 mm). The 3D printed dumbbell-shaped samples were inspired by a standard sample (D638 Type V) with a length of 54 mm, a gage length of 7.62 mm, a width of 9.53 mm, a gage width of 3.18 mm and a thickness of 2.6 mm.⁷⁵ The .stl files were generated using Autodesk Fusion 360 and printing parameters (slicing thickness and layer cure times) were generated using Photon Workshop software. The

dumbbell-shaped sample was then printed by using Anycubic Photon S DLP 3D printer. To ensure adhesion between the 3D printed material and the build stage, the first two (bottom) layers of the material were irradiated for 150 s/layer, after which the regular cure time per layer was 80 s/layer with a layer thickness of 50 μm . To obtain a high surface resolution, the last (top) layer of the material was irradiated for 150 s. The Z lift distance was 1 mm, the Z lift speed was 1 mm/s, and the Z retract speed was 3 mm/s. After the object was printed, the build stage was removed, and the residual polymerisation surface was briefly washed with ethanol. The material was then post-cured for 10 min through irradiation under violet light ($\lambda_{\text{max}} = 405 \text{ nm}$, $I_0 = 9.6 \text{ mW/cm}^2$) for further experiments. Due to the fast polymerisation kinetics of the resin without RAFT agents (near quantitative vinyl bond conversions after 30 s violet light irradiation), the regular cure time per layer for printing no RAFT samples was adjusted to 20 s. Moreover, the cure time for the first two (bottom) layers and the last (top) layer was decreased to 40 s/layer. With the addition of acrylic acid, the cure time per layer for the resin formulation of [DBTTC] : [AA] : [HEA] : [EGDMA] : [TPO] = 1 : 6 : 54 : 4 : 0.5 was increased to 100 s/layer. Also, the cure time for the first two (bottom) layers and the last (top) layer was increased to 100 s/layer.

3D printing procedures of rectangular samples

The resin formulation with a ratio of [DBTTC] : [HEA] : [EGDMA] : [TPO] = 1 : 60 : 4 : 0.5 was used to print simple rectangular samples with dimensions 40 \times 12 \times 2.6 mm (l, w, t). The .stl files were generated using Autodesk Fusion 360 and printing parameters (slicing thickness and layer cure times) were generated using Photon Workshop software. The object was then printed by using Anycubic Photon S DLP 3D printer. To ensure adhesion between the 3D printed material and the build stage, the first two (bottom) layers of the material were irradiated for 150 s/layer, after which the regular cure time per layer was 80 s/layer with a layer thickness of 50 μm . To obtain a high surface resolution, the last (top) layer of the material was irradiated for 150 s. The Z lift distance was 1 mm, the Z lift speed was 1 mm/s, and the Z retract speed was 3 mm/s. After the object was printed, the build stage was removed, and the residual polymerisation surface was briefly washed with ethanol. The material was then post-cured for 10 min through irradiation under violet light ($\lambda_{\text{max}} = 405 \text{ nm}$, $I_0 = 9.6 \text{ mW/cm}^2$) for further experiments. For the resin without RAFT agent, the samples were printed using a single layer cure time of 20 s/layer. Moreover, the cure time for the first two (bottom) layers and the last (top) layer was

decreased to 40 s/layer. For the resin formulation of [DBTTC] : [AA] : [HEA] : [EGDMA] : [TPO] = 1 : 6 : 54 : 4 : 0.5, the samples were printed using a single layer cure time of 100 s/layer. Also, the cure time for the first two (bottom) layers and the last (top) layer was increased to 100 s/layer.

3D printing procedures of complex objects

The resin formulation of [DBTTC] : [HEA] : [EGDMA] : [TPO] = 0.25 : 60 : 4 : 0.5 was used to print a violin model. The violin .stl file was downloaded from the internet.⁷⁶ The maximum width, length and height of the object were 32.8 mm, 89.3 mm and 7.0 mm, respectively. The printing parameters (slicing thickness and layer cure times) were generated using Photon Workshop software. The violin model was then printed by using Anycubic Photon S DLP 3D printer. To ensure adhesion between the 3D printed material and the build stage, the first 8 (bottom) layers of the material were irradiated for 150 s/layer, after which the regular cure time per layer was 40 s/layer with a layer thickness of 50 μm . The Z lift distance was 1 mm, the Z lift speed was 1 mm/s, and the Z retract speed was 3 mm/s. After the object was printed, the build stage was removed, and the residual polymerisation surface was briefly washed with ethanol. The material was then post-cured for 10 min through irradiation under violet light ($\lambda_{\text{max}} = 405 \text{ nm}$, $I_0 = 9.6 \text{ mW/cm}^2$) for further experiments.

The resin formulation of [DBTTC] : [HEA] : [EGDMA] : [TPO] = 1 : 60 : 4 : 0.5 was used to print a hook model. The hook .stl file was generated using Autodesk Fusion 360. The maximum width, length and height of the object were 17.3 mm, 50.0 mm and 3.0 mm, respectively. The printing parameters (slicing thickness and layer cure times) were generated using Photon Workshop software. The hook model was then printed by using Anycubic Photon S DLP 3D printer. To ensure adhesion between the 3D printed material and the build stage, the first 2 (bottom) layers of the material were irradiated for 150 s/layer, after which the regular cure time per layer was 80 s/layer with a layer thickness of 50 μm . The last (top) layer of the material was irradiated for 150 s to obtain a high surface resolution. The Z lift distance was 1 mm, the Z lift speed was 1 mm/s, and the Z retract speed was 3 mm/s. After the object was printed, the build stage was removed, and the residual polymerisation surface was briefly washed with ethanol. The material was then post-cured for 10 min through irradiation under violet light ($\lambda_{\text{max}} = 405 \text{ nm}$, $I_0 = 9.6 \text{ mW/cm}^2$) for further experiments.

DMA test of 3D printed rectangular samples

In DMA test, a 3D printed sample was measured with digital callipers, placed into the calibrated single cantilever clamp, and fixed into place with a torque wrench operated at a force of 3 in·lb. The GCA was used to adjust the temperature to -50°C and subsequently held at isothermal conditions for 3 min. The temperature was then ramped to 100°C at a rate of 2°C/min while the frequency was held constant at 1 Hz, using a displacement of 30 μm . The storage modulus was determined around room temperature (specifically at the closest temperature to 20 °C) and 1 Hz, while the glass transition temperature (T_g) was calculated as the temperature at which the 1 Hz Tan δ curve peaked. All DMA results were performed using duplicate samples.

Tensile test of 3D printed dumbbell-shaped samples

Tensile tests were performed at room temperature under a crosshead speed of 1.1 mm/min. Tensile strength was calculated by dividing the maximum load (N) by the average original cross-sectional area (m^2) in the gage length segment of the specimen and elongation at break was obtained by dividing the extension at the point of specimen rupture (change in gage length) by the original gage length and multiplying by 100.

Self-healing experiments

A typical self-healing procedure is as follows: the 3D printed dumbbell-shaped sample was cut into two approximately equal pieces with a sharp blade, and then the two parts were placed in close contact with the addition of 10 μL PEGDA ($M_n = 250 \text{ g mol}^{-1}$) between the contact area, which had dimensions of 8 mm^2 . Subsequently, the sample was fixed with double-side tape on a glass slide (dimensions 76 mm \times 19 mm \times 1 mm) and covered with another piece of glass slide with two binder clips (dimension 25 mm in width). An 80 W UV ($\lambda_{\text{max}} = 365 \text{ nm}$) light board (dimensions 70 mm \times 130 mm) was used for healing test in air at room temperature, with the sample placed 8 cm underneath.

5.3 Results and Discussion

5.3.1 Optimisation of resin formulations

The initial photocurable resins were composed of 2-hydroxyethyl acrylate (HEA) as the monomer and ethylene glycol dimethacrylate (EGDMA) as the crosslinker. Diphenyl (2,4,6-trimethylbenzoyl) phosphine oxide (TPO) was employed as the Norrish type I photoinitiator, due to its highly effective initiation performance reported in other works.^{11, 77-80} Moreover, the reactive radicals generated by TPO cleavage under violet light irradiation ($\lambda_{\text{max}} = 405 \text{ nm}$) can rapidly consume oxygen dissolved in the resins, enabling the printing system to be applied without deoxygenation.¹¹ Dibenzyl trithiocarbonate (DBTTC), a difunctional RAFT agent which consists of symmetric leaving R groups was selected as the RAFT agent for network formation. As noted previously, Z-connected RAFT agents such as DBTTC can display efficient self-healing due to the location of the TTC placement within the polymer main chain.^{35, 38, 63, 69} It has been shown that higher concentrations of TTC units within the polymer network can favour efficient self-healing. For instance, Matyjaszewski and co-workers demonstrated that increasing the concentration of thiuram disulfide can significantly promote the self-healing efficiency of polymer gels.⁶⁹ Based on these previous works, we hypothesised that a high concentration of RAFT agent in the 3D printing resin formulation would favor efficient self-healing for our 3D printed materials. However, an increase in RAFT concentration has also been shown to increase time to gelation, with longer printing times required to obtain well-defined 3D printed objects.^{60, 70} This motivated us to optimise the resin formulation prior to application in 3D printing. The molar ratio of [DBTTC] : [TPO] was initially selected to be 1 : 0.5 and the ratio of [DBTTC] : [HEA] was varied between 1 : 20 and 1 : 60 with a fixed ratio of [HEA] : [EGDMA] at 10 : 1. These reactions were performed in open-air droplets (20 μL) under violet light irradiation ($\lambda_{\text{max}} = 405 \text{ nm}$, $I_0 = 3.6 \text{ mW/cm}^2$) and monitored by following the decrease of the vinylic =C-H group via ATR-FTIR spectroscopy.

As shown in **Figure 5.1A**, an increased polymerisation rate was observed when the DBTTC concentration was decreased, with the system containing [DBTTC] : [HEA] = 1 : 60 displaying the fastest polymerisation kinetics ($\alpha = 31.3\%$ after 4 min irradiation). In comparison, both the [DBTTC] : [HEA] = 1 : 20 and 1 : 40 systems exhibited a long

induction period (> 2 min) and slower polymerisation kinetics with low vinyl bond conversion after 4 mins ($\alpha < 17.0\%$, **Figure 5.1A**), which can significantly increase 3D printing time and reduce practicality.^{60, 70} The long induction period observed when using the resin containing DBTTC was attributed to the poor reinitiating ability of the benzyl leaving R groups as well as the absorption of light by DBTTC at high concentrations.⁶⁰ The ratio of DBTTC relative to HEA was not decreased further, as the high concentration of the TTC units in the network can accelerate the self-healing reactions.⁶⁹ Therefore, a ratio of [DBTTC] : [HEA] = 1 : 60 was selected. Subsequently, the photoinitiator (TPO) concentration was optimised by varying between 0.1, 0.25, 0.5, 1 and 2 equiv. relative to DBTTC. As shown in **Figure 5.1B**, using 0.5 equiv. of TPO resulted in the fastest polymerisation while further addition of TPO reduced the polymerisation rate. This result was attributed to the increased light absorption of the resin containing higher concentrations of TPO, which limited the light penetration and decreased the cure depth through the system.⁸¹⁻⁸⁴ Thus, the ratio of the photoinitiator was fixed at 0.5 equiv. for further experiments. Additionally, as the crosslinking density has been shown by Matyjaszewski and co-workers to affect the chain mobility, and thus the self-healing efficiency, the molar ratio of HEA to EGDMA was varied.⁶⁹ As shown in **Figure 5.1C**, changing the concentration of [HEA] : [EGDMA] from 60 : 6 to 60 : 3 resulted in a negligible change in the kinetics. However, the gel formation rate was reduced with low EGDMA concentration; systems with [HEA] : [EGDMA] = 60 : 6 and 60 : 4 gelled after 3 min irradiation, while no free-standing gel was observed after 5 min irradiation for the system with [HEA] : [EGDMA] = 60 : 3. Consequently, the system with a molar ratio of [DBTTC] : [HEA] : [EGDMA] : [TPO] = 1 : 60 : 4 : 0.5 was selected as the optimised resin formulation to 3D print self-healing materials.

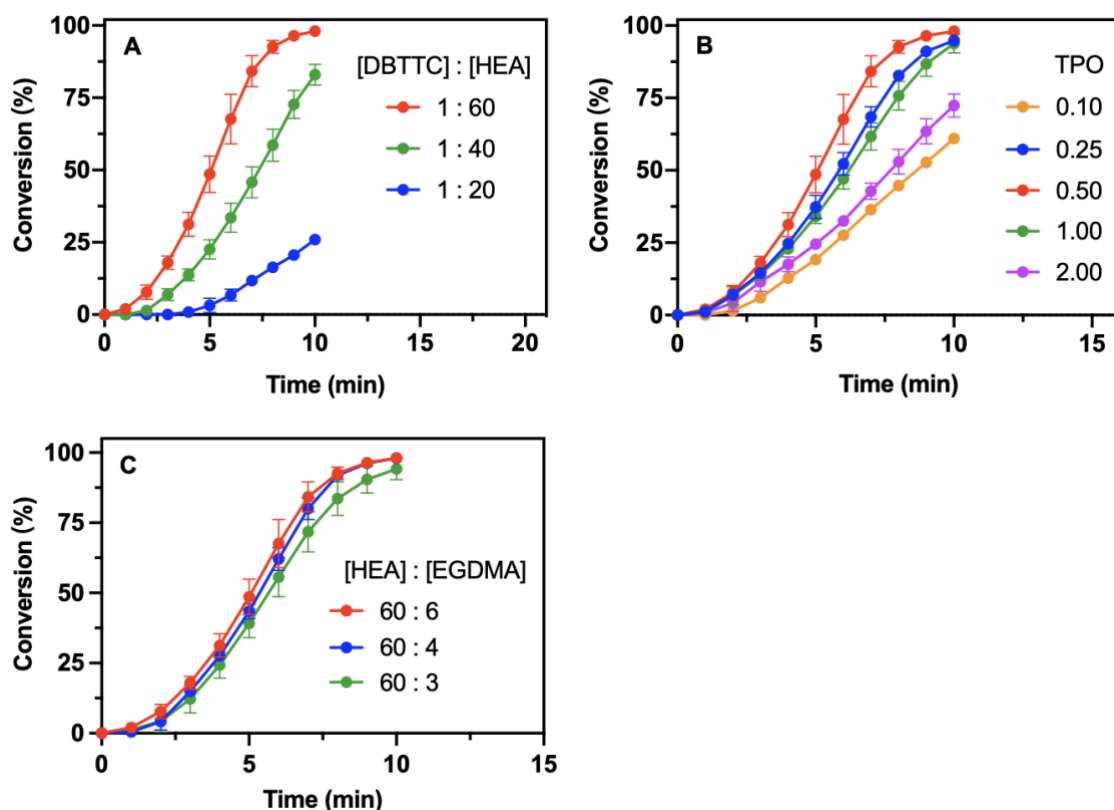


Figure 5.1 Kinetics of polymerisation for HEA/EGDMA mixtures using DBTTC as RAFT agent. (A) vinyl bond conversions *vs* time for varied [DBTTC] : [HEA] molar ratios with constant TPO molar ratio [DBTTC] : [TPO] = 1 : 0.5 and fixed molar ratio of [HEA] : [EGDMA] = 10 : 1; (B) vinyl bond conversion *vs* time for varied TPO molar ratios at molar concentration of [DBTTC] : [HEA] : [EGDMA] : [TPO] = 1 : 60 : 6 : [variable]; (C) vinyl bond conversion *vs* time for varied [HEA] : [EGDMA] molar ratios at a ratio of [DBTTC] : [TPO] = 1 : 0.5, the recipes were design to maintain fixed molar concentrations of DBTTC and TPO. As such, the molar ratios used in these experiments were [DBTTC] : [HEA] : [EGDMA] : [TPO] = 1 : 60 : 6 : 0.5 ([HEA] : [EGDMA] = 60 : 6), [DBTTC] : [HEA] : [EGDMA] : [TPO] = 1 : 63.2 : 4.2 : 0.5 (approximately [HEA] : [EGDMA] = 60 : 4), and [DBTTC] : [HEA] : [EGDMA] : [TPO] = 1 : 64.9 : 3.2 : 0.5 (approximately [HEA] : [EGDMA] = 60 : 3). Note: All reactions were performed under violet light ($\lambda_{\text{max}} = 405 \text{ nm}$ and $I_0 = 3.6 \text{ mW/cm}^2$).

5.3.2 Self-healing of 3D printed materials

After successful optimisation of the resin, we decided to 3D print objects using a commercial DLP 3D printer with a violet LED light board ($\lambda_{\text{max}} = 405 \text{ nm}$, $I_0 = 0.51 \text{ mW/cm}^2$). All 3D printing was performed without deoxygenation. The optimised resin

formulation i.e., [DBTTC] : [HEA] : [EGDMA] : [TPO] = 1 : 60 : 4 : 0.5, was used to print dumbbell-shaped objects (**Figure 5.2A**) for subsequent self-healing and mechanical tests. The dimensions of these objects were based on ATSM D638 Type V standards.⁷⁵ To obtain 3D printed objects with high resolution, a layer slicing thickness of 50 μm and a single layer cure time of 80 s/layer was used. A reduced curing time per layer (60 s/layer) was also attempted but resulted in ill-defined 3D printed objects (**Figure 5.2B**). Before performing the self-healing tests, the 3D printed objects were post-cured for 10 min under violet light irradiation ($\lambda_{\text{max}} = 405 \text{ nm}$, $I_0 = 9.6 \text{ mW/cm}^2$) to fully polymerise unreacted monomers. The vinyl bond conversions of the objects were determined by FTNIR spectroscopy by following the absorption peaks assigned to the stretching mode of the vinylic group. After post-curing, near quantitative vinyl bond conversions were observed for all 3D printed objects. As previously mentioned, the incorporation of photoiniferters into the network enables polymeric materials to undergo self-healing reactions via TTC reshuffling (Scheme 1).^{35-36, 39} However, previous works employed materials containing crosslinked polymers with low glass transition temperatures (T_g below room temperature). Low T_g enables high chain mobility for network rearrangement, which helps to facilitate efficient reshuffling reactions and therefore facilitates the self-healing process.^{35, 69}

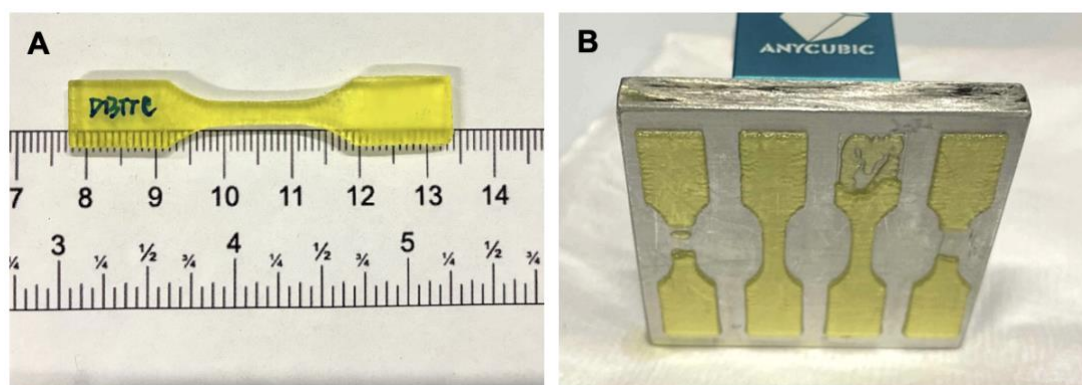


Figure 5.2 Dumbbell-shaped samples 3D printed using a resin formulation of [DBTTC] : [HEA] : [EGDMA] : [TPO] = 1 : 60 : 4 : 0.5 at a layer slicing thickness of 50 μm . (A) Dumbbell-shaped samples printed using a single layer cure time of 80 s/layer and (B) a single layer cure time of 60 s/layer.

Self-healing tests were conducted by cutting the 3D printed dumbbell-shaped samples into two pieces, and then placing the two parts in close contact under 365 nm light irradiation ($\lambda_{\text{max}} = 365 \text{ nm}$) (**Figure 5.3A**); these tests were performed at room

temperature and in an open-air environment. Unfortunately, the cut sample did not self-heal after 16 h of light exposure, which was attributed to the low mobility of polymer chains in these materials ($T_g = 37.9^\circ\text{C}$, **Figure 5.4A**). Consequently, the self-healing approach was modified to take advantage of the photo-reactivation of RAFT group under UV light (**Scheme 5.1**). Indeed, it is expected that the thiocarbonylthio groups can be activated under UV light irradiation to start a secondary polymerisation with freshly added monomer and crosslinker to produce a new network. As such, two different crosslinkers, namely EGDMA and poly(ethylene glycol) diacrylate (PEGDA), were investigated for their ability to aid in the network formation and self-healing process. Pleasingly, the system with PEGDA added at the cut material interfaces displayed noticeable self-healing behaviour after only 30 min irradiation with 365 nm light, as evidenced by the formation of a single piece, with the rupture on the surface hardly visualised (**Figure 5.3A**). For the system using EGDMA as the interface crosslinker, the self-healing process required 4 h which is an agreement with previous studies.^{35, 38} However, no self-healing was observed after 30 min due to the low propagation rate constant of EGDMA.⁸⁵ The healed samples retained integrity and withstood bending deformation without breakage (**Figure 5.3A**). This result was in alignment with Chen, Johnson and co-workers' work³⁸ which demonstrated that in the presence of PC only, the crosslinked gels containing TTC units resulted in poor healing. In contrast with the addition of a solution containing monomer, crosslinker and PC at the interface, the damaged gels were completely healed.

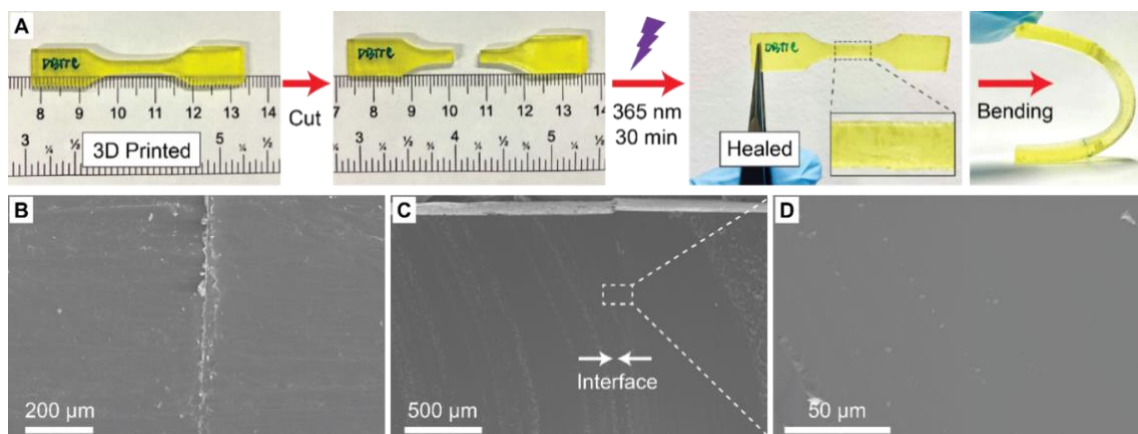


Figure 5.3 Self-healing process of 3D printed samples. (A) demonstration of the self-healing process on a dumbbell shaped object 3D printed using a resin formulation of [DBTTC] : [HEA] : [EGDMA] : [TPO] = 1 : 60 : 4 : 0.5; SEM images of (B) the top surface of the healed sample, (C) cross-sectional view of the healed sample, and (D) the magnified cross-sectional view of the healed sample showing disappearance of interfacial region after healing process.

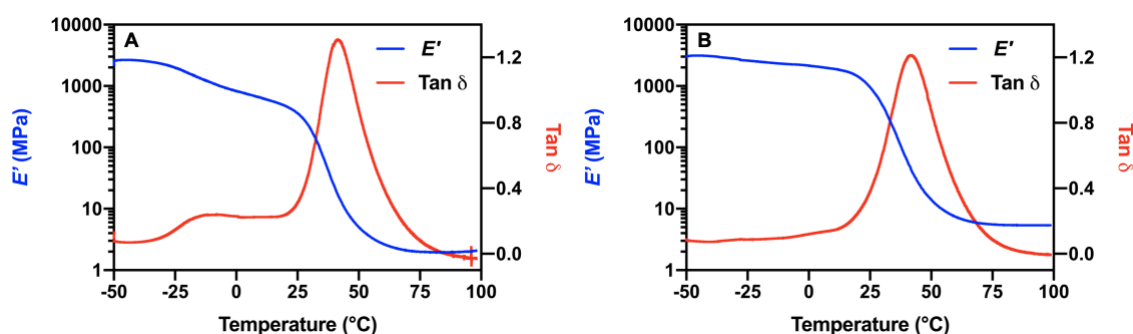


Figure 5.4 Storage modulus (E') and $\tan \delta$ for samples 3D printed with different resin formulations at a frequency of 1 Hz measured by DMA. (A) sample printed with the resin containing [DBTTC] : [HEA] : [EGDMA] : [TPO] = 1 : 60 : 4 : 0.5 at a cure time per layer of 80 s; (B) sample printed with the resin containing [DBTTC] : [HEA] : [EGDMA] : [TPO] = 0 : 60 : 4 : 0.5 at a cure time per layer of 20 s.

We also performed additional control experiments to demonstrate the importance of light irradiation and the presence of TTC units in this self-healing process. As expected, samples were not healed after 16 h in the absence of UV light, as the TTC units of DBTTC in the network cannot be activated without light irradiation at room temperature. Under white light irradiation for 24 h, $35 \pm 2\%$ tensile strength recovery was observed (**Table 5.1**), which was attributed to the low homolysis rate of C-S bonds under white light.⁵⁰ To

demonstrate the importance of TTC in the polymer network, control samples were printed in the absence of DBTTC and subsequently used in self-healing tests. For the non-TTC containing samples ($T_g = 41.2^\circ\text{C}$, **Figure 5.4B**), healing was not observed after 16 h even with the addition of PEGDA at the material interfaces. Furthermore, when PEDGA was replaced with a mixed solution containing free-RAFT agent at a ratio of [DBTTC] : [PEGDA] = 1 : 64, no self-healing was observed after 2 h irradiation. This demonstrates that the incorporation of TTC units in the polymeric network is essential for this self-healing reaction to occur. To better visualise the self-healed material printed with the resin of [DBTTC] : [HEA] : [EGDMA] : [TPO] = 1 : 60 : 4 : 0.5, the surface contact area was examined SEM. As shown in **Figure 5.3B**, the top surface of the healed sample shows the position of the cut, which is visible due to the slight misalignment of the severed pieces during sample preparation. In contrast, no cracks were observed in the cross-sectional view along the contact area, indicating that the two separated parts were successfully merged (**Figure 5.3C and D**).

Table 5.1 Mechanical properties of samples 3D printed with the resin of [DBTTC] : [HEA] : [EGDMA] : [TPO] = 1 : 60 : 4 : 0.5 self-healing at various healing time.

Healing time (min)	Tensile strength (KPa)	Tensile strength recovery (%)	Elongation at break (%)	Elongation at break recovery (%)
Pre-cut	1450 ± 50	-	150 ± 5	-
Pre-cut ^a	2150 ± 150	-	150 ± 10	-
5	700 ± 80	49 ± 5	40 ± 5	26 ± 2
15	1200 ± 50	83 ± 3	80 ± 15	53 ± 10
30	1450 ± 40	98 ± 3	110 ± 5	74 ± 3
60	1800 ± 90	123 ± 6	110 ± 1	76 ± 2
90	1700 ± 100	118 ± 7	95 ± 5	65 ± 2
60 ^b	850 ± 40	58 ± 2	80 ± 5	57 ± 4
60 ^c	450 ± 100	29 ± 8	40 ± 10	24 ± 9
60 × 24 ^d	500 ± 20	35 ± 2	80 ± 10	52 ± 5

^aOriginal 3D printed samples irradiated under 365 nm for 60 min before tension test. ^b3D printed samples self-healed three times with each healing performed for 60 min under 365 nm light irradiation. ^c3D printed samples self-healed with the addition of 50 vol% PEGDA in DMSO at the cut material interfaces under 365 nm light irradiation. ^d3D printed samples self-healed with the addition of PEGDA at the cut material interfaces under white light irradiation for 24 h.

To quantitatively evaluate the self-healing process, tensile tests were carried out to compare stress-strain properties between the original and healed samples at various healing times (**Figure 5.5**). Tensile tests were performed at room temperature under a crosshead speed of 1.1 mm/min. To determine the healing efficiency, the ratios of tensile strength and elongation at break between the healed samples and the original samples were considered (**Figure 5.6A and B, Table 5.1**). For the material fabricated using a resin with [DBTTC] : [HEA] : [EGDMA] : [TPO] = 1 : 60 : 4 : 0.5, the cut sample was rapidly healed, recovering 49 ± 5% of the original tensile strength and 26 ± 2% recovery in elongation at break in only 5 min irradiation. With increasing irradiation time, the material continued to recover, with the tensile strength reaching 98 ± 3% and elongation at break reaching 74 ± 3% of the original values in 30 min.

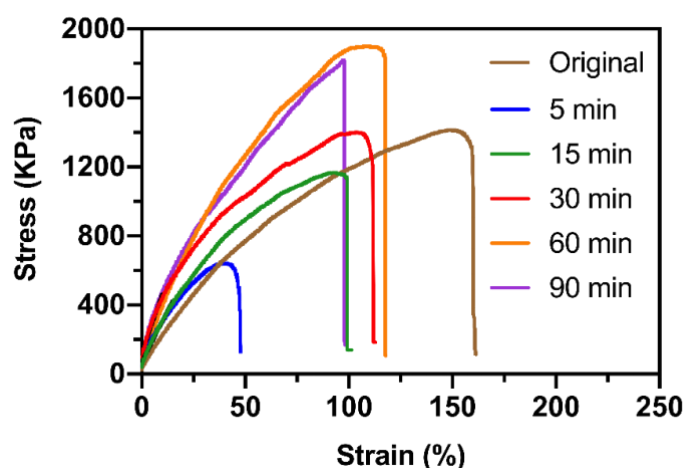


Figure 5.5 Stress-strain curves of the original sample and healed samples at various healing time. The dumbbell-shaped sample 3D printed by using the resin formulation of [DBTTC] : [HEA] : [EGDMA] : [TPO] = 1 : 60 : 4 : 0.5 at a layer slicing thickness of 50 μm and a single layer cure time of 80 s/layer.

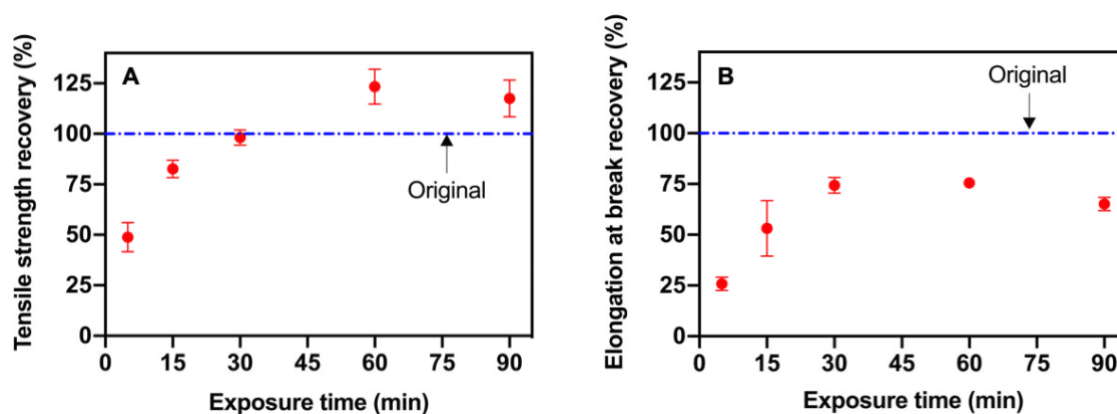


Figure 5.6 Healing efficiency of samples 3D printed with the resin of [DBTTC] : [HEA] : [EGDMA] : [TPO] = 1 : 60 : 4 : 0.5 at various healing time. (A) tensile strength recovery, and (B) elongation at break recovery of samples after irradiation under UV light at room temperature over time.

The recovered mechanical strength was ascribed to the increased PEGDA conversion with time, and thus the more complete reformation of crosslinked network. Overall, tensile strength recovery increased with extended healing time but plateaued at $123 \pm 6\%$ after 60 min irradiation (**Figure 5.6A**). As a control experiment, we also measured the tensile strength of the uncut material after exposure to UV light. Interestingly, the tensile strength increased by roughly 50% after 60 min UV light irradiation (**Table 5.1**), which

was attributed to the formation of new crosslinks in the material due to the reshuffling of the TTC units.⁸⁶⁻⁸⁷ The self-healing process under 60 min irradiation was successfully repeated three times by cutting and healing samples at the same point, with the tensile strength recovering $58 \pm 2\%$ and elongation at break recovering $57 \pm 4\%$ (**Table 5.1**). The reduced healing efficiency was attributed to the damaged contact surface caused by successive cutting. The impact of PEGDA concentration on self-healing efficiency was also investigated. Under 60 min irradiation, the tensile strength recovery and elongation at break recovery of samples healed with a 50 vol% solution of PEGDA in dimethyl sulfoxide was less than 30% (**Table 5.1**). To further explore the potential of the self-healing system, the self-healing test was conducted on more rigid materials. To obtain 3D printed objects with higher modulus and T_g , acrylic acid (AA) was incorporated in the resin formulation to yield [DBTTC] : [AA] : [HEA] : [EGDMA] : [TPO] = 1 : 6 : 54 : 4 : 0.5. As shown in **Figure 5.7**, the E' at 20 °C and T_g of the samples containing AA were 850 ± 70 MPa and 47.4 °C, respectively. The healing efficiency of the samples containing AA slightly decreased, with tensile strength recovery reaching $71 \pm 4\%$ and elongation at break recovery reaching $33 \pm 9\%$ (**Table 5.2**).

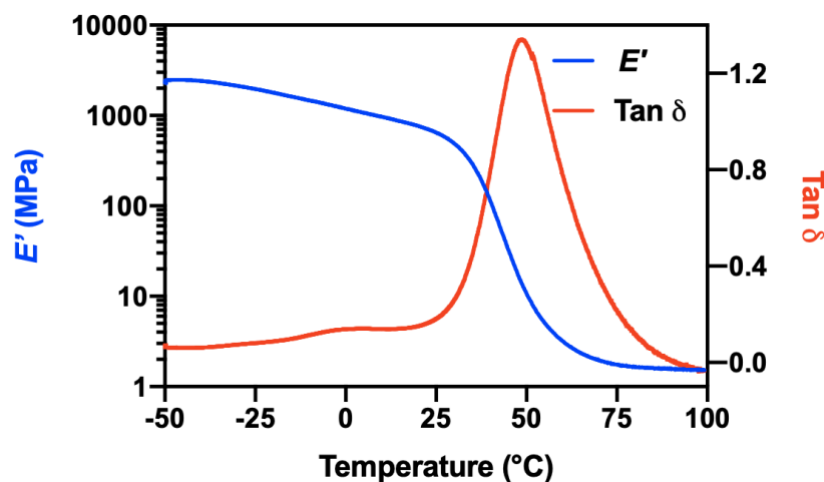


Figure 5.7 Storage modulus (E') and $\tan \delta$ for sample 3D printed with the resin containing [DBTTC] : [AA] : [HEA] : [EGDMA] : [TPO] = 1 : 6 : 54 : 4 : 0.5 at a cure time per layer of 100 s at a frequency of 1 Hz measured by DMA.

Table 5.2 Mechanical properties of samples 3D printed with the resin containing varied molar ratio of [AA] : [HEA] at a fixed molar ratio of [DBTTC] : [EGDMA] : [AA+HEA] : [TPO] = 1 : 4 : 60 : 0.5 self-healing under 365 nm irradiation for 60 min.

[AA] : [HEA]	Healing time (min)	Tensile strength (KPa)	Tensile strength recovery (%)	Elongation at break (%)	Elongation at break recovery (%)
0 : 60	Pre-cut	1450 ± 50	-	150 ± 5	-
	60	1800 ± 90	123 ± 6	110 ± 1	76 ± 2
6 : 54	Pre-cut	3750 ± 300	-	230 ± 10	-
	60	2650 ± 150	71 ± 4	80 ± 20	33 ± 9

Further experiments were conducted to gain a deeper insight into the impact of DBTTC concentration in the 3D printed samples on the healing efficiency. Due to the faster polymerisation rates at lower concentration of DBTTC, the layer cure time was adjusted to 40 s to obtain well-defined 3D printed samples with the resins containing 0.5 and 0.25 equiv. of DBTTC (**Figure 5.8**). Tensile tests were subsequently performed on the 3D printed samples with various concentrations of DBTTC in the resin. As is shown in **Table 5.3**, the tensile strength increased with a decreasing concentration of DBTTC, with the no RAFT sample exhibiting the highest tensile strength at 2800 ± 150 KPa. This is because the network formation of the samples containing TTC units undergoes an addition-fragmentation chain transfer process, which can dramatically alleviate shrinkage stress and promote relaxation of the network.⁸⁸⁻⁸⁹

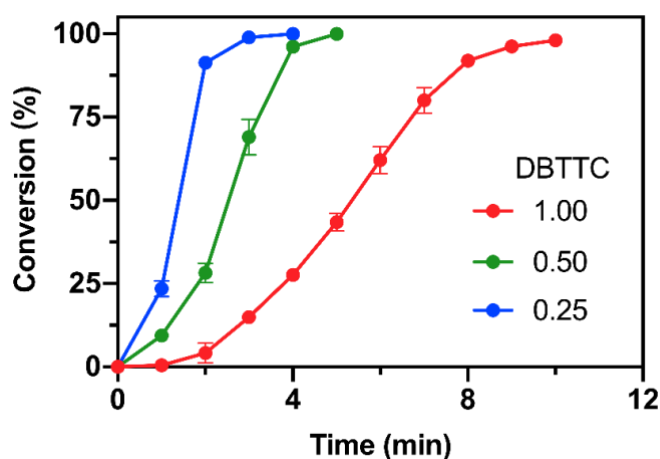


Figure 5.8 Kinetics of polymerisation with varied DBTTC concentration at fixed molar concentration of [HEA] : [EGDMA] : [TPO] = 60 : 4 : 0.5.

Table 5.3 Mechanical properties of original samples 3D printed with various concentrations of DBTTC in the resin at a fixed molar ratio of [HEA] : [EGDMA] : [TPO] = 60 : 4 : 0.5.

[DBTTC]	Tensile strength (KPa)	Elongation at break (%)
0.00	2800 ± 150	140 ± 5
0.25	2400 ± 150	140 ± 1
0.50	1950 ± 60	140 ± 10
1.00	1450 ± 50	150 ± 5

As previously described, the samples containing different concentrations of DBTTC were cut, and self-healing was performed by adding PEGDA at the interface and irradiating with UV light. While self-healing proceeded for all samples containing DBTTC, the healing efficiency was apparently reduced with decreased DBTTC concentrations (**Figure 5.9A and B, Tables 5.1, 5.4 and 5.5**). After 15 min irradiation, the tensile strength recovery was $83 \pm 3\%$ for the system with 1 equiv. DBTTC compared to $45 \pm 8\%$ for the sample printed using 0.25 equiv. of DBTTC. Furthermore, samples containing 0.25 equiv. DBTTC regained only 80% of their initial strength after 60 min irradiation, along with an elongation at break recovery of less than 50%.

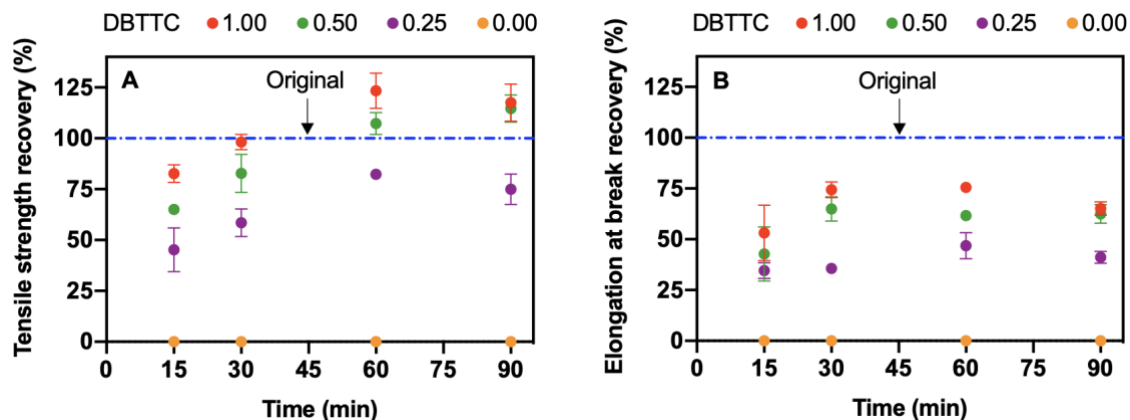


Figure 5.9 Mechanical property recovery vs time for 3D printed samples. (A) tensile strength recovery, and (B) elongation at break recovery for samples 3D printed using varied concentrations of DBTTC in the resin at a fixed molar ratio of [HEA] : [EGDMA] : [TPO] = 60 : 4 : 0.5. Self-healing was performed under UV light irradiation at room temperature with PEGDA at the material interface.

Table 5.4 Mechanical properties of samples 3D printed with the resin of [DBTTC] : [HEA] : [EGDMA] : [TPO] = 0.5 : 60 : 4 : 0.5 self-healing at various healing time.

Healing time (min)	Tensile strength (KPa)	Tensile strength recovery (%)	Elongation at break (%)	Elongation at break recovery (%)
Pre-cut	1950 ± 60	-	140 ± 10	-
15	1250 ± 5	65 ± 1	60 ± 10	43 ± 9
30	1600 ± 150	83 ± 7	90 ± 10	65 ± 4
60	2050 ± 70	107 ± 4	85 ± 1	62 ± 1
90	2200 ± 90	115 ± 5	85 ± 5	63 ± 3

Table 5.5 Mechanical properties of samples 3D printed with the resin of [DBTTC] : [HEA] : [EGDMA] : [TPO] = 0.25 : 60 : 4 : 0.5 self-healing at various healing time.

Healing time (min)	Tensile strength (KPa)	Tensile strength recovery (%)	Elongation at break (%)	Elongation at break recovery (%)
Pre-cut	2400 ± 150	-	140 ± 1	-
15	1100 ± 200	45 ± 8	50 ± 5	35 ± 3
30	1400 ± 100	58 ± 5	50 ± 1	36 ± 1
60	1950 ± 5	82 ± 1	70 ± 10	47 ± 5
90	1800 ± 150	75 ± 5	60 ± 5	41 ± 2

To further understand the effect of photoiniferter structure on self-healing efficiency, a monofunctional RAFT agent, 3-(((benzylthio)carbonothioyl)thio) propanoic acid (BSTP), was selected and compared with the difunctional DBTTC RAFT agent; BSTP has the same benzyl leaving R group as DBTTC but a different Z group (propanoic acid for BSTP vs benzyl for DBTTC). The resin formulation [BSTP] : [HEA] : [EGDMA] : [TPO] = 1 : 60 : 4 : 0.5 was applied to print dumbbell-shaped objects with layer cure times of 60 s/layer used to avoid overcuring in the comparatively fast BSTP system (**Figure 5.10**).

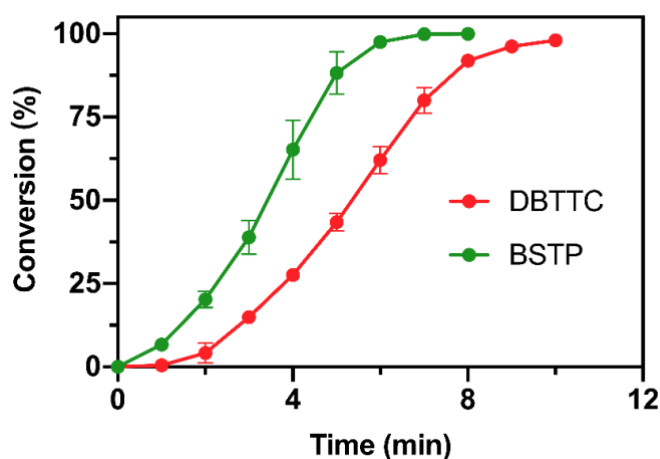


Figure 5.10 Kinetics of polymerization with different RAFT agents at fixed molar ratio of [RAFT] : [HEA] : [EGDMA] : [TPO] = 1 : 60 : 4 : 0.5.

As shown in **Table 5.6**, the healing efficiency of the 3D printed samples with the BSTP was significantly reduced compared to the samples containing DBTTC at the same concentration. As shown in **Figure 5.11A**, the tensile strength recovery for the BSTP sample was $70 \pm 4\%$ in 60 min, which was lower than that of DBTTC (tensile strength recovery = $123 \pm 6\%$). The elongation at break recovery was also lower for BSTP, reaching a plateau at $61 \pm 1\%$ after 60 min (**Figure 5.11B**). The different healing efficiency was attributed to the different structure of the RAFT agents. For DBTTC, the symmetric leaving R groups allow polymer chains to grow on both sides of the TTC unit, and also allows effective reshuffling of the TTC units to occur.^{35-36, 39, 90-92} In comparison, the asymmetric BSTP leads to polymerisation with the TTC units remaining pendent to the network at the terminus of all chains. The effective reshuffling with DBTTC provides more contact points between the two network fragments, thus allowing more effective strength recovery.³⁵⁻³⁶

Table 5.6 Mechanical properties of samples 3D printed with the resin of [BSTP] : [HEA] : [EGDMA] : [TPO] = 1 : 60 : 4 : 0.5 self-healing at various healing time

Healing time (min)	Tensile strength (KPa)	Tensile strength recovery (%)	Elongation at break (%)	Elongation at break recovery (%)
Pre-cut	3050 ± 70	-	200 ± 20	-
15	1300 ± 20	42 ± 1	85 ± 10	41 ± 4
30	1750 ± 250	57 ± 8	100 ± 10	48 ± 6
60	2150 ± 100	70 ± 4	130 ± 1	61 ± 1
90	2000 ± 150	65 ± 6	120 ± 15	58 ± 7

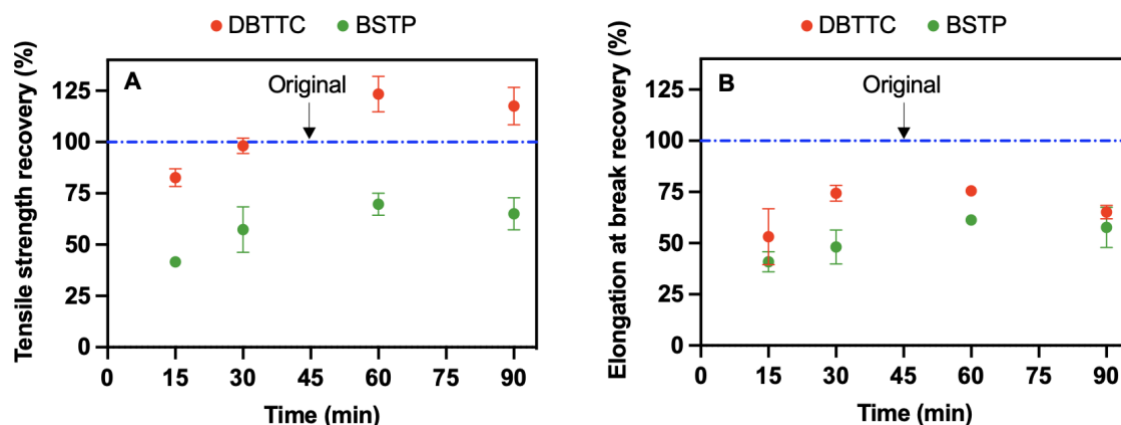


Figure 5.11 Mechanical property recovery vs time for 3D printed samples. (A) tensile strength recovery, and (B) elongation at break recovery for samples 3D printed with varied RAFT agents in the resin at a fixed molar ratio of [RAFT] : [HEA] : [EGDMA] : [TPO] = 1 : 60 : 4 : 0.5. Self-healing was performed under UV light irradiation at room temperature with PEGDA at the material interface.

To quantitatively demonstrate the healing ability of 3D printed objects, a hook model was 3D printed using a resin formulation containing a high concentration of DBTTC at a ratio of [DBTTC] : [HEA] : [EGDMA] : [TPO] = 1 : 60 : 4 : 0.5. As shown in **Figure 5.12**, the hook hang on a steel rod, with the torus end lifting a 200 g weight. Afterwards, the hook was cut in the middle and then self-healed under UV light with PEGDA at the interface. After 60 min, the hook successfully regained strength and was able to hold the 200 g weight with no obvious rupture at the cut area. To demonstrate the ability to 3D print more complex objects with self-healing functionality, a violin model was 3D printed using a resin formulation of [DBTTC] : [HEA] : [EGDMA] : [TPO] = 0.25 : 60 : 4 : 0.5. The lower DBTTC concentration was selected to provide a more practical build speed compared to resins with higher RAFT agent concentration. A slicing thickness of 50 μm and a single layer cure time of 40 s/layer were used to obtain the 3D printed violin model with high resolution. As shown in **Figure 5.12**, the tuning pegs and strings can be easily identified. After printing, the violin was rinsed with ethanol, followed by post-curing through irradiation under violet light ($\lambda_{\text{max}} = 405 \text{ nm}$) for 10 min. Subsequently, the fingerboard was cut in the middle and the two parts were placed in close contact with the addition of PEGDA at the contact surface. The object was then subjected to 365 nm light irradiation ($\lambda_{\text{max}} = 365 \text{ nm}$) in air at room temperature (**Figure 5.12**). After 60 min irradiation, the violin was repaired with fully recovered appearance.

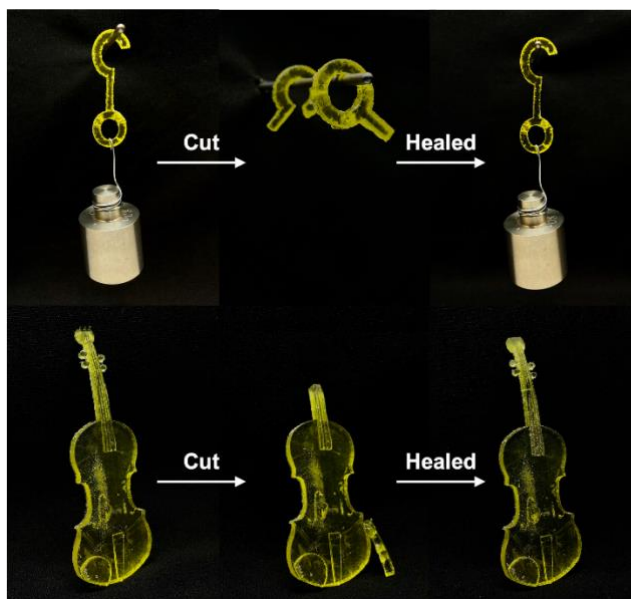


Figure 5.12 Photoinduced self-healing of geometrically complex objects 3D printed via photo-RDRP. Top: 200 g weightlifting test on a hook before and after self-healing. Hook was 3D printed using the resin formulation [DBTTC] : [HEA] : [EGDMA] : [TPO] = 1 : 60 : 4 : 0.5 and was self-healed under 365 nm irradiation for 60 min in air at room temperature. Bottom: model violin 3D printed using the resin formulation [DBTTC] : [HEA] : [EGDMA] : [TPO] = 0.25 : 60 : 4 : 0.5 self-healed under 365 nm irradiation for 60 min in air at room temperature.

5.4 Conclusion

In summary, RAFT agents were incorporated into photopolymerisation resins to investigate the fabrication of high-resolution 3D printed thermosets with self-healing functionality. Objects containing TTC units that were 3D printed under visible light ($\lambda_{\text{max}} = 405 \text{ nm}$) can perform rapid self-repair via a secondary polymerisation mechanism under UV light irradiation ($\lambda_{\text{max}} = 365 \text{ nm}$) under an open-to-air conditions and at room temperature. The concentration of TTC units in the resin played an important role in affecting the healing efficiency, with the object containing a high concentration of TTC units resulting in a higher tensile strength recovery and elongation at break recovery. Self-healing efficiency was also compared between the objects 3D printed with the resin containing symmetric difunctional RAFT agent DBTTC and asymmetric monofunctional RAFT agent BSTP. The objects 3D printed in the presence of DBTTC retained the TTC units in the middle of each polymer chain rather than the terminus of all chains, resulting in a superior self-repairing capability. This work promisingly paves the way for the fabrication of novel 3D printed thermosets with self-healing properties.

5.5 Reference

1. Layani, M.; Wang, X.; Magdassi, S., Novel Materials for 3D Printing by Photopolymerization. *Advanced Materials* **2018**, *30*(41), 1706344.
2. Zhang, J.; Xiao, P., 3D printing of photopolymers. *Polymer Chemistry* **2018**, *9*(13), 1530-1540.
3. Zheng, X.; Lee, H.; Weisgraber, T. H.; Shusteff, M.; DeOtte, J.; Duoss, E. B.; Kuntz, J. D.; Biener, M. M.; Ge, Q.; Jackson, J. A.; Kucheyev, S. O.; Fang, N. X.; Spadaccini, C. M., Ultralight, ultrastiff mechanical metamaterials. *Science* **2014**, *344*(6190), 1373-1377.
4. Dolinski, N. D.; Page, Z. A.; Callaway, E. B.; Eisenreich, F.; Garcia, R. V.; Chavez, R.; Bothman, D. P.; Hecht, S.; Zok, F. W.; Hawker, C. J., Solution Mask Liquid Lithography (SMaLL) for One-Step, Multimaterial 3D Printing. *Advanced Materials* **2018**, *30*(31), 1800364.
5. Schwartz, J. J.; Boydston, A. J., Multimaterial actinic spatial control 3D and 4D printing. *Nature Communications* **2019**, *10*(1), 791.
6. Peterson, G. I.; Schwartz, J. J.; Zhang, D.; Weiss, B. M.; Ganter, M. A.; Storti, D. W.; Boydston, A. J., Production of Materials with Spatially-Controlled Cross-Link Density via Vat Photopolymerization. *ACS Applied Materials & Interfaces* **2016**, *8*(42), 29037-29043.
7. Jung, K.; Corrigan, N.; Ciftci, M.; Xu, J.; Seo, S. E.; Hawker, C. J.; Boyer, C., Designing with Light: Advanced 2D, 3D, and 4D Materials. *Advanced Materials* **2020**, *32*(18), 1903850.
8. Sampson, K. L.; Deore, B.; Go, A.; Nayak, M. A.; Orth, A.; Gallerneault, M.; Malenfant, P. R. L.; Paquet, C., Multimaterial Vat Polymerization Additive Manufacturing. *ACS Applied Polymer Materials* **2021**, *3*(9), 4304-4324.
9. Tumbleston, J. R.; Shirvanyants, D.; Ermoshkin, N.; Januszewicz, R.; Johnson, A. R.; Kelly, D.; Chen, K.; Pinschmidt, R.; Rolland, J. P.; Ermoshkin, A.; Samulski, E. T.; DeSimone, J. M., Additive manufacturing. Continuous liquid interface production of 3D objects. *Science* **2015**, *347*(6228), 1349-1352.
10. Walker, D. A.; Hedrick, J. L.; Mirkin, C. A., Rapid, large-volume, thermally controlled 3D printing using a mobile liquid interface. *Science* **2019**, *366*(6463), 360-364.
11. Lee, K.; Corrigan, N.; Boyer, C., Rapid High-Resolution 3D Printing and Surface Functionalization via Type I Photoinitiated RAFT Polymerization. *Angewandte Chemie International Edition* **2021**, *60*(16), 8839-8850.
12. Ahn, D.; Stevens, L. M.; Zhou, K.; Page, Z. A., Rapid High-Resolution Visible Light 3D Printing. *ACS Central Science* **2020**, *6*(9), 1555-1563.
13. Ge, Q.; Sakhaei, A. H.; Lee, H.; Dunn, C. K.; Fang, N. X.; Dunn, M. L., Multimaterial 4D Printing with Tailorable Shape Memory Polymers. *Scientific Reports* **2016**, *6*, 31110.
14. Kaiser, T., Highly crosslinked polymers. *Progress in Polymer Science* **1989**, *14*(3), 373-450.
15. Wendel, B.; Rietzel, D.; Kühnlein, F.; Feulner, R.; Hülde, G.; Schmachtenberg, E., Additive Processing of Polymers. *Macromolecular Materials and Engineering* **2008**, *293*(10), 799-809.
16. Kloxin, C. J.; Bowman, C. N., Covalent adaptable networks: smart, reconfigurable and responsive network systems. *Chemical Society Reviews* **2013**, *42*(17), 7161-7173.
17. Zheng, J.; Suh, S., Strategies to reduce the global carbon footprint of plastics. *Nature Climate Change* **2019**, *9*(5), 374-378.

18. Jin, Y.; Yu, C.; Denman, R. J.; Zhang, W., Recent advances in dynamic covalent chemistry. *Chemical Society Reviews* **2013**, 42(16), 6634-6654.
19. Zhang, Z. P.; Rong, M. Z.; Zhang, M. Q., Polymer engineering based on reversible covalent chemistry: A promising innovative pathway towards new materials and new functionalities. *Progress in Polymer Science* **2018**, 80, 39-93.
20. Chakma, P.; Konkolewicz, D., Dynamic Covalent Bonds in Polymeric Materials. *Angewandte Chemie International Edition* **2019**, 58(29), 9682-9695.
21. Winne, J. M.; Leibler, L.; Du Prez, F. E., Dynamic covalent chemistry in polymer networks: a mechanistic perspective. *Polymer Chemistry* **2019**, 10(45), 6091-6108.
22. Zheng, N.; Xu, Y.; Zhao, Q.; Xie, T., Dynamic Covalent Polymer Networks: A Molecular Platform for Designing Functions beyond Chemical Recycling and Self-Healing. *Chemical Reviews* **2021**, 121(3), 1716-1745.
23. Shieh, P.; Hill, M. R.; Zhang, W.; Kristufek, S. L.; Johnson, J. A., Clip Chemistry: Diverse (Bio)(macro)molecular and Material Function through Breaking Covalent Bonds. *Chemical Reviews* **2021**, 121(12), 7059-7121.
24. Zhang, B.; Kowsari, K.; Serjouei, A.; Dunn, M. L.; Ge, Q., Reprocessable thermosets for sustainable three-dimensional printing. *Nature Communications* **2018**, 9(1), 1831.
25. Yuan, T.; Zhang, L.; Li, T.; Tu, R.; Sodano, H. A., 3D Printing of a self-healing, high strength, and reprocessible thermoset. *Polymer Chemistry* **2020**, 11(40), 6441-6452.
26. Durand-Silva, A.; Cortés-Guzmán, K. P.; Johnson, R. M.; Perera, S. D.; Diwakara, S. D.; Smaldone, R. A., Balancing Self-Healing and Shape Stability in Dynamic Covalent Photoresins for Stereolithography 3D Printing. *ACS Macro Letters* **2021**, 10(4), 486-491.
27. Liu, Z.; Hong, P.; Huang, Z.; Zhang, T.; Xu, R.; Chen, L.; Xiang, H.; Liu, X., Self-healing, reprocessing and 3D printing of transparent and hydrolysis-resistant silicone elastomers. *Chemical Engineering Journal* **2020**, 387, 124142.
28. Rahman, S. S.; Arshad, M.; Qureshi, A.; Ullah, A., Fabrication of a Self-Healing, 3D Printable, and Reprocessable Biobased Elastomer. *ACS Applied Materials & Interfaces* **2020**, 12(46), 51927-51939.
29. Wojtecki, R. J.; Meador, M. A.; Rowan, S. J., Using the dynamic bond to access macroscopically responsive structurally dynamic polymers. *Nature Materials* **2011**, 10(1), 14-27.
30. Roy, N.; Bruchmann, B.; Lehn, J.-M., DYNAMERS: dynamic polymers as self-healing materials. *Chemical Society Reviews* **2015**, 44(11), 3786-3807.
31. Blaiszik, B. J.; Kramer, S. L. B.; Olugebefola, S. C.; Moore, J. S.; Sottos, N. R.; White, S. R., Self-Healing Polymers and Composites. *Annual Review of Materials Research* **2010**, 40(1), 179-211.
32. Maeda, T.; Otsuka, H.; Takahara, A., Dynamic covalent polymers: Reorganizable polymers with dynamic covalent bonds. *Progress in Polymer Science* **2009**, 34(7), 581-604.
33. Stuart, M. A. C.; Huck, W. T. S.; Genzer, J.; Müller, M.; Ober, C.; Stamm, M.; Sukhorukov, G. B.; Szleifer, I.; Tsukruk, V. V.; Urban, M.; Winnik, F.; Zauscher, S.; Luzinov, I.; Minko, S., Emerging applications of stimuli-responsive polymer materials. *Nature Materials* **2010**, 9(2), 101-113.
34. Chung, C.-M.; Roh, Y.-S.; Cho, S.-Y.; Kim, J.-G., Crack Healing in Polymeric Materials via Photochemical [2+2] Cycloaddition. *Chemistry of Materials* **2004**, 16(21), 3982-3984.
35. Amamoto, Y.; Kamada, J.; Otsuka, H.; Takahara, A.; Matyjaszewski, K., Repeatable photoinduced self-healing of covalently cross-linked polymers through

- reshuffling of trithiocarbonate units. *Angewandte Chemie International Edition* **2011**, 50(7), 1660-1663.
36. Cheng, C.; Bai, X.; Zhang, X.; Li, H.; Huang, Q.; Tu, Y., Self-healing polymers based on a photo-active reversible addition-fragmentation chain transfer (RAFT) agent. *Journal of Polymer Research* **2015**, 22(4), 46.
 37. Gordon, M. B.; French, J. M.; Wagner, N. J.; Kloxin, C. J., Dynamic Bonds in Covalently Crosslinked Polymer Networks for Photoactivated Strengthening and Healing. *Advanced Materials* **2015**, 27(48), 8007-8010.
 38. Chen, M.; Gu, Y.; Singh, A.; Zhong, M.; Jordan, A. M.; Biswas, S.; Korley, L. T.; Balazs, A. C.; Johnson, J. A., Living Additive Manufacturing: Transformation of Parent Gels into Diversely Functionalized Daughter Gels Made Possible by Visible Light Photoredox Catalysis. *ACS Cent Sci* **2017**, 3(2), 124-134.
 39. Ida, S.; Kimura, R.; Tanimoto, S.; Hirokawa, Y., End-crosslinking of controlled telechelic poly(N-isopropylacrylamide) toward a homogeneous gel network with photo-induced self-healing. *Polymer Journal* **2017**, 49(2), 237-243.
 40. Nicolaÿ, R.; Kamada, J.; Van Wassen, A.; Matyjaszewski, K., Responsive Gels Based on a Dynamic Covalent Trithiocarbonate Cross-Linker. *Macromolecules* **2010**, 43(9), 4355-4361.
 41. Otsu, T.; Matsumoto, A., Controlled Synthesis of Polymers Using the Iniferter Technique: Developments in Living Radical Polymerization. In *Microencapsulation Microgels Iniferters*, DiMari, S.; Funke, W.; Haralson, M. A.; Hunkeler, D.; Joos-Müller, B.; Matsumoto, A.; Okay, O.; Otsu, T.; Powers, A. C.; Prokop, A.; Wang, T. G.; Whitesell, R. R., Eds. Springer Berlin Heidelberg: 1998; pp 75-137.
 42. Otsu, T., Iniferter concept and living radical polymerization. *Journal of Polymer Science Part A: Polymer Chemistry* **2000**, 38(12), 2121-2136.
 43. Cabannes-Boué, B.; Yang, Q.; Lalevée, J.; Morlet-Savary, F.; Poly, J., Investigation into the mechanism of photo-mediated RAFT polymerization involving the reversible photolysis of the chain-transfer agent. *Polymer Chemistry* **2017**, 8(11), 1760-1770.
 44. McKenzie, T. G.; Fu, Q.; Wong, E. H. H.; Dunstan, D. E.; Qiao, G. G., Visible Light Mediated Controlled Radical Polymerization in the Absence of Exogenous Radical Sources or Catalysts. *Macromolecules* **2015**, 48(12), 3864-3872.
 45. McKenzie, T. G.; Costa, L. P. d. M.; Fu, Q.; Dunstan, D. E.; Qiao, G. G., Investigation into the photolytic stability of RAFT agents and the implications for photopolymerization reactions. *Polymer Chemistry* **2016**, 7(25), 4246-4253.
 46. Xu, J.; Shanmugam, S.; Corrigan, N. A.; Boyer, C., Catalyst-Free Visible Light-Induced RAFT Photopolymerization. In *Controlled Radical Polymerization: Mechanisms*, American Chemical Society: 2015; pp 247-267.
 47. Corrigan, N.; Trujillo, F. J.; Xu, J.; Moad, G.; Hawker, C. J.; Boyer, C., Divergent Synthesis of Graft and Branched Copolymers through Spatially Controlled Photopolymerization in Flow Reactors. *Macromolecules* **2021**, 54(7), 3430-3446.
 48. Shanmugam, S.; Cuthbert, J.; Kowalewski, T.; Boyer, C.; Matyjaszewski, K., Catalyst-Free Selective Photoactivation of RAFT Polymerization: A Facile Route for Preparation of Comblike and Bottlebrush Polymers. *Macromolecules* **2018**, 51(19), 7776-7784.
 49. Carmean, R. N.; Sims, M. B.; Figg, C. A.; Hurst, P. J.; Patterson, J. P.; Sumerlin, B. S., Ultrahigh Molecular Weight Hydrophobic Acrylic and Styrenic Polymers through Organic-Phase Photoiniferter-Mediated Polymerization. *ACS Macro Letters* **2020**, 9(4), 613-618.

50. Xia, Y.; Scheutz, G. M.; Easterling, C. P.; Zhao, J.; Sumerlin, B. S., Hybrid Block Copolymer Synthesis by Merging Photoiniferter and Organocatalytic Ring-Opening Polymerizations. *Angewandte Chemie International Edition* **2021**, 60(34), 18537-18541.
51. Lalevée, J.; Blanchard, N.; El-Roz, M.; Allonas, X.; Fouassier, J. P., New Photoiniferters: Respective Role of the Initiating and Persistent Radicals. *Macromolecules* **2008**, 41(7), 2347-2352.
52. Pan, X.; Tasdelen, M. A.; Laun, J.; Junkers, T.; Yagci, Y.; Matyjaszewski, K., Photomediated controlled radical polymerization. *Progress in Polymer Science* **2016**, 6273-125.
53. Qin, S. H.; Qiu, K. Y., A new polymerizable photoiniferter for preparing poly(methyl methacrylate) macromonomer. *European Polymer Journal* **2001**, 37(4), 711-717.
54. Carmean, R. N.; Becker, T. E.; Sims, M. B.; Sumerlin, B. S., Ultra-High Molecular Weights via Aqueous Reversible-Deactivation Radical Polymerization. *Chem* **2017**, 2(1), 93-101.
55. Nothling, M. D.; Fu, Q.; Reyhani, A.; Allison-Logan, S.; Jung, K.; Zhu, J.; Kamigaito, M.; Boyer, C.; Qiao, G. G., Progress and Perspectives Beyond Traditional RAFT Polymerization. *Advanced Science* **2020**, 7(20), 2001656.
56. Roy, S. G.; Haldar, U.; De, P., Remarkable swelling capability of amino acid based cross-linked polymer networks in organic and aqueous medium. *ACS Applied Materials & Interfaces* **2014**, 6(6), 4233-4241.
57. Yu, Q.; Zhu, Y.; Ding, Y.; Zhu, S., Reaction behavior and network development in raft radical polymerization of dimethacrylates. *Macromolecular Chemistry and Physics* **2008**, 209(5), 551-556.
58. Norisuye, T.; Morinaga, T.; Tran-Cong-Miyata, Q.; Goto, A.; Fukuda, T.; Shibayama, M., Comparison of the gelation dynamics for polystyrenes prepared by conventional and living radical polymerizations: a time-resolved dynamic light scattering study. *Polymer* **2005**, 46(6), 1982-1994.
59. Shi, X.; Zhang, J.; Corrigan, N.; Boyer, C., PET-RAFT facilitated 3D printable resins with multifunctional RAFT agents. *Materials Chemistry Frontiers* **2021**, 5(5), 2271-2282.
60. Zhang, Z.; Corrigan, N.; Boyer, C., Effect of Thiocarbonylthio Compounds on Visible-Light-Mediated 3D Printing. *Macromolecules* **2021**, 54(3), 1170-1182.
61. Shanmugam, S.; Cuthbert, J.; Flum, J.; Fantin, M.; Boyer, C.; Kowalewski, T.; Matyjaszewski, K., Transformation of gels via catalyst-free selective RAFT photoactivation. *Polymer Chemistry* **2019**, 10(19), 2477-2483.
62. Cuthbert, J.; Balazs, A. C.; Kowalewski, T.; Matyjaszewski, K., STEM Gels by Controlled Radical Polymerization. *Trends in Chemistry* **2020**, 2(4), 341-353.
63. Amamoto, Y.; Otsuka, H.; Takahara, A.; Matyjaszewski, K., Changes in Network Structure of Chemical Gels Controlled by Solvent Quality through Photoinduced Radical Reshuffling Reactions of Trithiocarbonate Units. *ACS Macro Letters* **2012**, 1(4), 478-481.
64. Chiefari, J.; Chong, Y.; Ercole, F.; Krstina, J.; Jeffery, J.; Le, T. P.; Mayadunne, R. T.; Meijs, G. F.; Moad, C. L.; Moad, G., Living free-radical polymerization by reversible addition- fragmentation chain transfer: the RAFT process. *Macromolecules* **1998**, 31(16), 5559-5562.
65. Cuthbert, J.; Beziau, A.; Gottlieb, E.; Fu, L.; Yuan, R.; Balazs, A. C.; Kowalewski, T.; Matyjaszewski, K., Transformable Materials: Structurally Tailored and Engineered Macromolecular (STEM) Gels by Controlled Radical Polymerization. *Macromolecules* **2018**, 51(10), 3808-3817.

66. Lampley, M. W.; Harth, E., Photocontrolled Growth of Cross-Linked Nanonetworks. *ACS Macro Letters* **2018**, 7(6), 745-750.
67. Parkatzidis, K.; Wang, H. S.; Truong, N. P.; Anastasaki, A., Recent Developments and Future Challenges in Controlled Radical Polymerization: A 2020 Update. *Chem* **2020**, 6(7), 1575-1588.
68. Rasines Mazo, A.; Tran, T. N.; Zhang, W.; Meng, Y.; Reyhani, A.; Pascual, S.; Fontaine, L.; Qiao, G. G.; Piogé, S., Blue LED light-activated RAFT polymerization of PEG acrylate with high chain-end fidelity for efficient PEGylation. *Polymer Chemistry* **2020**, 11(32), 5238-5248.
69. Amamoto, Y.; Otsuka, H.; Takahara, A.; Matyjaszewski, K., Self-healing of covalently cross-linked polymers by reshuffling thiuram disulfide moieties in air under visible light. *Adv Mater* **2012**, 24(29), 3975-80.
70. Zhang, Z.; Corrigan, N.; Bagheri, A.; Jin, J.; Boyer, C., A Versatile 3D and 4D Printing System through Photocontrolled RAFT Polymerization. *Angewandte Chemie International Edition* **2019**, 131(50), 18122-18131.
71. Bainbridge, C. W. A.; Engel, K. E.; Jin, J., 3D printing and growth induced bending based on PET-RAFT polymerization. *Polymer Chemistry* **2020**, 11(25), 4084-4093.
72. Pawar, A. A.; Halivni, S.; Waiskopf, N.; Ben-Shahar, Y.; Soreni-Harari, M.; Bergbreiter, S.; Banin, U.; Magdassi, S., Rapid Three-Dimensional Printing in Water Using Semiconductor-Metal Hybrid Nanoparticles as Photoinitiators. *Nano letters* **2017**, 17(7), 4497-4501.
73. Darcos, V.; Monge, S.; Haddleton, D. M., In situ Fourier transform near infrared spectroscopy monitoring of copper mediated living radical polymerization. *Journal of Polymer Science Part A: Polymer Chemistry* **2004**, 42(19), 4933-4940.
74. Shanmugam, S.; Xu, J.; Boyer, C., Utilizing the electron transfer mechanism of chlorophyll a under light for controlled radical polymerization. *Chemical Science* **2015**, 6(2), 1341-1349.
75. ASTM-International, Designation: D 638 – 14 Standard Test Method for Tensile Properties of Plastics. 2015.
76. Thingiverse, Violin. <https://www.thingiverse.com/thing:515900> (accessed 24/9/2021).
77. Lu, L.; Yang, N.; Cai, Y., Well-controlled reversible addition–fragmentation chain transfer radical polymerisation under ultraviolet radiation at ambient temperature. *Chemical communications* **2005**, (42), 5287-5288.
78. Shi, Y.; Liu, G.; Gao, H.; Lu, L.; Cai, Y., Effect of Mild Visible Light on Rapid Aqueous RAFT Polymerization of Water-Soluble Acrylic Monomers at Ambient Temperature: Initiation and Activation. *Macromolecules* **2009**, 42(12), 3917-3926.
79. Miao, X.; Zhu, W.; Zhang, Z.; Zhang, W.; Zhu, X.; Zhu, J., Photo-induced cobalt-mediated radical polymerization of vinyl acetate. *Polymer Chemistry* **2014**, 5(2), 551-557.
80. Zhao, Y.; Yu, M.; Zhang, S.; Wu, Z.; Liu, Y.; Peng, C.-H.; Fu, X., A well-defined, versatile photoinitiator (salen)Co–CO₂CH₃ for visible light-initiated living/controlled radical polymerization. *Chemical Science* **2015**, 6(5), 2979-2988.
81. Lim, K. S.; Galarraga, J. H.; Cui, X.; Lindberg, G. C. J.; Burdick, J. A.; Woodfield, T. B. F., Fundamentals and Applications of Photo-Cross-Linking in Bioprinting. *Chemical Reviews* **2020**, 120(19), 10662-10694.
82. Zaquen, N.; Azizi, W. A. A. W.; Yeow, J.; Kuchel, R. P.; Junkers, T.; Zetterlund, P. B.; Boyer, C., Alcohol-based PISA in batch and flow: exploring the role of photoinitiators. *Polymer Chemistry* **2019**, 10(19), 2406-2414.

83. Lee, J. H.; Prud'homme, R. K.; Aksay, I. A., Cure depth in photopolymerization: Experiments and theory. *Journal of Materials Research* **2001**, *16*(12), 3536-3544.
84. Lin, H.; Zhang, D.; Alexander, P. G.; Yang, G.; Tan, J.; Cheng, A. W.-M.; Tuan, R. S., Application of visible light-based projection stereolithography for live cell-scaffold fabrication with designed architecture. *Biomaterials* **2013**, *34*(2), 331-339.
85. Odian, G., Radical Chain Polymerization. In *Principles of Polymerization*, John Wiley & Sons: 2004; pp 198-349.
86. Flory, P. J., Network Structure and the Elastic Properties of Vulcanized Rubber. *Chemical Reviews* **1944**, *35*(1), 51-75.
87. Langley, N. R.; Polmanteer, K. E., Relation of elastic modulus to crosslink and entanglement concentrations in rubber networks. *Journal of Polymer Science: Polymer Physics Edition* **1974**, *12*(6), 1023-1034.
88. Fenoli, C. R.; Wydra, J. W.; Bowman, C. N., Controllable Reversible Addition-Fragmentation Termination Monomers for Advances in Photochemically Controlled Covalent Adaptable Networks. *Macromolecules* **2014**, *47*(3), 907-915.
89. Leung, D.; Bowman, C. N., Reducing Shrinkage Stress of Dimethacrylate Networks by Reversible Addition-Fragmentation Chain Transfer. *Macromolecular Chemistry and Physics* **2012**, *213*(2), 198-204.
90. Zhou, H.; Johnson, J. A., Photo-controlled Growth of Telechelic Polymers and End-linked Polymer Gels. *Angewandte Chemie International Edition* **2013**, *52*(8), 2235-2238.
91. Dietrich, M.; Glassner, M.; Gruendling, T.; Schmid, C.; Falkenhagen, J.; Barner-Kowollik, C., Facile conversion of RAFT polymers into hydroxyl functional polymers: a detailed investigation of variable monomer and RAFT agent combinations. *Polymer Chemistry* **2010**, *1*(5), 634-644.
92. Moad, G., RAFT (Reversible addition-fragmentation chain transfer) crosslinking (co)polymerization of multi-olefinic monomers to form polymer networks. *Polymer International* **2015**, *64*(1), 15-24.

Chapter 6. Concluding Remarks and Outlook

6.1 Conclusion

In the past decades, VP as a promising additive manufacturing technology has been extensively employed in many applications, such as dentistry, tissue engineering, biomedical applications, and production of smart materials. Advanced VP techniques allows the fabrication of complex 3D objects in fast printing speed and high printing resolution. Moreover, the versatility of photochemistry applied behind these techniques enables the production of polymeric materials with diverse physical and chemical properties. Despite these advantages, non-living free radical or cationic polymerisation mechanism adopted by current VP photocuring methods produce inert polymers which are unable to be reactivated for further chain growth, significantly preventing post-functionalisation of 3D printed materials. Also, 3D printed thermosets with irreversibly crosslinked polymer networks cannot be repaired after damage, leading to wasted resources and materials.

Photomediated RAFT polymerisation is a versatile and robust RDRP technique which performs good control over polymer chain growth via photostimulation. Also, the retention of thiocarbonylthio polymer chain-ends in polymer materials can be reactivated by external stimuli to enable post-modification of pre-formed polymers. Therefore, the main purpose of this thesis was to apply photomediated RAFT polymerisation techniques in VP to fabricate materials in a controlled manner and impart living characteristics to these materials. This body of work has demonstrated that photomediated RAFT polymerisation can be applied in 3D printing under visible light irradiation in the open air using a commercial 3D printer. Further, the inclusion of RAFT agents in photoresins provides control over mechanical properties of 3D printed materials and allows post-functionalisation of pre-formed networks. Moreover, the incorporation of RAFT agents in the polymeric network enables 3D printing of thermosets with self-healing capabilities. The main outcomes of the work are summarised in the following paragraphs.

In **Chapter 3**, PET-RAFT polymerisation was firstly exploited in 3D printing by using a customised DLP 3D printer under green light irradiation ($\lambda_{\text{max}} = 525 \text{ nm}$) in an open-air condition. The photoinitiating system composed of an organic dye EB in conjunction with triethanolamine as co-catalyst allowed fast printing speeds. It was shown that the mechanical properties of 3D printed materials were tuned by varying the concentration

of the RAFT agent in resin formulations. Moreover, the retention of the RAFT functionality during the 3D printing process allowed the 3D printed materials to undergo surface post-modification after printing. The dormant RAFT agents on the surface of the 3D printed materials can be reinitiated in the presence of EB under green light irradiation, starting a secondary polymerisation with newly added monomers. Surface functionalisation was also able to be spatially controlled through selected irradiation during the post-functionalisation. The versatility of this photomediated RAFT polymerisation process provides access to a range of new functional and stimuli-responsive materials.

By utilising the same photoinitiating system as the previous chapter, **in Chapter 4**, photoresins containing various thiocarbonylthio species were investigated for their application in 3D printing. Both the activating Z groups and leaving R groups had a significant impact on the polymerisation rate, which affected the 3D printing process and the resulting mechanical properties of 3D printed materials. Photoresins containing BTPA or xanthate which provided fast polymerisation kinetics were in favour of network formation, leading to the production of rigid materials. The differences in mechanical properties between the objects 3D printed in the absence or presence of trithiocarbonates were further investigated. At the rubbery plateau region, the storage modulus of the sample printed with trithiocarbonates was lower than that of the sample printed without RAFT agents, indicating that the network of the sample 3D printed with trithiocarbonates was less crosslinked. Further, the impact of the concentration of trithiocarbonates on mechanical properties of 3D printed materials was demonstrated. The modulus in the glassy state of materials printed in the presence of increasing concentrations of trithiocarbonates increased to a point, and reduced thereafter, which was ascribed to reduction in polymerisation rates at higher RAFT concentrations. Finally, 3D printed materials with the incorporation of RAFT agents in the network were easily post-functionalised via one-pot *in situ* aminolysis and thiol-Michael additions.

In **Chapter 5**, RAFT polymerisation was applied to visible light-induced 3D printing to produce high-resolution 3D printed thermosets with self-healing capabilities. In this work, RAFT agents played roles as both a chain transfer agent during formation of the polymer network, and as an iniferter under UV light irradiation to enable post-modification of the network in the presence of additional monomer or crosslinker. A Norrish type I

photoinitiation system was adopted to facilitate RAFT photopolymerisation under violet light irradiation ($\lambda_{\text{max}} = 405 \text{ nm}$) in 3D printing, using symmetric difunctional RAFT agents to mediate the network formation. 3D printed materials (T_g above room temperature) containing TTC units can then perform rapid self-repair via a secondary polymerisation with freshly added crosslinker under UV light irradiation ($\lambda_{\text{max}} = 365 \text{ nm}$) in the open air at room temperature. The concentration of TTC units in the resin was critically important in affecting the healing efficiency, with the object containing a high concentration of TTC units resulting in a higher tensile strength recovery and elongation at break recovery. Self-healing efficiency was also influenced by the structure of RAFT agents incorporated in the network. It was demonstrated that the material 3D printed in the presence of symmetric difunctional RAFT agent resulted in a superior self-repairing capability over that 3D printed in the presence of asymmetric monofunctional RAFT agent. This work promisingly paves the way for the fabrication of novel 3D printed thermosets with self-healing properties.

As demonstrated throughout the work, photomediated RAFT polymerisation techniques can be applied in 3D printing to fabricate materials with controlled mechanical properties under visible light irradiation in the open air. More importantly, 3D printed materials incorporated with RAFT agents in the network can be easily post-functionalised via ω -end modification approaches, such as one-pot *in situ* aminolysis and thiol-Michael additions. Alternatively, the thiocarbonylthio species in the network can be reactivated under light irradiation, starting a secondary polymerisation with newly added monomers or crosslinkers to post-modify the pre-formed materials. This post-modification process can also be spatially controlled through selected irradiation to a specific area. The application of the versatile and robust photomediated RAFT polymerisation techniques in 3D printing provides access to a broad range of novel materials with diverse functionalities and properties.

6.2 Future Perspectives

Since the first SLA instruments introduced by Hull in 1980s,⁵⁸ various 3D printing techniques emerged and developed rapidly in the past decades, allowing the fabrication of materials with arbitrary geometries and functions tailored for individual demands and specific applications. Among these techniques, VP has garnered significant attention from material and polymer scientists, due to its fast build speed and high printing resolution as well as the versatility of photochemistry.²⁰² However, the current photocuring method adopts non-living radical polymerisation or cationic polymerisation, performing less control over chain growth and producing inert polymers incapable of post-functionalisation. The application of photomediated RAFT polymerisation in 3D printing allows the tuning of material mechanical properties, and more importantly imparts living characteristics into the network. The dormant thiocarbonylthio species in 3D printed materials can be repeatedly activated under external stimuli and then start a secondary polymerisation with freshly added monomers, generating materials with new functions, such as self-healing capability upon damage.

However, a great amount of work is required to fully reach the potential of photomediated RAFT polymerisation in 3D printing. A promising aspect is to develop 3D photopolymerisation systems toward longer wavelength irradiation, such as red light or NIR light induced system. In comparison with short wavelength irradiation, long wavelength with low energy irradiation causes less cellular photodamage, increasing the scope for potential application in 3D bioprinting.³⁴⁰ Moreover, long wavelength irradiation provides deeper light penetration, which is able to increase slicing thickness for each layer printing, in turn increasing printing speed. As mentioned in **section 2.3**, Page and co-workers demonstrated a rapid high-resolution DLP 3D printing activated by using red light irradiation ($\lambda_{\text{max}} = 615 \text{ nm}$) in the presence of ZnTPP as PC.⁶⁰ With the addition of coinitiators and opaquing agents, a high-resolution object was fabricated rapidly with the print speed of 11 s curing time per layer. However, no latent active sites were incorporated in the pre-formed materials, which were unable to be post-modified with new functions. Therefore, inspired by this work, it is expected that long wavelength induced RAFT polymerisation could provide fast fabrication of high-resolution 3D printed materials with dormant thiocarbonylthio species in the network which can be post-functionalised for various applications.

Another promising opportunity for photomediated RAFT processes in 3D printing is to apply photoorthogonal control over the polymerisation to fabricate materials with controlled properties. Employing distinct wavelengths to activate and control polymerisation enables photoorthogonal reactions; one reaction can proceed independently of another under specific wavelength irradiation, in turn producing materials with various functions. This strategy has been applied in organic chemistry and RDRP, but not in photomediated RAFT processes in 3D printing.^{46, 207-211, 214} Therefore, it is expected that the switch of light source during the printing process could be programmed, in turn activating polymerisation under selected wavelength irradiation to finally obtained 3D materials with controlled functions and properties.

Certainly, a great deal of work is still needed to explore more efficient and robust photoinitiation systems for 3D printing and develop new PCs or RAFT agents for specific applications. In addition, the development of VP techniques is also of great significance to facilitate the progress of the abovementioned new concepts, such as highly improved projection techniques to provide higher printing resolution and fast printing speed or 3D printers equipped with more light sources to provide programmable wavelength switch function. Taken all together, the advancement of photomediated RAFT processes in 3D printing will bring more opportunities to create new functional materials for numerous applications.